1971
Quarterly
Technical
Progress
Review
Volume 14-2

Reactor Technology

A publication of the
Division of Technical Information
U.S. Atomic Energy Commission
Prepared in Cooperation
with
The American Nuclear Society.

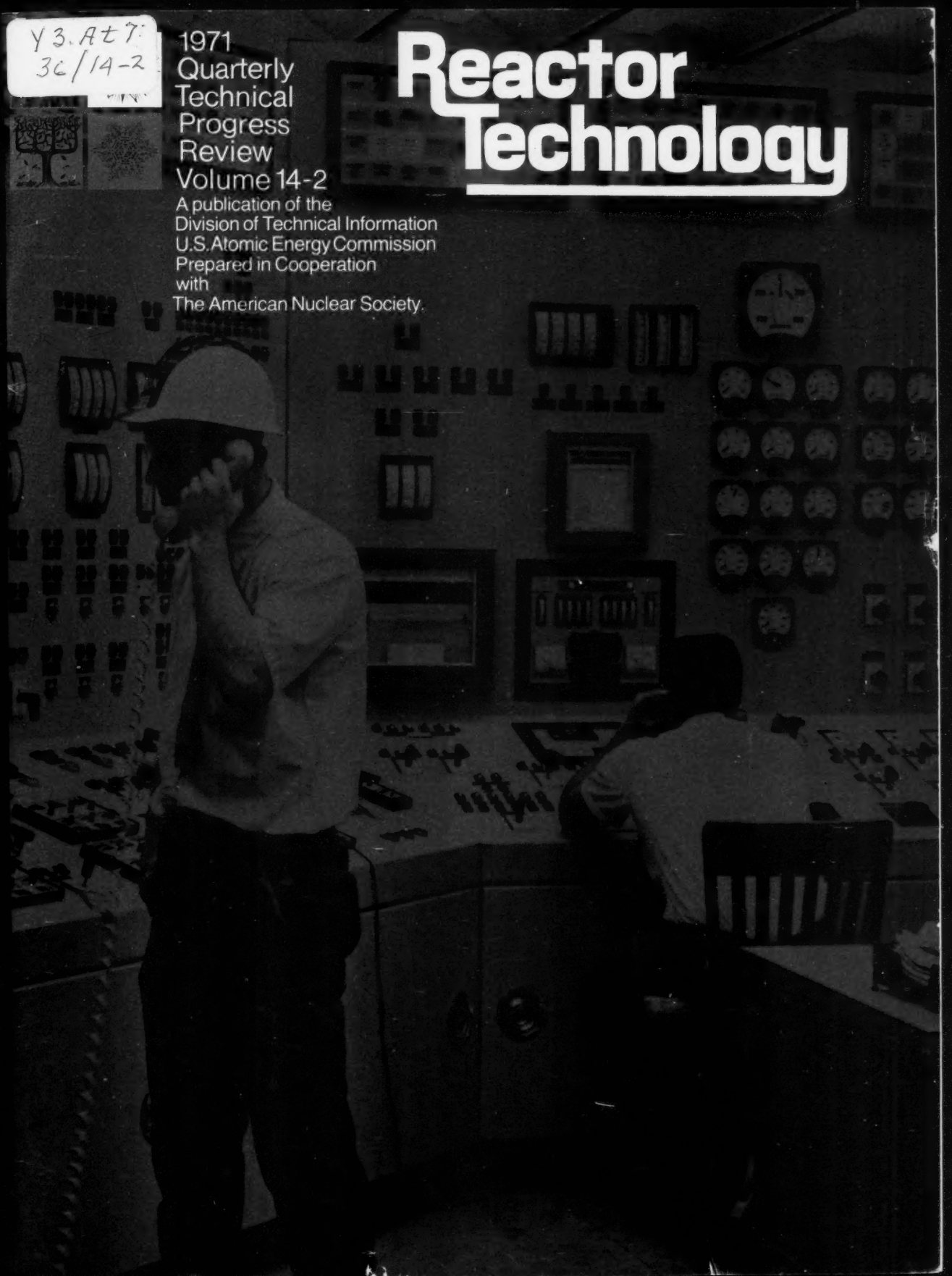

TECHNICAL PROGRESS REVIEWS

The United States Atomic Energy Commission publishes the Technical Progress Reviews to meet the needs of industry and government for concise summaries of current nuclear developments. Each journal digests and evaluates the latest findings in a specific area of nuclear technology and science. *Nuclear Safety* is a bimonthly journal; the other two are quarterly journals.

Isotopes and Radiation Technology
P. S. Baker, A. F. Rupp, and associates
Isotopes Information Center, Oak Ridge National Laboratory

Nuclear Safety
Wm. B. Cottrell, W. H. Jordan, J. P. Blakely, and associates
Nuclear Safety Information Center, Oak Ridge National Laboratory

Reactor Technology
Prepared in cooperation with the American Nuclear Society

All are available from the U. S. Government Printing Office. See the back cover for ordering instructions.

Availability of Reports Cited in This Review

United States Atomic Energy Commission (USAEC) reports are available at certain libraries that maintain collections of these reports. The libraries are listed on the inside front cover of each issue of *Nuclear Science Abstracts*. USAEC reports are also sold by the following governmental and international organizations: (1) National Technical Information Service (NTIS), U. S. Department of Commerce, Springfield, Va. 22151; (2) International Atomic Energy Agency (IAEA), Vienna, Austria; and (3) National Lending Library, Boston Spa, England.

Other U. S. Government agency reports identified in this journal are generally available from NTIS.

Reports from other countries are generally available at the same U. S. libraries as maintain collections of USAEC reports, and from IAEA and the originating country. **United Kingdom Atomic Energy Authority (UKAEA)** reports are sold by Her Majesty's Stationery Office, London. **Atomic Energy of Canada Limited (AECL)** reports are sold by the Scientific Document Distribution Office, Atomic Energy of Canada Limited, Chalk River, Ontario, Canada. UKAEA and AECL reports issued after March 1, 1967, are sold by NTIS to purchasers in the United States and its territories. IAEA publications are sold in the United States by UNIPUB, P. O. Box 433, New York, N. Y. 10016.

Private-organization reports should be requested from the originator.

REACTOR TECHNOLOGY

Vol. 14, No. 2 Summer 1971

Contents

COVER: Control room of the Robert Emmett Ginna Nuclear Power Plant on the south shore of Lake Ontario at Ontario, N. Y. See the article on page 139. (Rochester Gas & Electric Corp. photograph.)

Superintendent of Documents, U. S. Government Printing Office, Washington, D. C. 20402, $3.00 per year.

REACTOR TECHNOLOGY

is a quarterly review of progress and developments in the reactor field including the following subject areas:

Economics	Fuel Cycles
Physics	Fluid and Thermal Technology
Mechanics	Fuel Processing
Construction	Components
Fuel Elements	Operating Performance

Prepared for reactor physicists, reactor operators, designers, fuel-cycle specialists, administrators, and others interested in the field, this journal reviews, summarizes, critically evaluates and interprets the state of the art as reflected in the current literature.

The many reports and publications referenced merit further study, and readers are urged to consult them for additional details.

Qualified authors are invited to contribute review articles for consideration for publication.

U. S. Atomic Energy Commission
Division of Technical Information
Washington, D. C. 20545

Issued quarterly by the U. S. Atomic Energy Commission. Use of funds for printing this publication approved by the Director of the Bureau of the Budget on May 12, 1969.

A Review of Creep Behavior of Ceramic Nuclear Fuels

By M. S. Seltzer, J. S. Perrin, A. H. Clauer, and B. A. Wilcox*

INTRODUCTION

Substantial fuel-element dimensional changes can occur in-pile during reactor operation. Most of the dimensional changes can be caused by the fuel swelling from an accumulation of fission-product atoms. The gaseous atoms agglomerate and migrate into bubbles, thus internally stressing the fuel matrix, and the resulting growth of the fuel occurs in a manner thought to be analogous to creep deformation. As the fuel swells, from both the gaseous and solid fission products, part of the swelling is accommodated by fuel porosity introduced for this purpose, but the remaining growth is restrained by the fuel-element cladding. Thus the amount of fuel swelling is dependent on the creep strengths of both the fuel and cladding.

The importance of the creep strength of the fuel during reactor operation has made creep studies of reactor fuels necessary. These studies have usually consisted in out-of-pile creep tests, which are relatively easy to perform. However, there are predictions that the in-pile creep rate of reactor materials is increased relative to the out-of-pile creep rate owing to a fission-induced enhancement of the creep process. Hesketh[1,2] has predicted that substantial enhancement of creep rate in metals can occur during irradiation and that this enhancement is independent of temperature. Brucklacher, Dienst, and Thuemmler[3] have made a similar prediction for UO_2, predicting a fission-induced athermal component of creep which is substantially larger than the normal out-of-pile thermal component at lower temperatures ($T \lesssim 1200°C$). As a result of such predictions, several recent studies were made to determine the in-pile creep rate of nuclear fuels.

In this article, results of both out-of-pile and in-pile creep studies are presented and discussed. The materials reviewed include UO_2, UO_2–PuO_2, UO_2–ThO_2, UO_2–ZrO_2, BeO–UO_2, ThO_2, UC, and UN. The variables that are considered include temperature, stress, grain size, stoichiometry, density, impurities, and, in the case of in-pile creep tests, fission rate. In addition, currently proposed in-pile creep mechanisms are discussed and related to out-of-pile creep mechanisms.

OUT-OF-PILE CREEP

UO_2

Uranium dioxide crystallizes in the cubic fluorite structure and has a homogeneity range[4] extending over tens of at.% above 1000°C. Hypostoichiometric (oxygen deficient) compositions[5] are readily obtained only above 1700°C. Therefore studies of physical properties, including the creep characteristics of UO_2, have been performed on specimens containing an oxygen excess. The predominant point defects are believed to consist of oxygen interstitials and oxygen vacancies, perhaps in complexes of two oxygen interstitials and an oxygen vacancy.[6] The defect structure on the uranium sublattice has not been clearly established, but it is likely that uranium vacancies occur as a minority defect in hyperstoichiometric compositions. The diffusion data for UO_2 are summarized in Table 1, and the creep data are summarized in Table 2.

*Battelle Memorial Institute, Columbus Laboratories, Columbus, Ohio 43201.

Table 1 Self-Diffusion in Oxides

Oxide	Reference	Element	Temperature range, °C	Atm	Purity	D_0, cm²/sec	Q, kcal/mole	Comments*
$UO_{2\pm x}$	Auskern and Belle[37]	U	1450 to 1785	H_2	100 ppM Zr, ~100 ppM others	4.3×10^{-4}	88 ± 11	P, 20- to 40-μ g.s. >98% T.D.
$UO_{2\pm x}$	Hawkins and Alcock[23]	U	1350 to 1650	CO/CO_2	O/U = 2.01	2.04×10^{-3}	89 ± 2	S, P, 12-μ g.s., ^{233}U, $\alpha \rightarrow \gamma$-ray spect. At 1400°C, $\log D = 0.184 \log p - 12.78$ $D \propto x^2$
					O/U = 2.03	2.79×10^{-2}	95 ± 3.5	
					O/U = 2.10	1.09	105 ± 7	
					O/U = 2.15	6.79×10^{-3}	81 ± 13	
$UO_{2\pm x}$	Alcock et al.[38]	U	1450 to 1700	H_2		4×10^{-7}	70 ± 8	S, P, 12-μ g.s., ^{233}U, α-ray spect.
						4×10^{-2}	70	← g.b. diffusion, 5-Å g.b. width
						1.2	108	← g.b. and volume diffusion. Surface activity decreases method
$UO_{2\pm x}$	Lindner and Schmitz[39]	U	1300 to 1600	H_2		0.23	105 ± 7	P, 50-μ g.s., 97.4% T.D., ^{233}U, γ-ray spect.
$UO_{2\pm x}$	Yajima et al.[40]	U	1900 to 2150	Ar		5.82×10^{-5}	72.7	P, >100-μ g.s., >99% T.D., volume diffusion
						5.2×10^{-2}	47.2	^{233}U sectioning, g.b. diffusion, 5-Å g.b. width
$UO_{2\pm x}$	Nagels et al.[41]	U	1300 to 1800	10^{-5} torr vacuum		4×10^{-4}	88 ± 6	S, ^{235}U sectioning
UO_{2+x}	McNamara[42]	U	1500 to 1600			0.12	108	S
	Marin et al.[24]	U	1500		130 ppM Fe, 50 ppM Si		$D \propto x^2$	S, P, 10-μ g.s. ^{235}U sectioning, $D \propto x^2$
UO_{2+x}	Matzke[25]	U	1200 to 1600	Various	40 ppM Ca, 25 ppM Si		110 ± 7	S, P, 20-μ g.s., >98% T.D., $D \propto x^{1.5}$ at 1500 C, ^{233}U, α-ray spect.
UO_{2+x}	Marin and Contamin[43]	U	1275 to 1650	Ar to O_2		$0.13\,x^2$ $[1 + 10^3\,x^3]$	85 ± 7	P, 20 to 100 μ g.s., ^{235}U, α-ray spect., $0.03 < x < 0.20$
UO_{2+x}	Reimann and Lundy[44]	U	1620 to 2010	H_2		6.8×10^{-5}	98.3 ± 9.7	S, ^{233}U, α-ray spect. Crystals may be hypostoichiometric
UO_{2+x}	Auskern and Belle[45]	0	550 to 780	CO_2 $CO_2 + H_2$	O/U = 2.002	1.2×10^2	65.3	UO_2 powder, ^{18}O, mass spect.
			445 to 602	CO_2	O/U = 2.004	7.0×10^{-6}	29.7	
			317 to 1100	CO_2	O/U = 2.004	2.06×10^{-3}	29.7	

Table 1 (Continued)

Oxide	Reference	Element	Temperature range, °C	Atm	Purity	D_0, cm²/sec	Q, kcal/mole	Comments*
UO_2+x	Dornelas and Lacombe[46]	O	900 to 1100	Ar	O/U = 2.01	3.8	65	P, 97% T.D., measurement of anion transport number
UO_2+x	Roberts et al.[47]	O	1370 to 1480	CO/CO_2	O/U = 2.001		69.0	S, ^{18}O, mass spect.
			1200 to 1400	CO/CO_2	O/U = 2.01		30.0	
			1240 to 1370	CO/CO_2	O/U = 2.03		23.0	
UO_2+x	Marin and Contamin[43]	O	780 to 1250	H_2, Ar	O/U ≈ 2.000	0.26	59.3	S, P, ^{18}O, mass spect.
UO_2-PuO_2	Lindner et al.[48]	U	1000 to 1600	H_2/H_2O	O/M ≈ 2.000	2.84×10^{-10}	37.0	P, 15% Pu, ^{232}U, α-ray spect. >98% T.D. ^{238}Pu, α-ray spect.
		Pu	1000 to 1600	H_2/H_2O		3.45×10^{-10}	33.0	
ThO_2	Hawkins and Alcock[23]	Th	1600 to 2100	Air, vacuum, CO/CO_2, hydrogen	Reactor grade	1.25×10^{-7}	58.8 ± 3	P, g.s. = 100 μ, ^{230}Th. D was independent of atm
ThO_2	King[49]	Th	1850 to 2000	Argon in Ta or W furnace	300 ppM Al 100 to 3000 ppM Y 1 to 1000 ppM Ca	0.35	~150	S, ^{228}Th, sectioning, probably ThO_{2-x} non-Gaussian
ThO_2	Morgan and Poteat[50]	Th	1300 to 2300	Argon for $T >$ 1800°C		2×10^{-7}	74	S, ≤1800°C for penetrations, ≤0.6 μ
				Oxidizing atm for lower temperature		4.1×10^{-9}	68.1	P, near surface
						2.6×10^{-7}	69	P, 0.2 to 0.6 μ
						7×10^{-6}	65.2	P, deeper penetration
ThO_2	Roberts and Roberts[51]	O	1000 to 1650		High		50	
			1300 to 1600		99%		46	

*S = single crystal; P = polycrystal; g.b. = grain boundary; g.s. = grain size.

Single Crystals. Creep of UO_2 single crystals has been studied by Seltzer, Clauer, and Wilcox[7] in compression and by Armstrong, Causey, and Sturrock[8] in bending. Seltzer et al.[7] examined the influence of nonstoichiometry, whereas Armstrong et al.[8] investigated the effect of crystallographic orientation on the creep behavior. These experiments provide a basis of comparison for results obtained in studies of the creep properties of polycrystalline uranium dioxide,[9-22] where, in addition to the above-mentioned parameters, the grain size, density, and foreign-atom concentrations have been treated as variables. Therefore the single-crystal results are presented first, and then the polycrystalline data are reviewed.

Seltzer, Clauer, and Wilcox[7] found that both the temperature and the stress dependence of the steady-state creep rate varied with O/U ratio. For O/U values above 2.001 at 1100°C, creep rates could be fitted by a power-law stress dependence of the form $\dot{\epsilon} \propto \sigma^n$, where σ = applied stress, $\dot{\epsilon}$ = steady-state creep rate, and

Table 2 Activation Energy and Stress Dependence of Steady-State Creep Rate in Uranium Dioxide and Mixed UO_2-Base Oxides

	Activation-energy determinations			Stress-dependence determinations							
Composition	Q_c, kcal/mole	Stress, psi	Temperature range, °C	Stress exponent,* n	Temperature, °C	Stress range, psi	% T.D.	Grain size, μ	Deformation mode	Atmosphere	Reference
$UO_{2.00}$	91 ± 8	10,000	1250 to 1400	–	–	–	96.1	6	3-point bend	Dry H_2	Armstrong et al.[16]
$UO_{2.00}$	–	–	–	1.3	1300, 1400	700 to 10,000	96.1	6	3-point bend	Dry H_2	Armstrong et al.[16]
$UO_{2.00}$	–	–	–	4	1400	10,000 to 16,000	96.1	6	3-point bend	Dry H_2	Armstrong et al.[16]
$UO_{2.00}$	–	–	–	1	1400	4,000 to 8,000	94.5 to 98.0	13 to 40	3-point bend	Dry H_2	Armstrong et al.[16]
$UO_{2.00}$	–	–	–	4	1400	8,000 to 13,000	94.5 to 98.0	13 to 40	3-point bend	Dry H_2	Armstrong et al.[16]
$UO_{2.02-2.08}$	56 ± 5	5,000	975 to 1350	–	–	–	96.0	6	3-point bend	Ar + O_2†	Armstrong and Irvine[17]
$UO_{2.02-2.08}$	–	–	–	1	1300	1,000 to 7,000	96.0	6	3-point bend	Ar + O_2†	Armstrong and Irvine[17]
$UO_{2.16}$	63 ± 8	5,000	975 to 1300	–	–	–	96.0	6	3-point bend	Ar + O_2†	Armstrong and Irvine[17]
$UO_{2.16}$	–	–	–	>1	1300	1,000 to 3,000	96.0	6	3-point bend	Ar + O_2†	Armstrong and Irvine[17]
$UO_{2.00}$	>95	5,000	1000 to 1650	–	–	–	95	2 to 10	3-point bend	H_2(?)	Scott et al.[15]
$UO_{2.06}$	72	5,000	850 to 1000	–	–	–	95	2 to 10	3-point bend	Ar	Scott et al.[15]
$UO_{2.16}$	65	5,000	800 to 1000	–	–	–	95	2 to 10	3-point bend	Ar	Scott et al.[15]
$UO_{2.16}$	–	–	–	>1	975	800 to 6,500	95	2 to 10	3-point bend	Ar	Scott et al.[15]
$UO_{2.00}$	98 ± 7	10,000	1220 to 1400	–	–	–	97.7	24	3-point bend	Dry H_2	Armstrong and Irvine[18]
$UO_{2.00}$	–	–	–	2	1400	2,000 to 6,000	97.7	24	3-point bend	Dry H_2	Armstrong and Irvine[18]
$UO_{2.00}$	–	–	–	5	1400	6,000 to 10,000	97.7	24	3-point bend	Dry H_2	Armstrong and Irvine[18]
$UO_{2.00}$ – 0.5 ZrO_2	121 ± 8	10,000	1325 to 1450	–	–	–	97.2	26	3-point bend	Dry H_2	Armstrong Irvine[18]
$UO_{2.00}$ – 0.5 ZrO_2	–	–	–	1	1400	6,000 to 12,000	97.2	26	3-point bend	Dry H_2	Armstrong and Irvine[18]
$UO_{2.00}$ – 1.0 ZrO_2	–	–	–	1	1400	8,000 to 14,000	97	31	3-point bend	Dry H_2	Armstrong and Irvine[18]
$UO_{2.00}$ – 0.5Y_2O_3	127 ± 13	10,000	1325 to 1400	–	–	–	96	19	3-point bend	Dry H_2	Armstrong and Irvine[18]
$UO_{2.00}$ – 0.5 CaO	130 ± 11	10,000	1300 to 1425	–	–	–	97.3	25	3-point bend	Dry H_2	Armstrong and Irvine[18]
$UO_{2.00}$ – 0.5 CaO		–	–	1	1400	6,000 to 10,000	97.3	25	3-point bend	Dry H_2	Armstrong and Irvine[18]
$UO_{2.00}$ – 1.0 SiO_2	105 ± 10	10,000	1200 to 1400	–	–	–	99	10	3-point bend	Dry H_2	Armstrong and Irvine[18]
$UO_{2.00}$	117 ± 10‡	3,600 to 8,000	1340 to 1685	–	–	3,600 to 5,000	>99	Single crystal§	4-point bend	Dry H_2	Armstrong et al.[8]
$UO_{2.00}$	–	–	–	3.3 ± 0.1	1400	3,600 to 8,000	>99	Single crystal§	4-point bend	Dry H_2	Armstrong et. al.[8]
$UO_{2.00}$	71	3,000	1600 to 2000	–	–	–	98.5	55	Compression	?	Wolfe and Kaufman[9]
$UO_{2.00}$	–	–	–	4.5	1800 to 2000	1,500 to 5,000	98.5	55	Compression	?	Wolfe and Kaufman[9]
$UO_{2.00}$	–	–	–	1	1800	1,000 to 3,000	97.5	18	Compression	?	Wolfe and Kaufman[9]
$UO_{2.00}$	–	–	–	4.8	1800	3,000 to 5,000	97.5	18	Compression	?	Wolfe and Kaufman[9]

Table 2 (Continued)

	Activation-energy determinations			Stress-dependence determinations							
Composition	Q_c, kcal/mole	Stress, psi	Temperature range, °C	Stress exponent,* n	Temperature, °C	Stress range, psi	% T.D.	Grain size, μ	Deformation mode	Atmosphere	Reference
$UO_{2.00}$	84	3,000	1430 to 1666	–	–	–	97.5	10	Compression	?	Poteat and Yust[10]
$UO_{2.00}$	90	10,000	1430 to 1666	–	–	–	97.5	10	Compression	?	Poteat and Yust[10]
$UO_{2.00}$	–	–	–	1 to 1.1	1430 to 1666	2,000 to 5,500	97.5	10	Compression	?	Poteat and Yust[10]
$UO_{2.00}$	–	–	–	4.8	1430 to 1666	5,500 to 11,000	97.5	10	Compression	?	Poteat and Yust[10]
$UO_{2.0001}$	134	10,000	1100 to 1300	7	1100	16,000 to 24,000	100	Single	Compression	H_2	Seltzer et al.[7]
$UO_{2.001}$	115	10,000	1100 to 1400	13	1100	12,000 to 18,000	100	Single	Compression	CO/CO_2	Seltzer et al.[7]
$UO_{2.003}$	80.5	10,000	1100 to 1400	17	1100	12,000 to 14,000	100	Single	Compression	CO/CO_2	Seltzer et al.[7]
$UO_{2.01}$	63.5	10,000	1100 to 1300	17	1100	7,000 to 12,000	100	Single	Compression	CO/CO_2	Seltzer et al.[7]
$UO_{2.062}$	57.5	10,000	1100 to 1300	17	1100	5,000 to 10,000	100	Single	Compression	O/CO_2	Seltzer et al.[7]
$UO_{2.0001}$	129	3,000	1250 to 1400	1	1300	–	100	Single	Compression	H_2	Seltzer et al.[7]
$UO_{2.01}$	131	3,000	1250 to 1400	17	1400	3,000 to 5,000	100	Single	Compression	CO/CO_2	Seltzer et al.[7]
$UO_{2.001}$	117	8,000	1100 to 1300	7	1100 to 1300	7,000 to 10,000	97.8	27	Compression	CO/CO_2	Seltzer et al.[12]
$UO_{2.01}$	75	6,000	1100 to 1300	17	1100 to 1300	6,000 to 9,000	97.8	27	Compression	CO/CO_2	Seltzer et al.[12]
$UO_{2.10}$	54	4,000	1100 to 1300	17	1100 to 1300	2,000 to 5,000	97.8	27	Compression	CO/CO_2	Seltzer et al.[12]
$UO_{2.001}$	108	15,000	1100 to 1300	4	1100 to 1300	7,000 to 10,000	95	7	Compression	CO/CO_2	Seltzer et al.[12]
$UO_{2.001}$	68.5	2,000	1100 to 1300	1	1100 to 1300	1,250 to 5,000	95	7	Compression	CO/CO_2	Seltzer et al.[12]
$UO_{2.01}$	55	2,000	1100 to 1300	1	1100 to 1300	350 to 4,000	95	7	Compression	CO/CO_2	Seltzer et al.[12]
$UO_{2.05}$	45	2,000	1100 to 1300	1	1100 to 1300	200 to 5,000	95	7	Compression	CO/CO_2	Seltzer et al.[12]
$UO_{2.0001}$	132	7,000 to 15,000	1440 to 1760	4.5	1440 to 1760	7,000 to 15,000	92 to 98	4 to 35	Compression	H_2	Bohaboy et al.[11]
$UO_{2.0001}$	90	1,000 to 4,000	1440 to 1760	1	1440 to 1760	1,000 to 4,000	92 to 98	4 to 35	Compression	H_2	Bohaboy et al.[11]
$UO_{2.000}$	93 to 127	2,000 to 5,000	1150 to 1500	1.5 to 2.8	1150 to 1500	2,000 to 5,000	94 to 99	10 to 80	Compression	H_2/H_2O	Marples and Hough[13]
$UO_{2.000}$	–	–	–	5 to 7	1250	5,000 to 7,000	94 to 99	10 to 80	Compression	H_2/H_2O	Marples and Hough[13]
$UO_{2.00}$	106	8,640	1200 to 1600	~2	1600	1,440 to 5,760	92 to 95	10	Compression	10^{-5} mm Hg vacuum	Kummerer and Vollath[14]
$UO_{2.00}$	80 to 200	2,870 to 5,380	1000 to 1350						Torsion	10^{-5} mm Hg vacuum	Solomon and Gebner[22]

*The exponent, n, is defined by the expression $\dot{\epsilon} \propto \sigma^n$, where σ = applied stress.
†The O_2 pressure maintained by heating U_3O_8 to desired temperature inside furnace chamber.
‡This is Q_c for constant deflection rate in a sigmoidal creep curve and is not a Q_c for steady-state creep.
§Various orientations of a single crystal.

$n \approx 17$ (see Fig. 1). At lower O/U levels, n decreased to a value of 7. As can be seen in Fig. 1, creep rates increase with oxygen excess, x, as $\dot{\epsilon} \propto x^2$ in the region of constant-stress exponent, i.e., for O/U > 2.001, where x is given by UO_{2+x}. Similarly, uranium diffusion rates have been found to increase with the square of the oxygen excess in several diffusion and sintering studies (see Table 1, Refs. 23–25). This dependence was predicted by Lidiard[27] on the basis that uranium diffuses via vacancies in the uranium sublattice as a U^{4+} species.

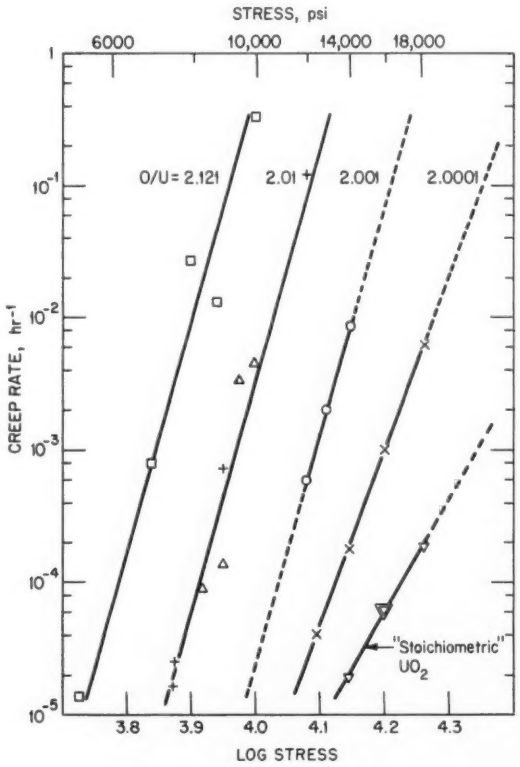

Fig. 1 Creep rate as a function of applied stress for UO_2 single crystals tested in compression at 1100°C. From Seltzer, Clauer, and Wilcox.[7]

At a stress of 10,000 psi, creep activation energies of the single crystals decreased from 134 to 58 kcal/mole as the O/U ratio increased from ~2.0001 to 2.062. The activation energies are plotted (circles) as a function of $\log x$ in Fig. 2. As will be discussed later, these values are in good agreement with activation energies determined in other studies on polycrystalline

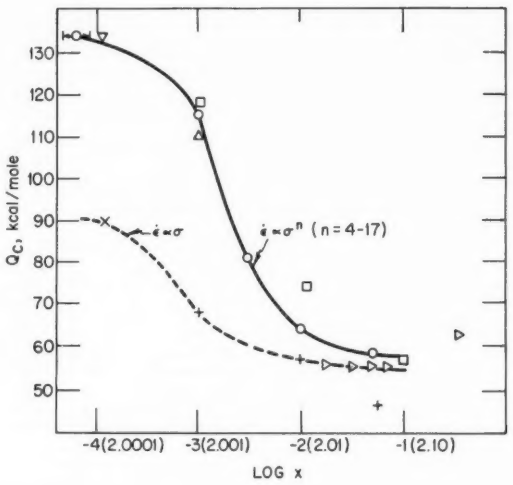

Fig. 2 Activation energies for compression creep of UO_{2+x} as a function of log x: ○, single crystals (from Seltzer, Clauer, and Wilcox[7]); □, polycrystals–27-μ g.s. (grain size), enriched (from Seltzer, Clauer, and Wilcox[8,9]); +,△, polycrystals –7-μ g.s. (from Seltzer, Clauer, and Wilcox[8,8]); ×, ▽, polycrystals, 4 to 35-μ g.s. (from Bohaboy, Asamoto, and Conti[11]); ▷, polycrystals, 6-μ g.s., from Armstrong and Irvine[17] (four-point bending).

UO_{2+x} where the composition has been controlled. In most cases, however, the O/U ratio has not been treated as a variable, and activation energies obtained for so-called "stoichiometric" UO_2 have a range of values from 71 to 117 kcal/mole, as seen in Table 2.

The creep activation energies for "stoichiometric" UO_2 that have values of 130 to 135 kcal/mole are some 20 kcal higher than the highest reported uranium self-diffusion activation energies.[28] A correction in Q_c for the temperature dependence of the elastic modulus[29] is less than 3 kcal/mole. Also, the values of 55 to 70 kcal/mole for creep of highly hyperstoichiometric UO_2 are considerably lower than the uranium self-diffusion activation energies reported in this O/U region by Hawkins and Alcock.[23] More recently, however, Lay[26] has reported an activation energy for uranium diffusion of 55 kcal/mole, determined from sintering experiments, for materials with an O/U ratio of 2.08.

Figure 3 shows the results obtained by Armstrong, Causey, and Sturrock[8] in bending creep of stoichiometric UO_2 single crystals having various orientations and tested over the stress range of 4000 to 8000 psi. On the average, the relation $\dot{\epsilon} \propto \sigma^{3.3}$ is obeyed. In some cases where higher creep rates were found in specimens tested at lower temperatures, the dis-

crepancies may have been caused by variations in orientation, stoichiometry, or impurity level in the crystals studied. In the temperature range of 1350 to 1685°C, the average activation energy for creep in bending was 117 ± 10 kcal/mole.

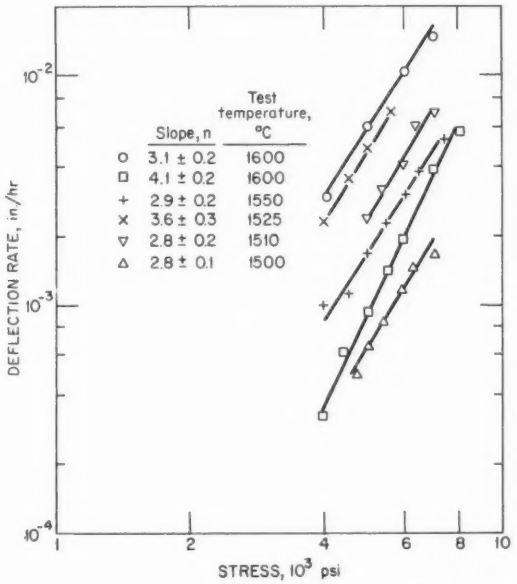

Fig. 3 Deflection rate as a function of stress for single-crystal UO_2 tested in bending. From Armstrong, Causey, and Sturrock.[8]

Polycrystals. Creep of polycrystalline UO_2 has been studied, using compression,[9-14,88,89] bending,[15-20] tension,[21] and torsion[22] testing methods, as a function of temperature, stress, stoichiometry, grain size, foreign-atom additions, and density. Selected results from these studies are discussed in the following paragraphs.

Figure 4 includes data for the influence of stress on creep rates of polycrystalline stoichiometric UO_2 tested in compression.[9-11] The creep data can be approximated by two straight lines, one in which creep rates vary as stress to the power 1 and the other in which creep rates are proportional to stress to the power 4 to 5. Although the transition from one stress dependence to the other occurs over a range of stresses, a sharp transition is drawn for the data presented in Fig. 4. It was first observed by Wolfe and Kaufman[9] that the transition stress, σ_t, was dependent on grain size, decreasing as the grain size increases, and that σ_t

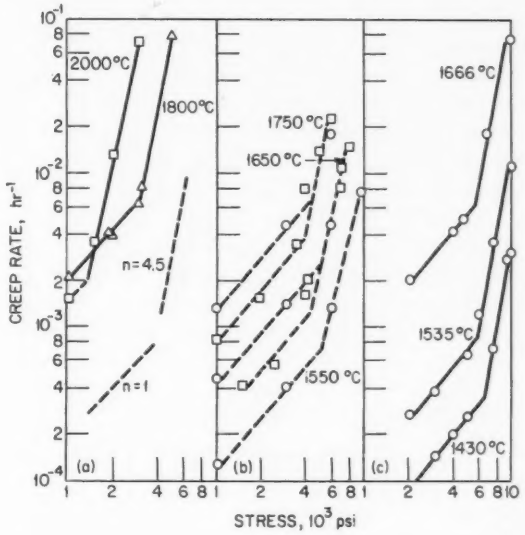

Fig. 4 Creep rate vs. stress for stoichiometric UO_2 tested in compression: (*a*) △, 18-μ g.s., 98.5% T.D., □, 55-μ g.s., 98.5% T.D. From Wolfe and Kaufman;[9] (*b*) □, 17- to 19-μ g.s., 94.8% T.D., ○, 12- to 14-μ g.s., 97% T.D. From Bohaboy, Asamoto, and Conti;[11] (*c*) ○, 10-μ g.s., 97% T.D. From Poteat and Yust.[10]

was relatively independent of temperature. The latter condition holds only when the creep activation energies are similar in the two stress regimes and when the temperature range is small. This was the case for a number of the early studies[9,10] performed on nearly stoichiometric UO_2.

It has also been observed that creep rates are independent of grain size in the region where $\dot{\epsilon} \propto \sigma^{4-5}$ [see the (*b*) data in Fig. 4 for 1650 and 1750°C]. This result is in accord with dislocation models of power-law creep,[30,31] in which the creep rate is independent of grain size. At low stresses where a linear stress dependence of the creep rate has been observed, the creep rates are proportional to the reciprocal of the grain size squared, in both compression[11] and bending[16] experiments. This is shown in Fig. 5. This behavior is in accord with the Nabarro–Herring model of diffusional creep[32] and with models based on grain-boundary sliding,[33] as the rate-controlling process. On the basis of these findings, Seltzer, Clauer, and Wilcox[34] have outlined an approximate method that can be utilized to predict the transition stress at which the change in creep mechanism occurs for polycrystalline stoichiometric UO_2 tested in compression.

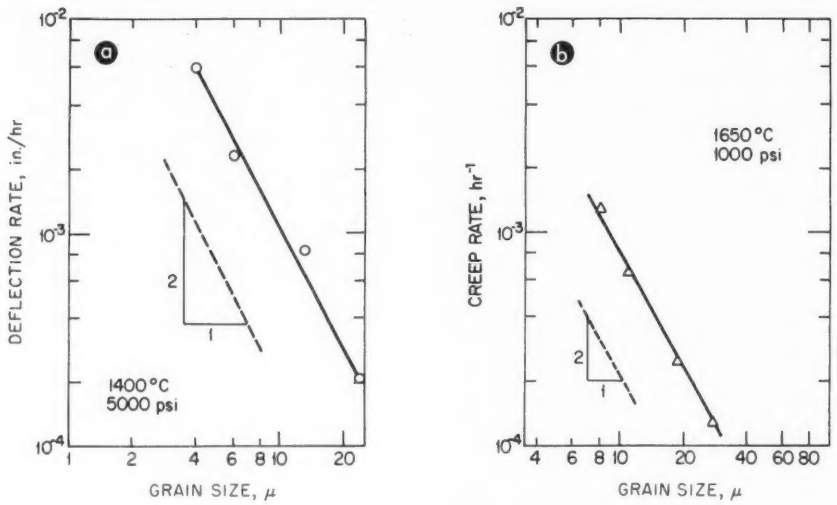

Fig. 5 Creep rate as a function of grain size: (*a*) in bending, from Armstrong, Irvine, and Martinson;[16] (*b*) in compression, from Bohaboy, Asamoto, and Conti.[11]

In Fig. 6 the values of the transition stress, σ_t, are presented for various grain sizes. The transition stresses were determined from the intersection of straight lines extrapolated from the power-law and linear stress regions, as in Fig. 4. These data were taken at different test temperatures, but temperature variations do not significantly affect the stress at which the break occurs in the cases examined. The open squares at 7, 10, and 25 μ represent transition points obtained by Bohaboy, Asamoto, and Conti,[11] and the creep data for these points are not included in Fig. 4. In Fig. 6, for a given grain size, creep rates are proportional to the first power of the stress at stresses below σ_t and to some high power of the stress for stresses above σ_t. Most of the compression data fall on a straight line whose least-squares slope gives $\sigma_t \propto L^{-0.61}$, where L is the grain size.

The following analysis was offered to provide a rationale for the experimental slope.[34] At low stresses, creep rates vary approximately with stress and grain size as

$$\dot{\epsilon}_A = A \frac{\sigma}{L^2} \tag{1}$$

where $\dot{\epsilon}_A$ = steady-state creep rate for low stresses
A = a constant at a given temperature
σ = stress
L = grain size

At high stresses the creep rates appear to be independent of grain size, so

$$\dot{\epsilon}_B = B\sigma^n \tag{2}$$

where $\dot{\epsilon}_B$ is the steady-state creep rate for high stress, and B is a constant at a given temperature.

Then at the transition stress, σ_t,

$$A \frac{\sigma_t}{L^2} = B\sigma_t^n \tag{3}$$

and, if A, B, and n are independent of σ and L,

$$\sigma_t^{n-1} = \frac{A}{B} \frac{1}{L^2} \tag{4}$$

or

$$\sigma_t \propto L^{-[2/(n-1)]} \tag{5}$$

If A and B have the same temperature dependence and n is independent of temperature, σ_t will be independent of temperature. As pointed out by Langdon,[35] even if Q_c is the same above and below σ_t, over wide temperature intervals the temperature dependence of the shear modulus also must be considered in B, and σ_t will have a small temperature dependence. Values of n are commonly found in the range of 4 to 5, which yield theoretical slopes for Eq. 5

of −0.67 to −0.50. The least-squares slope of −0.61 in Fig. 6 is within the expected region. Clearly the kind of analysis presented above is applicable for an understanding of the results presented in Fig. 6. Although caution should be exercised, this plot should serve as a useful operating diagram to predict the stress at which the predominant creep mechanism changes for polycrystalline, stoichiometric, high-density UO_2 tested in compression.

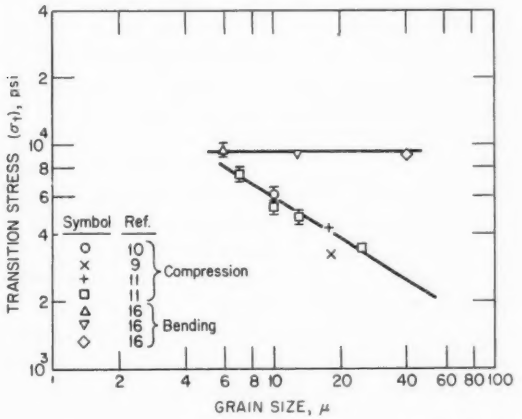

Fig. 6 Stresses at which a change in creep mechanism occurs for creep of UO_2 specimens of various grain sizes. From Seltzer, Clauer, and Wilcox.[3,4]

Finally, note that the break in the stress-dependence data appears to be nearly independent of grain size for the bending experiments in Fig. 6. The bending specimens[16] showed networks of intercrystalline cracks on their tension edges after strains as low as 0.6%. It is suggested that the apparent independence of the transition stress on grain size may be associated with this grain separation. In bending experiments, both plastic strain and grain-boundary separation contribute to the measured outer-fiber deflection. The simultaneous occurrence of these two processes could mask the grain-size-dependent transition in creep mechanism observed in compression, where σ_t depends on grain size.

Figure 7 shows results by Armstrong and Irvine[17] regarding the effect of changes in stoichiometry on the bending creep rate in the stress region where $n = 1$. No break is observed in the deflection rate vs. stress plots, for O/U values below 2.08. The dashed lines shown for higher O/U levels suggest the beginning of a transition region at high stresses for these compositions. This would be expected since according to Fig. 6 the break should occur at about 10,000 psi, but experiments were performed only to 8000 psi. It was also shown[12] that the transition stress decreases with increasing O/U, and this may account for the beginning of a transition region shown in Fig. 7. Deflection rate increases with increasing oxygen content, with the rate being proportional to x.

A linear dependence of creep rate on oxygen excess, x, has also been observed in the compression experiments performed by Seltzer, Clauer, and Wilcox[12,88] at 1100°C under conditions where creep

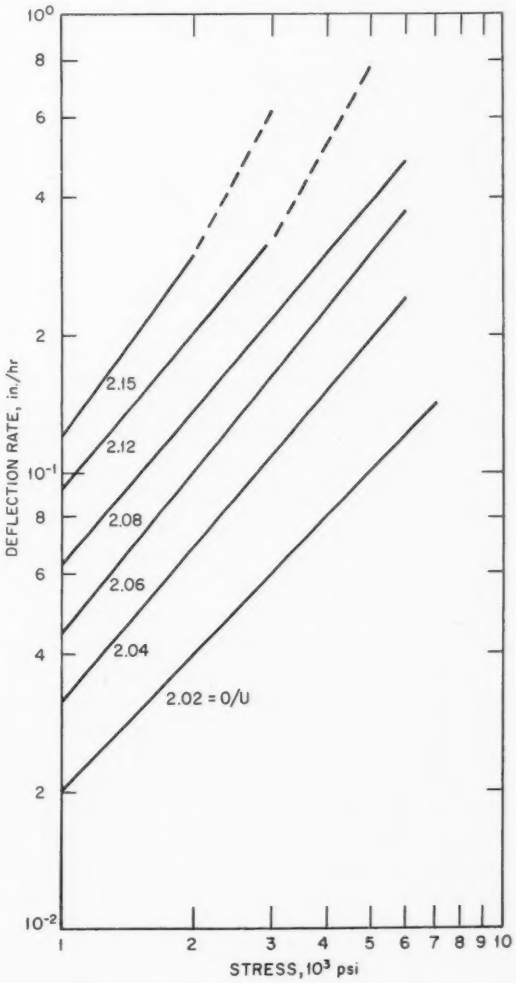

Fig. 7 Deflection rate as a function of stress for polycrystalline UO_{2+x}. Tested in bending at 1300°C; 6-μ g.s., 96% T.D. From Armstrong and Irvine.[17]

rates increased linearly with stress. These results are included in Fig. 8 for specimens having compositions in the range of $2.001 < O/U < 2.05$. The tests were conducted at 1100°C and 1300°C under stresses of 150 to 24,000 psi on specimens of 95% of theoretical density (T.D.) with an average grain size of 6 to 7 μ

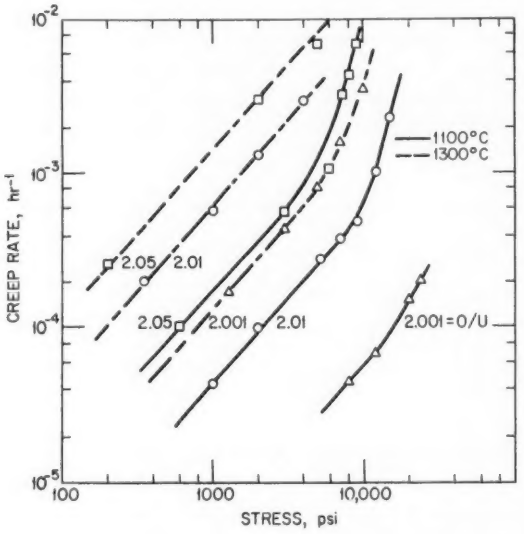

Fig. 8 Steady-state creep rate vs. applied stress for polycrystalline UO_{2+x} tested in compression at 1100°C and 1300°C, 6- to 7-μ g.s., 95% T.D. From Seltzer, Clauer, and Wilcox.[88]

The creep rates increase linearly with stress for low stresses, where $\dot{\epsilon} \propto \sigma$, but the stress dependence of the creep rates increases at high stresses, where, if described by a power-law stress dependence, $n \geq 4$. These results are similar to those reported previously[9-11] for compression creep of stoichiometric polycrystalline UO_2. Two important features of the results shown in Fig. 8 are that the two different stress dependences occur for a number of different compositions, and that the transition stress, σ_t, decreases with increasing O/U ratio. For the data at 1100°C, the transition stress decreases from ~20,000 psi to ~10,000 psi to ~5500 psi as the O/U ratio increases from 2.001 to 2.01 to 2.05.

The variation in transition stress is caused by the difference in the composition dependence of the creep rates in the two different stress regions. In the region of linear stress dependence, the creep rates increase linearly with x. In the power-law stress-dependence region, on the other hand, creep rates increase with $x^{1.75}$. This is close to the x^2 dependence found in the single-crystal creep studies, which suggests that similar processes control creep of single crystals and polycrystals in the power-law stress region, with possibly some grain-boundary contribution entering into the polycrystalline results.

An estimate of the creep activation energies can be obtained from the data in Fig. 8 for the two temperatures studied. For an O/U of 2.001, in the high-stress region $Q_c \approx 108$ kcal/mole,* whereas, in the low-stress region, $Q_c \approx 68.5$ kcal/mole. For O/U values of 2.01 and 2.05, Q_c values in the low-stress region are ~55 kcal/mole and ~45 kcal/mole, respectively. These activation energies have been plotted as triangles (Δ) and pluses (+) in Fig. 2. Also included in Fig. 2 are creep activation energies obtained by Bohaboy, Asamoto, and Conti[11] for polycrystalline UO_2 tested in hydrogen. It is assumed that their Q_c of 132 kcal/mole for the power-law regime corresponds to an $O/U \approx 2.0001$ based on our results. Their Q_c for the linear stress region, 90 kcal/mole, has been accordingly placed at the same O/U ratio.

Creep activation energies have also been obtained as a function of O/U ratio for enriched polycrystalline UO_2 specimens tested in compression in the power-law stress region.[8,9] The specimens were prepared from 24.48% enriched powder, had 97.8% T.D., and an average grain size of 27 μ. Major impurities in these specimens were 100 ppM iron and 150 ppM silicon. Results for the stress dependence of the creep rates obtained from creep tests conducted at 1100°C and 1300°C are shown, respectively, in Figs. 9 and 10 for O/U ratios of 2.001, 2.01, and 2.10.

The data for an O/U ratio of 2.10 at 1300°C (Fig. 10) best illustrate how the stress dependence of the steady-state creep rate can vary with stress. At the lowest stresses used, 150 to 500 psi, the creep rates increase linearly with stress, but the stress dependence increases with increasing stress so that above 3000 psi creep rates are best fitted by a power-law stress dependence of the form, $\dot{\epsilon} \propto \sigma^n$, where $n = 7$. These results are similar to those obtained by other investigators,[9,11] where the high stress dependence suggests a dislocation creep mechanism, whereas the linear stress dependence indicates the predominance of Nabarro–Herring or grain-boundary diffusional creep or a grain-boundary sliding process. For the lower O/U ratios at 1300°C and in all cases at 1100°C, a complete

*It was necessary to extrapolate to higher stresses for both 1100° and 1300°C tests to obtain this value.

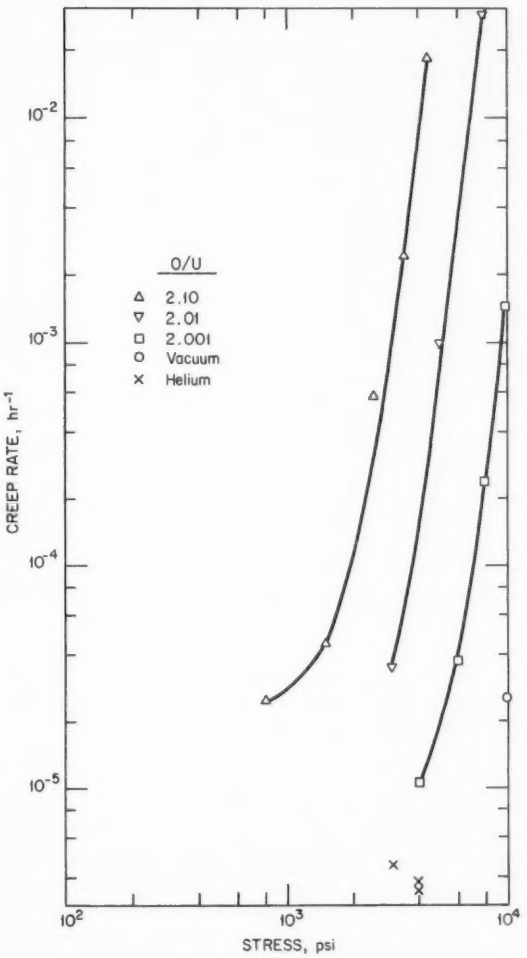

Fig. 9 Steady-state creep rates vs. applied stress for enriched uranium dioxide tested in compression at 1100°C. 27-μ g.s., 97.8% T.D. From Seltzer, Clauer, and Wilcox.[89]

transition to the linear stress dependence was not observed because the required creep rates were too low to be accurately measured.

The absolute values for the creep rates in Figs. 9 and 10 at a given temperature, stress, O/U ratio, and grain size are several orders of magnitude higher than those of uranium dioxide containing natural or depleted uranium.[9-11,88] According to an investigation by Goodyear, Speidel, and Kizer,[36] this appears to be related to the high silicon content of the enriched uranium dioxide. Scanning electron microscopy showed that very small amounts of a phase containing silicon were present at the grain boundaries of the enriched UO_2 creep specimens. If this is a glassy phase, such as SiO_2, it might be expected to appreciably weaken the uranium dioxide creep specimens. This could occur by facilitating grain-boundary sliding in the low-stress region. In the high-stress range, a doping effect might account for enhanced diffusion-controlled creep by some dislocation mechanism, such as climb. In an early study, Armstrong and Irvine[18] showed that deflection rates from bending experiments were higher for UO_2 containing SiO_2 than for undoped UO_2.

Although the absolute values for the creep rates of the enriched specimens do not agree with those of the specimens bearing natural or depleted uranium, the

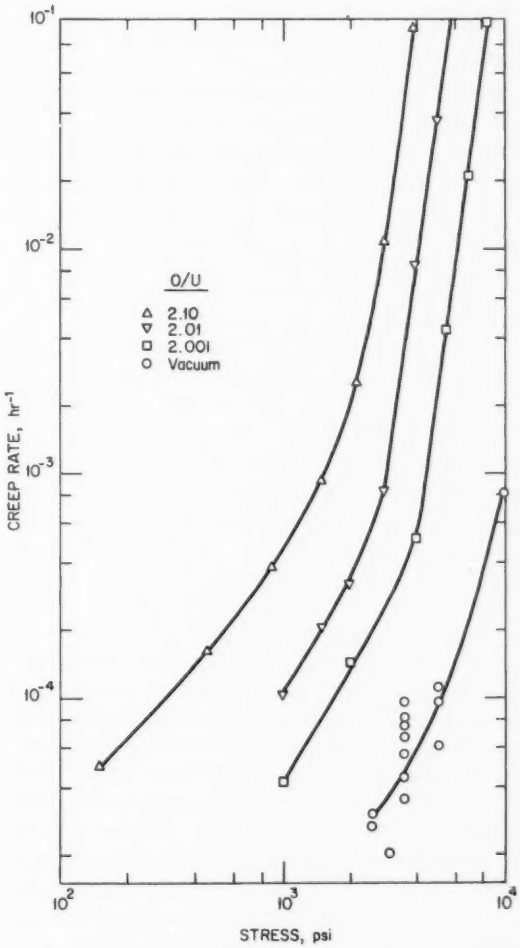

Fig. 10 Steady-state creep rate vs. applied stress for enriched uranium dioxide tested in compression at 1300°C. 27-μ g.s., 97.8% T.D. From Seltzer, Clauer, and Wilcox.[89]

composition dependence of creep rates of enriched UO_2 is similar to that found for the unenriched specimens. At 1100°C, $\dot{\epsilon} \propto x^2$ in the high-stress region, whereas at 1300°C the value for the exponent on x is between 1 and 2. In the low-stress region, the stoichiometry dependence is not well-defined; at 1300°C and 1000 psi $\dot{\epsilon}_{2.10}/\dot{\epsilon}_{2.01} \approx 4.5$ and $\dot{\epsilon}_{2.01}/\dot{\epsilon}_{2.001} \approx 2.5$. Furthermore, the activation energies for creep of enriched, polycrystalline uranium dioxide are similar to those for creep of UO_{2+x} single crystals. Figure 2 includes the activation energies for creep of enriched polycrystalline UO_{2+x} estimated from the high-stress portions of the data given in Figs. 9 and 10 for O/U ratios of 2.001, 2.01, and 2.10. These values are 117 kcal/mole, 75 kcal/mole, and 54 kcal/mole, respectively.

Figure 2 shows that, in the high-stress region, the activation energies and the composition dependence of creep are similar for single crystals and for enriched and natural polycrystals, and the creep mechanism is believed to be controlled by uranium self-diffusion. In the low-stress region, the creep activation energies and composition dependences are somewhat lower and possibly correspond to uranium grain-boundary-diffusion activation energies.

The influence of porosity on creep of UO_2 was first investigated by Armstrong, Irvine, and Martinson.[16] Unfortunately these experiments were performed on specimens with varying grain size, but apparently there was no influence of porosity on creep for less than 5% porosity. More recently, Bohaboy, Asamoto, and Conti[11] determined creep rates for 10-μ grain-size UO_2 at three different densities, 97, 95, and 92% T.D. The creep rates increased with increasing porosity, as shown in Fig. 11. Over this density range at 1650°C, the variation of creep rates with density was similar in the low-stress region, 1000 psi, and in the high-stress region, 8000 psi.

The creep properties of UO_2 containing foreign-atom additions have been studied by Christie and Williams[19] and Armstrong and Irvine.[18] The latter investigators studied creep of sintered compacts containing from 0.1 to 1.0 mole % calcia (CaO), yttria (Y_2O_3), zirconia (ZrO_2), and silica (SiO_2), whereas the former group reported only on the influence of yttria.

The influence of stress on deflection rates for UO_2 containing 1.0 mole % ZrO_2 and 0.5 mole % ZrO_2 or CaO is shown in Fig. 12 for work done in bending at 1400°C on material of 97.4% T.D. with grain sizes in the range of 24 to 31 μ. The authors had plotted these results on Cartesian coordinates and reported a linear stress dependence at low stresses and an increasing

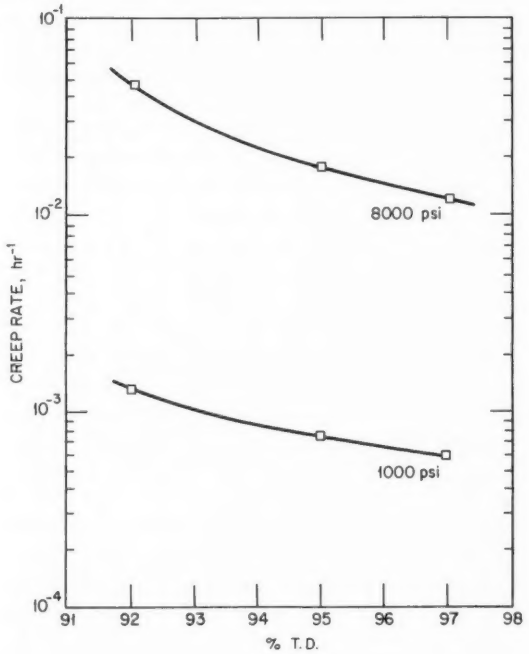

Fig. 11 Creep rate as a function of density for uranium dioxide tested in compression at 1650°C, 10-μ g.s. From Bohaboy, Asamoto, and Conti.[11]

stress dependence at high stresses. Here the results have been replotted on a log-log scale, and all the results lie on straight lines with slopes of 4, suggesting that a dislocation-controlled creep mechanism is operative.

The temperature dependence of the steady-state deflection rate for various UO_2 alloys containing 0.5 mole % CaO, ZrO_2, and Y_2O_3, and 1.0 mole % SiO_2 is shown in Fig. 13. The samples doped with CaO, ZrO_2, and Y_2O_3 were single phase, whereas the SiO_2 precipitated as a second phase at grain boundaries and within the grains. The activation energies for creep of all the doped samples were somewhat higher than the value for undoped UO_2. Addition of the soluble foreign atoms served to depress creep rates, whereas the SiO_2 additions resulted in enhanced creep behavior. These results cannot be explained in terms of the different valences of the cation additions influencing the atomic-defect concentrations of the UO_2, since substitution of divalent Ca^{2+}, trivalent Y^{3+}, or tetravalent Zr^{4+} seems to have roughly the same effect on the creep activation energy. Apparently the atomic-defect concentration in these samples was fixed either by the stoichiometry of the crystals or by other impurities.

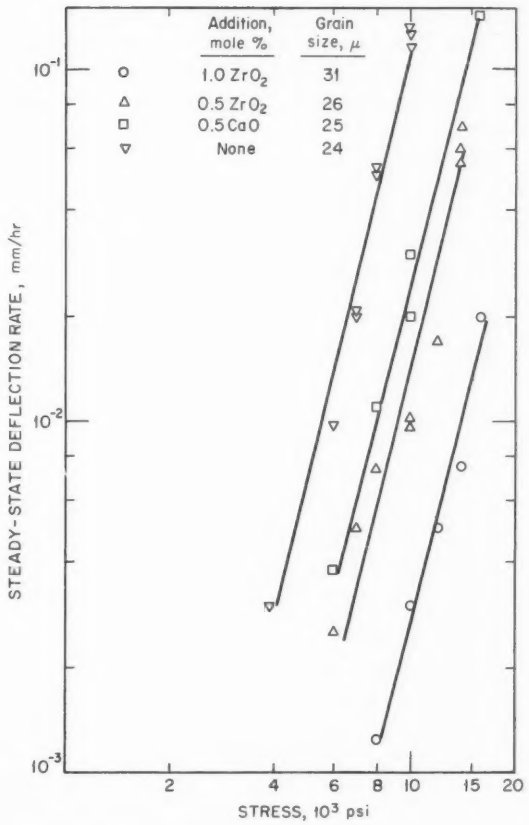

Fig. 12 Steady-state deflection rate as a function of stress for uranium dioxide containing foreign-atom additions. Tested in bending at 1400°C. From Armstrong and Irvine.[18]

One possible explanation for the observed influence of these foreign atoms is that they have a solid-solution hardening effect.[18] This argument is strengthened by considering that (1) the lowest creep rates are observed in zirconia-doped crystals, (2) the smallest effect is found in calcia-doped UO_2, and (3) yttria doping has an intermediate effect. This is in accord with the degree of ionic misfit between the various cations and uranium in UO_2, i.e., U^{4+}, 0.97 Å; Ca^{2+}, 0.99 Å; Y^{3+}, 0.93 Å; Zr^{4+}, 0.80 Å.

Microstructural changes resulting from creep have been observed in compression[10] and bending[16-18] experiments. Poteat and Yust[10] observed that in the low-stress region intergranular voids were created from the formation and growth of chains of pores on the grain boundaries. The displacement of reference marks across grain boundaries showed that grain-boundary sliding had occurred. In the high-stress region, less plastic deformation was observed and the structure contained many intergranular cracks rather than porosity. Armstrong, Irvine, and Martinson[16] observed grain separation in all their bending samples. The grain separation in these specimens occurred primarily along grain boundaries lying transverse to the direction of the fiber stresses on the tension side of the neutral axis. Grain-boundary sliding was also observed.

Later, Armstrong and Irvine[17] found that stoichiometric UO_2 tested in bending exhibited intercrystalline cracks on the tension side after 0.6% strain and that a sample of $UO_{2.015}$ was completely sound after 2.0% strain. However, grain-boundary separation was observed in $UO_{2.012}$ specimens, but the fissures had not linked together to form fully developed intergranular cracks. Grain-boundary migration occurred during creep of both stoichiometric and nonstoichiometric specimens. Additions of CaO, Y_2O_3, or SiO_2 increased the tendency toward intercrystalline cracking.[18] Thus it is clear that grain-boundary sliding occurs during creep of polycrystalline UO_2 and that failure due to intercrystalline cracking is a distinct possibility for stoichiometric UO_2, either undoped or containing various foreign atoms and subjected to high stress.

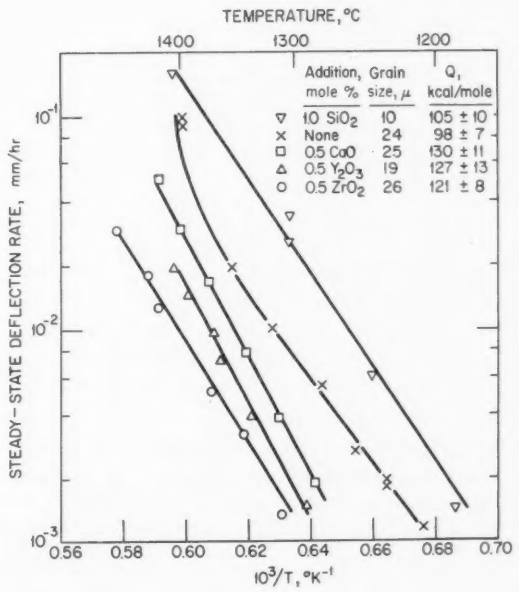

Fig. 13 Steady-state deflection rate as a function of temperature for uranium dioxide containing foreign-atom additions. Tested in bending at 10,000 psi. From Armstrong and Irvine.[18]

The creep behavior of UO_2 has been studied more extensively than that of any other ceramic fuel, or for that matter, than any other oxide. Thus it is possible to formulate expressions relating creep rate to stress, temperature, and material parameters, and it is appropriate to summarize these here. Yet, even with the extensive information available, the formulations are necessarily restricted to ranges of the various parameters that affect creep. Following are expressions relating the creep rate of UO_2 to parameters that influence creep. The expressions generally relate to data obtained from compression creep tests. However, the formulations can be extended in some cases to include results from bending creep tests; e.g., the influence of stoichiometry on Q_c and the stress dependence and grain-size dependence of creep rate.

A general expression in functional form is

$$\dot{\epsilon} = f(\sigma,T,x,L,P,i,O) \tag{6}$$

where $\dot{\epsilon}$ = steady-state creep rate
σ = applied stress
T = test temperature
x = composition, as in UO_{2+x}
L = grain size
P = porosity
i = impurities or dopants
O = orientation in single crystals

There are not enough results available concerning the influence of P, i, and O on creep of UO_2, and thus these factors are not considered here. The following formulations are derived from the previous discussion and the data in Table 2.

Case 1: Single Crystals Tested in Compression at High Stresses

$$\dot{\epsilon} \propto \sigma^{n(x)}\, x^2 \exp -\left[\frac{Q_c(x)}{RT}\right] \tag{7}$$

The stress exponent, n, increases from 7 for "stoichiometric" crystals to 17 for $x \lesssim 0.001$.
The x^2 dependence holds only for $x > 0.001$.
The activation energy decreases from 134 kcal/mole for "stoichiometric" crystals to 58 kcal/mole for $x = 0.062$.
The stress exponent for "stoichiometric" single crystals tested in bending is $n = 3.3$.
Single crystals tested in compression at very low stresses tend to exhibit $\dot{\epsilon} \propto \sigma$.

Case 2: Undoped Polycrystals Tested at High Stresses

$$\dot{\epsilon} \propto \sigma^n\, x^{\sim 2} \exp -\left[\frac{Q_c(x)}{RT}\right] \tag{8}$$

In general, the stress exponent, n, is 4 to 5.
As for single crystals, the activation energy for creep decreases with increasing x; e.g., $Q_c = 132$ kcal/mole for $x = 0.0001$ and 54 kcal/mole for $x = 0.10$.

Case 3: Undoped Polycrystals Tested at Low Stresses

$$\dot{\epsilon} \propto \frac{\sigma x}{L^2} \exp -\left[\frac{Q_c(x)}{RT}\right] \tag{9}$$

The activation energy for creep decreases with increasing x; e.g., $Q_c \approx 90$ kcal/mole for $x \approx 0.0001$ and 45 kcal/mole for $x = 0.05$.
The L^{-2} dependence occurs for both compression and bending creep.

The Transition Stress for Polycrystals Tested in Compression

$$\sigma_t \propto L^{-[2/(n-1)]}\, f(T,x) \quad \text{where } n = 4 \text{ to } 5 \tag{10}$$

There appears to be no grain-size dependence of the transition stress in bending creep studies.
The above dependence of σ_t on L holds only when the values of Q_c in the high σ and low σ ranges are approximately equal.
The dependence of σ_t on T appears to be minor.
σ_t appears to depend on x, such that σ_t decreases with increasing x.
There really is not a sharp transition stress. Rather, the stress dependence of the creep rate increases gradually from $\dot{\epsilon} \propto \sigma$ in the low stress range to $\dot{\epsilon} \propto \sigma^{4-5}$ in the high-stress region. When investigators report that $(4 \text{ to } 5) > n > 1$, they are probably measuring creep in the transition region, which leads to an apparently anomalous value of n.

The above expressions show various relations between creep rate and stress, temperature, stoichiometry, and grain size. Yet these are of limited usefulness in *predicting* absolute creep rates. Rather a more detailed analysis is required. For example, there are now enough data on compression creep of polycrystalline UO_2 as a function of T, σ, x, and L to derive an

explicit quantitative expression relating these factors. This is presently being undertaken at Battelle Memorial Institute using a regression analysis. A dominant factor will be stoichiometry since x influences Q_c and the transition stress, σ_t.

From this review it is clear that, although much work has been done on creep of UO_2, a number of serious gaps exist in our knowledge. These include:

1. An understanding of the effect of porosity on creep rates in both the high- and low-stress regions of creep. These experiments should be done at constant grain size. Also, if possible, the ratio of amount of grain-boundary porosity to amount of intragranular porosity should be constant.

2. Knowledge of creep mechanisms in the power-law region. Creep here may be controlled by dislocation climb, nonconservative motion of jogged screw dislocations, or the formation and dissolution of dislocation loops and tangles. Transmission electron microscopy of crept structures can be used here to distinguish among the possibilities.

3. The importance of grain-boundary sliding vis-à-vis grain-boundary diffusion or Nabarro–Herring creep in polycrystals tested in the low-stress region. The creep activation energies indicate that grain-boundary diffusion-controlled models are predominant, but it is not clear whether it is diffusion creep as suggested by Coble[90] or grain-boundary sliding. Resolution of this question can be helped by a detailed investigation of crept structures utilizing metallographic techniques.

ThO_2

Although thoria crystallizes in the same fluorite structure as UO_2 and CeO_2, it does not exist as a single-phase oxide over an appreciable range of composition.[52] The creep behavior of polycrystalline ThO_2 has been studied by Morgan and Hall,[53] Poteat and Yust,[10,54] and by Wolfe[55] (see Table 3). Wolfe and Kaufman[9] have presented a detailed review of these investigations.

Poteat and Yust performed compression creep tests on specimens having 97.5% T.D. density and an average grain size of 10 μ over the temperature range of 1430 to 1790°C under initial stresses of 4000, 7500, 11,000, and 15,000 psi. Wolfe examined specimens whose grain size was 15 or 220 μ having a density of 98.5% T.D. Experiments were performed in compression in the range of 3000 to 7500 psi at temperatures of 1700 to 1800°C. This is approximately 0.50 to 0.55 T_M (thoria melts at 3260°C).

Figure 14 shows the stress dependence of the creep rate obtained in these studies. Poteat and Yust found that the stress exponent varied from 1.04 to 1.59 as the temperature increased from 1430°C to 1790°C. Data obtained above 11,000 psi show an increasing stress dependence of the creep rate, suggesting that the creep mode was changing at higher stresses, typical of the results reported for creep of polycrystalline UO_2. The stress dependences of the creep rates for the 15-μ grain-size specimens tested by Wolfe at 1800°C and the 10-μ grain-size specimens reported by Poteat and Yust

Table 3 Creep Properties of ThO_2 *

Ref.	% T.D.	Temp., °C	Atm	Grain size μ	Purity	n	Q_c, kcal/mole	Remarks
Morgan and Hall[53]	98	1465	Argon	5 to 20	350 ppM impurities	–	–	
	98	1400 to 1465		4 to 8	0.45 to 8.10 wt.% CaO	–	–	Grain growth occurred for CaO-doped specimens
Poteat and Yust[10,54]	97.5	1430 to 1790	Neutral	10	0.0025 wt.% Ca 0.0008 wt.% Mg <0.0002 wt.% Si <0.0002 wt.% Cu 0.0040 wt.% C <0.0005 wt.% S <0.0002 wt.% Fe	1.04 to 1.59	112 ± 7	4000 to 15,000 psi, n increased with T
Wolfe[55]	98.5	1700 to 1800	–	15	–	1		3000 to 7500 psi
	98.5	1700 to 1800	–	220	–	4	163	

*All tests performed in compression.

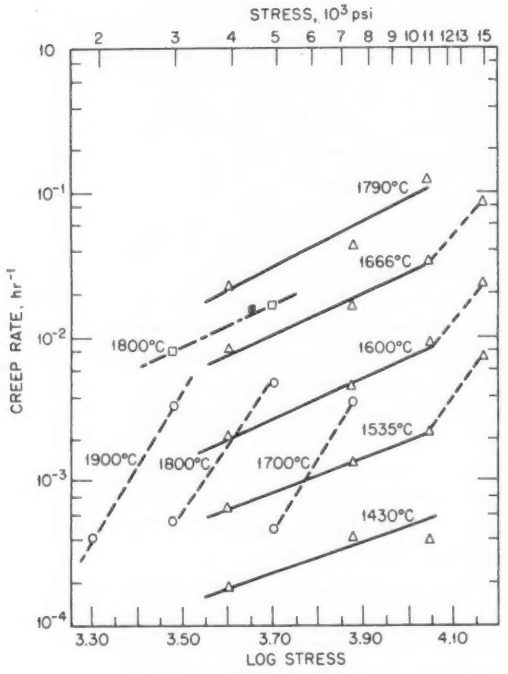

Fig. 14 Steady-state creep rate vs. applied stress for polycrystalline thoria tested in compression: △, 10-μ g.s., from Poteat and Yust;[10] ○, 220-μ g.s., from Wolfe,[55] □, 15-μ g.s., from Wolfe.[55]

at 1790°C are in reasonable agreement considering the differences in grain size and density of the specimens used in the two studies. The stress dependence for the coarse-grained ThO_2 (220 μ) tested by Wolfe is seen in Fig. 14 to be of the form $\dot{\epsilon} \propto \sigma^4$, indicating a different creep mechanism is operative in the coarse-grained material compared with the fine-grained material.

The temperature dependence for steady-state creep of ThO_2 with 10- and 220-μ grain diameters for various stress levels is presented in Fig. 15. The average activation energy for creep of the 10-μ samples is 112 ± 7 kcal/mole, whereas the Q_c values for the coarse-grained ThO_2 is 163 kcal/mole. These values may be compared with the reported values for the diffusion activation energies of thorium (58.8 to 158 kcal/mole) and oxygen (46 kcal/mole) in ThO_2 (see Table 1). Clearly, the creep activation energies are larger than the oxygen self-diffusion activation energies. If ThO_2 is analogous to UO_2, then the creep activation energy might be expected to correlate with that for thorium diffusion. However, since Hawkins and Alcock[23] and Morgan and Poteat[50] made their diffusion measurements over a wide range of temperatures and oxygen partial pressures on relatively coarse-grained specimens, apparently there is no obvious reason why a better correlation between creep activation energies and diffusion activation energies does not exist. The creep activation energy of 112 kcal/mole is in the range of values found for creep and uranium self-diffusion in UO_2 and in fair agreement with the thorium-diffusion activation energy determined by King.[49] The thorium-diffusion measurements may therefore include a considerable contribution from grain-boundary diffusion or some other short-circuiting effect.

Morgan and Hall[53] studied the compression creep of polycrystalline ThO_2 and ThO_2–CaO annular specimens of about 98% T.D. Quantitative information was not obtained, but a number of interesting observations were made concerning the creep behavior of these specimens. The addition of CaO in amounts from 0.45 to 8.10 mole % resulted in a substantial decrease in the

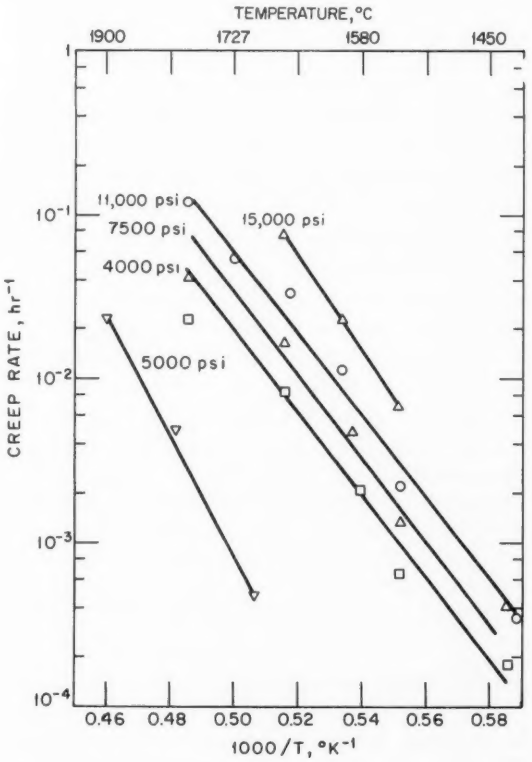

Fig. 15 Steady-state creep rate as a function of temperature for polycrystalline thoria tested in compression: □, ○, △, 10-μ g.s., from Poteat and Yust;[54] ▽, 220-μ g.s., from Wolfe.[55]

initial creep strength of ThO_2 at 1465°C under an applied stress of 8000 psi. After several hundred hours into the creep test, however, the minimum creep rate for the mixed oxide approached that of "pure" ThO_2. Considerable grain growth occurred in the CaO-doped specimens from a grain size of 4 to 8 μ before testing, to as much as 20 μ after testing. However, the grain size of undoped ThO_2 specimens remained at 5 to 20 μ during testing.

Poteat and Yust[10] examined the microstructure of specimens before and after creep and made some useful observations relative to understanding the creep mechanisms operative in the low-stress region. Grain-boundary sliding was apparent from displacements in surface scratches at grain boundaries (see Fig. 16). Voids were found to form as a necklace type of porosity at boundaries that were parallel to the compression axis (see Fig. 17). These pores eventually joined up to form cracks. Thus the creep deformation was attributed to grain-boundary sliding, with a contribution from Nabarro–Herring diffusion creep. The increase in the stress exponent with increasing temperature was then attributed to a contribution to the total creep strain from a dislocation mechanism. The high-stress exponents found for the coarse-grained specimens and for the 10-μ grain-size specimens at high stresses suggests that a dislocation mechanism for creep predominates in these cases.

UO_2–PuO_2

Both oxides crystallize in the fluorite structure and mix with complete solid solubility. Hypostoichiometric compositions are easily attained with PuO_2, and most of the mixed oxides tested are in the oxygen-deficient region with O/M ratios of 1.95 to 2.00. Two methods are used to prepare the mixed oxides: mechanical blending of powders of the two individual oxides or a coprecipitation technique.

Table 4 includes the experimental conditions utilized in the five investigations of the creep behavior of UO_2–PuO_2. The first reported work was performed by Slagle[58] on UO_2–20 mole % PuO_2 samples prepared from coprecipitated powders. Experiments were performed in four-point bending at 1475 and 1560°C. Under a maximum fiber stress of 4130 psi, the creep activation energy was 110 kcal/mole. With the use of the incremental-stress-change technique, the stress dependence of the creep rate depended on the direction in which stresses were applied. At 1475°C, by successively increasing the stress, $n = 1.08$, but under decreasing stress, $n = 1.75$. At 1560°C, $n = 1.53$ in the range of applied stresses from about 2500 psi to 8000 psi regardless of direction in which stress was changed. As for the case of bending experiments with UO_2, Slagle found that extensive cracking occurred on the tensile faces of crept mixed-oxide specimens. In addition, enlargement of porosity was found ahead of the cracks.

Houston, Kruger, and Pardue[57] studied creep of mechanically blended UO_2–22 wt.% PuO_2 under the conditions given in Table 4. Both solid and annular specimens were tested in this program, and no discernible difference was observed between the two configurations. Grain growth of the fine-grained samples was observed, primarily in the triaxially stressed region near the contact faces. At 1210°C over the stress range of 1500 to 3200 psi, creep rates increased as stress to the 1.4 power, and, at 1500 psi in the temperature range of 1100 to 1330°C, the creep activation energy was 77 kcal/mole. For the two grain sizes tested, the ratios of the creep rates fitted a $1/L^2$ relation.

The most extensive studies to date on the creep properties of UO_2–PuO_2 over a range of compositions have been conducted by Bohaboy and Evans[56] and by Marples and Hough.[13] These investigators performed compression experiments in N–6% H and Ar–12% H atmospheres, respectively. In both cases slight additions of water vapor were used to control the O/M ratios of the test specimens.

The experimental results of Bohaboy and Evans,[56] shown in Fig. 18, were fitted by summing two Arrhenius-type equations of the form

$$\dot{\epsilon} = A\sigma \exp(-Q_1/RT) + B\sigma^{4.5} \exp(-Q_2/RT) \qquad (11)$$

The samples had a grain size of 22 to 25 μ, were 92.8% T.D., and were tested in the temperature range 1475 to 1625°C at initial stress levels between 900 and 8000 psi. For $(Pu_{0.2}U_{0.8})O_{1.95}$, the constants were

$A = 5.32 \times 10^4$
$B = 0.00183$
$Q_1 = 110 \pm 10$ kcal/mole
$Q_2 = 140 \pm 10$ kcal/mole

They also found that, when the O/M level was increased from 1.95 to 2.00, the creep rate of UO_2–20 wt.% PuO_2 was increased by a factor of about 10 (see Fig. 18). The activation energies were virtually unchanged by composition at 4000 psi, being $Q_c = 140$ kcal/mole and 145 kcal/mole for O/M values of 1.95 to 2.00. At 1000 psi, $Q_c = 110$ kcal/mole and 90 kcal/

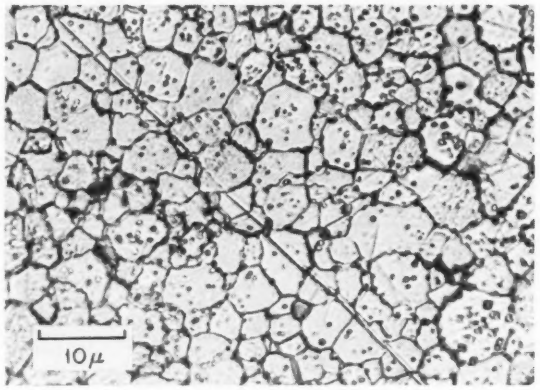

Fig. 16 Axial surface polished, etched, and inscribed with a line before compression testing. Note displacement of line at grain boundaries due to creep. From Poteat and Yust.[54]

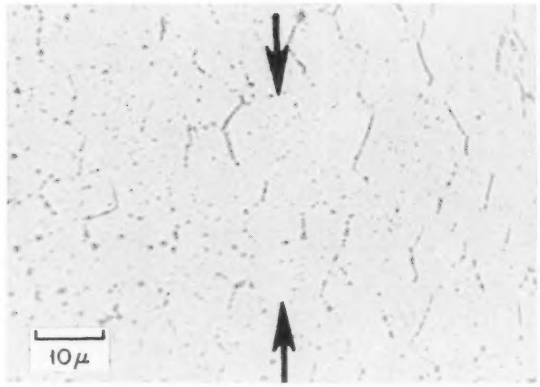

Fig. 17 Axial section of a specimen after creep test. Arrows indicate compression axis. Note necklace of pores on boundaries parallel to stress axis which result in formation of intergranular voids (unetched). From Poteat and Yust.[54]

Table 4 Creep Properties of UO_2–PuO_2

Reference	Preparation	Grain size, μ	% T.D.	O/M	Pu content, wt.%	Atm	Type of test*	Temp., °C	Stress, psi	n	Q_c, kcal/mole
Bohaboy and Evans[56]	Coprecipitated	20 to 28	89 to 95	1.95 to 2.00	20, 30, 100	N_2–6% H_2 + H_2O	C	1475 to 1625	900 to 8000	1	110
Houston et al.[57]	Mechanically blended	3 to 5 10 to 15	94 90	1.99	22	5×10^{-6} torr vacuum	C	1100 to 1330	1100 to 3200	4.5 1.4	140 77
Marples and Hough[13]	Coprecipitated and mechanically blended	3 to 80	94 to 99	1.995 to 2.00	2, 5, 10, 15, 20, 30, 40	Ar–12% H_2 + H_2O	C	1150 to 1500	1200 to 2000	1 4.5	103 133
Kummerer and Vollath[14]	Mechanically blended	5 to 30	92 to 95		19.5	10^{-5} torr vacuum	C	1200 to 1700	425 to 3560		98
Slagle[58]	Coprecipitated	20	96	1.98	20	Ar–8% H_2	B	1475 to 1560	2500 to 9000	1.08 to 1.75	110

*C = compression; B = bend.

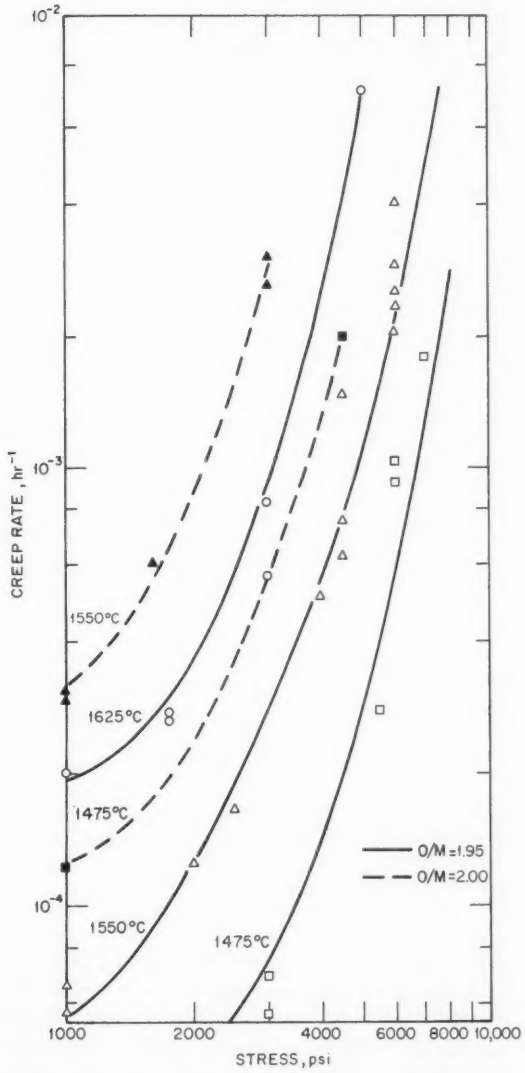

Fig. 18 Steady-state compression creep rate vs. applied stress for coprecipitated $(Pu_{0.2}U_{0.8})O_{1.95}$ and $(Pu_{0.2}U_{0.8})O_{2.00}$. Curves drawn to fit Eq. 11; 22- to 25-μ g.s., 93.9% T.D., from Bohaboy and Evans.[56]

mole, respectively, for these two O/M levels.[56] These results were essentially duplicated by Marples and Hough[13] for mixed oxides containing 10 and 20 wt.% PuO_2. For UO_2–10 wt.% PuO_2 with 99% T.D. and 30-μ grain size tested at 2000 psi, $\dot{\epsilon}_{2.000}/\dot{\epsilon}_{1.995} \approx 10$ and $Q_c = 133$ and 137 kcal/mole for the high and low O/M material, respectively. Similarly, for UO_2–20 wt.% PuO_2 with 99% T.D. and 20-μ grain size tested at 2000 psi, $\dot{\epsilon}_{2.000}/\dot{\epsilon}_{1.995} \approx 10$ but $Q_c = 103$ kcal/mole for O/M = 2.000 and 117 kcal/mole for O/M = 1.995.

These results[7] are in opposition to those found for hyperstoichiometric UO_{2+x} and hypostoichiometric CeO_{2-x} where creep activation energies[59] varied by a factor of 2 with increase or decrease in O/M ratio, respectively, and the creep rates increased with increasing nonstoichiometry. This may be due to the fact that, for the mixed-oxide system, the O/U ratio is fixed at 2.000 but that the O/Pu ratio varies to accommodate the change in O/M level. Then, if the creep behavior is controlled essentially by the uranium dioxide phase, small changes in creep rates will occur as the PuO_{2-x} weakens or strengthens the mixed oxide, but large effects due to drastic changes in uranium diffusion rates will not occur. As for the case of UO_2, creep rates increased with decreasing density in the range 89 to 94% T.D., the increase being a factor of 4 over this density range[56] in both the low-stress region, 1000 psi, and in the power-law region, 6000 psi, as shown in Fig. 19.

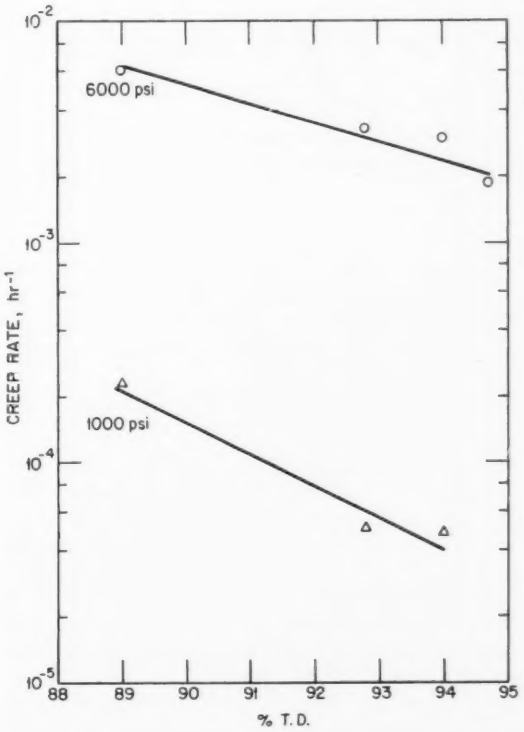

Fig. 19 Steady-state creep rate as a function of density for coprecipitated $(Pu_{0.2}U_{0.8})O_{1.95}$ tested in compression at 1550°C; 20- to 25-μ g.s., from Bohaboy and Evans.[56]

Increasing the plutonium content increased the creep rate at both stress levels[5,6] examined, as shown in Fig. 20. At 1000 psi, for example, the creep rate for PuO_2 is about 50 times faster than for UO_2–20 wt.% PuO_2. The data of Marples and Hough[13] with regard to the effect of plutonia, normalized to a grain size of 20 μ, are presented in Fig. 21 for 0, 2, 5, 10, and 15 wt.% Pu. These results show that small additions greatly enhance creep rates over a wide temperature range. However, little effect was observed as the PuO_2 content was increased from 20 to 40%.

Results obtained by Kummerer and Vollath[14] under the conditions given in Table 4 are in some respects considerably different from those obtained by other investigators. These workers used specimens with an initial grain size of 5 μ and performed their tests under a vacuum of 10^{-5} mm Hg, which gave an unknown O/M ratio in the test samples. Compression tests were performed to strains of 40%, which is a factor of 4 higher than normally recommended. In some cases primary creep extended up to 25% strain, compared with the several percent or less normally observed. Apparently the material was tending toward superplastic behavior. A similar tendency has been observed by Roberts and Wrona[87] for UO_2–PuO_2 specimens (0.6–2.0 μ, 88–95% T.D.) deformed by bending at constant $\dot{\varepsilon}$ over the temperature range 1400 to 1600°C. In all cases Kummerer and Vollath found that grain growth occurred, giving a final grain size of 10 to 30 μ. At 1700°C the creep rates were said to follow an exponential stress law of the form $\dot{\varepsilon} \propto \exp(B\sigma/RT)$ and yielded a creep activation energy of 98 kcal/mole at a stress of 1850 psi.

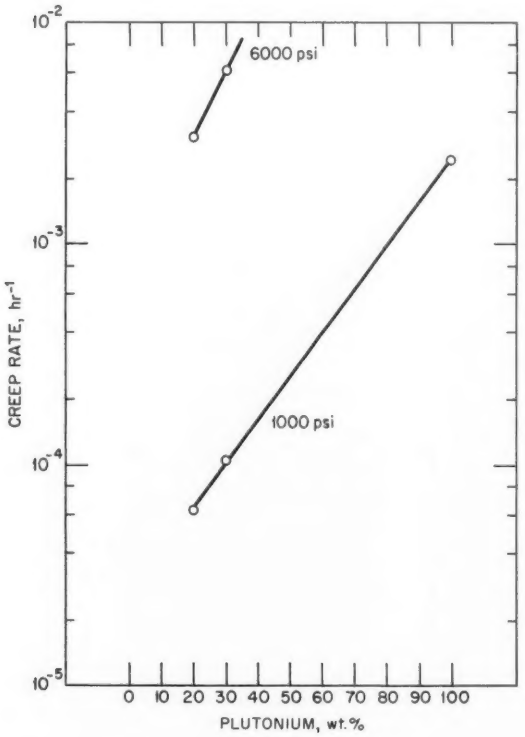

Fig. 20 Steady-state creep rate vs. weight percent plutonium for coprecipitated UO_2–PuO_2 tested in compression at 1550°C; 22- to 28-μ g.s., 93% T.D. O/Pu = 1.78; from Bohaboy and Evans.[56]

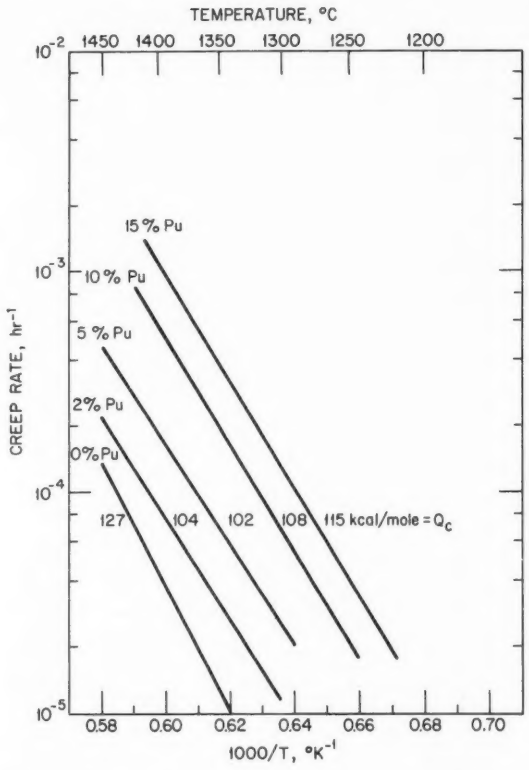

Fig. 21 Steady-state creep rate vs. temperature for polycrystalline mechanically mixed UO_2–PuO_2 tested in compression at 2070 psi. Normalized to 20-μ g.s., 94 to 98% T.D., O/M = 2.000. From Marples and Hough.[13]

ThO_2–UO_2

Wolfe[55] performed compression creep tests on ThO_2–10 wt.% UO_2, which is a single-phase oxide crystallizing in the fluorite structure. Experiments were

performed under constant stress in the range of 1000 to 7500 psi at temperatures from 1600 to 2100°C. The specimens had average grain diameters of 30, 85, or 120 μ with the density of the fine-grain-size material being 97% T.D. The creep rates decreased with increasing grain size at 1800°C, as shown in Fig. 22. As expected, the grain-size dependence of creep decreases at higher stresses in the coarser-grained specimens where the stress exponent, n, is increasing. In the coarsest-grained material, $n = 4$ to 5 above 500 psi. The 30-μ specimens exhibited a linear stress dependence of the creep rate at low stresses and an increasing stress dependence at higher stresses, as shown in Fig. 23.

However, the 120-μ grain-size material tested at higher temperatures (to 2100°C) exhibited a power-law creep-rate dependence with $n = 4$ over most of the stress range studied. This is shown in Fig. 24. Creep rates for this mixed oxide are slightly lower than those for pure ThO_2, which are given in Fig. 14. This may be

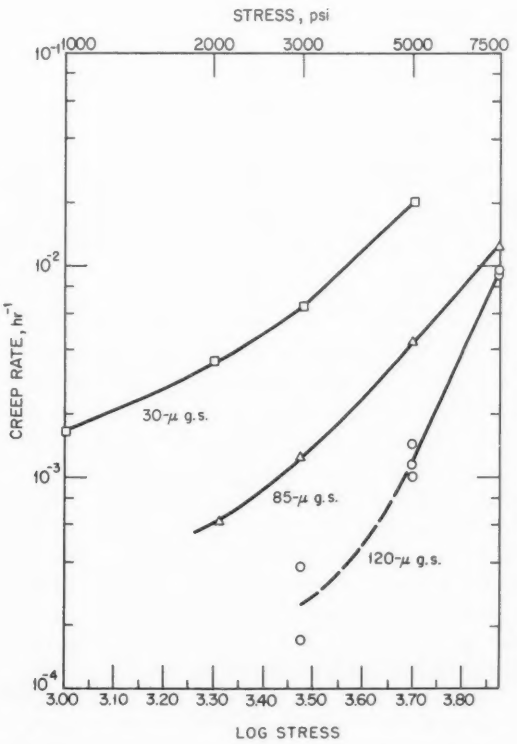

Fig. 22 Steady-state creep rate as a function of applied stress for ThO_2 –10 wt.% UO_2 tested in compression at 1800°C; 97% T.D. From Wolfe.[55]

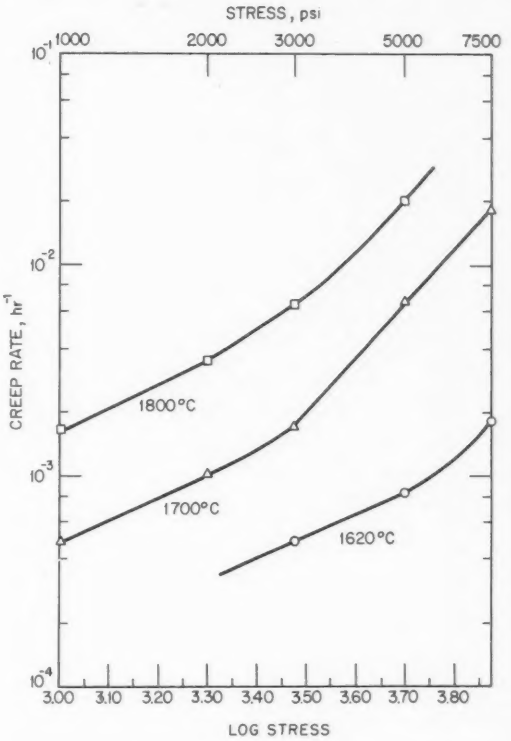

Fig. 23 Steady-state creep rate vs. applied stress for polycrystalline ThO_2 –10 wt.% UO_2 tested in compression; 30-μ g.s., 97% T.D. From Wolfe.[55]

due to variations in grain size, density, or diffusion rates between the two materials. The steady-state creep rates for the 120-μ ThO_2–10 wt.% UO_2 specimens were best fitted by the expression

$$\dot{\epsilon} = 9.2 \times 10^{-6}\ \sigma^4 \exp(-120{,}000/RT) \qquad (12)$$

where the creep rate is in hr^{-1}, the stress is in psi, and the activation energy is in kcal/mole.

ZrO_2–UO_2

In his comprehensive investigation of creep of oxide fuels, Wolfe[55] has performed constant-stress compression tests on ZrO_2–30 wt.% UO_2 and ZrO_2–41 wt.% UO_2. The 30 wt.% UO_2 specimens had a face-centered tetragonal structure, average grain sizes of 15 and 25 μ, and a 99.4% T.D. The material with 41 wt.% UO_2 was a two-phase structure with a 99.7% T.D. and an average grain size of 10 μ in the matrix phase. The matrix phase had a tetragonal structure.

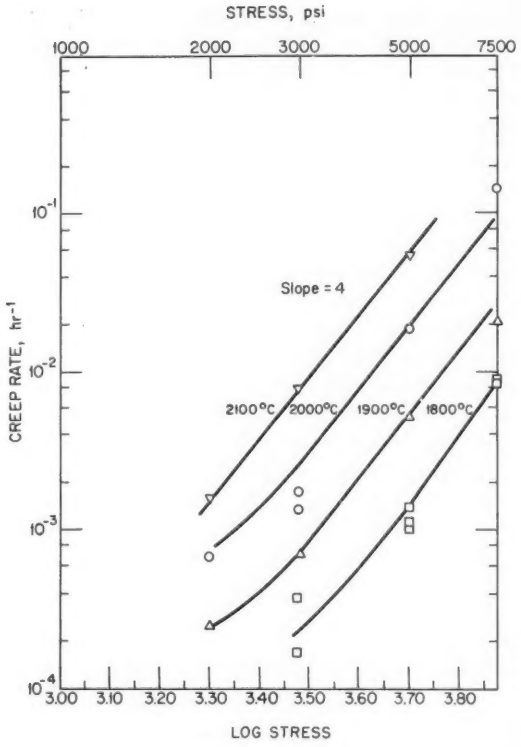

Fig. 24 Steady-state creep rate vs. applied stress for polycrystalline ThO_2 –10 wt.% UO_2 tested in compression; 120-μ g.s., 97% T.D.; from Wolfe.[55] Curves drawn to fit Eq. 12 in high-stress range.

The stress dependence of the creep rates of these mixed oxides is shown in Fig. 25, which has been redrawn on a log-log plot. Here, n is low and varied from less than 1 to 2, increasing with increasing stress. As Wolfe and Kaufman[9] point out, the grain-size dependence observed over the entire range of stress indicates a considerable contribution of diffusional creep or grain-boundary sliding to the total deformation. The temperature dependence for steady-state creep of ZrO_2–30 wt.% UO_2 and ZrO_2–41 wt.% UO_2 is shown in Fig. 26. Both mixed oxides are single-phase, face-centered cubic fluorite structures above 2000°C. At lower temperatures the 30 wt.% UO_2 oxide is a single phase having the tetragonal structure, whereas the 41 wt.% UO_2 oxide contains both phases. The authors suggest that the higher creep rates for the two-phase material may result from the effect of interphase boundary sliding, in a manner similar to the results found by Armstrong, Causey, and Sturrock[8] for UO_2 containing a small amount of SiO_2. An activation energy of 102 kcal/mole was determined for creep of the tetragonal 30 wt.% material and the two-phase 41 wt.% UO_2 specimens. Creep data for the latter material are best fitted by an expression of the form

$$\dot{\epsilon} = 6.3 \times 10^5 \, \sigma \exp(-102{,}000/RT) \qquad (13)$$

for a grain size of 10 μ and a stress of 3000 psi.

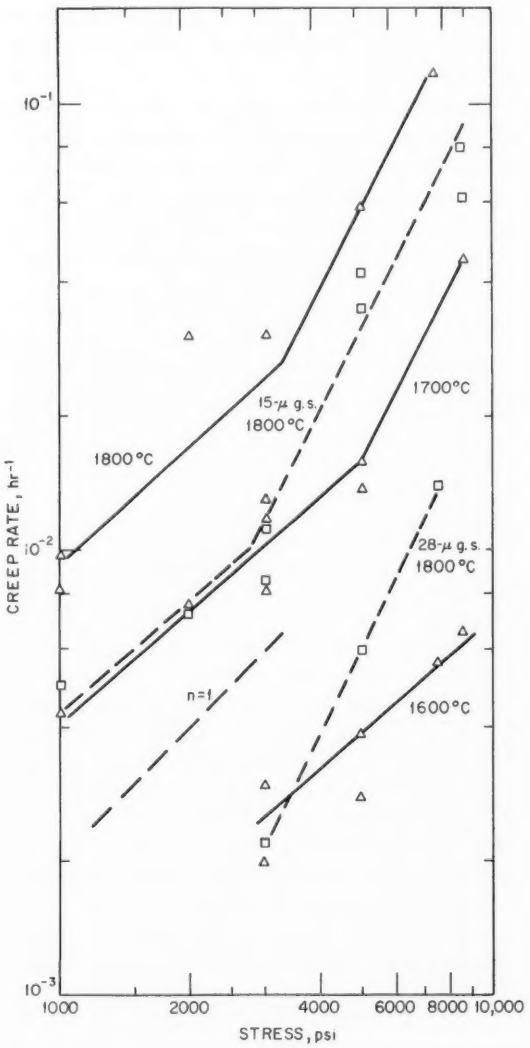

Fig. 25 Steady-state creep rate as a function of applied stress for ZrO_2–UO_2 tested in compression: △, ZrO_2–41 wt.% UO_2, 10-μ g.s., 99.7% T.D.; □, ZrO_2–30 wt.% UO_2, 99.4% T.D. From Wolfe.[55]

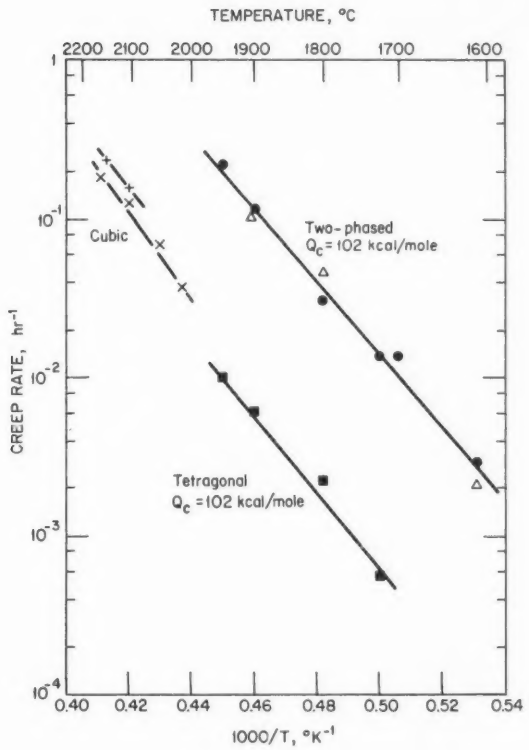

Fig. 26 Steady-state creep rate vs. temperature for ZrO_2–UO_2 tested in compression: +,■, ZrO_2–30 wt.% UO_2, 28-μ g.s.; X,●, ZrO_2–41 wt.% UO_2, 10-μ g.s.; △ ZrO_2–41 wt.% UO_2, 10-μ g.s. Change of temperature. From Wolfe.[55]

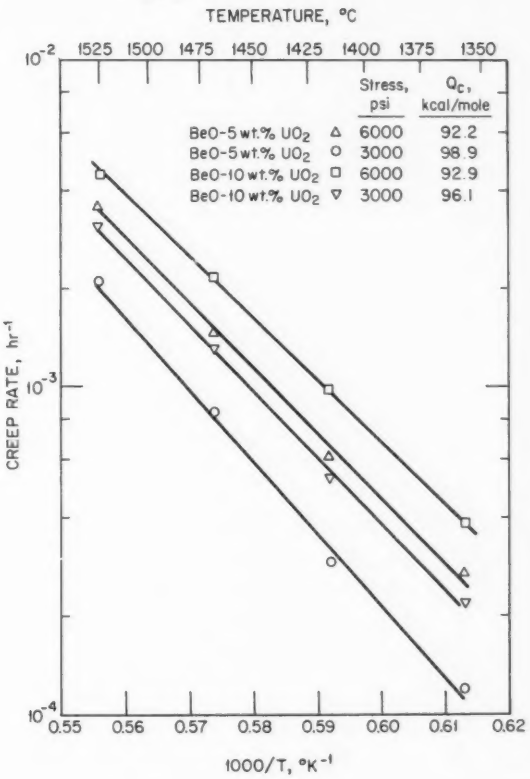

Fig. 27 Steady-state creep rate vs. temperature for BeO–UO_2 tested in compression. From Vandervoort and Barmore.[60]

BeO–UO_2

The compressive creep of BeO–5 wt.% UO_2 and BeO–10 wt.% UO_2 has been studied by Vandervoort and Barmore[60] over the temperature range 1375 to 1540°C. The grain sizes of the creep specimens were 6 to 10 μ, whereas densities varied from 98.0% T.D. for the BeO–5 wt.% UO_2 to 99.0 T.D. for BeO–10 wt.% UO_2. Total metallic-impurity concentrations were on the order of 220 ppM (primarily Si, Al, and Fe). No mutual solubility has been reported in the BeO–UO_2 system, and apparently the specimens contain a uniform dispersion of UO_2 particles ranging in size from 0.1 to 1.0 μ. All tests were conducted in air. The activation energies for creep were independent of applied stress at 3000 and 6000 psi for both compositions. The values in Fig. 27 are in the range of 92 to 99 kcal/mole, which compare with the value of 96 kcal/mole reported for "pure" BeO.[61] As for the case of pure BeO, creep rates of the mixed oxides were found to be linearly dependent on the applied stress, as shown in Fig. 28.

At 1540°C the creep rates for BeO–10 wt.% UO_2 having grain sizes of 7.5 μ and 16.5 μ were found to vary as $\dot{\epsilon} \propto 1/L^2$. By normalizing the data with respect to grain size and stress, Vandervoort and Barmore[61] were able to demonstrate that no significant difference exists between creep behavior of pure BeO and the mixed oxides. The authors concluded that all observations were consistent with the Nabarro–Herring model for diffusional creep.

UC

Uranium carbide[62] has the NaCl structure with a melting temperature of 2400 ± 50°C. The width[63] of the homogeneity range varies with temperature, but it extends roughly from 4.55 wt.% C to 4.90 wt.% C in the temperature region of 1300 to 1900°C with the stoichiometric composition corresponding to 4.80

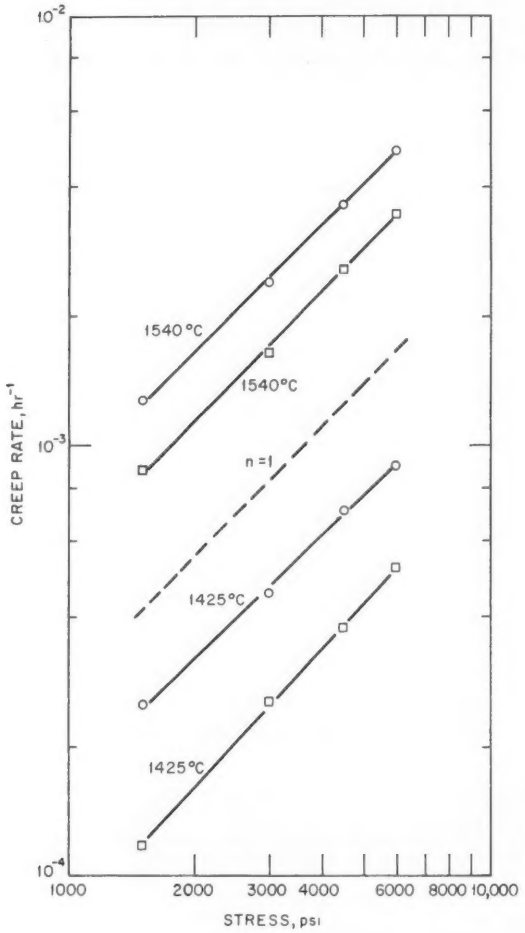

Fig. 28 Steady-state creep rate vs. applied stress for BeO–UO_2 tested in compression: □, BeO–5 wt.% UO_2, 6- to 10-μ g.s.; ○, BeO–10 wt.% UO_2, 6- to 10-μ g.s. From Vandervoort and Barmore.[60]

wt.% C. At lower carbon levels UC_{1-x} + U forms, and at higher carbon levels, above about 4.90 wt.%, UC_{1+x} + U_2C_3 or UC_2 forms.

Most high-temperature creep studies of UC have been performed in compression[63-68,92,93] under vacuums from 10^{-4} to 10^{-6} torr (see Table 5 and Fig. 29). Recently a few tensile creep experiments have been reported.[69] Except for two studies on single crystals,[65,93] the creep experiments have been conducted on coarse-grained arc-cast polycrystals.

Table 5 reveals that, for a power-law stress dependence of the creep rate, the stress exponents vary from 2.3 to 6. The low value of 2.3 was estimated from

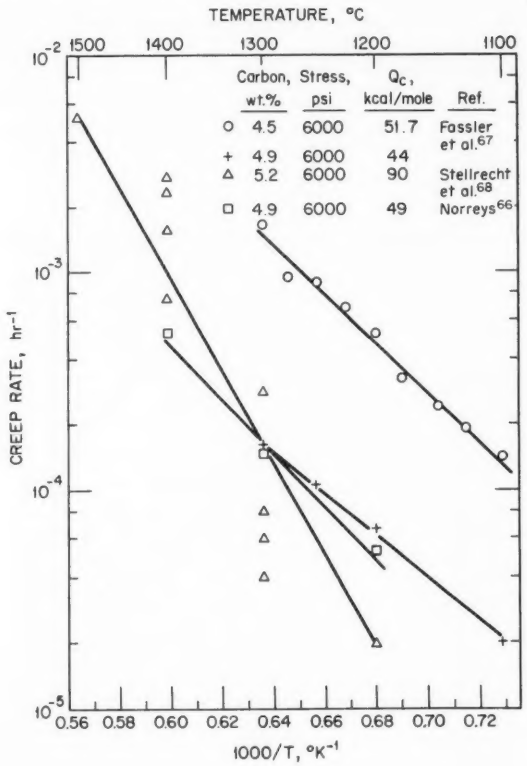

Fig. 29 Steady-state creep rate vs. temperature for uranium carbide tested in compression.

creep rates at only two stresses, 6000 and 8000 psi, at 1300°C, on the finest-grain-size uranium carbide tested. This may be in a transition region from the linear dependence associated with a diffusion-creep or grain-boundary-sliding process to the high-power-law dependence of dislocation-creep models. Norreys[66] found that minimum creep rates in the range of 2000 to 8000 psi at 1300°C could best be fitted by an exponential stress dependence. However, replotting his data to a power law gave $n = 1.8$. The stress exponents of 1.79 and 4.15 found by Killey[93] also result from a power-law treatment of data that could be fitted by an exponential stress dependence.

Uranium diffusivities are some three orders of magnitude lower than are those for carbon diffusion in uranium carbide,[70,71] and it is therefore expected that the high-temperature creep of UC will be controlled by a uranium-diffusion process. Although considerable data are available on both creep and self-diffusion activation energies for uranium carbide, it is not possible to simply relate the creep activation energies

Table 5 Creep Properties of UC*

Reference	Temperature, °C	Atm	Grain size, μ	Purity	Carbon, wt.%	n†	Q_c, kcal/mole	Remarks
Chang[64]	1500 to 1900	10^{-5} torr vacuum	300 to 400	50 ppM Fe 40 ppM Si 15 ppM Ni		5	37.5	Arc-cast, some metallic uranium. For transient creep, Q = 80 kcal/mole. Voids on grain boundaries parallel to compression axis
Chang[65]	1600 to 2000	10^{-4} torr vacuum	Single		Stoichiometric	5 to 6	69 to 92	Grown by electron-beam, floating-zone technique
Norreys[66]	1200 to 1400	5×10^{-5} torr vacuum	300	0.05 wt.% Al 0.01 wt.% Ti 0.005 wt.% Fe 200 ppM O_2 100 ppM N_2	4.9	1.8	49 ± 8	Free U increases $\dot{\epsilon}$ at 1300°C, W decreases $\dot{\epsilon}$. Arc cast
Fassler et al.[67]	1100 to 1300	10^{-6} torr vacuum	30	0.05 wt.% Si 0.05 wt.% Fe 0.02 wt.% Cr	4.9	2.3	44	1850 ppM O_2, 400 ppM N_2, 95% T.D.
				0.02 wt.% Ni	4.5		51.7	3200 ppM O_2, 1150 ppM N_2
Magnier et al.[63]	1600 to 2300	10^{-5} torr vacuum		300 ppM (O_2 + N_2)	4.5 to 5.0			Specimens are strengthened as C increases from 4.5 to 5.0 wt.%
Stellrecht et al.[68]	1200 to 1600	10^{-5} torr vacuum		50 ppM O_2 50 ppM N_2 100 ppM metals	5.2	3	90	Arc cast
Killey[92]	900 to 1100	2×10^{-5} torr vacuum	150 to 500	100 ppM N_2 200 ppM O_2 500 ppM Al 100 ppM Ni	4.7 to 4.78	1	45 ± 3	Arc cast
Killey[93]	1225 to 1600	2×10^{-5} torr vacuum	120	100 ppM N_2 200 ppM O_2 500 ppM Al 100 ppM Ni	4.81 to 5.18	1.79 4.18	68.6 141.6	Low temperature; low stress. High temperature; high stress. Single crystals also tested

*All the tests are in compression.
†The creep data are fitted to the relation $\dot{\epsilon} \propto \sigma^n$.

to atomic diffusion. Careful study of Table 5 suggests that the creep activation energies increase from 37.5 kcal/mole to 141.6 kcal/mole as the U/C ratio decreases from a carbon-deficient composition where free uranium is present to a carbon-excess composition in which a carbon-rich second phase is expected. According to Table 6 the activation energies for carbon diffusion either decrease with or are independent of any decreasing U/C ratio.[71,73] The trend is no different, however, for uranium diffusion,[72,73] although at high temperatures Lindner, Riemer, and Scherff[72] did find that the uranium activation energy increased from 70 kcal/mole to 90 kcal/mole as the carbon content increased from 4.68 to 4.83 wt.%. However, the absolute values of the activation energies for creep and diffusion are not in good agreement in this case. The diffusion activation-energy data can be used to make a case for the diffusion of either species being rate controlling in the creep behavior.

Killey[92,93] has performed the most extensive investigation of the influence of stoichiometry on the creep behavior of uranium monocarbide. He suggests that, at temperatures between 900 to 1100°C and for stresses in the range of 4000 to 8000 psi, where $\dot{\epsilon} \propto \sigma^1$, creep of slightly hypostoichiometric UC (4.70–4.78 wt.% C) is controlled by the diffusion of carbon vacancies. Differences between the creep activation energy of 45 kcal/mole and carbon-diffusion activation energies of 62 to 89 kcal/mole for this range of U/C compositions are explained by the fact that the creep measurements are performed at low temperatures where diffusion of carbon via monovacancies pre-

Table 6 Self-Diffusion in UC

Reference	Element	Temp., °C	Atm	Purity	Carbon, wt.%	D_0, $(cm^2)/(sec)$	Q, kcal/mole	Comments*
Chubb et al.[70]	^{14}C	1200 to 1940	Vacuum in graphite holder		5.0	0.02	50 ± 20	Sectioning method for U and C. Arc cast
	^{235}U	1600 to 2120			5.0	0.0013	64 ± 20	
Lee and Barrett[71]	^{14}C	1266 to 1684	10^{-5} torr vacuum in UC capsule		4.7	32.3	89 ± 6	Sectioning method for U and C, 97% T.D. All arc cast except 5.1 wt.% C which was sintered.
				~100 ppM O	4.82	1.75	63 ± 1	
				~125 ppM N	5.0	3.21×10^{-2}	55 ± 8	
				100 ppM W	5.1	2.95×10^{-2}	54 ± 15	
				150 ppM Fe	5.6	2.76×10^{-3}	45 ± 6	
	^{235}U	1505 to 1863			4.82	8.47	104 ± 7	
Lindner et al.[72]	^{233}U	1600 to 2100	10^{-5} to 10^{-6}		4.68	6.53×10^{-6}	70 ± 5	Arc-cast and single crystals. Alpha energy degradation. Same results for single crystals and arc cast
		800 to 1600	torr vacuum		4.68	6.33×10^{-11}	33 ± 2	
		1400 to 2000		1000 ppM O	4.83	1.85×10^{-4}	90 ± 6	
		1000 to 1400			4.83	1.21×10^{-12}	28 ± 4	
Bentle and Ervin[73]	^{235}U	1700 to 2050	10^{-5} to 10^{-6} mm Hg vacuum 1500°C	500 to 700 ppM, non-metallic	4.4		125 ± 15	ZM Sectioning
		1700 to 2050			4.6		125 ± 15	ZM
		1750 to 2050			4.8		125 ± 15	ZM
		1350 to 1700		1000 ppM metallic	4.4		32 ± 2	ZM
		1150 to 1750	10^{-8} to 10^{-9} mm Hg vacuum below 1500°C		4.6		32 ± 2	ZM
		1150 to 1750			4.8		32 ± 2	ZM, A.C.
		1400 to 2050			4.9		70 ± 5	ZM, A.C.
Bentle and Ervin[73]	^{14}C	1500 to 1900			4.6		94 ± 6	ZM
		1600 to 1900			4.7		92 ± 6	ZM
		1500 to 1900			4.8		84 ± 6	ZM
		1150 to 1500			4.6		53 ± 6	ZM
		1150 to 1600			4.7		54 ± 4	ZM
		1150 to 1500			4.8		51 ± 4	ZM
		1100 to 1900			4.9		60 ± 5	ZM
Villaine[74]	^{235}U	1450 to 2000		250 to 500 ppM O_2 100 ppM N_2	4.63 to 5.00	7.5×10^{-5}	81 ± 10	Diffusivities decrease with increase in % C. Sectioning, autoradiography. Alpha spectrometry
Krakowski[75]	^{14}C	1065 to 1499	10^{-5} torr vacuum	60 to 1250 ppM oxygen	4.68 to 4.75	0.1	62.5 ± 2	Decrease in surface activity

*S.C. = single crystal; P.C. = polycrystal; A.C. = arc cast; ZM = zone melted.

dominates, whereas the carbon-diffusion activation energies were determined at higher temperatures, where diffusion through divacancies is important. This is in agreement with the recent results of Bentle and Ervin[73] shown in Table 6, where the carbon activation energies are in the range of 51 to 54 kcal/mole for 1150 to 1500°C and in the range of 84 to 94 kcal/mole for 1500 to 1900°C.

The model proposed by Killey to explain creep of hypostoichiometric UC involves the dissolution of free uranium from grain boundaries into the UC lattice, along with the formation of carbon vacancies. The carbon vacancies then migrate into the substructure formed during primary creep, where they may condense. It is assumed that uranium diffuses rapidly along the substructure so that uranium diffusion is not the rate-limiting step. In these experiments grain-boundary sliding was not observed.

Killey[93] has also performed a series of compressive creep tests on arc-cast, polycrystalline [120-μ grain size (g.s.)] hyperstoichiometric UC (4.81–5.18 wt.%) in the temperature range of 1225 to 1600°C and under stresses of 1500 to 10,000 psi. It was found that the creep data could be fitted either to an expression of the form

$$\dot{\epsilon} = A' \exp -\left[\frac{\Delta H' - (\beta RT - \alpha)\sigma}{RT}\right] \qquad (14)$$

where $A' = 0.0189\ \text{hr}^{-1}$

$\Delta H' = 25 \pm 25$ kcal/mole

$\beta = 6.28 \times 10^{-3} \pm 2.61 \times 10^{-3}$ in.^{2}lb^{-1}

$\alpha = 18.7 \pm 4.26$ cal mole^{-1} lb^{-1} in.^{2}

or to one of the form

$$\dot{\epsilon} = A'' \sigma^n \exp\left(-\frac{\Delta H''}{RT}\right) \qquad (15)$$

where, for low temperatures and low stresses,

$A'' = 2.28 \times 10^{-2}$

$n = 1.79 \pm 0.67$

$\Delta H'' = 68.6 \pm 23.4$ kcal/mole

or where, at high temperatures and high stresses,

$A'' = 1.13 \times 10^{-1}$

$n = 4.18 \pm 1.36$

$\Delta H'' = 141.6 \pm 21.6$ kcal/mole

At a stress of 6000 psi, the transition occurs in the temperature range of 1300 to 1400°C.

Under equivalent conditions of stress and temperature, the creep rates for hyperstoichiometric UC are several orders of magnitude lower than are those for hypostoichiometric material. The high creep activation energies and the form of the stress exponents obtained from Eq. 15 are consistent with several of the creep models involving diffusion-limited dislocation motion, with the creep being controlled by uranium diffusion. Killey suggests that the low-temperature, low-stress results may be interpreted in terms of a model in which the activated step is that of overcoming the Peierls stress for the dislocations.

Creep tests on single crystals of varying orientation, in conjunction with metallographic observations, determined the principal active slip system at 1400°C and below to be $\langle 110 \rangle \{100\}$. From 1300 to 1500°C at 6000 psi, the slip plane became increasingly wavy. This behavior corresponded with the transition of creep behavior with stress and temperature given by Eq. 15.

Information concerning rate-controlling processes can sometimes be obtained from the influence of composition on creep rates. Norreys,[66] Killey,[92,93] and Magnier, Marchal, and Accary[63] found that creep rates for uranium carbide decreased with increasing carbon content. For example, at 1300°C and 6000 psi, Norreys found that samples containing 4.7 wt.% C plastically deformed some 25% in 30 hr, whereas samples containing 4.9 and 5.2 wt.% C strained less than 2% in the same time interval. This was attributed to the presence of free uranium along grain boundaries in the hypostoichiometric specimens. The same effect was found by Magnier, Marchal, and Accary[63] over the range of 4.49 to 5 wt.% carbon at 1900°C and a stress of 3850 psi.

However, if the observed dependence of creep rates on carbon concentration is attributed to variations in diffusion rates rather than to the presence of varying amounts of a second phase, then the diffusion data suggest uranium diffusion is the rate-controlling process. Lindner, Riemer, and Scherff,[72] Bentle and Ervin,[73] and Villaine[74] all found that uranium-diffusion coefficients decreased with increasing carbon content, which is the behavior consistent with decreasing creep rates, whereas Lee and Barrett[71] and Bentle and Ervin[73] found that carbon diffusivities increased with increasing carbon concentration. There have been no systematic studies of the influence of grain size or density on the creep behavior of uranium carbide.

UN

Compression creep of uranium mononitride has been investigated by Fassler, Huegel, and DeCresente[67]

and by Vandervoort, Barmore, and Cline,[76] while Stellrecht and Moak[77] have performed tensile creep tests on this compound (see Table 7).

Fassler, Huegel, and DeCresente[67] studied specimens that had a 95% T.D., a grain size of 30 μ and a nitrogen content of 5.25 wt.%. These samples contained 1100 ppM carbon and 2600 ppM oxygen as the primary nonmetallic impurities. The principal metallic impurities, in weight percent, were Si, 0.05; Fe, 0.05; Cr, 0.02; and Ni, 0.02 wt.%. Tests were performed in a vacuum of 10^{-6} torr. At 6000 psi and over, in the temperature range of 1100 to 1250°C, the creep rates could be fitted by a relation of the form

$$\dot{\epsilon} = 2.75 \times 10^5 \exp\left(-\frac{62{,}000}{RT}\right) \qquad (16)$$

whereas, at 8000 psi and over, in the temperature range of 1100 to 1350°C, the relation was

$$\dot{\epsilon} = 6.9 \times 10^5 \exp\left(-\frac{60{,}800}{RT}\right) \qquad (17)$$

From these two stress levels, a stress exponent of 4.15 was estimated.

Several tests were performed on samples containing 430 ppM oxygen and 1550 ppM carbon. At 1100°C and 6000 psi, creep rates for the low-oxygen-content material were an order of magnitude higher than those found for the UN containing 2600 ppM oxygen discussed earlier. The experimental results obtained by Fassler, Huegel, and DeCresente are included in Fig. 30.

Vandervoort, Barmore, and Cline[76] performed their study on stoichiometric UN in the temperature range of 1500 to 1800°C at stresses from 2000 to 5000 psi in a partial pressure of 200 mm nitrogen. The specimens had theoretical density and contained 400 ppM oxygen and 100 ppM carbon with a nitrogen content of 5.56 wt.%. Primary metallic impurities were 50 ppM Ca, 30 ppM Fe, and 20 ppM Si. The average grain size was 140 μ except for one specimen having a grain size of 2000 μ. The results obtained are plotted in Fig. 30. An average stress exponent, $n = 6.0 \pm 1.0$, was obtained, and the average creep activation energy was 75 ± 10 kcal/mole. Although the activation energies obtained by Vandervoort, Barmore, and Cline[76] differ from those determined by Fassler, Huegel, and DeCresente,[67] the relative positions for specimens of equivalent oxygen content are consistent if the data are corrected for the difference in stress. This may be somewhat fortuitous since the U/N ratios for the two studies must be different and creep rates may be expected to vary with composition.

Comparison of the creep activation energies given in Fig. 30 with the diffusion activation energies in Table 8 shows that the creep process may involve uranium volume diffusion. Reimann and Lundy[79] found that the uranium-diffusion activation energy increased from 60 kcal/mole to 105 kcal/mole as the nitrogen pressure and temperature increased. This is precisely the effect observed in the creep studies,

Table 7 Creep Properties of UN

Ref.	% T.D.	Temp., °C	Atm	Grain size, μ	Purity	n	Q_c kcal/mole	Remarks
Fassler et al.[67]	95	1100 to 1350	10^{-6} torr vacuum	30	1100 ppM C 2600 ppM O 0.05 wt.% Si 0.05 wt.% Fe 0.02 wt.% Ni 0.02 wt.% Cr	4.15	62	Compression, 6000 to 8000 psi, 5.25 wt.% N
Vandervoort et al.[76]	~100	1500 to 1800	200 torr N_2	140	400 ppM O 100 ppM C 50 ppM Ca 30 ppM Fe 20 ppM Si	6 ± 1	75 ± 10	Compression 2000 to 5000 psi, 5.56 wt.% N
Stellrecht and Moak[77]	~100	1400 to 1700	10^{-4} atm N_2 4×10^{-3} atm N_2	25	130 ppM O 400 ppM C 100 ppM others	~3 –	– –	Tension, 2500 to 5000 psi

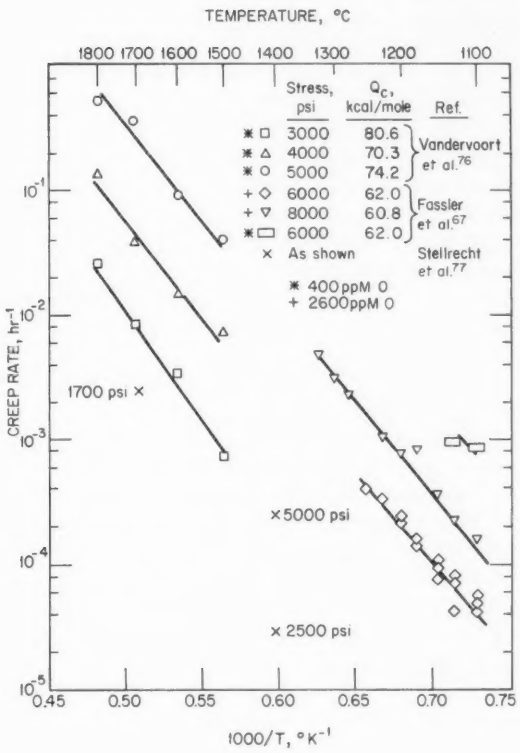

Fig. 30 Steady-state creep rate as a function of temperature for uranium mononitride tested in compression.

although the creep activation energy at high temperatures is somewhat lower than the uranium-diffusion activation energy.

Stellrecht and Moak[77] have performed a limited number of tensile creep tests on high-density, polycrystalline UN. Tests were performed at 1400°C under a nitrogen pressure of 10^{-4} atm and at 1700°C under 4×10^{-3} atm nitrogen. These pressures were expected to maintain a U/N ratio near the center of the composition range for UN. At 1400°C and 5000 psi, a specimen was elongated 11% before failure occurred, and, at 1700°C and 1700 psi, a specimen failed after 4% elongation. At 1400°C it was estimated that $n \cong 3$ for tests at 2500 and 5000 psi. This may represent a transition region from a linear stress behavior to the high-power-law stress region found by the previous workers. The creep rates obtained by Stellrecht and Moak[77] are included in Fig. 30.

$(U_{0.85}Pu_{0.15})(C_{0.65}N_{0.35})$

The compressive creep properties of mixed uranium–plutonium carbonitride have been studied by de Novion et al.[82] In the temperature range of 1150 to 1700°C, creep activation energies for $(U_{0.85}Pu_{0.15})(C_{0.65}N_{0.35})$ were found to vary from 83 kcal/mole to 101 kcal/mole over a range of applied stresses from 1940 to 9400 psi (see Fig. 31). The stress dependence of the creep rate over this range of stresses is $n \simeq 2.3$. These experiments, performed in vacuum on specimens

Table 8 Self-Diffusion in UN

Reference	Element	Temp., °C	Atm	Purity	D_0, $(cm^2)/(sec)$	Q, kcal/mole	Comments
Sturiale and DeCrescente[78]	^{15}N	1560 to 1900 1250 to 1500	100 torr N_2		2.6×10^{-4}	55 29	25- and 125-μ grain size. ^{14}N–^{15}N exchange method
Reimann and Lundy[79]	^{233}U	1100 to 1600 1420 to 1830	Low N_2 pressure Higher N_2 pressure		3.24×10^{-7} 7.54×10^{-2}	60 105	Alpha-energy degradation Large-grained polycrystals
Holt and Almassy[80]	^{15}N	1700 to 2000	7 to 603 torr nitrogen	784 ppM O 211 ppM C		56	$^{15}N \rightarrow {}^{15}F$. Composition unknown. Large grains. $D_N \propto P_N 0.36$ for $0.01 < P_N < 1.0$ atm
Droege and Alexander[81]	^{15}N	1360 to 1800	0.5 to 10 torr nitrogen				Arc-melted, large grains. D_N increases with increasing nitrogen pressure

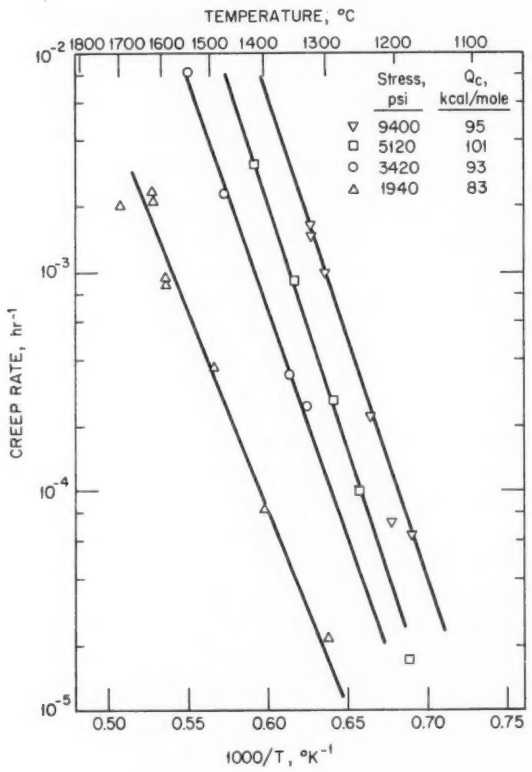

Fig. 31 Steady-state creep rate vs. temperature for $U_{0.85}Pu_{0.15}$) ($C_{0.65}N_{0.35}$) tested in compression; 91% T.D. From de Novion, Amice, Groff, Guerin, and Padel.[82]

of 91% T.D., gave higher creep rates than those reported for UN or UC for comparable conditions. This result was attributed to the lower density of the mixed carbonitride specimens.

IN-PILE CREEP STUDIES

UO_2

Sykes and Sawbridge[83,91] studied the in-pile creep behavior of natural UO_2 in an atmosphere of purified argon. The test specimens, which had a grain size of 17 μ and a density of >97% T.D., were in the form of helical springs with an outside diameter of 20 mm (0.788 in.) and with six active coils having a 1-mm (0.039 in.) square cross section. A constant load was maintained on the specimen through a pretensioned spring in the capsule which was in contact with a free end of the specimen. Strain was measured continuously by an electrical displacement transducer, and the temperature was measured by two thermocouples located near the specimen.

Creep tests have been conducted using six different capsules in the temperature range of 525 to 880°C. The shear stress for the two specimens in the region located at 44% of the distance from the side of the square cross section ranged from 505 to 2670 psi, which is an equivalent compressive stress range of 875 to 4620 psi. Tests were conducted at a maximum fission rate of 1.5×10^{12} fissions/(cm^3)(sec). The experimental conditions employed for all the in-pile creep tests performed to date on ceramic fuels are included in Table 9.

Data obtained by Sawbridge and Sykes[83] are given in Fig. 32, which is a plot of in-pile creep rates vs. reciprocal temperature. All points in this plot have been normalized to a compressive stress of 3500 psi on the assumption that creep rate is directly proportional to stress, which is a reasonable assumption for the relatively low stresses used for these tests. Tests 1* and 2* were stopped before steady-state creep-rate conditions were reached, and the points for 1* and 2* in Fig. 32 are therefore slightly higher than the steady-state points would be.

There is a moderate variation in the fission rate, ranging from 7.3×10^{11} fissions/(cm^3)(sec) (test 3B) up to 1.5×10^{12} fissions/(cm^3)(sec) (tests 1, 2, 3A, and 4). Even though there is some scatter in the data, it shows that the creep rates are not a strong function of temperature as are out-of-pile creep rates extrapolated from higher temperatures to 525 to 800°C. Furthermore, out-of-pile creep rates would be expected to be at least two orders of magnitude below the in-pile data points at 720°C (1.007×10^{-3} °K^{-1}).

A recent in-pile experiment was conducted by Solomon and Routbort.[84] The specimen used in this study was a helical spring with 16 active turns. The outside diameter was 0.932 in., and the wire diameter was 0.073 in. This stoichiometric UO_2 had an enrichment of 1.82%, a 10-μ grain size, and a 96% T.D. with porosity distributed uniformly within the grains. The capsule had a device to apply load on the specimen by deadweight loading. The creep strain was measured during testing by a linear variable differential transducer. The measured surface temperature of the spring was 102°C. The calculated outer-fiber shear stress was 2890 psi, which is an equivalent outer-fiber tensile stress of 5005 psi. The test was run at a fission rate of 2×10^{12} fissions/(cm^3)(sec) and yielded a creep rate of approximately 4×10^{-6} hr^{-1}. This creep rate represents an enhancement of many orders of magnitude with respect to the out-of-pile creep rate extrapolated

Table 9 In-Pile Creep Investigations of Nuclear Fuels

Reference	Material	Type of test	Temp., °C	Atm	Grain size, μ	% T.D.	Maximum fission rate fissions/(cm³)(sec)	Remarks
Sykes and Sawbridge[83,91]	UO_2	Compression of spring	525 to ~880	Argon	17	>97	1.5×10^{12}	In-pile creep rate enhanced orders of magnitude with respect to the extrapolated out-of-pile creep rate
Solomon and Routbort[84]	UO_2	Spring in tension	102	NaK	10	96	2.6×10^{12}	In-pile creep rate enhanced by many orders of magnitude over the extrapolated out-of-pile creep rate. Initial composition stoichiometric
Brucklacher and Dienst[85]	UO_2	Compression	220 to 600	NaK	30 to 40	95	1.0×10^{14}	In-pile creep rate enhanced by orders of magnitude over the extrapolated out-of-pile creep rate
Clough[20]	UO_2	Bend and creep	500 to 750	–	8 to 10	96 to 97	1.6×10^{13}	In-pile creep rate enhanced by orders of magnitude over the out-of-pile creep rate. Initial O/U ratio <2.0005
Clough[20]	UC	Tensile	802	–	30	95.5	6×10^{12}	In-pile creep rate enhanced by orders of magnitude over the out-of-pile creep rate
Perrin[86]	UO_2	Compression	1000 to 1180	Helium	27	98	1.2×10^{13}	In-pile creep rate enhanced by a factor of five over out-of-pile creep rate. Stoichiometry during testing ~2.0003

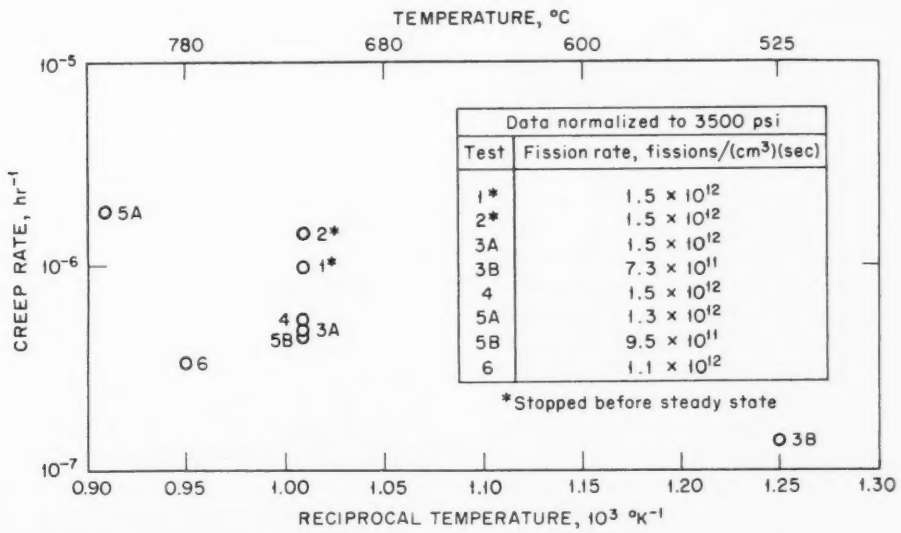

Fig. 32 Creep rate vs. reciprocal temperature for in-pile creep tests (from Sykes and Sawbridge).[83,91]

to 102°C. It should be noted, however, that extrapolating high-temperature creep data ($T > 1000$°C) to 102°C may not be valid. It is entirely likely that different creep mechanisms operate in the two different temperature ranges, and that these have different activation energies.

Brucklacher and Dienst[85] have performed in-pile compression creep experiments on 15% enriched UO_2. The test specimen consisted of 19 alternating rings of UO_2 and Mo (TZM). The purpose of the metal rings was to reduce the temperature gradients in the UO_2 rings. The UO_2 had a 30- to 40-μ grain size and a 95% T.D. The load on the specimen was applied by gas pressure, and the strain was measured by an electrical displacement transducer. Temperature was measured by means of thermocouples located near the specimen. Tests were run at a fission rate of 1.0×10^{14} fissions/(cm^3)(sec), under compressive stresses up to 4950 psi and a maximum specimen surface temperature of 410°C that corresponded to a maximum specimen internal temperature of 600°C.

Figure 33 is a plot of creep rate vs. stress for in-pile creep tests of UO_2. The two points near a zero stress

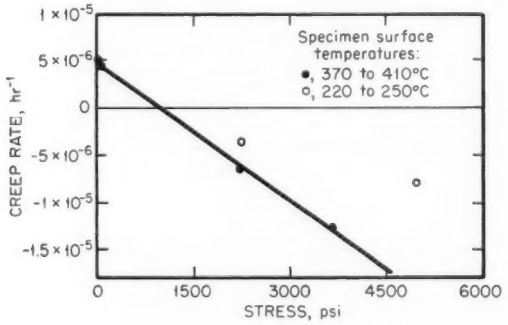

Fig. 33 Creep rate vs. stress for in-pile creep of UO_2. From Brucklacher and Dienst.[85]

show that some swelling occurs owing to irradiation. Thus the actual in-pile creep rates may be larger than the observed values since any swelling would tend to decrease the apparent compressive creep rate. The highest creep rate observed was 1.3×10^{-5} hr^{-1} at a stress of 3700 psi. In the temperature range studied, it was concluded that the creep rate increases only slightly with increasing temperature.

Clough[20] performed creep relaxation and three-point bend tests on UO_2. The tests were performed on 96 to 97% T.D. material with a grain size of 8 to 10 μ, with an initial O/U ratio of <2.0005, and at three levels of enrichment. The specimens were rectangular, each having length, outside diameter, and inside diameter of 0.98, 0.79, and 0.195 in., respectively. The three-point bend tests were conducted under approximately constant-stress conditions, with an initial stress of about 4930 psi, using a spring-loaded plunger stressing the center of the specimen. The amount of bending in the test specimens was determined by postirradiation measurements. Creep rates were calculated by dividing total deflection by the total test time.

Figure 34 is a plot of creep rate over stress ($\dot{\epsilon}/\sigma$) vs. reciprocal temperature for the six irradiated bend specimens. This normalization assumes that $\dot{\epsilon} \propto \sigma^1$, which is reasonable for the stress employed. Two unirradiated compression creep tests run at 1200 and

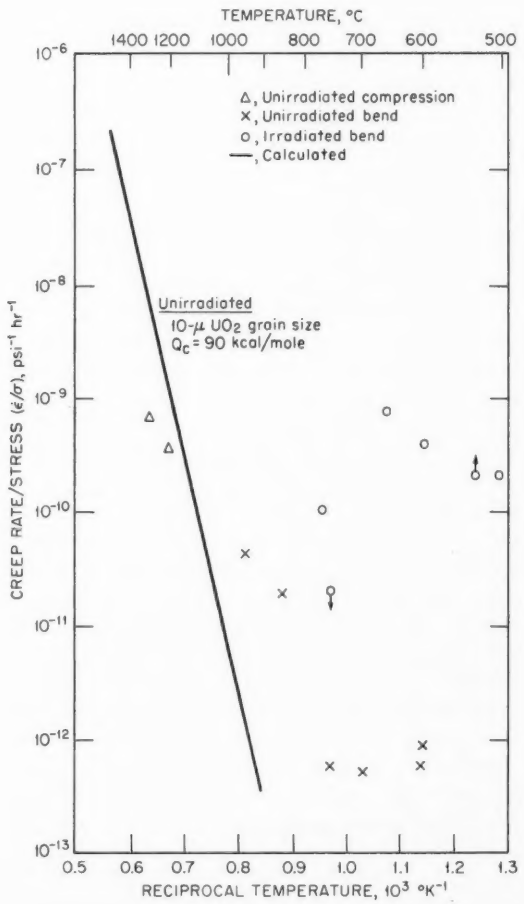

Fig. 34 Creep rate divided by stress vs. reciprocal temperature for out-of-pile and in-pile UO_2 creep tests. After Clough.[20]

1300°C are shown, and six unirradiated bend tests in the range 600 to 950°C are shown. A plot of creep rate of unirradiated UO_2 with a 10-μ grain size at stresses below 3050 psi, according to the relation $\dot{\epsilon}/\sigma = 1.41 \times 10^3 \exp(-90{,}000/RT)$, is also shown which predicts creep rates very close to the unirradiated compression creep rates measured by Clough. The equation is based on a literature survey by Sykes and Sawbridge.[83] Also shown in the figure are six tests run on irradiated specimens in the temperature range 500 to 770°C. These in-pile tests have creep rates that are over two orders of magnitude more rapid than the unirradiated creep rates in the temperature range 600 to 750°C. It is not known why creep rates for unirradiated UO_2 are athermal. The results suggest that out-of-pile creep at low temperatures is controlled by a mechanism different from those operative above 1000°C.

Perrin and coworkers[86] studied the in-pile compressive creep behavior of 24.48% enriched UO_2 in a series of three capsules. To minimize temperature gradients, they prepared the test specimens as hollow cylinders with a length of 0.750 in., an outside diameter of 0.250 in., and an inside diameter of 0.150 in. The grain size was 27 μ, and the density was 98% T.D. The residual porosity was spherical and mainly located within the grains. The stoichiometry during the in-pile tests was not controlled but was, on the basis of out-of-pile controlled-stoichiometry experiments,[89] estimated to be 2.0003. The capsule contained heaters for controlling the specimen temperature, and the temperature was measured by three thermocouples attached directly to the specimen surface. Constant load was applied to the specimen by externally controlled gas pressure. Creep strain was measured continuously by a transducer that converted the relative linear movement of two probes attached to the specimen into induced pressure changes across a variable orifice. Tests were conducted in a temperature range of 1000 to 1180°C and in a stress range of 1500 to 4000 psi. Most tests were run at a fission rate of 1.2×10^{13} fissions/(cm^3)(sec), although one test was run at 4×10^{12} fissions/(cm^3)(sec).

To show the effect of fission rate and stress, the investigators[86] normalized the data to a single effective temperature of 1100°C and plotted them as creep rate vs. stress, as shown in Fig. 35. The activation energies used for the normalization were determined separately for the in-pile and out-of-pile data. The out-of-pile tests ($\varphi = 0$) show a creep rate proportional to stress to the first power, i.e., $\dot{\epsilon} \propto \sigma$. This indicates a creep mechanism such as grain-boundary sliding[33] or

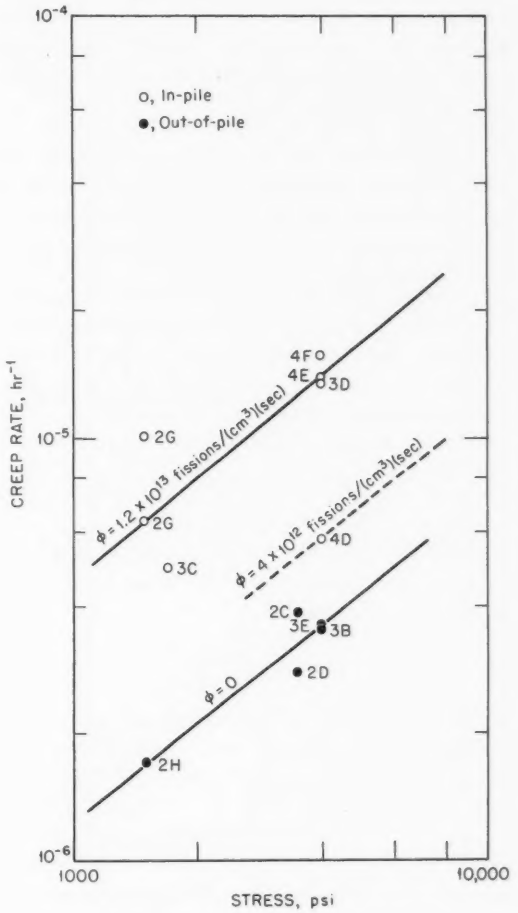

Fig. 35 Creep rate vs. stress for out-of-pile and in-pile UO_2 creep tests, normalized to T = 1100°C. After Perrin.[86]

Nabarro–Herring creep,[32] rather than a mechanism such as dislocation climb where creep rate is proportional to stress to the fourth to fifth power. The same type of creep-rate dependence on stress is seen for the in-pile tests at a fission rate of 1.2×10^{13} fissions/(cm^3)(sec). Further, the creep rates at this fission rate are enhanced in comparison to the zero-fission-rate creep rates by a factor of 4 to 5. One creep test was run at an intermediate creep rate of 4×10^{12} fissions/(cm^3)(sec). This result, together with the data at 1.2×10^{13} fissions/(cm^3)(sec), indicates that the creep rate increases about linearly with the fission rate. Additional data points at the intermediate fission rate would be needed to better define the exact dependence of creep rate on fission rate.

A further important result is that the out-of-pile tests on a given specimen before and after in-pile tests fall on the same curve. For example, tests 2C and 2D were out-of-pile, test 2G was run in-pile, and then test 2H was run out-of-pile. In addition, 3B was run out-of-pile, 3D was then run in-pile, and finally 3E was run out-of-pile. Out-of-pile and in-pile tests were normally separated at 24-hr or greater periods of time, but the specimen was maintained at temperature. There was, therefore, time for relaxation of the defect structure produced during irradiation, such as annealing out of any excess vacancies above the equilibrium number or mutual annihilation of vacancies and interstitials.

These results indicate that $\dot{\epsilon} \propto \sigma$. In general, for a constant fission rate, we can write

$$\dot{\epsilon} = K\sigma e^{-Q/RT} \tag{18}$$

where K is a constant depending on such factors as grain size, density, and stoichiometry. Equation 16 can be rewritten as

$$\dot{\epsilon}/\sigma = Ke^{-Q/RT} \tag{19}$$

where $\dot{\epsilon}/\sigma$ is the stress-compensated creep rate. Figure 36 is a plot of the stress-compensated creep rate as a function of reciprocal temperature for fission rates of 0, 4×10^{12}, and 1.2×10^{13} fissions/(cm^3)(sec). There is a strong temperature dependence of the stress-compensated creep rate for the in-pile tests as well as for the out-of-pile tests. The activation energies for the out-of-pile tests and the in-pile tests at 1.2×10^{13} fissions/(cm^3)(sec) are about the same, being in the range of 90 to 100 kcal/mole. These results show that the in-pile creep-rate curve in this temperature range of 1000 to 1180°C is displaced above and approximately parallel to the out-of-pile creep-rate curve.

It is difficult to plot quantitatively all the data available on in-pile creep of UO_2 because of uncertainties in temperature in some investigations, variations in density, grain size, stoichiometry, amount of enrichment, fission rate, and state of stress. However, on the basis of the tests performed by several other groups in the range of 100 to 825°C and the results of our investigation in the range 1000 to 1180°C, the qualitative behavior appears to be as follows: The in-pile creep rate in the low-temperature region (~100 to 750°C) is athermal or only moderately dependent on temperature and is two to three orders of magnitude greater than the out-of-pile thermal creep rate,

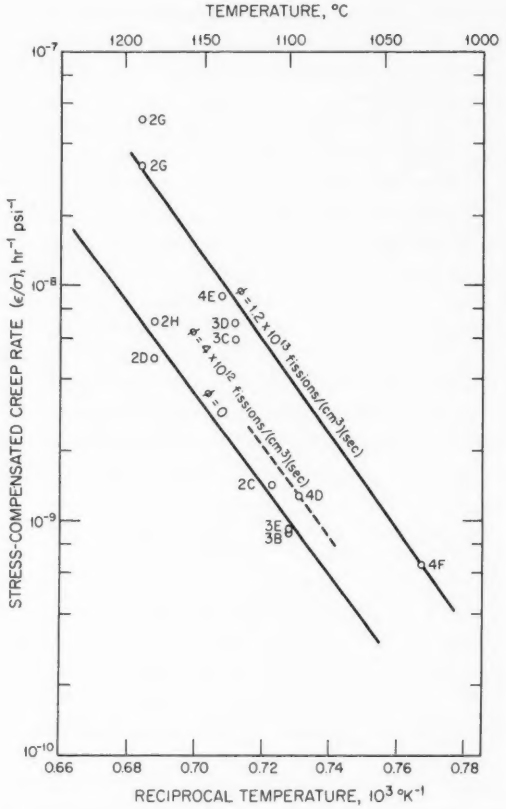

Fig. 36 Creep rate divided by stress vs. reciprocal temperature for out-of-pile and in-pile UO_2 creep tests. After Perrin.[86]

which may also be athermal at low temperatures. However, in the high-temperature region, the in-pile creep rate is strongly dependent on temperature with an activation energy (90 to 100 kcal/mole) of the order of the out-of-pile creep. This suggests a model where the in-pile creep rate is always greater than the out-of-pile creep, at least to temperatures of approximately 1200°C for fission rates greater than 1×10^{13} fissions/(cm^3)(sec).

UC

Clough[20] performed a uniaxial tensile test on hyperstoichiometric UC containing 4.85 wt.% carbon. Platelets of UC_2 existed within grains, and platelets of U_2C_3 existed along grain boundaries and at triple points. The grain size varied from 5 to 100 μ, with the mean grain size being 30 μ, and the density was 95.5% T.D. The tensile specimen had a 1-in.-gauge length and

a 0.120-in.-gauge diameter. A screw mechanism located at the top of the capsule adjusted a compressible spring that applied the load to the tensile specimen. Strain was measured by means of a micrometer located in the capsule. Temperature was controlled by a heater in the capsule and measured by two thermocouples on the specimen.

For the in-pile tensile creep test, the effective specimen temperature was 802°C, the stress was 3770 psi, and the fission rate was 6×10^{12} fissions/(cm^3)(sec). The result is shown in Fig. 37 along with

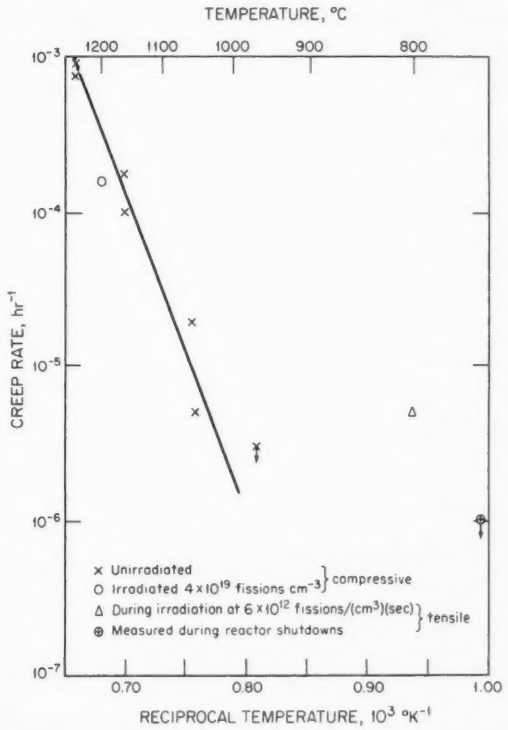

Fig. 37 Creep rate vs. reciprocal temperature for out-of-pile and in-pile UC creep tests. After Clough.[20]

the creep rate measured without irradiation during the reactor shutdown at the same stress and a temperature of approximately 733°C.

Also shown in Fig. 37 are compressive creep tests of unirradiated UC run in argon. The cylindrical test specimens were 0.197 to 0.295 in. long and 0.125 in. in diameter. Tests were run at 4640 psi at temperatures from 1060°C to 1300°C. In addition, a single post-irradiation compression test was run on a specimen machined from the in-pile tensile specimen. It was tested at 1200°C and 4640 psi and had a creep rate very close to the unirradiated specimens.

The in-pile creep rate was approximately 5×10^{-6} hr^{-1} at 3770 psi and 802°C. An extrapolation of the unirradiated creep data (determined at 4640 psi) to the same temperature is a creep rate more than two orders of magnitude below the in-pile creep rate. Thus the UC creep rate in-pile is substantially enhanced over the out-of-pile creep rate if it can be assumed that extrapolation of out-of-pile high-temperature creep data to low temperatures is a valid procedure.

ACKNOWLEDGMENTS

The authors' studies on compression creep of uranium dioxide were performed for Argonne National Laboratory and the U. S. Atomic Energy Commission under Contract W-7405-Eng-92. Figures 16 and 17 were kindly provided by C. S. Yust of Oak Ridge National Laboratory.

We wish to thank E. C. Sykes of the Central Electricity Generating Board, Berkeley Nuclear Laboratories, and N. M. Killey of the General Electric Company Limited's Hirst Research Center for permission to use their results prior to publication.

REFERENCES

1. R. V. Hesketh, in Proceedings of the Conference on Solid State Physics Research with Acceleration, Allen N. Goland (Ed.), USAEC Report 50083, p. 389, Brookhaven National Laboratory, 1967.
2. R. V. Hesketh, *J. Nucl. Mater.*, **29:** 217 (1969).
3. D. Brucklacher, W. Dienst, and F. Thuemmler, German Report KFK-817 (EUR-3975) (in German), July 1968. A translation of this report is USAEC Report EURFNR-585.
4. L. Lynds, W. A. Young, J. S. Mohl, and G. G. Libowitz, *Nonstoichiometric Compounds,* R. F. Gould (Ed.), Advances in Chemistry Series, No. 39, p. 58, Washington, D. C., 1963.
5. E. A. Aitken, H. C. Brassfield, and R. E. Fryxell, Thermodynamic Behavior of Hypostoichiometric UO_2, in *Thermodynamics,* Symposium Proceedings, Vienna, 1965, p. 435, International Atomic Energy Agency, Vienna, 1966 (STI/PUB/109) (Vol. 2).
6. B. T. M. Willis, *Proc. Brit. Ceramic Soc.*, **1:** 9 (1964).
7. M. S. Seltzer, A. H. Clauer, and B. A. Wilcox, USAEC Report BMI-1886, Sec. C, pp. C-36–C-48, Battelle Memorial Institute, 1970.
8. W. M. Armstrong, A. R. Causey, and W. R. Sturrock, *J. Nucl. Mater.*, **19:** 42 (1966).
9. R. A. Wolfe and S. F. Kaufman, USAEC Report WAPD-TM-587, Bettis Atomic Power Laboratory, October 1967.

10. L. E. Poteat and C. S. Yust, *Ceramic Microstructures,* R. M. Fulrath and J. A. Pask (Eds.), p. 646, John Wiley & Sons, Inc., New York, 1968.
11. P. E. Bohaboy, R. R. Asamoto, and A. E. Conti, USAEC Report GEAP-10054, General Electric Company, May 1969.
12. M. S. Seltzer, A. H. Clauer, and B. A. Wilcox, USAEC Report BMI-1882, Battelle Memorial Institute; April 1970.
13. J. A. C. Marples and A. Hough, in Plutonium 1970 and Other Actinides, Nuclear Metallurgy, Vol. 17, William N. Miner (Ed.), USAEC Report 701001, p. 497, The Metallurgical Society, 1970.
14. K. Kummerer and D. Vollath, International Meeting on Fast Reactor Fuel and Fuel Elements, Karlsruhe, Sept. 28–30, 1970, paper 49.
15. R. Scott, A. R. Hall, and J. Williams, *J. Nucl. Mater.,* **1**: 39 (1959).
16. W. M. Armstrong, W. R. Irvine, and R. H. Martinson, *J. Nucl. Mater.,* **7**: 133 (1962).
17. W. M. Armstrong and W. R. Irvine, *J. Nucl. Mater.,* **9**: 121 (1963).
18. W. M. Armstrong and W. R. Irvine, *J. Nucl. Mater.,* **12**: 261 (1964).
19. G. Christie and J. Williams, *J. Nucl. Mater.,* **5**: 1 (1962).
20. D. J. Clough, *Fast Reactor Fuel and Fuel Elements,* Karlsruhe, Sept. 28–30, 1970, Paper No. 6.
21. P. R. Mertens, The Creep Strength of Polycrystalline Uranium Dioxide, Thesis, Rennselaer Polytechnic Institute, Troy, N. Y., 1964.
22. A. A. Solomon and R. H. Gebner, USAEC Report ANL-7726, p. 121, Argonne National Laboratory, July 1970.
23. R. J. Hawkins and C. B. Alcock, *J. Nucl. Mater.,* **26**: 112 (1968).
24. J. M. Marin, H. Michaud, and P. Contamin, *Compt. Rend.,* **264**: 1633 (1967).
25. Hj. Matzke, *J. Nucl. Mater.,* **30**: 26 (1969).
26. K. W. Lay, *J. Amer. Ceram. Soc.,* **54**: 18 (1971).
27. A. B. Lidiard, *J. Nucl. Mater.,* **19**: 106 (1966).
28. J. Belle, *J. Nucl. Mater.,* **30**: 3 (1969).
29. C. R. Barrett, A. J. Ardell, and O. D. Sherby, *Trans. AIME, Met. Soc.,* **230**: 200 (1964).
30. J. Weertman, *J. Appl. Phys.,* **28**: 362 (1957).
31. R. Chang, *The Physics and Chemistry of Ceramics,* p. 275, Gordon and Breach, Science Publishers, Inc., New York, 1963.
32. F. R. N. Nabarro, in *Conference on the Strength of Solids,* p. 75, London Physics Society, 1948.
33. R. C. Gifkins, *J. Amer. Ceram. Soc.,* **51**: 69 (1968).
34. M. S. Seltzer, A. H. Clauer, and B. A. Wilcox, *J. Nucl. Mater.,* **34**: 351 (1970).
35. T. G. Langdon, *J. Nucl. Mater.,* **38**: 88 (1971).
36. M. U. Goodyear, E. O. Speidel, and D. E. Kizer, USAEC Report BMI-1868, p. C-25, Battelle Memorial Institute, July, 1969.
37. A. B. Auskern and J. Belle, *J. Nucl.Mater.,* **33**: 311 (1961).
38. C. B. Alcock, R. J. Hawkins, A. W. D. Hills, and P. McNamara, A Study of Cation Diffusion in Stoichiometric UO_2 Using α-Ray Spectrometry, in *Thermodynamics,* Symposium Proceedings, Vienna, 1965, p. 57, International Atomic Energy Agency, Vienna, 1966 (STI/PUB/109) (Vol. 2).
39. R. Lindner, and F. Schmitz, *Z. Naturforsch,* **16A**: 1373 (1961).
40. S. Yajima, H. Furuya, and T. Hirai, *J. Nucl. Mater.,* **20**: 162 (1966).
41. P. Nagels, W. Van Lierde, R. De Batist, M. Denayer, L. DeJonghe, and R. Gevers, Migration and Reorientation of Oxygen Interstitials, and Migration and Self-Diffusion of Uranium in UO_2, in *Thermodynamics,* Symposium Proceedings, Vienna, p. 311, 1965, International Atomic Energy Agency, Vienna, 1966, (STI/PUB/109) (Vol. 2).
42. P. McNamara, Thesis, London, 1963, quoted in Ref. 38.
43. J. F. Marin and P. Contamin, *J. Nucl. Mater.,* **30**: 16 (1969).
44. D. K. Reimann and T. S. Lundy, *J. Amer. Ceram. Soc.,* **52**: 511 (1969).
45. A. B. Auskern and J. Belle, *J. Nucl. Mater.,* **3**: 267 (1961).
46. W. Dornelas and P. Lacombe, *J. Nucl. Mater.,* **21**: 100 (1967).
47. L. E. J. Roberts et al., quoted by J. Belle, *J. Nucl. Mater.,* **30**: 3 (1969).
48. R. Lindner, D. Reimann, and F. Schmitz, in *Plutonium as a Reactor Fuel,* Symposium Proceedings, Brussels, 1967, International Atomic Energy Agency, Vienna, 1967 (STI/PUB/153).
49. A. D. King, Canadian Report AECL-3655, August 1970.
50. C. S. Morgan and L. E. Poteat, Oak Ridge National Laboratory Metals and Ceramics Division Annual Progress Report, June 30, 1968.
51. E. W. Roberts and J. P. Roberts, *Bull. Soc. Fr. Ceram.,* **77**: 3 (1967).
52. I. Bransky and N. M. Tallen, *J. Amer. Ceram. Soc.,* **53**: 625 (1970).
53. C. S. Morgan and L. L. Hall, *Proc. Brit. Ceram. Soc.,* **6**: 233 (1966).
54. L. E. Poteat and C. S. Yust, *J. Amer. Ceram. Soc.,* **49**: 410 (1966).
55. R. A. Wolfe, High Temperature Creep of Oxide Fuel Materials, quoted in Ref. 9.
56. P. E. Bohaboy and S. K. Evans, in Plutonium 1970 and Other Actinides, Nuclear Metallurgy, Vol. 17, William N. Miner (Ed.), USAEC Report 701001, p. 478, The Metallurgical Society, 1970.
57. M. D. Houston, O. L. Kruger, and W. M. Pardue, *ibid.,* p. 488.
58. O. D. Slagle, USAEC Report BNWL-1223, p. 21, Battelle–Northwest, 1969.
59. D. N. Polubayarinov, E. Ya. Shapiro, V. S. Bakunov, and F. A. Akopov, *Inorg. Mater. (USSR) (Engl. Transl.),* **2**: 336 (1966).
60. R. R. Vandervoort and W. L. Barmore, *J. Amer. Ceram. Soc.,* **48**: 587 (1965).
61. R. R. Vandervoort and W. L. Barmore, *J. Amer. Ceram. Soc.,* **46**: 180 (1963).
62. G. Ervin, A. K. Smalley, and H. Nadler, *Mater. Research Bull.,* **1**: 151 (1966).
63. P. Magnier, M. Marchal, and A. Accary, *Proc. Brit. Ceram. Soc.,* **7**: 141 (1967).
64. R. Chang, *J. Appl. Phys.,* **33**: 858 (1962).
65. R. Chang, *Physics and Chemistry of Ceramics,* C. Klingsberg (Ed.), p. 282, Gordon and Breach, Science Publishers, Inc., 1963.

66. J. J. Norreys, *Carbides and Nuclear Energy, Vol. 1*, L. E. Russell (Ed.), p. 435, MacMillan & Co. Ltd., London, 1964.
67. M. H. Fassler, F. J. Huegel, and M. A. DeCresente, USAEC Report PWAC-482 (Pt. 1), Pratt and Whitney Aircraft, October 1965.
68. D. E. Stellrecht, M. S. Farkas, and D. P. Moak, *J. Amer. Ceram. Soc.*, **51**: 455 (1968).
69. D. E. Stellrecht and D. P. Moak, USAEC Report BMI-1859, Battelle Memorial Institute, February 1969.
70. W. Chubb, R. W. Getz, and C. W. Townley, *J. Nucl. Mater.*, **13**: 63 (1964).
71. L. M. Lee and L. R. Barrett, *Proc. Brit. Ceram. Soc.*, **7**: 159 (1967).
72. R. Lindner, G. Riemer, and H. L. Scherff, *J. Nucl. Mater.*, **23**: 222 (1967).
73. G. G. Bentle and G. Ervin, Jr., USAEC Report AI-AEC-12726, Atomics International, August 1968.
74. P. Villaine, Report CEA-R-3436 (in French), September 1968.
75. R. A. Krakowski, *J. Nucl. Mater.*, **32**: 120 (1969).
76. R. R. Vandervoort, W. L. Barmore, and C. F. Cline, *Trans. AIME, Met. Soc.*, **242**: 1466 (1968).
77. D. E. Stellrecht and D. P. Moak, USAEC Report BMI-1886, p. 894, Battelle Memorial Institute, Columbus, July 1970.
78. T. J. Sturiale and M. A. DeCrescente, USAEC Report PWAC-477, Pratt & Whitney Aircraft, September 1965.
79. D. K. Reimann and T. S. Lundy, *J. Metals*, **20**: 54 (1968).
80. J. B. Holt and M. Y. Almassy, *J. Amer. Ceram. Soc.*, **52**: 3 (1969).
81. J. Droege and C. A. Alexander, USAEC Report BMI-1886, p. A16, Battelle Memorial Institute, July 1970.
82. C. H. de Novion, B. Amice, A. Groff, Y. Guerin, and A. Padel, Plutonium 1970 and Other Actinides, Nuclear Metallurgy, Vol. 17, William N. Miner (Ed.), USAEC Report 701001, p. 509, The Metallurgical Society, 1970.
83. E. C. Sykes and P. T. Sawbridge, British Report RD/B/N-1489, November 1969.
84. A. A. Solomon and J. L. Routbort, Argonne National Laboratory (U.S.A.), presentation at ACS Basic Science and Nuclear Divisions Meeting, Gatlinburg, Tenn., Nov. 5,
85. D. Brucklacher and W. Dienst, *J. Nucl. Mater.*, **36**: 244 (1970).
86. J. S. Perrin, Irradiation-Induced Creep of Uranium Dioxide, to be published in *J. Nucl. Mater.*, 1971.
87. J. T. A. Roberts and B. J. Wrona, USAEC Report ANL-7742, p. 112, October 1970.
88. M. S. Seltzer, A. H. Clauer, and B. A. Wilcox, USAEC Report BMI-1898, Battelle Memorial Institute, January 1971.
89. M. S. Seltzer, A. H. Clauer, and B. A. Wilcox, USAEC Report BMI-1893, Battelle Memorial Institute, October 1970.
90. R. L. Coble, *J. Appl. Phys.*, **34**: 1679 (1963).
91. E. C. Sykes, personal communication to J. S. Perrin, Jan. 18, 1971.
92. N. M. Killey, The Secondary Creep Behaviour of Uranium Monocarbide in Compression, I: Hypostoichiometric Uranium Monocarbide, to be published in *J. Nucl. Mater.*, 1971.
93. N. M. Killey, The Secondary Creep Behaviour of Uranium Monocarbide in Compression, II: Hyperstoichiometric Uranium Monocarbide, personal communication to M. S. Seltzer.

Operating Experience at the Connecticut Yankee Reactor October–December 1970

By Myrna L. Steele*

OPERATIONS

At the beginning of October 1970, the plant[1] was operating at the nominal full-power level of 600 MW(e). At 0537 hr on October 12, a momentary decrease in the indicated reactor coolant flow from loop 2 initiated an automatic trip. Normal steam dump was actuated, and all 10 steam-dump valves opened to reduce the reactor coolant average temperature from 545 to 535°F; however, a coil stop for one of the 10 steam-dump-valve positioners was out of adjustment and prevented one valve from closing when the average temperature reached 535°F. The average coolant temperature continued decreasing to a minimum of 502°F while efforts to isolate the dump valve were made, then began recovering after the main-steam-line trip valves and the steam-dump-header manual isolation valve were closed. Because the trip was initiated from an indicated loss-of-coolant flow, the constant-voltage-supply unit, the rectifier circuit, and the optical-meter relay associated with the loop 2 flow-transmitter system were replaced. Also, the faulty coil stop for the steam-dump-valve positioner was cleaned and readjusted, and all other positioner assemblies were inspected to assure proper adjustment. The plant was returned to full power until October 24 when it was shut down at 0849 for examinations of prospective reactor operators and for miscellaneous maintenance.

During the shutdown a complete calibration of one of the three level-monitoring channels for the pressurizer was effected because of an unexplained indicated-drift problem. The drifting had been observed on a small scale following the startup of Core II in June 1970, and a check-out of the channels during a plant shutdown on Sept. 11, 1970, had failed to locate the cause. During the 2 weeks prior to the shutdown for operator examinations, the drift had increased. Even though several new components had been installed in the channel before it was calibrated, the channel was still considered to be malfunctioning when returned to service.

At 2130 on October 24, the plant was returned to the nominal 600-MW(e) level without the drifting pressurizer-level-monitoring channel. Further investigation showed that the instrumentation was properly aligned and that the problem was other than the electronics. The difficulty appeared to result either from one of the reference legs or from a malfunction of the other two level-monitoring channels. After a check-out of the static reference leg for the drifting channel yielded no answers, the plant was removed from service at 2106 on October 26, and at 2210 the reactor was scrammed. The plant was removed from service so that the other two pressurizer-level-monitoring channels could be checked. The check revealed a partial loss of the common high-side static reference leg of these two channels. Both the high- and low-side reference legs were blown down and refilled, and, when returned to service, these two channels indicated the same as the third channel. The pressurizer level was then raised slowly to 80% to verify proper response of the channels.

Although the cause of the partial loss of the reference leg could not be positively identified, the bypass valve on a Δp cell, which had leaked slightly from the packing gland, was adjusted. At 0308 on October 27, as the reactor was just critical in prepara-

*U. S. Atomic Energy Commission, Division of Technical Information Extension, Oak Ridge, Tenn. 37830.

tion for a return to full power, the reactor was scrammed by a momentary high-level signal from two of the pressurizer-level-monitoring channels. A Δp cell for one of the pressurizer-level channels had been returned to service with its low-side isolation valve in the open position. All channel checks were completed, all channels were restored to service, and the plant was back on line at 0454.

Plant output remained[2] at the nominal 600-MW(e) level until November 11 when the output was reduced to 540 MW(e) for sensitivity tests of the instrumentation, and then the power was returned to the 600-MW(e) level. At 0210 on November 24, the load was rapidly reduced to 400 MW(e) because of a failure of a circulating-water pump. By 0335 the load was further reduced to about 300 MW(e), and a second circulating-water pump was removed from service while plant conditions were evaluated. At 1318 on November 25, one of the circulating-water pumps was returned to service, and the plant load was increased to ~500 MW(e); however, an hour later the load was reduced to 390 MW(e) so that one coolant loop could be removed from service and a leaking lower flange in the feedwater-control valve could be repaired. The repairs were completed at 2150, and the load was returned to ~500 MW(e), where it remained until November 27. At 0707 on that day, the load was reduced to ~400 MW(e) so that the other repaired circulating-water pump could be returned to service. Then the plant load was again increased to the nominal full-power level.

On December 3 while the plant[3] was still at nominal full power, a steam-flow–feedwater-flow mismatch signal coincident with a steam-generator low-level signal caused an automatic reactor trip. The mismatch–low-level signal was generated when the shift supervisor switched from what he assumed to be a faulty power supply for a semivital bus to an alternate power supply. Actually he had switched from an operable alternate power supply to a faulty normal power supply. All systems functioned normally to bring the plant to a hot-standby condition. The power was switched back to the functioning alternate power supply, the faulty normal power supply was repaired, and the plant was returned to full power. The next day the load was reduced to 400 MW(e), and another circulating-water pump was removed from service for maintenance.

An increase in plant load to ~540 MW(e) while the pump was out was followed, on December 7, by a reduction to 400 MW(e) while the pump was being put back into service and then by a return to nominal full power. On the following day the output was reduced to 400 MW(e) to permit not only a check for leaking condenser tubes but also the removal of another of the four circulating-water pumps for maintenance. Output was increased to ~600 MW(e) during the three-circulating-water-pump mode of operation and again reduced to 400 MW(e) on December 9 to return the pump to service. The fourth and final pump was removed from service for maintenance at this time, and plant load was returned to full power with three circulating-water pumps operating. On December 12 the load was decreased to 400 MW(e), and the repaired circulating-water pump was returned to service. Load was then increased to full power until December 17 when a reduction to 300 MW(e) was necessary because of a leaking drain on one of the steam-generator feed pumps. Repairs were completed, and the load was returned to normal [600 MW(e)] for the remainder of 1970.

MAINTENANCE, MODIFICATIONS, AND REPAIRS

The items listed below are selected from the referenced reports to give the reader an idea of the minor, but noteworthy, problems that can be encountered during routine operations.

Plant Systems

October 1970 (Ref. 1)

Drain valves were installed on the air headers for both diesel generators.

A time-delay relay associated with the half-power resistor circuitry for the slave cycler of a control-rod subgroup was replaced.

A new gasket was installed on the cascading-vent orifice for a feedwater heater.

A leak in the bonnet of a level-control valve on the heater-drain tank was repaired by welding the bonnet and capping the studs and nuts.

A leaking bonnet on a manual isolation valve in the feedwater system was welded.

A leak in the recirculation line from the steam-generator feed pump to the condenser was repaired.

A heater-drain pump was repacked.

New bodies were installed on each recirculation-control valve on the steam-generator feed pump.

A leaking diaphragm for a manway for a moisture-separator reheater was repaired.

The failed bearings in a cooling-fan motor for one of the control-rod drives were replaced.

November 1970 (Ref. 2)

New bearings were installed in a cooling-fan motor for another control-rod drive.

A leaking bonnet gasket on a control valve for a reheater-drain tank was replaced.

The moisture separator for a compressor in the control air system was replaced because of a cracked flange.

The circulating-water pump that failed in service was removed and repaired. A stainless-steel liner that was located at the point of highest impingement had broken away from the intake bell and lodged between the impeller and the pump casing. The liner was removed, the holes were filled with epoxy, the impeller and shaft were balanced, and the pump was reassembled and returned to service.

A leaking bottom flange on a feedwater-control valve was repaired by welding a cap over the bottom flange.

December 1970 (Ref. 3)

A new outboard bearing was installed in a charging pump, and the motor for the pump was realigned and doweled.

The edges of the propeller blades in three circulating-water pumps were trimmed, the stainless-steel bands on the intake bells were removed, and all impingement holes in the intake bells were filled with epoxy.

Failed bearings on the motor for the aerated-drain-tank pump were replaced, and the pump and motor were realigned.

Failed bearings in the fan of a vapor extractor for the generator were replaced, the shaft seal was replaced, and the fan was balanced.

Instrumentation

October 1970 (Ref. 1)

A hot-leg resistance-temperature detector in the ΔT circuitry for one of the reactor coolant loops was replaced.

A fourth level-monitoring channel for the pressurizer was modified for use at operating temperature and pressure.

The pilot valve in the level-control-valve positioner for the heater-drain tank was replaced.

November 1970 (Ref. 2)

A pressure transmitter was installed in the residual heat-removal system.

A faulty capacitor and a diode for one of the coolant-loop $\Delta T\,R/I$ converters were replaced.

A new Δp cell was installed across the letdown prefilter.

December 1970 (Ref. 3)

A torque tube was replaced in the level controller for a reheater-drain tank.

A volume booster was replaced on the pressure controller for the well-water system.

ACKNOWLEDGMENT

I would like to thank F. W. Hartley, Plant Superintendent at the Connecticut Yankee Reactor, for his many helpful suggestions and contributions and for his continuing cooperation.

REFERENCES

1. Connecticut Yankee Atomic Power Company, Connecticut Yankee Atomic Power Plant, Operation Report No. 70-10, October 1970, USAEC Report DOCKET-50213-84, Nov. 24, 1970.

2. Connecticut Yankee Atomic Power Company, Connecticut Yankee Atomic Power Plant, Operation Report No. 70-11, November 1970, USAEC Report DOCKET-50213-87, Dec. 17, 1970.

3. Connecticut Yankee Atomic Power Company, Connecticut Yankee Atomic Power Plant, Operation Report No. 70-12, December 1970, USAEC Report DOCKET-50213-94, Jan. 22, 1971.

Suggested Reading List

Southwest Research Institute, Connecticut Yankee Nuclear Power Plant, 1970 Inservice Inspection, USAEC Report DOCKET-50213-85, Sept. 17, 1970.

Teledyne Materials Research Company, Connecticut Yankee Atomic Power Plant, Effect of Oil and Extinguisher Material on Reactor-Coolant Piping and Pump, USAEC Report DOCKET-50213-80, Oct. 22, 1970.

Connecticut Yankee Atomic Power Company, Connecticut Yankee Atomic Power Plant, Malfunction of Pressurizer Level Instrumentation, USAEC Report DOCKET-50213-81, Nov. 4, 1970.

Connecticut Yankee Atomic Power Company, Connecticut Yankee Atomic Power Plant, Automatic Plant Trip and Reactor Coolant System Cooldown to 502°F, USAEC Report DOCKET-50213-82, Nov. 4, 1970.

Connecticut Yankee Atomic Power Company, Connecticut Yankee Nuclear Power Plant, Containment Operation and Testing, May 1967–April 1970, USAEC Report DOCKET-50213-86, Nov. 30, 1970.

Connecticut Yankee Atomic Power Company, Connecticut Yankee Atomic Power Plant, Thermal Stress Evaluation of the Reactor Vessel During a Cooldown Transient, USAEC Report DOCKET-50213-89, Jan. 5, 1971.

Operating Experience at the Ginna Reactor

By Myrna L. Steele*

Unit 1 of the Robert E. Ginna nuclear power plant, located on the south shore of Lake Ontario about 16 miles east of Rochester, N. Y., and owned by the Rochester Gas & Electric Corp., is a 420-MW(e) pressurized-water reactor (PWR). Initial criticality[1] was achieved on Nov. 9, 1969, and the designed power rating was reached in March 1970. By the end of 1970, the plant had generated in excess of 2.2 million MWh (net) of electricity.

The three-region core[2] is composed of 121 Zircaloy-clad, slightly enriched UO_2 fuel elements and 33 rod-cluster control assemblies, 29 of which are full length and 4 are part length. The rod-cluster control assemblies are inserted into the guide thimbles of the fuel assemblies. The lower core support structure and the core barrel serve to provide passageways and control for the coolant flow of 33.65×10^6 lb/hr from each of the two loops. The coolant flows from the vessel inlet nozzles down the annulus between the core barrel and the vessel wall, then along both sides of the thermal shield, and into a plenum at the bottom of the vessel. The coolant then turns and flows up through the lower support plate, through the intermediate diffuser plate, and then through the lower core plate. The flow holes in the diffuser plate and the lower core plate are arranged to give a very uniform entrance-flow distribution to the core. After passing through the core, the coolant enters the area of the upper support structure and then flows generally radially to the core-barrel outlet nozzles and directly through the vessel outlet nozzles. A small amount of water also flows between the baffle plates and the core barrel to provide additional cooling of the barrel. Similarly, a small amount of the entering flow is directed into the vessel head plenum and exits through the vessel outlet nozzles. Boric acid, dissolved in the coolant of the two-loop closed cooling system, is used for control of long-term reactivity effects.

The turbine[3] is a three-element, tandem-compound, four-flow exhaust, 1800-rpm unit with 40-in. last-row blades. It has a maximum gross rating of slightly more than 496 MW with inlet steam conditions of 730 psia, 508°F, exhaust at 1.35 in. Hg absolute, 0% makeup, and five-stage feedwater heating. Steam leaving the high-pressure section of the turbine passes through moisture separators and is reheated by live steam to 480°F before entering the low-pressure turbine sections.

The hydrogen inner-cooled main steam generator is rated 608 MVA at 19,000 V with a power factor of 0.85. It is equipped with a 2600-kW rotating rectifier exciter that is directly connected to the generator shaft.

Emergency power adequate for all engineered-safeguard equipment and instrumentation and control is provided by redundant diesel-driven generators, each rated at 1950 kW, 480 V.

The turbine exhausts to two condensers cooled by lake water drawn from an intake tunnel extending 3100 ft out under the lake bottom. Total cooling-water flow is 356,000 gal/min with a temperature rise of 19.6°F at full power.

OPERATIONS FROM INITIAL CRITICALITY THROUGH DEC. 31, 1970

Low-power testing activities[4] were begun on Nov. 9, 1969, immediately after initial criticality of the

*U. S. Atomic Energy Commission, Division of Technical Information Extension, Oak Ridge, Tenn. 37830.

reactor, and, as soon as these tests were completed, the plant had to be shut down on Nov. 19, 1969, because of problems with the pressurizer-level instrumentation. The sealed tubing of the reference-leg level indicator for the pressurizer was removed, and open-type tubing was installed. This was a temporary measure, and the sealed tubing for the reference leg will be installed again at a later date after further development work and verification for this type of level indication. The reactor was returned to the critical condition on Nov. 28, 1969. On November 29, with the reactor at 2% power, a false high-pressure signal from a condenser tripped the reactor. A valve to the bistable had been closed during calibration of the high-condenser-pressure logic and had not been reopened.

The generator was initially phased to the line on December 2, and, while the power level was being increased on Dec. 3, a trip signal caused by a low-low steam-generator level was initiated when the suction valve to the operating feedwater pump was closed by mistake. The reactor was again brought up to the 20% power level, and again the low-low steam-generator-level reactor trip was actuated because the reactor operator had not manually reset the feedwater bypass valve after a high water level had occurred in the steam generator. The reactor was again brought back to the 20% power level, and again the low-low steam-generator-level reactor trip was actuated. This time the feedwater bypass valves were placed in the automatic-operation mode before the turbine-stop valves were latched.

Once again the reactor was brought back up, and on December 4, with the reactor at 24% power, the operator removed the field from the generator before he transferred the 4160-V-bus power supply to the 34.5-kV auxiliary supply. This caused the loss of both reactor coolant pumps, which in turn caused a reactor trip. The reactor was brought critical again, and on December 6 a reactor trip was again initiated by a low-low steam-generator level. Excessive vibration had caused the differential-pressure mercoid switch in the seal-water system to trip the feedwater pump, which in turn caused the low-low level in the steam generator. The reactor was returned to operation for tests at 30% thermal power, which were completed in about a week. On December 15 a feedwater-pump trip caused a reactor trip due to a low-low steam-generator level. Low seal-water differential pressure had caused the feedwater pump to trip.

The reactor was placed in the hot-shutdown condition at 1400 hr on Dec. 16, 1969, in compliance with a Technical Specifications requirement because of the failure of an engineered-safety-system valve to open completely during a monthly surveillance test. During the regular testing of all the engineered-safety-system valves, one of the 10-in. double-disk gate valves from containment sump B to the pumps of the residual-heat-removal (RHR) system failed to open fully. After the valve had been disassembled, inspection showed that both disks in the double-disk valve were bowed. Since damage was limited to the stainless-steel centers of the disks, the valve was reassembled using new internals. Stringent tests on the RHR system with the valve in place indicated no leaks, and so the reactor was again brought critical.

On Dec. 30, 1969, during operation at 1% reactor power, a steam-flow–feedwater-flow mismatch concurrent with a low steam-generator-level signal tripped the reactor. The 1A auxiliary feedwater pump was not operable, and the trip occurred before the steam-driven feedwater pump could be put into service. The 1B feedwater pump could not supply enough water for the load.

On Jan. 3, 1970, with the reactor at 2% power, the reactor was scrammed by a safety-injection signal resulting from a two-out-of-three-logic low-pressure signal from the main steam line. Personnel who were calibrating one of the pressure channels had closed a valve to another pressure channel because steam was leaking from the gasket around the valve bonnet. At the time of the actuation of the safety-injection-system signal, it was noted that one set of the engineered-safety-system equipment and valves did not operate. Dirty contacts on a relay were cleaned, a test signal was initiated, and both logic trains then operated. However, three safeguard valves (two air-operated and one motor-operated) did not indicate proper operation on the status board in the control room. Further investigation showed that the two air-operated valves were operating properly but that their respective position-indicator switches were out of position and unable to make contact for proper position indication; the switches were adjusted. The motor-operated valve was found to have an open contact in the limit switch, and this was adjusted. The valve was then exercised satisfactorily seven times.

On Jan. 16–17, 1970, tests were performed to demonstrate the capability of the reactor instrumentation to detect and verify the misalignment of a control-rod cluster with respect to its bank before core design limits are exceeded. The reactor was manually shut down twice on January 17; one trip was effected to repair a steam leak through the gasket on a

turbine-stop valve, and the other trip was necessitated by a malfunction of the control-rod-step counters.

Testing at 50% thermal rating was begun on January 21 and was completed in about a week. During the 50% power testing, a turbine trip on January 27 was caused by a loss of pressure in the pump for the electrohydraulic (EH) governor. The operator had put the feedwater-pump control in the pull-stop position when the steam-generator level reached 80%. The feedwater pump was not put back in service soon enough with manual feedwater control to avoid a low-low steam-generator-level signal, and thus a reactor trip resulted. The reactor was returned to the 50% power level and was again tripped when the overtemperature ΔT bistable was tested. Further testing could not reproduce the problem, and so the reactor was returned to operation. On January 28, with the reactor at 23% power, a second trip from the overtemperature ΔT channel occurred while personnel were checking for the cause of the first one. Dirty contacts on one of the relays had allowed only one trip breaker to open on the two-out-of-four logic. Later that same day another trip occurred because of a feedwater-flow–steam-flow mismatch concurrent with a low steam-generator-level signal. Severe water-level fluctuations in the A steam generator caused the A feedwater valve to close on a high-level signal. The feedwater-valve controller was put in the manual mode, and the valve was reset, but the operator was unable to control the swing in the steam-generator level.

The reactor was kept at 50% of full power from January 28 until February 5 because of a condensate-pump failure. By February 12 the plant had been slowly brought to 75% power. Problems with condensate pumps and heater-drain pumps limited operation to between 50 and 75% of full power until March 11. The only trip in February occurred on February 22 during testing of the underfrequency trips on the 4160-V buses.

On March 2 the plant was removed from service for 39.5 hr so that the pressurizer-spray valves could be repacked. The power level was returned to 75% of full power, and testing at this level was begun on March 3 and was completed in about 4 days. On March 6, during tests of the seals for the personnel- and equipment-hatch air locks, an excessive amount of leakage was noted. The leaks were traced to two shaft penetrations for the inside handwheels. Repacking of the handwheel shafts reduced the air leak to about one-eighth of the original leakage. On March 11, when the heater-drain-pump repairs were finished, the plant was brought to the 100% power level, and the 100-hr acceptance run at 100% power was initiated. After this test was finished at 0200 on March 16, the 10 and 50% load-reduction tests were completed satisfactorily. On March 30, while plant personnel were performing a surveillance test, they asked the control operator to switch the automatic feedwater control to the manual position. The plant was at 100% power. When the operator switched from automatic to manual, the A steam-generator level began to oscillate, and the operator could not catch it on manual control. The reactor tripped on the low steam-generator-level signal in conjunction with feedwater-flow–steam-flow mismatch. The plant was left out of service for scheduled maintenance on the primary and secondary systems in preparation for commercial operation. On Apr. 24, 1970, the plant was returned to service.

The plant remained at 100% of its rated power[5,6] until May 14 when the turbine and reactor were tripped for the full-power trip test and for the scheduled turbine inspection and primary-system maintenance. The primary system was held in hot-shutdown condition until the resistance-temperature detectors (RTDs) could be checked. When these checks were completed, the reactor operator tripped the main-steam-line isolation valves in preparation for reactor cooldown, but the position-indicating lights on the control board showed that one valve had failed to close. Investigations showed that the valve trip mechanism had operated to close the valve but that the valve had not closed fully. The packing gland was loosened, and then the valve did close fully. During the ensuing scheduled shutdown, which lasted until June 19, the malfunctioning main-steam-line isolation valve and a section of blading on the low-pressure side of the turbine were repaired. Also, two RTDs were replaced in the primary loops.

The reactor was brought critical on June 18 in preparation for plant operation, but the fluttering of a safety-injection-system relay initiated a trip signal that caused one of the reactor trip breakers to open. The terminal screws in the relay were found to be loose. The reactor was again made critical, and the next day the reactor was tripped by a low-low water-level signal from a steam generator subsequent to a turbine overspeed-trip test. During the test the water level in the steam generators was being controlled manually by the use of the feedwater-bypass-system control valves. The pressure transient from the turbine trip depressed the water level in the steam generator and thereby initiated the low-low level signal. The plant was returned to service that day and remained at about 85% of full power until July 5 when a steam leak was

located in a high-pressure turbine-gauge line. Since the turbine had to be shut down for the necessary repairs, further maintenance was also effected. This maintenance included adding packing to a pressurizer-spray valve, checking the stroke on another spray valve, and adjusting the turbine-trip pilot valve. The plant was returned to about 85% of full power the same day and was kept at this level until July 12, when excess leakage of one of the primary-system valves necessitated that the reactor be manually shut down. Subsequent to repairs of the valve, the plant load was increased to 100% of full power and was kept at that level until one of the feedwater pumps tripped on July 25. That trip initiated a feedwater-flow–steam-flow mismatch signal concurrent with a low steam-generator-level signal and tripped the reactor. The plant load was returned to the nominal full-power level where it remained throughout August and until September 5.

A manual turbine trip was initiated on September 5 because noises coming from the turbine room were interpreted as turbine vibrations. The turbine trip resulted in a low-steam-generator-level–low-feedwater-flow signal, and this tripped the reactor. An investigation revealed that loose packing in one of the main feedwater-control valves had caused oscillations in the feedwater supply to the steam generator. The packing was repaired, and the plant was returned to service. With the plant at about 45% turbine load, a failure of the EH governor system caused one turbine-control valve to close and two turbine-control valves to open wide, which in turn caused a load increase. The reactor control system followed this increase with no difficulty. The load was maintained manually at 50% until the next morning when the turbine was manually tripped so that the EH governor system and a suction relief valve for a feedwater pump could be repaired. On September 8 the plant load was increased to nominal full power where it remained until September 30 when the plant was removed from the line for a 2-week maintenance shutdown. The maintenance included replacing a bonnet gasket on a pressurizer-spray valve, welding a pipe leak on the high-pressure turbine, replacing two failed RTDs in the primary loop, and inspecting the moisture-separator reheaters.

During the shutdown it was necessary to reroute[7] the flow for the RHR system so that a diaphragm on the discharge check valve from the 1A accumulator could be seal welded. As procedures were being followed to reroute the flow from the RHR system through the core-deluge valves, one of the valves failed to indicate a wide-open position. An investigation showed that the overload switch for the Limitorque operator had tripped the breaker open but that the valve was only half open. The Limitorque valve operator was disassembled for a complete inspection of why the valve opened only halfway. Disassembly was effected by cutting the valve yoke in half. An inspection of the valve operator revealed that the stem nut had seized to the valve stem. Removal and inspection of the stem nut showed that a chip from the thread of the stem nut was the reason for the seizure. Since the stem threads were undamaged, the stem nut was replaced with a new one. The valve yoke was welded, the valve operator was reassembled, and the proper functioning of the valve was checked out. Since the plant was in the cold-shutdown condition, the remaining valves of this type were also tested to ensure proper operability.

On October 14, while the plant was being brought from the cold-shutdown to the hot-shutdown condition, one of the containment B sump valves failed to operate properly. The valve could be operated manually, although not smoothly. An investigation revealed that the valve operator was being tripped because it required excessive torque. A locknut on the stem nut of the valve operator had loosened and backed off. This allowed the stem to be free to move vertically and bind the driving gear. The locknut was retightened, the valve stem and stem nut were lubricated, and proper operation of the valve and valve operator was verified. Later that day the plant was returned[8] to nominal full power. On October 29 it was removed from the line by a turbine trip that resulted when a tree, cut down by a beaver in a swampy area, fell across a distribution line. Relays isolated the fault, but a distance relay at the plant did not operate properly, and the turbine tripped while at 100% power. Plant load was returned to 100% later in the day.

On November 1 the plant was tripped from 100% of full power when the automatic voltage regulator for the generator "acted up." This occurrence removed the plant from the line. The unit was off line for 9 hr for a check of the voltage regulator, and, when no problem could be found, the unit was slowly brought back up to 100% power. The next day another trip from full power was again caused by erratic operation of the automatic voltage regulator for the generator. This time the plant was out of service for 14.75 hr for further investigation of the voltage-regulating system. Since no cause of the problem could be found, special recorders were connected to monitor the regulating-potential transformers. The plant was again removed from the line on Nov. 5, 1970, for a check of the

regulating-potential-transformer leads. This time the plant was off the line for 6 hr and then slowly brought back to 100% power. Although problems were discovered in one of the phase-regulating-potential transformers, the plant was kept on the line until a new transformer arrived. The generator was removed from the line on Nov. 6, 1970, and the defective phase-regulating-potential transformer was replaced. The plant was back on the line at 0131 on Nov. 7, 1970. Load was maintained at about 100% power until Nov. 15, 1970, when a manual shutdown was initiated so that a $\frac{3}{4}$-in. bypass valve for a pressurizer-spray valve could be repacked.

On Nov. 23, 1970, the generator was manually tripped at 2030 for the following items of maintenance: repacking the bypass valve for a pressurizer-spray valve, checking a negative ground on the battery, and removing an in-core drive unit from the containment. While the maintenance personnel were checking for the battery ground, they unintentionally tripped the reactor. The ground was found in a limit switch on one of the power-operated relief valves. The reactor was brought critical at 2229 on November 23, and the generator was synchronized to the line at 0235 on Nov. 24, 1970.

The plant remained at a nominal 100% power until Dec. 12, 1970, when the generator was manually taken off line at 0223. At 0304 the reactor was placed in the subcritical condition so that maintenance personnel could repack a power-operated stop valve for a pressurizer-relief valve, repack the bypass valve for a pressurizer-spray valve, and find and plug leaky condenser tubes. The reactor was brought critical at 1712 on Dec. 13, 1970, and the generator was synchronized to the line at 2258 and slowly brought up to 100% power.

The power level was maintained at nominal full power until Dec. 31, 1970, when it was manually shut down for repairs on the moisture-separator reheaters, repair of condenser tube leaks, and other secondary plant maintenance. The reactor was made critical at 0100 on Jan. 4, 1971, and the generator was synchronized to the line at 0545 on Jan. 4,1971, and then slowly brought back up to 100% power.

MAINTENANCE AND REPAIRS

The items listed below are selected from the referenced reports to give the reader an idea of minor problems which can be encountered during routine operations and which can affect plant performance.

Plant Systems

November–December 1969 (Ref. 4)

A seal was replaced on a reactor coolant pump.

An oil-deflection baffle was installed on a reactor coolant pump to stop the leakage of oil from the lubricating system.

The condensing pots for the four upper-level channels on the pressurizer were repiped and relocated to correct erratic readings.

The plungers for one of the charging pumps were replaced, and the pump was repacked.

Deformed disks on an isolation valve from a containment sump to one of the pumps of the RHR system were replaced.

Two condensate pumps were extensively overhauled. Many flange belts and nuts had come loose or sheared, and many of the nuts and washers had been pumped into the condensate system but were recovered.

One of the thimbles for the in-core flux monitors was replaced.

January 1970 (Ref. 4)

Leaking gaskets for the safety-valve flanges on three of the six reheater safety valves were replaced.

Leaking gaskets on the valve cover of the main-steam-line isolation valves were replaced.

A leaking stem plug in the atmospheric steam-dump valve for one of the main steam generators was replaced.

The bypass valves for the turbine-stop valves were repacked.

The inboard and outboard floating seals for both main feedwater pumps were replaced.

One of the condensate pumps was repaired. Repairs consisted of straightening and metallizing the lower stub shaft and adding new flange bolts at each end of the spool piece.

A leaking letdown relief valve in the primary system was removed and then reinstalled unrepaired since the cuts in the seat and disk were too deep to lap. The valve was replaced a few days later.

Two power-operated relief valves, both pressurizer-spray valves, and both bypass stop valves for the pressurizer-spray valves were repacked.

A new accumulator for one of the charging pumps was installed.

One of the discharge check valves on the containment-spray pump was inspected and the valve seat was lapped.

Both canned pumps for the boric acid tanks were replaced because of excessive wear on the thrust collars.

The relief valve on one of the charging pumps was repaired.

The Teflon mechanical-type seals on one of the main feedwater pumps were changed to a new style.

One of the charging pumps was completely repacked.

February 1970 (Ref. 4)

One of the condensate pumps was disassembled, the lower pump shaft was straightened, and four new shaft bearings were installed.

Two seal-water booster pumps were installed for the main feedwater pumps.

The discharge valves in one of the compressors in the instrument air system were replaced.

The damaged outlet valve on one of the seal-water filters was repaired.

Leaking tubing fittings on two of the level transmitters for the pressurizer were repaired.

March 1970 (Ref. 4)

Both pressurizer-spray valves were repacked.

The ruptured tubes and the inlet expansion joint on the condensate cooler were repaired.

The oil pump was replaced on one of the auxiliary feedwater pumps.

The severely damaged motor and internals of one of the two heater-drain pumps were repaired. The damage had occurred because a setscrew for the pump-throttle bushing came loose, lodged in the seat of the discharge check valve for the pump, and caused the pump to rotate backward when shut down.

The pump plungers and throat bushings on one of the charging pumps were replaced, and the pump was repacked.

New Satellite plungers, spacers, and throat-bushing sleeves were installed on another charging pump, and the pump was repacked.

The failed pump associated with the gas and particulate monitor for the auxiliary building was rebuilt.

April 1970 (Ref. 4)

The leaking inboard and outboard-shaft seal assemblies on a main feedwater pump were changed from the Teflon-insert type to a new type with no inserts.

Both sleeve nuts and the inboard motor bearing for another main feedwater pump were replaced, and the outboard seal was cleaned and reassembled.

A boric acid transfer pump that had seized was replaced.

A failed inboard bearing that had caused the pump for a waste-gas compressor to seize was replaced.

A condensate pump was completely overhauled by replacing the shaft with a two-piece shaft and rebabbitting the lower guide bearing for the motor.

Packing shafts for two of the personnel-hatch outer doors were replaced with stainless-steel shafts; grease fittings were installed on the stuffing boxes, and the stuffing boxes were repacked.

A bronze gear was replaced in the discharge valves for each of two auxiliary feedwater pumps.

A reactor coolant pump was completely disassembled so that new gaskets could be installed on the pump bowl.

A loose lower separator plate in one of the moisture separators was repaired. The plate-to-shell weld had cracked and failed on each side from 6 to 7 ft back from the inlet edge. Backup plates were also installed over the weld areas that had failed.

Two leaking tubes in the condenser were plugged, and a 2-in. makeup-water distribution header was replaced with a stainless-steel multihole header to improve deaeration of the makeup water.

A leaking cover diaphragm for the manway to a high-pressure feedwater heater was replaced.

The stem and plug in the power-operated atmospheric relief valve for one of the main steam lines were replaced.

A valve body was replaced on one of the pressurizer-spray valves. A defect in the body had been confirmed by X-raying the casting.

All connections on the isophase ground system for the main generator were inspected and cleaned, and the loose grounding lugs were tightened.

May–December 1970 (Ref. 5)

All the 10th stage and four of the 11th stage blades were replaced on a low-pressure turbine because of damage from a foreign object in the turbine.

A separate leakoff-collection system for the glands of the charging pumps was installed. The collection system was vented to the vent header, and the collected leakoff was pumped back to the three containment-vessel collection-system holdup tanks instead of to the waste-holdup tank.

Pipe stabilizers were installed on the main steam lines to the turbine to prevent pipe vibration which had restricted full-power operation.

The outboard seals in one of the feedwater pumps were replaced.

Eighty-four high-efficiency particulate-air (HEPA) filters and 84 prefilters were replaced, and the filter framework was reinforced.

A new style single-sleeve-type seal was installed on a main feedwater pump.

All 56 anchor bolts for a primary coolant pump and steam generator were replaced because 4 anchor bolts were found broken. The new bolt material was ultrasonic and magnetic-particle tested, and double nuts were installed on the new anchor bolts and only tightened hand tight.

A total of 239 reheater U-tube bundles were either repaired or plugged.

The B-phase-regulating-potential transformer for one of the generators was replaced because of a failure of the windings.

Faulty servo cards were replaced in the solid-state control system for the EH governor for the turbine.

Both source-range BF_3 detectors were replaced because of noisy output.

Two primary-system RTDs were replaced.

A seal of new design was installed in the main feedwater pump because the previous seal had a short lifetime.

The original plungers in the charging pumps were replaced with tungsten carbide plungers that have somewhat longer lifetimes.

Stainless-steel first-stage impellers were added to the condensate pump as an interim measure against cavitation. (The cause of the cavitation was traced to a design deficiency, and impellers of new design will be installed.)

In steps to alleviate high-temperature-induced materials problems, bearings were replaced and rotor journals were reworked in the canned-type boric acid transfer pumps and evaporator pumps.

REFERENCES

1. *Hearings Before the Joint Committee on Atomic Energy, Congress of the United States, Ninety-First Congress, Second Session on Civilian Power Reactors, Mar. 11, 1970, Part 3,* pp. 1131-1190, Superintendent of Documents, U. S. Government Printing Office, Washington, 1970.
2. Rochester Gas & Electric Corp., Robert Emmett Ginna Nuclear Power Plant, Unit 1, Final Facility Description and Safety Analysis Report, Amendment 6, Vol. 1, USAEC Report DOCKET-50244-1, Jan. 24, 1968.
3. Rochester Gas & Electric Corp., Robert Emmett Ginna

Nuclear Power Plant, Unit 1, Final Facility Description and Safety Analysis Report, Amendment 6, Vol. 2, USAEC Report DOCKET-50244-2, Jan. 24, 1968.

4. Rochester Gas & Electric Corp., Robert Emmett Ginna Nuclear Power Plant, Unit 1, Semiannual Report No. 1, Nov. 9, 1969–Apr. 25, 1970, USAEC Report DOCKET-50244-44, June 24, 1970.
5. Rochester Gas & Electric Corp., Robert Emmett Ginna Nuclear Power Plant, Unit 1, Semiannual Report No. 2, Apr. 26, 1970–Dec. 25, 1970, USAEC Report DOCKET-50244-66, Feb. 23, 1970.
6. Rochester Gas & Electric Corp., Robert Emmett Ginna Nuclear Power Plant, Unit 1, Failure of Main Steam Line Isolation Valve To Close, USAEC Report DOCKET-50244-42, May 22, 1970.
7. Rochester Gas & Electric Corp., Robert Emmett Ginna Nuclear Power Plant, Unit 1, Malfunction of Core Deluge Valve, USAEC Report DOCKET-50244-51, Oct. 14, 1970.
8. Rochester Gas & Electric Corp., Robert Emmett Ginna Nuclear Power Plant, Unit 1, Malfunction of Containment Sump Valve, USAEC Report DOCKET-50244-52, Oct. 23, 1970.

Operating Experience at the Nine Mile Point Reactor

By Myrna L. Steele*

The Nine Mile Point Nuclear Station, located in Oswego County, N. Y., and owned by Niagara Mohawk Power Corporation, is a 500-MW(e) direct-cycle boiling-water reactor (BWR). Criticality[1] was achieved on Sept. 5, 1969, and the initial licensed power of 1538 MW(t) was reached on Jan. 18, 1970, although the plant had gone into commercial operation the previous month. By Dec. 31, 1970, the plant had produced about 2×10^6 MW(e)-hr.

On Apr. 20, 1970, the Niagara Mohawk Power Corporation requested permission to increase the power level to the design rating of 1850 MW(t), or 625 MW(e). On Feb. 6, 1971, the Advisory Committee on Reactor Safeguards (ACRS) reported favorably on this request.

The core lattice[2] for the Nine Mile Point reactor approximates a cylinder with an equivalent diameter of 156.12 in. and an active length of 144 in. The four-zoned core is comprised of 532 Zircaloy-clad slightly enriched UO_2 fuel-element assemblies and 129 cruciform-shaped B_4C movable control rods. The fuel elements are held in place by upper and lower grid plates that are supported from the stainless-steel shroud which surrounds the core and which acts as a barrier to separate the core cooling water and the downcomer recirculation flow. The control rods are mounted in guide tubes that extend from the control-rod-drive housings through the lower core grid plate.

OPERATIONS

Fuel loading began[3] at Nine Mile Point on Aug. 23, 1969, and was completed September 4. Initial criticality was achieved at 1:09 p.m. on September 5. During the process of bringing a pressure regulator for the steam system into service on October 5, a high-pressure signal from the primary system initiated an automatic reactor trip. The reactor was returned to service but was manually scrammed the next day for adjustments and repairs to the pressure regulator. The reactor was brought back to criticality on October 9.

On October 11 the reactor was scrammed from 20 MW(t) by a low-water-level signal on a channel of the protection system, followed by a high intermediate-range neutron-flux signal on the second protection-system channel. These system disturbances were initiated by operator error. The reactor was brought back up, and the next day the reactor was automatically tripped when the main-steam-line isolation valves were closed as a test at the rated pressure. After the reactor was returned to service, water hammers in the steam lines to the emergency condenser caused the reactor to be manually scrammed. The reactor remained shut down from October 12 to 18 so that drain lines could be installed in the steam lines to the emergency condenser. The drain lines eliminated the water hammer that was being caused by flashing when the unit was started up.

After having been returned to service on October 18, the reactor was automatically tripped on October 23 when the operator failed to switch ranges on the neutron-flux intermediate-range monitor. On October 26 the plant was intentionally shut down because a factory radiograph indicated a crack in the body of a recirculation-pump discharge valve. A field radiograph disclosed no crack. While the plant was down, a test of the electromagnetic relief valves

*U. S. Atomic Energy Commission, Division of Technical Information Extension, Oak Ridge, Tenn. 37830.

revealed leaking seats in the valves. The seats were relapped, and the damaged internal cones on the discharge expansion bellows of the relief valves were replaced.

The reactor was returned to service on November 1 and held at minimum thermal power for testing at rated pressure and temperature. The next day the turbine was rolled at about 16% power for balancing measurements. Following these measurements, reactor pressure was lowered below 600 lb to allow taking the turbine out of service for balance-weight installation. When again the reactor was brought up to critical for continued turbine testing, the reactor was scrammed because of a feedwater-control malfunction. The reactor was again brought critical but was again scrammed by an oscillation of the control sensor for the reactor coolant level. The reactor was immediately returned to service for continued no-load testing. Tests during this period included control-rod-drive (CRD) scram and friction measurements and turbine-control and -balance testing. When the turbine was not rolling, the reactor was held in hot-standby condition.

On November 8 a malfunction of the feedwater control system initiated a high-neutron-flux scram from two channels of the intermediate-range-monitor system. The reactor was immediately restarted, and the next day the generator was phased to the line for the first time. On November 10 a malfunction of a pressure regulator again caused the reactor to scram. The reactor was again brought critical, and the pressure was increased to 530 psig on November 11. The reactor was then shut down so that a bearing could be replaced in the CRD pump and so that repairs and adjustments on the steam regulator could be continued. As a test, the operator had manually switched an intermediate-range flux monitor downrange on each safety channel, and this scrammed the reactor.

The plant was returned to the line and 2 days later was again scrammed by a malfunction of the pressure regulator. The regulator had caused a rapid opening and closing of the bypass valves which resulted in a pressure spike and then an overpressure trip signal. The reactor was returned to service for continued startup testing until November 21, when it was shut down for 16 days to change the inner filters on all the control-rod drives (CRDs). Shutdown was accomplished by completion of the startup test calling for closure of the main-steam-line isolation valves.

For about 6 weeks prior to the November 20 shutdown,[4] 30 of the control rods had been hooked to a brush recorder to monitor scram times for these control rods. During this time the 30 rods had averaged 4.17 sec for 90% insertion, compared to the original 90% insertion times of 3.00 sec for all rods. During a scram on November 20, one rod had a scram time that exceeded the 5.3-sec Technical Specifications limitation by 0.02 sec. Since similar excessive scram times had been experienced at Oyster Creek 1 because of partially plugged 400-mesh strainers in the inner rod drive, it was decided to replace the strainers with 10-mil strainers. At the same time, a leaking tube in the nonregenerative heat exchanger for the cleanup system was plugged.

On December 7 the plant[5] was returned to the line, and the first commercial power was generated on December 14. On the same day a turbine trip–reactor scram was initiated by a high-flux-level signal caused by a pressure spike. The reactor was returned to the line and, later in the day, was scrammed by a high-pressure signal from the condenser. On December 15, after the reactor had been returned to the line, a level switch in the moisture separator inadvertently tripped and caused a turbine trip–reactor scram.

From December 20 to 22, the steam plant was placed in hot standby so that the vent lines on the high-level trips for the moisture separator could be relocated and snubbers could be added to the supports for the steam bypass lines. On December 21, with the steam system in hot standby and the reactor critical, the reactor was scrammed while a functional check-out of the flow comparator for the average-range power monitor (ARPM) was being made.

The plant was returned to the line on December 22 but had to be scrammed manually on December 24 because icing at the cooling-water intake had caused the primary-system water temperature to become excessive. Later that day the plant was returned to the line where it remained until December 30, when it was manually scrammed because of an indication of no recirculating-water flow during a trip test of five of the pumps. A subsequent investigation showed that the zero flow had been indicated because of a temperature difference between the two water legs of the flow instrumentation. This problem was corrected by installing additional insulation in the water legs.

Final stages[5] in the startup program were completed in February 1970. On January 9, with the reactor power at almost half the rated value, a reactor shutdown was initiated so that the clutch for the shaft-driven feedwater pump could be adjusted. When these adjustments were completed, the plant was returned to service. On January 12, with the plant load at about 360 MW(e), a load reduction test was ef-

fected. This reduction test initiated a turbine trip that, in turn, caused the reactor to scram on a high-flux signal.

The plant was returned to the line, and on January 19, during testing activities, the turbine was tripped because of high moisture-separator level indications. Subsequent to the turbine trip with the plant at 800-psig hot standby, a reactor scram was initiated by a false low-condenser-vacuum signal that was generated during repairs to the turbine governor. The reactor was brought back to critical, and the power level was increased to about 410 MW(e) for turbine- and generator-trip tests.

The plant was returned to an output of about 350 MW(e) until February 8, when a scram was initiated by a turbine trip when a ramp decrease in power was induced by using the recirculation pumps. On February 14, closure tests of the main-steam-line isolation valves resulted in an expected reactor scram, and startup testing was completed on February 16.

On February 17 an oil leak at the reduction gear for the main-generator exciter necessitated a manual scram. Subsequent to repairs, the plant was returned to service, and on February 20 another oil leak at the reduction gear for the main-generator exciter initiated an emergency generator trip that resulted in a high-neutron-flux signal and scrammed the reactor. The reactor was brought back to critical 5 days later, and, as the steam system was being brought into service, a low-low water-level signal was generated while the cleanup system was being changed from the low-pressure to the high-pressure control valve. This signal scrammed the reactor, but an immediate restart was made.

On March 2 excessive vibration in the reduction gear for the main-generator exciter caused the reactor to be shut down. During the outage for the removal and replacement of the gear for the main-generator exciter, small cracks were found in a safe end for one of the core spray nozzles.[5,6] Extensive investigations and repairs extended the plant outage to July 12, 1970.

On July 4, 1970, after the reactor[7] had been brought back to critical subsequent to the 4-month shutdown to repair the reactor-vessel safe ends, a low-reactor-water-level signal initiated a scram. The pumps for the CRD system were being used as reactor feedwater pumps during the startup, and the steam generation had exceeded the pump capacity. On July 12 the generator was phased to the line, and the plant was again generating electricity.

On July 20, large pressure oscillations occurred when operations personnel switched from an electric pressure regulator to a mechanical pressure regulator and caused a high-pressure signal that tripped the plant off-line. The plant was returned to service that day and was scrammed again the next day. This scram was caused by a high-neutron-flux signal that was generated by a turbine trip that had resulted from a high-level moisture-separator signal following a rapid 200-MW load reduction. This was a test of the station capability to make rapid load changes within the range of the recirculation flow control of reactor power and showed that the operation of the moisture separator was the most limiting function. Major design changes in the moisture-separator reheater systems are in progress. The plant was returned to the line and on July 28 was again separated from the line by an inadvertent operation of high-flow sensors in the main steam line during surveillance testing. The plant was returned to service, where it remained until August 8.

On August 8 a disturbance of the feedwater flow-control system during surveillance testing tripped the plant off-line for about 10.27 hr. The trip resulted from a low primary-system water-level signal that had been caused by the feedwater-system disturbance. The plant was returned to service that day and remained at base-load power until October 9.

During October the plant was out of service for 228.43 hr. Since the unit was scheduled to be shut down for reactor-operator-licensing examinations, the plant was left off-line when it was scrammed on October 9. The scram had occurred when pressure oscillations had been induced by switching from an electrical pressure regulator to a mechanical pressure regulator in the primary system.

Subsequent to the maintenance activities and operator examinations, the plant was returned to the 500-MW(e) level. The station was shut down on Nov. 14, 1970, for a scheduled outage to repair a leaking flange on the second stage of the reheater-drain tank. The plant was returned to service 41.92 hr after shutdown and remained there until December 4.

On December 4 a low primary-system water-level signal initiated a scram. Two of the three reactor feedwater pumps were being used to supply the reactor when one of the operating pumps tripped out. This caused the low-flow signal that tripped the reactor. As the reactor was being restarted, a failure of valve-seat bolts caused one of the steam-admission valves on the turbine to stick. The outage was extended for 391.75 hr for inspection and repair of the turbine-control valves.

MAINTENANCE, MODIFICATIONS, AND REPAIRS

The items listed below are selected from the referenced reports to give the reader an idea of the minor, but noteworthy, problems that can be encountered during routine operations.

Plant Systems

September 1969 (Ref. 3)

Two control-rod drives (CRDs) were overhauled, and one of these was installed in-core.
A third CRD was removed from the reactor.
The feet on a moisture separator interfered with the vibration sensors in the reactor vessel, and so $4\frac{1}{4}$ in. was removed from the feet, and one hold-down bolt was shortened.
Several leaks found during hydrostatic testing of the primary system were repaired, and the vessel-head insulation and the piping were installed.
A coupling capacitor was installed on one of the breakers.
An air compressor on a second breaker was overhauled.

October 1969 (Ref. 3)

The check valves were removed from the steam bleed line for the emergency condenser to the main steam line, and provisions were made for the automatic closure of the bleed-line isolation valves on a signal for isolation of the reactor vessel.
Additional drain connections were installed in the horizontal portion of the steam supply lines to the emergency condenser to ensure complete drainage of any trapped condensate.
A new seat was installed in a scram inlet valve for one of the CRDs.
Three of the CRDs were overhauled, and one was installed in the reactor vessel.

December 1969 (Ref. 3)

Six CRDs were replaced with rebuilt CRDs, and the drives that were removed from the reactor vessel were overhauled.
The mechanical seals were replaced on the electric and the motor-driven feedwater pumps.
The clutch on the shaft-driven feedwater pump was overhauled, and the pump was realigned.
Additional hangers and snubbers were installed on the bypass steam piping for the turbine.

January 1970 (Ref. 5)

New hangers and supports were installed for the condenser-bypass piping because piping motion had caused some of the original supports to break.
All welds in the condenser-bypass piping system were inspected using the dye-penetrant method because of the motion.
A 2-in. ventilation tie line was installed between the drain line and the ventilation line on each of the four moisture separators.
A broken tube that had been plugged previously was anchored inside the nonregenerative heat exchanger for the cleanup system.
Three CRDs were changed because of excessive in-leakage.
Seals on the two scram inlet valves were replaced.
Position-indicator probes for eight CRDs were removed and repaired.
Three breakers that had been damaged by a fire, caused by loose connections, were repaired.
The force-control clutch for the shaft-driven feedwater pump was disassembled and repaired.
New valve rings and instrument connections were installed on one of the intercept valves.

February 1970 (Ref. 5)

Three CRDs that had been removed in January were rebuilt.
The inboard and outboard seals on two of the feedwater pumps were rebuilt.
A new seat was installed on a scram inlet valve.
The exciter reduction gear was dismantled and repaired because of an oil pipe break.
New bearings and seals were installed on a CRD supply pump.
Two seats on the isolation valves for the condensate return to the emergency condenser were lapped.
The seats of the check valves for the second stage on two of the reheater-stop systems were lapped.
One of the check valves in the feedwater system was disassembled, and a defective Teflon seat was removed.

March 1970 (Ref. 5)

A new outboard bearing and new internals were installed in a CRD supply pump.
An inboard bearing was replaced on a feedwater pump.
New internals were installed on three recirculating-water valves in the feedwater system.
A new seat ring was installed on a scram inlet valve.
All safe ends on the reactor vessel and the reactor-vessel head were inspected by X-ray, dye-penetrant, and ultrasonic techniques.
Position-indicator probes for four CRDs were removed and repaired.
The thermocouples on all 129 position-indicator probes for the CRDs were grounded.

April 1970 (Ref. 5)

The safe ends for both core spray nozzles were replaced with new nonsensitized stainless-steel safe ends.
A reducing elbow at the connection for the safe end on each core spray line was replaced with a smaller elbow and a straight reducer.
A new support system for the core spray piping was installed in the dry well.
An electrical interlock was installed between the turbine-building exhaust fan and the reheater-system drying fans.
The 2-in. vent tie that was installed in January was replaced by a 6-in. vent system.
A bearing and a hydrogen seal on the exciter end of the generator and new insulation for the bearing were installed.
New impellers and a shaft were installed on a supply pump to a CRD.

May 1970 (Ref. 5)

New impellers were installed on a supply pump for another CRD.
One CRD was replaced.
Position-indicator probes for three CRDs were removed and repaired.
The Limitorque switch on the main steam valves was repaired and reset.
New flexible hoses were installed on the drying system for the reheaters.

June 1970 (Ref. 5)

Flange gaskets were replaced on an emergency check valve.
Flange O rings were replaced on two CRDs.
Position-indicator probes for two CRDs were repaired.

July 1970 (Ref. 7)

One CRD was replaced, and O rings were replaced at the flanges of two other CRDs.
A seat was replaced on a scram inlet valve for a CRD.
The O rings in a hydraulic accumulator for one of the CRDs were replaced.
New internals were installed in a feedwater pump, and the strainers (used for startup) were removed from the suction line.
Leaks in the air supply to all scram valves in the CRD system were repaired.
A burned-out motor on an oil cooler for the main transformer was replaced.

August 1970 (Ref. 7)

The mechanical seals on one of the cleanup pumps were replaced.
New internals were installed on another feedwater pump, and the strainer was removed from the suction pipeline.
The sump pumps in the screenhouse were rebuilt.
The bearings on one of the a-c generators were replaced.
The brushes on the motors for two recirculating-water pumps were replaced.
The O rings in a hydraulic accumulator for another CRD were replaced.
A feedwater pump was dismantled to remove debris from disintegration of the startup strainer.

September 1970 (Ref. 5)

New internals were installed in the dismantled feedwater pump.
A rebuilt perimeter-drain pump was installed.
The O rings were replaced in the hydraulic accumulator for another CRD.
A 115-kV breaker was overhauled.

October 1970 (Ref. 7)

The safety valves for a moisture-separator reheater were overhauled.
The Limitorque switch on a feedwater valve was repaired.
The hold-down bolts on the mechanical seals of all the recirculating-water pumps were replaced by bolts of a new material.
The gaskets on a feedwater-flow orifice were replaced.
The gaskets in the check valve to an emergency condenser were replaced.
Three CRDs were replaced.
The O ring on a flange of a CRD was replaced.
The position-indicator probes for eight CRDs were replaced.
The seat on an inlet scram valve was replaced on a CRD.
The seal housings on a feedwater pump were replaced with housings of a new design.

November 1970 (Ref. 7)

The mechanical seals on a cleanup pump were rebuilt.
The expansion joints on three of the condensate pumps were replaced.

December 1970 (Ref. 7)

All turbine-control valves were dismantled; all valve seats were removed, machined, and reinstalled; the seats were pinned to the valve bodies with 1-in. pins; and the valves were reassembled.
The shrinkage cracks in the body of the drain valve for the moisture separator were ground out and rewelded.
Position-indicator probes for six CRDs were replaced.
Two CRDs were replaced.
The pilot valve on one of the electromagnetic relief valves was overhauled.
Two of the diesel generators were realigned.
New equipment for measuring the temperature and the differential level was installed in the cooling-water intake and discharge tunnel.
A new thrust collar and thrust shoes were installed on a feedwater booster pump.

ACKNOWLEDGMENT

I would like to thank M. A. Silliman, Results Supervisor, of the Nine Mile Point Nuclear Station for his very helpful comments and suggestions.

REFERENCES

1. *Hearings Before the Joint Committee on Atomic Energy, 91st Congress, Second Session on Civilian Power Reactors, March 11, 1970, Part 3,* pp. 1131-1190, Superintendent of Documents, U. S. Government Printing Office, Washington, 1970.
2. Niagara Mohawk Power Corporation, Nine Mile Point Nuclear Station, Final Safety Analysis Report, Amendment 2, Volume 1, USAEC Report DOCKET-50220-9, June 1, 1967.
3. Niagara Mohawk Power Corporation, Nine Mile Point Nuclear Station, Semiannual Report of Operation, August 23–December 31, 1969, USAEC Report DOCKET-50220-46, July 10, 1970.
4. Niagara Mohawk Power Corporation, Nine Mile Point Nuclear Station, Results of Pre-Operational Control Rod Scram Tests, USAEC Report DOCKET-50220-29, Dec. 6, 1969.

5. Niagara Mohawk Power Corporation, Nine Mile Point Nuclear Station, Semiannual Report of Operation, January 1–June 30, 1970, USAEC Report DOCKET-50220-55, Dec. 9, 1970.
6. Niagara Mohawk Power Corporation, Nine Mile Point Nuclear Station, Temporary Change in Technical Specifications, USAEC Report DOCKET-50220-36, Mar. 11, 1970.
7. Niagara Mohawk Power Corporation, Nine Mile Point Nuclear Station, Third Semiannual Report of Operation, July 1, 1970–December 31, 1970, USAEC Report DOCKET-50220-58, Feb. 18, 1971.

Suggested Reading List

Niagara Mohawk Power Corporation, Nine Mile Point Nuclear Station, Reactor Primary System Investigation, Report DOCKET-50220-40, May 1, 1970.

Niagara Mohawk Power Corporation, Nine Mile Point Nuclear Station, Reactor Primary System Investigation Report No. 2, Report DOCKET-50220-42, May 11, 1970.

Niagara Mohawk Power Corporation, Nine Mile Point Nuclear Station, Program for Restoration to Service: Based on Reports of Primary System Investigation, Report DOCKET-50220-41, May 11, 1970.

Niagara Mohawk Power Corporation, Nine Mile Point Nuclear Station, Request for Amendment to License To Increase Power Level, USAEC Report DOCKET-50220-39, Apr. 20, 1970.

Niagara Mohawk Power Corporation, Nine Mile Point Nuclear Station, Technical Supplement to Petition To Increase Power Level, First Addendum, USAEC Report DOCKET-50220-49, Oct. 12, 1970.

Niagara Mohawk Power Corporation, Nine Mile Point Nuclear Station, Technical Supplement to Petition To Increase Power Level, Second Addendum, USAEC Report DOCKET-50220-50, Oct. 29, 1970.

Niagara Mohawk Power Corporation, Nine Mile Point Nuclear Station, Technical Supplement to Petition To Increase Power Level, Third Addendum, USAEC Report DOCKET-50220-54, Dec. 4, 1970.

Niagara Mohawk Power Corporation, Nine Mile Point Nuclear Station, Technical Supplement to Petition To Increase Power Level, Fourth Addendum, USAEC Report DOCKET-50220-56, Dec. 22, 1970.

Operating Experience at and Physics Characteristics of SEFOR

By Myrna L. Steele*

The operations summary presented here is basically problem or malfunction oriented and is written with the premise that all systems are functioning satisfactorily unless otherwise noted. An attempt has been made to gather information on the operations problems and component malfunctions so that it can be tabulated or otherwise assembled for whatever use the reader may make of it. This is simply a digest of several reports to present their most essential content as an objective, open account. It should be emphasized that no attempt has been made to evaluate the material. The reader should note that a Suggested Reading List is included which contains references to detailed topical reports on the SEFOR project.

The Southwest Experimental Fast Oxide Reactor (SEFOR) is a 20-MW(t) sodium-cooled fast test reactor that is fueled with mixed PuO_2–UO_2. The reactor is located about 19 miles south-southwest of Fayetteville, Ark., and is owned by a group of 17 investor-owned electric utilities called Southwest Atomic Energy Associates (SAEA). General Electric Company operates the reactor.

The SEFOR core[1] was designed with characteristics similar to the large, soft-spectrum fast breeder reactors so that physics and engineering data may be obtained for compositions, temperatures, and crystalline states for fuels for these large power reactors. The primary purpose of the experimental measurements made in SEFOR will be for evaluating and identifying reactivity coefficients, particularly the Doppler coefficient, which are important to fast reactor development.

*U. S. Atomic Energy Commission, Division of Technical Information Extension, Oak Ridge, Tenn. 37830.

The core is 34.7 in. in diameter (cylindrical equivalent) and has an active fuel length of 33.8 in. One-hundred-nine hexagonal stainless-steel-clad fuel elements, enriched to 18.7% ^{239}Pu and ^{241}Pu, comprise the active part of the core. Each of these fuel elements is, in turn, made up of six fuel rods and one central BeO tightener rod. In-core positions are also provided for six instrumented fuel assemblies and a maximum of 18 fixed (in-core) B_4C control rods; the core is surrounded by 10 movable reflector pieces (36° segments) that are used for reactor control.

OPERATIONS HIGHLIGHTS

By April 1969 the preoperational testing[2] of SEFOR was completed, the reactor-building personnel and emergency-access locks were placed in service, and pressure control was established in the building. The reactor-vessel head was removed on April 6, and fuel loading was begun on April 8. Malfunctions of some of the fuel grapples necessitated that the grapples be bagged out of the refueling cell, and a man-entry into the refueling cell was required to repair two low speeds on the 10-ton hoist because the speed control had become inoperative during the fuel-loading operations. Excessive plugging temperatures of the primary sodium necessitated suspending fuel-loading activities for about three shifts so that cold trapping could reduce the temperature to <225°F. Thereafter, frequent cold-trap operation kept the plugging temperatures at <225°F, and a 500 gal/min sodium flow rate maintained a very clean sodium surface. By the end of April about 91 fuel elements had been loaded into the core.

During the February–April 1969 quarter, a major overhaul of the emergency diesel was required after the

engine developed leaks from the water cooling system into the crankcase and cylinder. Sleeves and pistons were replaced on eight cylinders, and the piston rings were modified to prevent scoring. Metal particles from the scored pistons also had passed through the turbochargers, and so both of these were replaced.

A modification of the man-entry-suit system was necessitated by a collapse of one of the suits on Apr. 5, 1969, as two operators were preparing to make a routine exit from the refueling cell. While the operator with the failed suit was being assisted through the emergency exit, the other operator made a routine exit. An investigation revealed that the normal air-supply line which provides air for both suits had iced closed and that the emergency air supply for the suits had to be relied on. In the suit that failed, the modulating vacuum-exhaust valve had become clogged with lint and could not close fully. As a result the vacuum-exhaust system reduced the pressure in the suit, and the suit collapsed. As corrective steps, a valve that will close when the normal air supply is lost was installed in the suit, a low-pressure alarm was added to the suit, and the air-refrigeration system was provided with a manually valved bypass so that normal air flow could be restored if the cooling line iced closed. Additional safety procedures were also invoked.

After initial criticality[3,4] was achieved on May 3, 1969, startup testing was begun immediately, and 133 startups were made in the May–July quarter. Of the 20 reactor scrams that occurred, 4 were manually initiated as specified by test procedures; of the other 16, 12 were from noise in the neutronics instrumentation, 2 from low accumulator pressure that occurred when a reflector was dropped manually, 1 from an operator's failure to switch ranges on a neutronics channel, and 1 from low flow caused by a malfunction of the flow controller in the main line of the primary sodium system. Total operating time for the reactor over the May–July quarter was about 140 hr. Although most of the startup tests were conducted at about 400 W, a maximum power of approximately 19 kW(t) was attained.

The reactor was operated for an extended period during the quarter with the pressure-vessel head removed. Accomplished at this time were the annual checks for containment leaks, as well as work on maintenance and modifications in the refueling cell and nitrogen zone. During operation without the vessel head, the sodium was maintained at the refueling level with a flow rate of about 500 gal/min, and frequent cold trapping kept a proper temperature to prevent plugging. When the vessel head was replaced and the reactor sodium level was raised so that reactor noise and reflector worth could be measured, the plugging temperature rose to about 340°F. This increase in plugging temperature was attributed not only to oxides that had formed on the upper structures during operation with the sodium at the refueling level but also to a decrease in the performance of the cold traps. Plugging in inappropriate places in the cold traps caused instabilities in sodium flow through the traps. The performance of the traps was improved not only by heating but also by carefully programming the temperature decreases.

After a planned 2-month outage[5,6] for leak checks of the containment and for maintenance, tests at essentially zero power were resumed on Sept. 1, 1969. Reactor startups numbered 154 during the tests, the majority of which were run at about 400 W. Of a total of 19 automatic scrams, 11 were caused by noise in the neutronics instrumentation, 7 were attributable to operator errors, and 1 was from an undetermined cause.

On Aug. 16, 1969, the thermocouple on the dome for the auxiliary intermediate heat exchanger (IHX) registered a temperature greater than full scale (1200°F). The primary sodium temperature at this time was 600°F. The IHX dome was vented, and the thermocouple reading returned to the 600° bulk-sodium temperature. Visual examinations and measurements gave no indication of distortion or damage, but reactor operations were suspended until a full analysis of the occurrence was completed. Results of the analysis indicated that the IHX dome had reached 900 to 1000°F.

On Sept. 15, 1969, during some routine test procedures, the emergency diesel failed to start. About 1.5 min later an overcrank alarm annunciated, and an unsuccessful attempt was made to start the diesel from the panel switch. The diesel started the second time the switch was actuated. An investigation showed that two of the starting motors had been wired incorrectly, and the diesel had been starting with one motor. The wiring error was corrected, and the starting motor and solenoid were repaired.

On Sept. 11, 1969, during an approach to critical, one of the wide-range monitors (WRM) indicated a decreasing power level whereas the other two showed the power to be increasing. The reactor was shut down, and the problem was traced to a broken positive high-voltage cable at the instrument chassis. The cable was repaired, and the WRM was returned to service. On October 15 another one of the WRMs did not respond correctly when a change in the range was initiated. A

defective solder joint in one of the coils in the range-switching relays had caused the erratic behavior.

The ground-detection relay on the 125-V d-c switchgear annunciated a ground alarm that was traced to a plug-in socket for one of the relays. Investigations revealed that the relays for one of the very-high-radiation containment-building monitors had failed. The relays and relay sockets were replaced, and all associated wiring and components were inspected and tested.

On Sept. 3, 1969, a reflector rundown occurred when a low-flux trip was actuated by a switching transient. The rundown action is initiated by a signal from a two-out-of-three coincidence logic, and subsequent investigations revealed that the contacts on one of the downscale-trip relays were stuck closed. The malfunction was repaired, and the electrical load on the contacts was checked.

By November 1 the zero-power testing program[7,8] was completed, and a planned outage was begun for maintenance and modifications prior to approach to power. On Jan. 10, 1970, the core was returned to the premaintenance configuration. The core was then rearranged to facilitate the imminent full-power operations, a criticality check was made, and one of the reflector segments was recalibrated. Subsequently 15 reactor startups were effected, and six automatic scrams occurred: two were caused by noise in the neutronics channels, three resulted from operator errors, and one was caused by a spurious trip from the primary-system low-flow indicator. A license for operation up to 20 MW(t) in the steady-state and pulsed modes was received on Jan. 2, 1970.

On Jan. 16, 1970, two failed silicon-controlled rectifiers in the inverter power supply caused a fuse to blow. The reactor was shut down at the time, and, since the inverter provides the power for the neutronic instrumentation in case of loss of off-site power, reactor operation was postponed until the inverter was repaired.

Zero-power testing continued[9,10] into the February–April quarter, and on March 20 the reactor was secured for an outage to repair and replace, where necessary, the thermocouples on the reflector guide structure. Fourteen reactor scrams occurred during the 192.4 hr of operation. Of these scrams, two were caused by malfunctions in the neutronics channels, two by operator errors, three by spurious low-level signals from the expansion tanks, three by full-scale failure of the thermocouples on the reflector guide structures, one by a spurious signal from the high-level indicator for the primary sodium system, one by a malfunction of a radiation monitor in the containment, and the remaining two were manual scrams.

Recurring failures of the thermocouples on the reflector guide structure in 1969 prompted a survey in November which showed that 8 out of 55 had failed. In March 1970 a second survey showed 16 open thermocouples and 8 reading incorrectly. Two additional thermocouple failures caused a reactor scram on March 7. After the scram a third survey showed 23 open thermocouples and 9 reading incorrectly. An alternate system that consists of replaceable thermocouples was designed, and installation was under way at the end of April. (Experience gained with the old and new thermocouple designs is discussed in Ref. 14.)

In February 1970 the oscillator rod was calibrated, and effects of the rod on core kinetics were observed at the maximum permissible reactivity amplitude. Since preliminary analyses of the static calibrations indicated a linear relation for the rod worth as a function of position for locations from 0 to 8 in. above core midplane, dynamic calibrations were carried out, using amplitudes of 2, 4, 6, and 8 in., from the full-out position to the full-in (core-midplane) position of the oscillator rod. A static-worth measurement was obtained by lowering the rod to a location 2 in. below core midplane. These data showed that the rod worth vs. position was not linear and that some of the dynamic-worth measurements had exceeded the Technical Specifications limits of ±10 cents. A site safety committee review determined that no safety problem had resulted but set procedural requirements for further testing with the oscillator rod.

On Apr. 23, 1970, when off-site power was lost because of an electrical storm, the emergency diesel started as it should have and supplied power until the off-site power was restored. However, when the diesel started, the louvers failed to open and had to be opened manually. A ground on the feed line to the oil-pressure switch kept the solenoid energized regardless of the position of the pressure-switch contacts, and this energized solenoid kept the louvers closed. The ground was eliminated, and the louvers operated properly.

The outage that began on March 20 was terminated[11,12] on June 26 when the replacement of the temperature-monitoring system on the reflector guide structure was completed. Eight scrams occurred during the 357 hr of operation in the May–July quarter. Four of the scrams were caused by spurious signals from either the nuclear or cooling-system instrumentation, two were attributed to operator error, one resulted from actuation of an undervoltage relay while a

nitrogen blower was being started, and one was caused by a high-winding-temperature signal from a main secondary pump.

On July 24, with the reactor at 5 MW(t), smoke was observed to be coming from the power supply for the auxiliary primary pump. A reflector rundown was immediately initiated, and the auxiliary primary pump was secured. Investigations revealed that the power supply had developed an open circuit on one set of windings. A spare power supply was installed, and capacitors were obtained to improve the power factor and reduce the load on the power supply.

MAINTENANCE, MODIFICATIONS, AND REPAIRS

Plant Systems

February–April 1969 (Ref. 2)

Resistance-temperature-detector (RTD) and thermocouple wells in the main primary and secondary systems were replaced with wells of a new design.
The seal between the refueling cell and the nitrogen zone was repaired.

May–July 1969 (Refs. 3 and 4)

A particulate-sample panel was fabricated for the reactor cover gas and gaseous-radwaste systems.
An additional argon vent was installed on the vacuum pump.
The clutch on the refueling-cell crane was repaired.
A rapid vent valve was installed on the primary drain tank.
A gate valve on the vacuum-distillation station was repaired.
Gasket seals between the refueling cell and the nitrogen zones were repaired.
A sampling device was installed in the NaK bubbler discharge.

August–October 1969 (Refs. 5 and 6)

I-type sodium-level probes were fabricated and installed in the reactor-vessel head.
A thin, all-welded cover plate was installed over the existing refueling-cell floor seal that encircles the reactor vessel.
The isolation valve and elbows were removed from the refueling cell, and the NaK that was deposited in the valve and elbows was removed by water.
The malfunctioning rupture diaphragms in the primary vent tank and on the argon cooling loop were replaced.
Check valves on the gaseous-radwaste header were cleaned and lapped.
Manual-reset oil-pressure switches on the gaseous-radwaste compressors were replaced with automatic-reset switches.
The motor bearings were replaced on a nitrogen blower.
The main bearings were replaced in a Freon compressor.
The fan bearings were replaced on a Freon condenser unit.
An additional vaporizer unit was installed on the liquid-nitrogen supply tank.

November 1969–January 1970 (Refs. 7 and 8)

Both primary-system cold traps were replaced.
One of the reactor-vessel sodium-level J probes was replaced.
The main IHX level probe was replaced.
A reactor cover-gas monitor was installed.
The stator on the blower motor for the nitrogen-circulation system was rewound.
The leaking seal on the shaft of the argon blower was replaced, and an oil bath was added.
A faulty time-delay relay in one of the main electrical buses was replaced.
Two failed silicon-controlled rectifiers in the inverter power supply were replaced.

February–April 1970 (Refs. 9 and 10)

Thermocouples were installed in the lower end of each reflector segment to monitor reflector-system temperatures.
Both the I and J probes for the reactor sodium-level-indication system were removed, cleaned and repaired, and replaced.

May–July 1970 (Refs. 11 and 12)

A new sodium-leak-detector system was installed to augment the six detectors on the auxiliary primary-IHX return to the reactor vessel.
Flow-control valves were added to the discharge lines of each of the two vacuum pumps on the argon-vent system.
A failed connector for the lower-region core thermocouples, located in the refueling cell, was replaced, and the thermocouples were restored to service.

Instrumentation and Control Systems

May–July 1969 (Refs. 3 and 4)

Transient-voltage suppressors were installed in parallel with all lower solenoids on the reflector segments to prevent recurring solenoid failure.
Two relays with burned contacts were replaced in the auxiliary primary-pump trip circuit.
A failed pair of detectors in the wide-range-monitor system was replaced.

August–October 1969 (Refs. 5 and 6)

A trip and an alarm for high- or low-pressure reactor-building isolation were installed for the ventilation makeup fan.

November 1969–January 1970 (Refs. 7 and 8)

A system to monitor the reactor cover gas for indications of fuel-cladding failures was installed and tested.
Ammeters were installed in the electric-power cables to each starting motor on the emergency diesel.

February–April 1970 (Refs. 9 and 10)

Position lights were installed on the louvers on the enclosure for the emergency diesel to indicate louver position in the control room.
An alarm that indicates an overspeed trip on the emergency diesel was installed to annunciate in the control room.
A time-delay relay was added to the period-scram-suppressor circuit.

May–July 1970 (Refs. 11 and 12)

An electrical interlock was added to the circuitry for the fast-reactivity-excursion device (FRED). This interlock prevents firing of the FRED unless all three latches are withdrawn.

LOW-POWER TESTING

Determination of Minimum Critical Core

Initial criticality[3,13] was achieved in SEFOR with 9 cents of excess reactivity at 1945 CDT on May 3, 1969, and the maximum power level attained by the end of July 1970 was 5 MW(t).

The core configuration (Fig. 1) with which initial criticality was attained consisted of 550 fuel rods (about 91 fuel elements), 96 BeO tightener rods, and no B_4C rods. Subsequent to the addition of 13 more fuel rods and 4 BeO tightener rods to the core periphery, the reactivity worths of the fuel rods were measured at different core locations. These measurements revealed that some of the rods were low in reactivity worth by as much as 40% when compared with a standard rod. An extensive investigation showed that these rods had an insufficient amount of plutonium. The very-low-worth rods were removed and replaced with rods from the core periphery. With this configuration a minimum critical loading (Fig. 2) of 522 rods and 100 BeO tightener rods was achieved. Some of the fuel rods were then moved to the core periphery, and B_4C rods, as well as additional fuel and BeO tightener rods, were added to completely fill the 108 fuel-element channels. This full-size core loading (Fig. 3) is the configuration that was used for the low-power tests that will be summarized in this article.

For this discussion the tests are divided into two types: (1) basic physics (neutronics) characteristics and (2) integral physics parameters pertinent to reactor operation. The first type includes material worths, fission-rate distributions and fission ratios, and noise measurements to determine l/β; the second type includes reflector calibrations, flow and pressure coefficients of reactivity, temperature coefficients of reactivity, and zero-power-reactivity transfer functions.

Neutronics Characteristics

Material Reactivity Worths. Although some material-worth measurements were made in the second core configuration in SEFOR, extensive data were not obtained until the fourth configuration.[5,13]

The reactivity worths of fuel (18.7% fissile Pu), B_4C, stainless-steel, guinea-pig (25% fissile Pu), depleted-UO_2, and BeO tightener rods were measured at the several locations shown in Fig. 4.

The reactivity-worth data were obtained by recording reactor temperature and critical reflector position with:

1. The original fuel rod in place.
2. The fuel rod removed and this location filled with the sodium coolant.
3. The original fuel rod replaced by one of the following: the reference fuel rod, a B_4C rod, a stainless-steel rod, a guinea-pig rod, or a depleted-UO_2 rod.
4. The original rod reinserted.

The worths of the BeO tightener rods were determined by replacing the original BeO rods with special stainless-steel tightener rods. The results of the reactivity-worth measurements are shown in Figs. 5 to 8 with the calculated values included for comparison. The calculated reactivity worths (shown in the curves) were obtained from one-dimensional perturbation-diffusion codes.

Neutron Fission-Rate Distributions and Fission Ratios. Foil-activation techniques[7,9,13] were used to measure the spatial distribution of the fission rates for ^{239}Pu, ^{238}U, and ^{235}U. In addition, fission ratios were determined at core center from the ^{140}La decay.

The spatial distributions of the fission rates were obtained by irradiating fission foils at selected radial locations for about 1 hr at a nominal reactor power of 1 kW and then using scintillation methods to obtain count rates. Figure 9 illustrates the scheme used to designate fuel-rod positions in the SEFOR core. The fission-rate-measurement positions are shown in Fig. 10. Calculated and measured-fission-rate distributions are shown in Figs. 11 to 18. The fission-rate distributions in rod FB near core center are shown in Figs. 11 to 13 for ^{239}Pu, ^{238}U, and ^{235}U, respectively; axial fission-rate distributions at the core radial boundary are shown in Figs. 14 and 15 for ^{235}U and ^{238}U, respectively; radial fission-rate distributions at 37 cm above core bottom are shown in Figs. 16 to 18 for ^{239}Pu, ^{235}U, and ^{238}U, respectively. The calculated values shown in the figures were obtained using both a 13-energy-group two-dimensional synthesis code and a two-dimensional diffusion code.

Additional count-rate data were taken on the foils that were near core center (position FB) to obtain the fission ratios. Table 1 compares the calculated cross-section ratios with the neutron-cross-section values that were obtained from measured fission-ratio data.

Noise Measurements. Neutron noise[7,13] was measured with two sensitive ^3He detectors that were mounted in the central channel of the core. The fluctuating components of the chamber current were amplified, digitized with a sampling frequency of 10^4 samples/sec, and recorded on magnetic tape. These

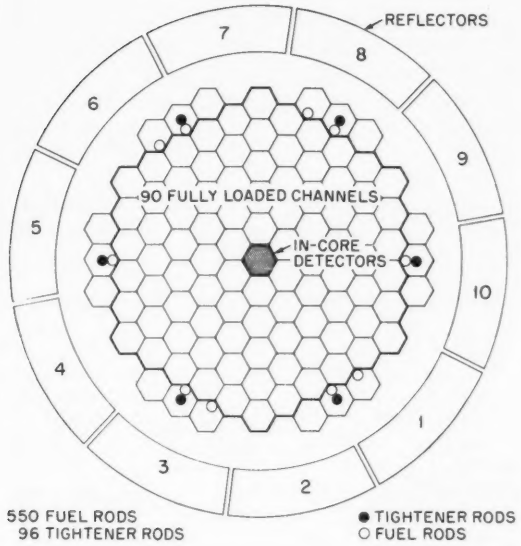

Fig. 1 SEFOR initial critical core loading.[13]

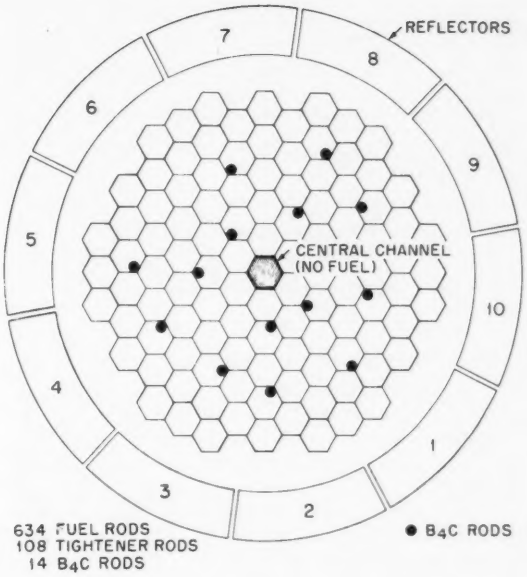

Fig. 3 Full-size core loading for low-power testing.[13]

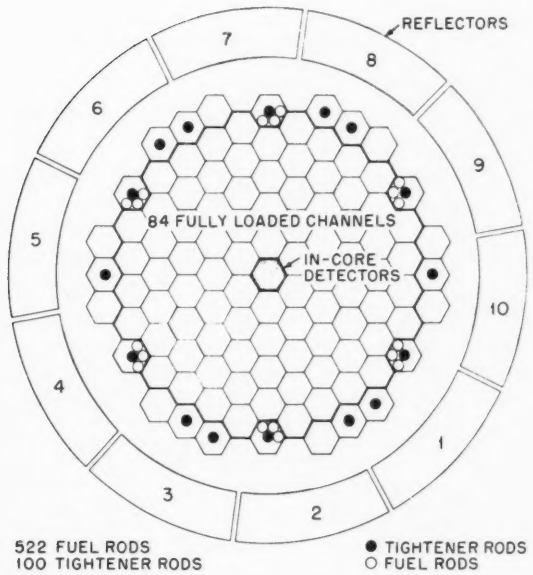

Fig. 2 SEFOR minimum critical loading.[13]

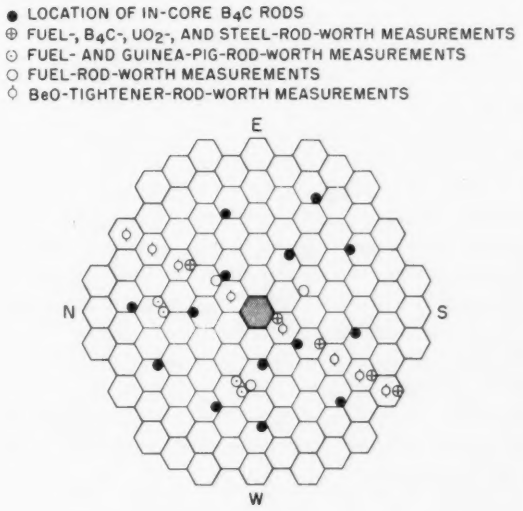

Fig. 4 Locations of material-worth measurements.[13]

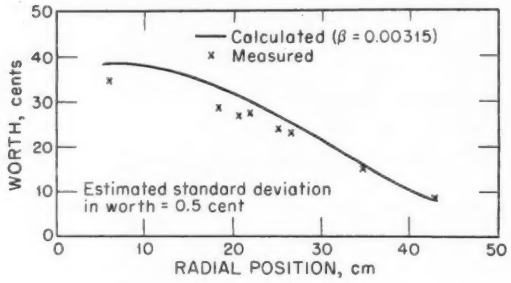

Fig. 5 Radial dependence of fuel-rod worth.[13]

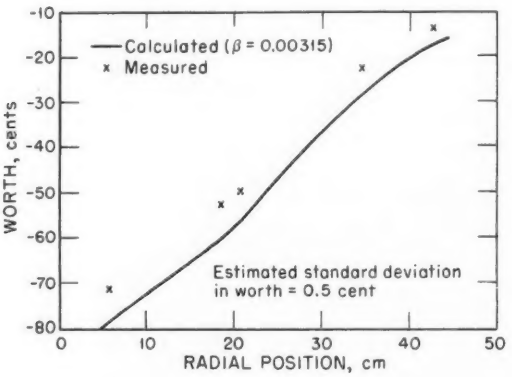

Fig. 6 Radial dependence of B_4C-rod worth.[13]

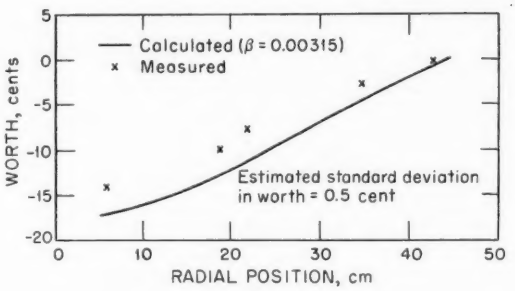

Fig. 7 Radial dependence of depleted-UO_2-rod worth.[13]

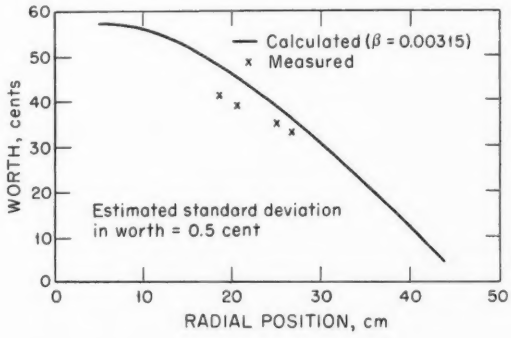

Fig. 8 Radial dependence of guinea-pig-rod worth.[13]

data were then analyzed in the time domain by using a digital computer to obtain the autocorrelation and cross-correlation functions. The β/l values were, in turn, obtained by semilogarithmic plots of the correlation function. The correlation functions are shown in Fig. 19. Results of the noise analysis are given in Table 2. Measurements were attempted at higher power levels, but the detectors appeared to saturate, and the frequency response of the detectors was apparently changed. The delayed-neutron fraction β in Table 2 was calculated using the two-dimensional synthesis code BISYN, and the neutron lifetime l was calculated from the reactivity effects caused by introducing a $1/v$ absorber. Results obtained from a two-dimensional synthesis code and a two-dimensional diffusion code are both tabulated.

Integral Physics Parameters

Reflector Calibrations. The SEFOR core is controlled by a reflector consisting of ten 36° segments. Eight of these are for coarse control of the reactor, and the other two (segment Nos. 3 and 8) are used for fine control.

The coarse-reflector worths[5,13] were measured according to the following procedures: The segment to be calibrated was completely raised, fine reflector No. 3 was completely lowered, and criticality was achieved with reflector segment No. 8 at a mid position. The coarse-reflector segment was then lowered, reflector No. 3 was raised, and the coarse-reflector worth was determined from the worth of reflector No. 3 (the "substituting" segment) and the change in the position of segment No. 8.

Fine-reflector calibrations were effected as follows: The reactor was brought critical with the fine-reflector segment that was to be calculated in the completely lowered position and the other fine reflector completely raised. Criticality was maintained with a coarse-reflector configuration such that the coarse segments on either side of the fine segment, which was being calibrated, were moved to the full-out position. The reflector segment that was being calibrated was then raised a few centimeters to produce a positive period,

the period was measured, and the incremental worth of the segment was determined from the measured period using the inhour equation. Finally, the other fine reflector was lowered to bring the reactor back to critical at the original flux level. Representative results of the reflector-segment worth measurements are given in Table 3.

Reactivity Coefficients. *Flow Coefficient.* The relation between reactivity and coolant flow[7,9,13] was determined by incrementally altering the coolant flow rate between the maximum and minimum values and adjusting the reflector position to maintain a constant flux level. The data for the coolant-flow–reactivity measurements are given in Table 4.

Pressure Coefficient. The effects of reactor-vessel hydraulic pressure on reactivity[7,9,13] were measured by varying the reactor-vessel cover-gas pressure and noting the change in reactivity while a constant flux level was maintained by reflector positioning. Table 5 gives the results of these measurements.

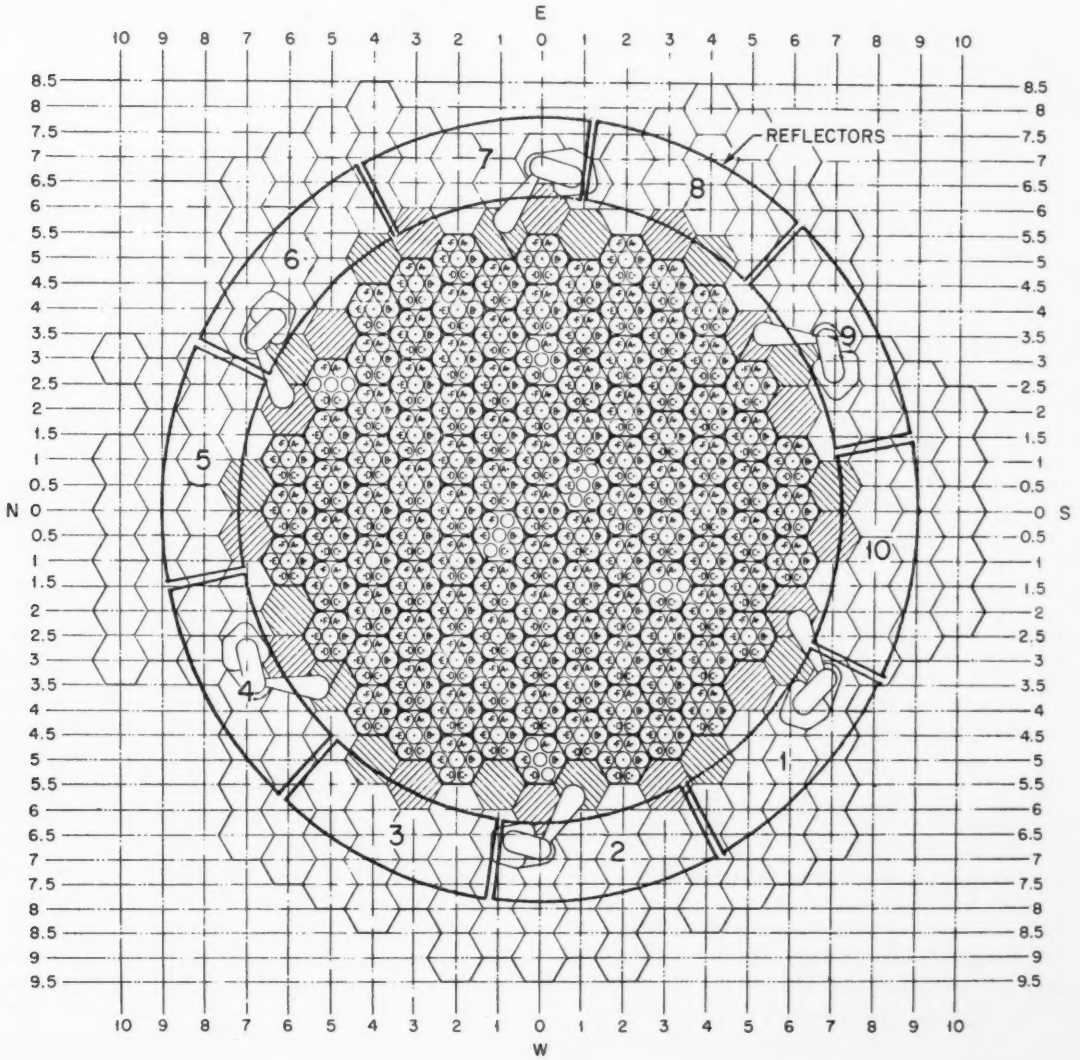

Fig. 9 Core-loading locations.[13]

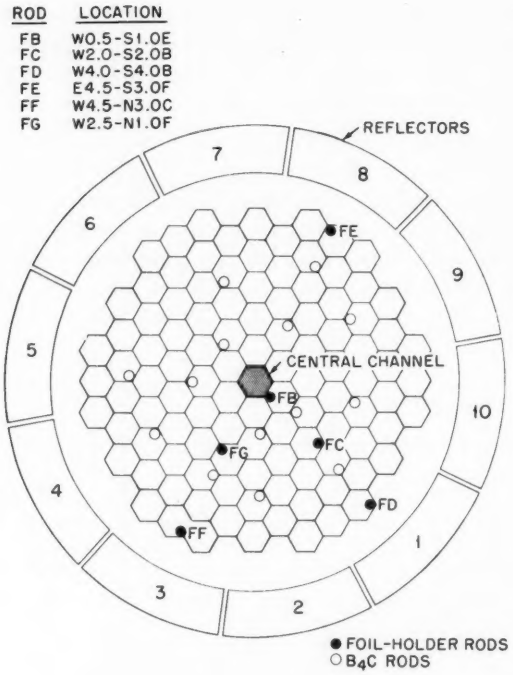

Fig. 10 Foil-holder-rod locations.[13]

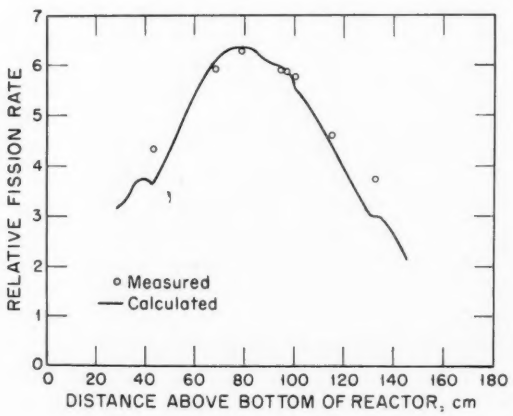

Fig. 11 ^{239}Pu fission distribution in rod FB.[13]

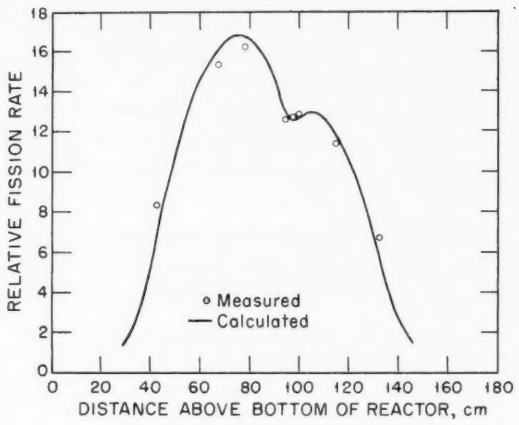

Fig. 12 ^{238}U fission distribution in rod FB.[13]

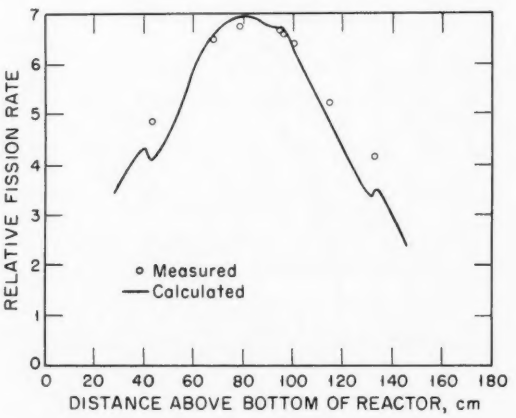

Fig. 13 ^{235}U fission distribution in rod FB.[13]

Temperature Coefficient. Preliminary temperature-coefficient measurements[7,9,13] were performed with the fully loaded core by heating the primary sodium from 350 to 400°F and noting the critical positions of the fine reflector. The temperature was maintained at 400°F for about 2 hr; it was then dropped back to 350°F, and critical reflector positions were recorded. During the heating and cooling periods, the reactor was shut down, but after steady-state temperatures were achieved, the critical reflector positions were noted. Data obtained during these measurements are shown in Table 6. A least-squares fit of these data gives a value of -0.59 ± 0.01 cent/°F for the temperature coefficient as compared to a calculated value of -0.68 cent/°F.

More extensive measurements of the temperature-dependent reactivity-feedback coefficients were taken with a full-power core-loading configuration except that seven of the fuel rods were replaced with guinea-pig rods. The primary sodium coolant was heated from 350 to 760°F, cooled to about 700°F,

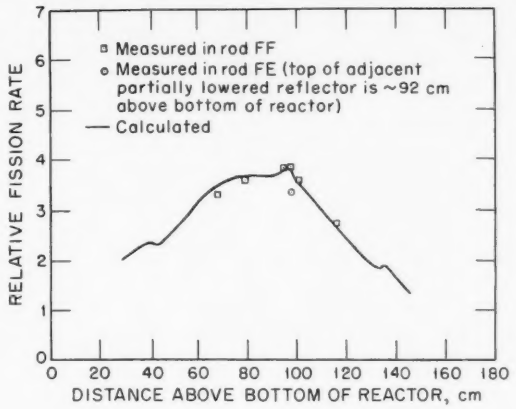

Fig. 14 ^{235}U axial fission distribution at core radial boundary.[13]

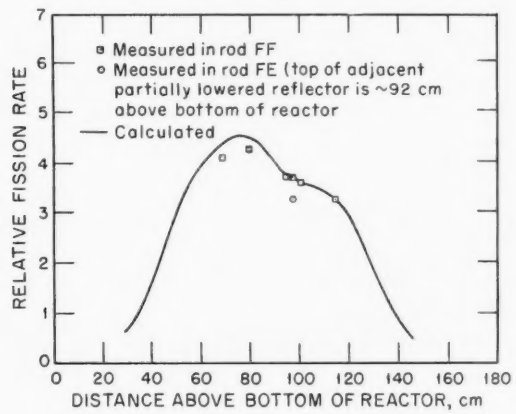

Fig. 15 ^{238}U axial fission distribution at core radial boundary.[13]

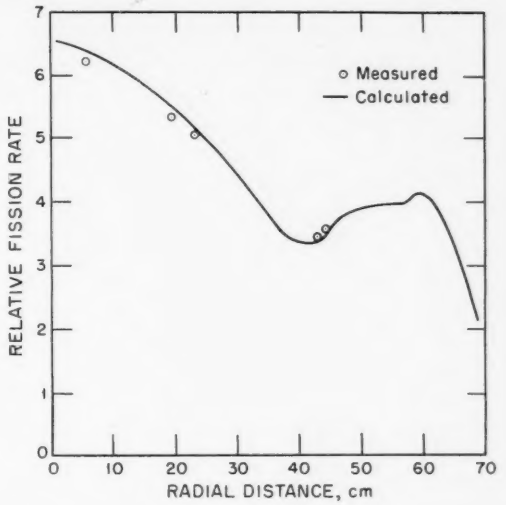

Fig. 16 ^{239}Pu radial fission distribution[13] at axial position 3.

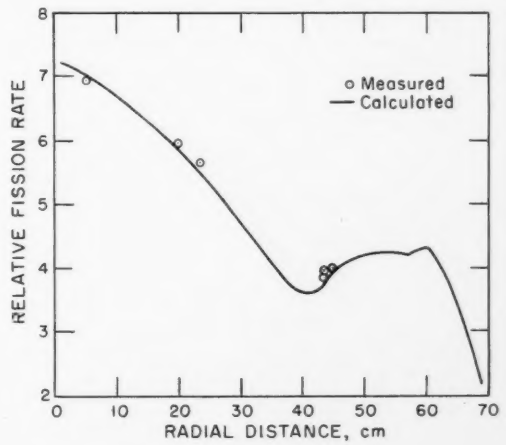

Fig. 17 ^{235}U radial fission distribution[13] at axial position 3.

and then reheated to 760°F. The reactor power level was held constant at about 600 W throughout the cooling and heating periods by compensating for reactivity-feedback effects by positioning the control reflector. RTDs were used to monitor the reactor inlet and outlet temperatures, and temperatures and reflector positions were recorded about every 15 min. The total temperature reactivity-feedback coefficient (including expansion–sodium-density effects) is shown in Fig. 20, and Table 7 summarizes the data.

Transfer-Function Measurements. Oscillator experiments[9] were performed with the poison rod being oscillated in the central channel at 11 different frequencies between 0.25 and 0.00175 cycle/sec while the reactor power level was maintained at about 1 kW. The zero-power transfer functions were measured while the mean position of the oscillator was 5.5 in. from the core center. Three sets of measurements were made, each covering the whole range of frequencies. Rod oscillation during the first two sets of measurements produced about a 10% variation in power level, and during the third set, 2 to 10% variations in power level.

The measured and calculated values of the amplitude of the zero-power transfer function are shown in

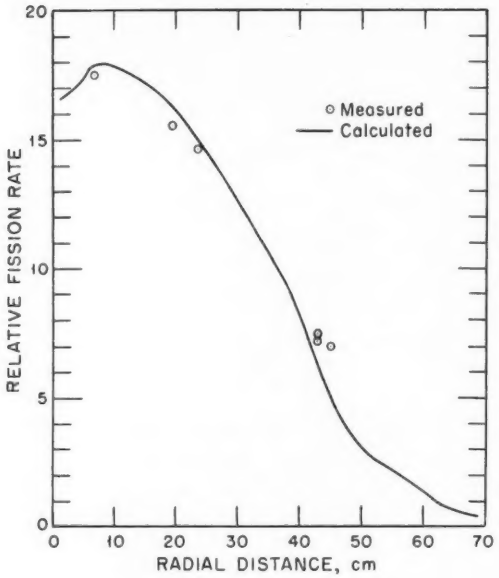

Fig. 18 ^{238}U radial fission distribution[13] at axial position 3.

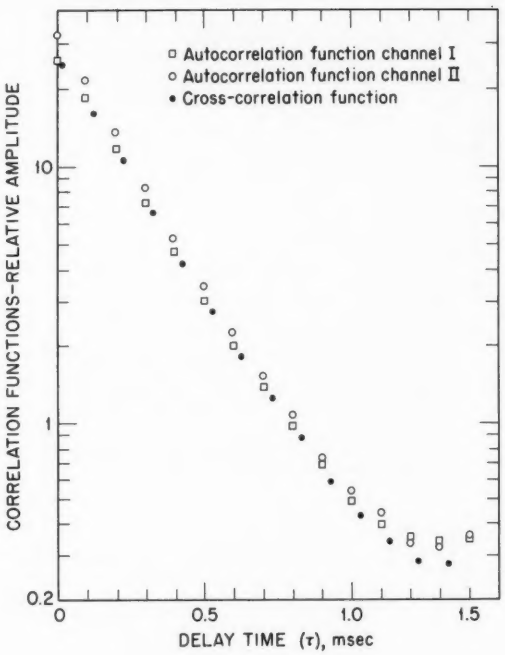

Fig. 19 Correlation functions.[13]

Table 1 Fission-Cross-Section Ratios Near Core Center[9,13]

Ratio	Measured	Predicted*
$^{238}\sigma_f/^{235}\sigma_f$	0.0252	0.0256
$^{239}\sigma_f/^{235}\sigma_f$	0.905	0.894

*From Ref. 2.

Table 2 Results of Noise Analysis[7,13]

Power obtained from noise analysis, W	Reactivity, cents	Cross-correlation function, V	Auto-correlation function 1, V	Auto-correlation function 2, V	l/β, sec*
22.28	-1.2 ± 0.5	0.0108	0.0105	0.0120	0.205×10^{-3}
1036	0.0	0.305	0.286	0.352	0.232×10^{-3}
6180	0.0	0.647	0.616	0.770	0.244×10^{-3}

*Estimated uncertainty of ±1%. Calculated results: two-dimensional-synthesis-program $l/\beta = 0.214 \times 10^{-3}$ sec; true two-dimensional-diffusion-program $l/\beta = 0.184 \times 10^{-3}$ sec.

Table 3 Reflector Segment Worths[5,13]

Reflector segment number	Reactivity worth, dollars	
	Measurement No. 1*	Measurement No. 2†
1	1.25	
2	1.28	1.02
3	1.27‡	
4	1.24	0.99
5	1.25	1.20
6	1.28	
7	1.14	1.29
8	1.25‡	
9	1.09	1.24
10	1.26	

*Substituted for No. 3 reflector segment (No. 8 at ~50 cm, or about halfway up).

†Substituted for No. 8 reflector segment (No. 3 at ~50 cm, or about halfway up).

‡Worths obtained from period measurements.

Fig. 21 and the measured and calculated values of the phase angle in Fig. 22.

The first series[11] of at-power oscillator tests was carried out at 2 MW with a coolant flow of 2000 gal/min. This series of tests, like the zero-power tests, included three sets of measurements at 11 different frequencies. The amplitude of the at-power transfer function is shown in Fig. 23 and the phase angle in Fig. 24.

SUMMARY

This is the fourth in a series of articles on the operating experience and physics characteristics of liquid-metal-cooled fast breeder reactors now in operation. The SEFOR data presented here will be updated (as will the data for EBR-II, Fermi, and Rapsodie in previous articles) as additional information becomes publicly available.

Table 4 Flow–Reactivity[7,9,13] Measurements*

Coolant flow, gal/min	Reflector No. 8		Temperature, °F	Relative system† reactivity at 390°F, cents
	Position, cm	Worth, cents		
500	55.94	43.90	393.82	46.50
1000	53.70	48.47	386.25	45.92
1500	52.56	49.53	384.50	45.79
2000	52.46	50.21	383.33	45.68
3000	52.08	50.34	382.75	45.41
3500	52.20	50.15	382.67	45.16
4000	58.64	39.42	399.94	46.18
4450	58.83	39.12	400.31	46.12
4900	59.60	37.85	402.19	46.14

*Average of data from tables in Ref. 13.

†Using a temperature coefficient at 390°F of −0.68 cent/°F.

Note: Variations in reactor temperature were held to less than 20°F.

Table 5 Pressure–Reactivity[7,9,13] Measurements*

Cover-gas pressure, psig	Reflector No. 8		Temperature, °F	Relative System† reactivity at 350°F, cents
	Position, cm	Worth, cents		
0	39.27	71.99	348.75	71.14
5	39.13	72.23	349.50	71.89
10	39.13	72.23	349.50	71.89
15	39.00	72.46	349.63	71.87
20	38.80	72.80	348.69	71.90

*Average of data from tables in Ref. 13.

†Using a temperature coefficient at 390°F of −0.68 cent/°F.

Table 6 Temperature-Coefficient[7,9,13] Measurements*

Temperature, °F	Reflector No. 3		Reflector No. 8		Reactivity change relative to 350°F, cents
	Position, cm	Worth, cents†	Position, cm	Worth, cents†	
350.0	0.44	0.00	51.71	73.33	0.00
352.0	0.75	0.19	52.09	74.02	−0.88
397.0	0.75	0.19	68.67	101.03	−27.89
397.5	0.75	0.19	68.88	101.33	−28.19
398.25	0.44	0.00	69.21	101.80	−28.47
398.5	0.75	0.19	69.07	101.60	−28.46

*Average values from Ref. 13 for a core comprised of 634 fuel rods, 108 tightener rods, and 14 B_4C rods.

†Relative to the worth with the reflector lowered.

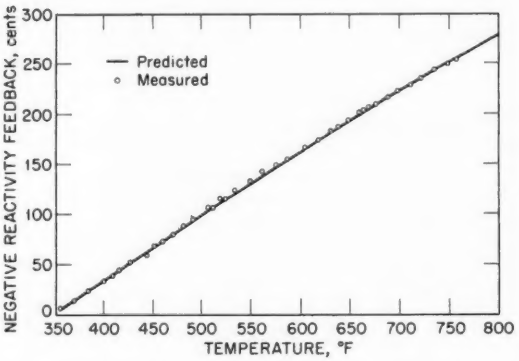

Fig. 20 Temperature reactivity feedback.[13]

Table 7 Uniform Temperature Coefficient[7,9,13] of Reactivity Between 350°F and 760°F

Temperature range, °F	Average temperature reactivity coefficient in indicated temperature range, cents/°F	
	Measured	Predicted
350 to 450	−0.67	−0.66
450 to 550	−0.64	−0.63
550 to 650	−0.60	−0.61
650 to 750	−0.57	−0.58

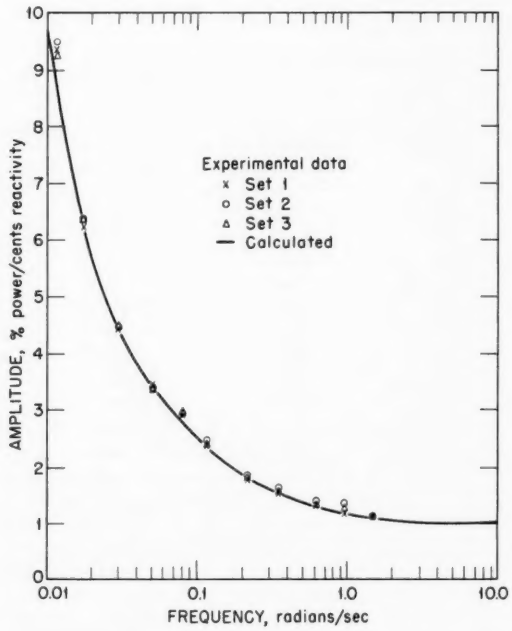

Fig. 21 Amplitude of SEFOR zero-power transfer function.[9]

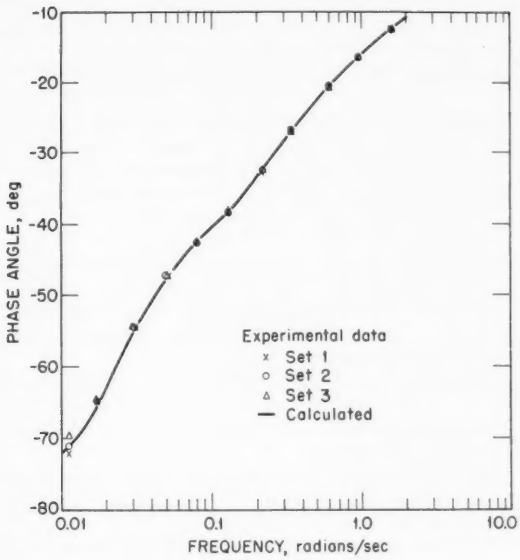

Fig. 22 Phase angle of SEFOR zero-power transfer function.[9]

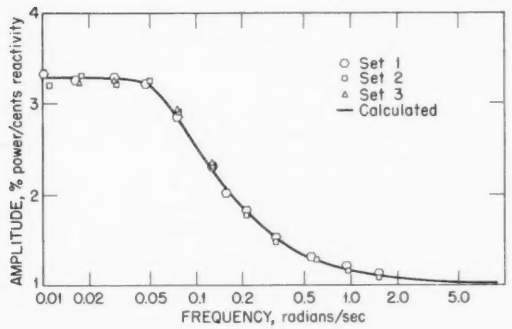

Fig. 23 Amplitude of power-reactivity transfer function[11] at 2 MW.

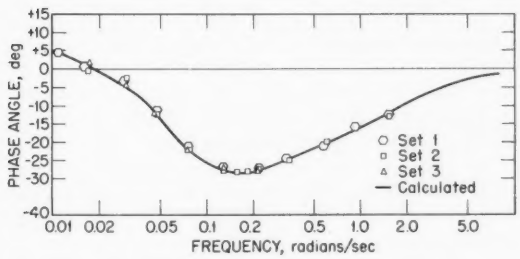

Fig. 24 Phase of the power-reactivity transfer function[11] at 2 MW.

ACKNOWLEDGMENTS

I would like to thank Dr. G. R. Pflasterer and the SEFOR R&D Staff of GE's Breeder Reactor Development Operation for their review and comments.

REFERENCES

1. General Electric Company, Southwest Experimental Fast Oxide Reactor, Facility Description and Safety Analysis Report, Vol. 1, USAEC Report DOCKET-50231-30, July 21, 1967.
2. General Electric Company, Southwest Experimental Fast Oxide Reactor Development Program, Twentieth Quarterly Report, February–April 1969, USAEC Report GEAP-10010-20, May 1969.
3. General Electric Company, Southwest Experimental Fast Oxide Reactor Development Program, Twenty-first Quarterly Report, May–July 1969, USAEC Report GEAP-10010-21, August 1969.
4. General Electric Company, Southwest Experimental Fast Oxide Reactor, Quarterly Plant Operation Report No. 1, May 1, 1969–July 31, 1969, USAEC Report DOCKET-50231-65, Nov. 7, 1969.
5. General Electric Company, Southwest Experimental Fast Oxide Reactor Development Program, Twenty-second Quarterly Report, August–October 1969, USAEC Report GEAP-10010-22, December 1969.
6. General Electric Company, Southwest Experimental Fast Oxide Reactor, Quarterly Plant Operation Report No. 2, August 1, 1969–October 31, 1969, USAEC Report DOCKET-50231-66, Dec. 30, 1969.
7. General Electric Company, Southwest Experimental Fast Oxide Reactor Development Program, Twenty-third Quarterly Report, November 1969–January 1970, USAEC Report GEAP-10010-23, February 1970.
8. General Electric Company, Southwest Experimental Fast Oxide Reactor, Quarterly Plant Operation Report No. 3, November 1, 1969–January 31, 1970, USAEC Report DOCKET-50231-43, Mar. 30, 1970.
9. General Electric Company, Southwest Experimental Fast Oxide Reactor Development Program, Twenty-fourth Quarterly Report, February–April 1970, USAEC Report GEAP-10010-24, May 1970.
10. General Electric Company, Southwest Experimental Fast Oxide Reactor, Quarterly Plant Operation Report No. 4, February 1–April 30, 1970, USAEC Report DOCKET-50231-48, June 18, 1970.
11. General Electric Company, Southwest Experimental Fast Oxide Reactor Development Program, Twenty-fifth Quarterly Report, May–July 1970, USAEC Report GEAP-10010-25, August 1970.
12. General Electric Company, Southwest Experimental Fast Oxide Reactor, Quarterly Plant Operation Report No. 5, May 1–July 31, 1970, USAEC Report DOCKET-50231-57, Sept. 30, 1970.
13. L. D. Noble et al., Results of Zero Power Experiments, USAEC Report GEAP-13588, General Electric Company, March 1970.

14. J. O. Arterburn, G. Billuris, and G. B. Kruger, SEFOR Operating Experience, paper presented at First National Division Conference of the ASME Nuclear Engineering Division, Palo Alto, Calif., Mar. 7, 1971.

Suggested Reading List

P. E. Novak and R. R. Asamoto, A Survey for a High Temperature Sensor for SEFOR, USAEC Report GEAP-4903, General Electric Company, Sunnyvale, July 1965.

E. P. Quinn, Vibration of SEFOR Fuel Rods in Parallel Flow, USAEC Report GEAP-4966, General Electric Company, Sunnyvale, September 1965.

M. L. Johnson, A Description of Fuel and Other Core Materials Procured for SEFOR Critical Experiments in ZPR-III, USAEC Report GEAP-5133, General Electric Company, Sunnyvale, December 1965.

R. Protsik, Epithermal Capture and Fission Rate Distribution in a Fuel Rod: The Computer Code REAX, USAEC Report GEAP-4973, General Electric Company, Sunnyvale, April 1966.

P. E. Novak and R. R. Asamoto, An Out-of-Pile Evaluation of W–Re Thermocouple Systems for Use to 4700°F in Mixed Oxide, USAEC Report GEAP-5166, General Electric Company, Sunnyvale, May 1966.

R. P. Morrell, SEFOR Beta/l Measurements by Noise Analysis Techniques, USAEC Report IDO-17210, Phillips Petroleum Co., August 1966.

R. F. Williams and E. E. Polomik, Pressure Drop and Dye Tests with Water on the SEFOR Prototype Fuel Bundle, USAEC Report GEAP-5129, General Electric Company, Sunnyvale, February 1966.

C. N. Craig, C. M. Ryer, and M. L. Thompson, Plutonium–Uranium Mixed Oxide Fuel Pellet Fabrication Development for the Southwest Experimental Fast Oxide Reactor, USAEC Report GEAP-5285, General Electric Company, Sunnyvale, October 1966.

E. E. Polomik and R. F. Williams, Coolant Surface Turbulence Study, SEFOR Reactor Vessel, USAEC Report GEAP-5099, General Electric Company, Sunnyvale, December 1966.

L. Wilkinson, Use of Neutron Filters for Fast Reactor Fuel Irradiations in a Thermal Core, USAEC Report GEAP-5035, General Electric Company, Sunnyvale, April 1967.

L. Wilkinson et al., Devices for Cyclic and Transient Power Control in a Steady-State Neutron Flux Gradient, USAEC Report GEAP-5036, General Electric Company, Sunnyvale, May 1967.

D. Wilkinson, Weighted Doppler Analysis Code, WEDOP, USAEC Report GEAP-5513, General Electric Company, Sunnyvale, October 1967.

E. R. Craig, R. H. Fulton, and J. J. Damon, Design and Testing of Solenoid and Instrument Lead Connector for Use in SEFOR Reactor Vessel, USAEC Report GEAP-5307, March 1967.

R. R. Asamoto, K. J. Perry, and E. L. Zebroski, The Effective and Diametral Thermal Expansion of UO_2 Under a Radial Temperature Gradient, USAEC Report GEAP-5284, General Electric Company, Sunnyvale, October 1966.

R. L. McVean et al., Critical Studies of the Southwest Experimental Fast Oxide Reactor (SEFOR) in ZPR-3, USAEC Report ANL-7348, Argonne National Laboratory, pp 560-568, Oct. 10–13, 1966.

E. E. Polomik, Fluid Flow and Vibration Tests, ½-Scale Model of SEFOR Reactor Vessel, USAEC Report GEAP-5440, General Electric Company, Sunnyvale, April 1967.

J. H. Field, M. L. Johnson, and P. E. Novak, An Evaluation of the Effect of Design and Operating Variables on SEFOR Fuel and Fuel Cladding, USAEC Report GEAP-5309, General Electric Company, Sunnyvale, December 1967.

C. E. Russell, Flow Distribution Measurements in a 3-Scale Model of the SEFOR Fuel Bundle, USAEC Report GEAP-5184, General Electric Company, Sunnyvale, May 1968.

J. T. Cochran, SEFOR Core Clamping Model Tests, One-Sixth Segment, USAEC Report GEAP-5465, General Electric Company, Sunnyvale, May 1968.

R. R. Asamoto and P. E. Novak, An In-Pile Evaluation of W–Re Thermocouple Systems for Use to 4700°F in SEFOR Fuel, USAEC Report GEAP-5466, General Electric Company, Sunnyvale, October 1968.

J. T. Cochran, SEFOR Fuel Assembly Sodium Flow Tests, USAEC Report GEAP-5466, General Electric Company, Sunnyvale, September 1968.

J. T. Cochran, SEFOR Fuel Rod Sodium Thermal Shock Tests, USAEC Report GEAP-5467, General Electric Company, Sunnyvale, August 1968.

E. R. Craig, SEFOR Instrumented Fuel Assembly Design and Development, USAEC Report GEAP-5615, General Electric Company, Sunnyvale, April 1968.

A. G. Steamer, G. V. Brynsvold, and L. C. Franckx, Fuel Handling and Other Tests in the SEFOR Refueling Cell Mockup, USAEC Report GEAP-5701, General Electric Company, Sunnyvale, March 1969.

M. L. Johnson, R. A. Becker, and J. M. Haar, SEFOR Fuel Handling, USAEC Report GEAP-13565, General Electric Company, Sunnyvale, December 1969.

M. Audoux, L. Caldarola, P. Giordano, H. Rohrbacher, and C. Russell, The Balanced Oscillator Tests in SEFOR, USAEC Report ANL-7320, pp 456-474, Argonne National Laboratory, Oct. 10–13, 1966.

A. B. Reynolds and S. L. Stewart, Application of the SEFOR Critical Experiments in ZPR-3 to SEFOR, USAEC Report ANL-7320, pp 569-585, Argonne National Laboratory, Oct. 10–13, 1966.

L. Noble, G. R. Pflasterer, C. D. Wilkinson, and L. Caldarola, Recent Developments in the SEFOR Experimental Program, USAEC Report ANL-7320, pp 746-758, Argonne National Laboratory, Oct. 10–13, 1966.

A. B. Reynolds and S. L. Stewart, Analysis of the SEFOR Mockup Critical Experiments in ZPR-3, USAEC Report GEAP-5294, General Electric Company, Sunnyvale, March 1967.

L. D. Noble and C. D. Wilkinson, Final Specifications for the SEFOR Experimental Program, USAEC Report GEAP-5576, General Electric Company, Sunnyvale, January 1968.

G. R. Pflasterer, SEFOR, Experimental Program Planning. Vol. I, Specifications for the Plant and Experimental Equipment, USAEC Report GEAP-5092, General Electric Company, San Jose, August 1966.

G. R. Pflasterer and L. Caldarola, SEFOR Experimental Program Planning. Vol. II, Descriptions of Planned Tests, USAEC Report GEAP-5092, General Electric Company, San Jose, August 1966.

JACK CHERNICK

Reactor Technology expresses its sorrow and regret for the loss of Jack Chernick, who was the Senior Physicist and Head of the Reactor Physics Division at Brookhaven National Laboratory. He died April 8 at age 59. Mr. Chernick was a valued member of the ANS Critical Review Advisory Committee.

AMERICAN NUCLEAR SOCIETY—CRITICAL REVIEWS

The Atomic Energy Commission has contracted with the American Nuclear Society to prepare for publication on a regular basis detailed Critical Review articles written by experts selected from the ANS membership and reviewed by an advisory committee of top leaders and scientists in the field. In this issue the articles are on pages 169-209.

Comments on the articles should be communicated directly to the ANS Critical Review Advisory Committee or Editor, 244 E. Ogden Avenue, Hinsdale, Ill. 60521.

ANS GUIDELINES FOR PREPARING CRITICAL REVIEWS FOR *REACTOR TECHNOLOGY*

One interpretation of the words "Critical Review" emphasizes the word *critical.* That type of article would have as its purpose the discussion of a single subject, which has been uncertain and perhaps controversial, in considerable depth. An example might be a critical review of the values of alpha for plutonium, assessing all the work done and arriving at a best current estimate. This paper is primarily addressed to specialists on the particular subject, and serves as an authoritative source for the information they use.

In the second interpretation of a Critical Review, the emphasis is on the word *review,* in the sense of survey. Such a paper would be broader and probably more descriptive in scope. A paper on "Solubility of Metallic Elements in Liquid Sodium" is an example of this category. Such a paper would be addressed to a much broader group of readers and written in a fashion that would be of interest to the majority of reactor technologists. It would provide enough of an introduction that the specialist from another field could immediately appreciate why the subject is important.

The criteria for these two types of articles may not be very different:

1. The paper should be based on a thorough coverage of relevant work on the subject from many sources. A review based on the work of only one individual or group is better suited for publication in one of the regular society journals. The review should be critically selective, reporting only the most valid results and indicating why some prior results have a questionable status. The review should call attention to significant gaps where more work is required in the subject of the article.

2. The paper should be timely, on a subject of active current interest.

3. The scope of articles acceptable as Critical Reviews includes all the subject areas identified for *Reactor Technology* (Economics, Physics, Mechanics, Construction, Fuel Elements, Fuel Cycles, Fluid and Thermal Technology, Fuel Processing, Components, Operating Performance), as well as Materials (including Source and Special Nuclear), Environmental Effects, and Effluent Management. Not desired are (1) reports of original research proposed for first publication and (2) review articles directed toward the specialist in the field of nuclear safety (which is covered by the AEC's bimonthly review *Nuclear Safety*).

4. The paper should be organized so that it is of immediate practical use to the readers. Such organization requires: attention to consistent use of units, presentation of important data in summary curves or tables, and a fully adequate bibliography to the original literature. Details on size, honorarium, style, etc., can be obtained from ANS.

Space- and Energy-Dependent Neutronics in Reactor Transient Analysis

By Weston M. Stacey, Jr.*

Abstract: *Spatial and spectral neutronic effects that influence reactor transient analyses are discussed, and methods developed for treating these effects (quasi-static, coupled core, synthesis, direct numerical integration, etc.) are reviewed. The status of computational methods development is evaluated, and results of intracomparison of methods and comparison with experiment are summarized.*

Evaluation of reactor performance for design, optimization, and safety purposes is generally based on an analysis of the ability of the reactor core not only to operate in the steady-state condition but also to undergo a transient arising from some postulated change in operating condition without sustaining unacceptable damage or, in the case of safety analyses, leading to a catastrophic event. Although the criteria used in defining initiating mechanisms and "acceptable" damage vary considerably, depending on reactor type and whether a routine performance or safety analysis is being considered, an adequate prediction of the transient neutron-flux level and distribution is essential to all such analyses. The point-kinetics neutronics model, or some variant thereof, is almost universally employed in transient analyses made for the purpose of establishing performance limits for reactors. The point-kinetics model is defined in terms of integral reactor parameters and is exact if these parameters are correctly defined.

In recent years, ample theoretical evidence has accumulated to demonstrate that the spatial and spectral distributions of the neutron flux and the importance function,† which are used in averaging the nuclear properties to obtain the parameters of the point-kinetics model, vary with time during a transient. For certain reactor types and transients, the resulting changes in the point-kinetics parameters are sufficient to produce a dramatic effect on the outcome of the transient analysis, relative to the standard procedure of using one set of parameters throughout the transient. Reactor physicists responsible for such analyses have attempted to choose sufficiently pessimistic neutron-flux and importance distributions for averaging point-kinetics parameters so that the prediction of the resulting point-kinetics analysis is conservative with respect to the prediction of a more costly analysis in which changes in the flux and/or importance distributions are explicitly calculated.

On the other hand, methods for explicitly calculating the changes in the spatial and spectral neutron-flux and/or importance distributions have been actively developed in recent years. These activities range from the quest for more-efficient numerical integration schemes for the "exact" multigroup finite-difference kinetics equations to the quasi-static schemes for updating the point-kinetics parameters at different times during a transient calculation. Intermediate to these efforts is the large body of work on the development of modal (synthesis) and nodal (coupled-core) approximations for the spatial depen-

*Applied Physics Division, Argonne National Laboratory, Argonne, Ill. 60439.

†The importance, or adjoint, function determines the reactivity worth of a given change in reaction rate due to a perturbation and is included in the definition of point-kinetics parameters.

dence of the neutron flux, and more recently the development of synthesis approximations for the spectral dependence of the neutron flux. Verification of these methods has been primarily by intercomparison, although some experimental comparisons have recently been published.

The purpose of this article is to review recent work in identifying spatial and spectral effects that are important in reactor transient analyses and recent work in developing and verifying calculational models. With few exceptions, the material included was published subsequent to 1964, when a comprehensive review was made.[1] Since this article is limited to material relating to reactor transient analysis, excluding xenon transients, certain logically related material is excluded. Xenon transients are excluded because they were felt to be sufficiently important to warrant separate treatment.[2] Similarly, spatial and spectral effects in pulsed-neutron, noise, neutron-wave, stability, and control analyses would seem to constitute a sufficiently large body of work to warrant a separate review. Semi-analytic excursion models were omitted on the basis of the contention that their discussion is more germane to a review of reactor safety methods.

SPATIAL AND SPECTRAL NEUTRONICS PHENOMENA

Several interrelated phenomena combine to determine the changes in the spatial and spectral neutron-flux and importance distributions, and their consequences, in an actual transient. One class of phenomena involves changes in the spatial flux distribution ensuing from a localized perturbation in the reactor properties such as may be caused by movement of a control rod. Prompt neutrons respond to a change in reactor properties on a time scale characteristic of the prompt-neutron generation time.

Because the prompt-neutron generation time is short compared to characteristic times associated with other physical processes of interest in reactor transient analyses, it might seem that the transient spatial flux distributions at any instant would be approximated by the static distribution that would occur for the identical physical configuration; in fact, this is the basis of the adiabatic approximation to be discussed subsequently. However, under certain conditions, there are two phenomena that tend to invalidate this approximation. First, the delayed-neutron precursors are spatially distributed in a manner determined by the fission rate, and hence the flux, at prior times (for a reactor with fixed fuel). Thus the delayed neutrons are emitted with a spatial distribution more typical of previous than present fission-rate distributions, effectively holding back any flux tilt. This effect is important in delayed-critical and subcritical transients where the delayed neutrons have an important effect on the spatial neutron-flux distribution. A second type of phenomena becomes important in superprompt-critical transients. When the neutron density is increasing rapidly, the spatial flux distribution may differ considerably from the static distribution that would occur in the same reactor if the fission rate could be reduced artificially to achieve criticality (the artifice used in making a static eigenvalue calculation). Mathematically the time derivative of the neutron flux introduces an added term into the neutron-balance equation which has the effect of a distributed absorber with strength w/v, where w is the instantaneous period and v is the neutron speed.

Yasinsky and Henry[3] published the first extensive study of spatial effects in reactor transient analyses. They considered prompt-supercritical and delayed-critical transients in two cores representative of small (60-cm slab) and large (240-cm slab) thermal reactors. Their calculations, which ignored feedback effects, indicated that spatial flux tilting caused the point-kinetics model to be substantially in error for both cores and that for the larger core the delayed-neutron holdback effect was significant in determining the spatial flux distribution during the delayed-critical transient. Figure 1 shows the flux amplitude function as computed exactly (finite difference) by the point-kinetics model and by the adiabatic model (mentioned above and discussed later) for a ramp increase, followed by a ramp decrease, in the fission cross section in the left quarter of the larger core. Flux distributions following a ramp increase in fission cross section in the left quarter of the larger core are shown in Fig. 2, together with the initial flux distribution. The effect of delayed neutrons in holding back the flux tilt is indicated by the difference between the exact and the adiabatic results. Ott and Madell[4] and Stacey and Adams[5] have also examined the effect of delayed neutrons in holding back flux tilts.

In general, the magnitude of a spatial flux tilt resulting from a given local perturbation and the magnitude of the delayed-neutron holdback are directly proportional to the size of the reactor measured in neutron migration lengths. Both magnitudes can be increased by material zoning, which tends to flatten the spatial flux distribution. Analyses[6,7] and experiment[6] have shown that both magnitudes are inversely related to the separation between the fundamental and

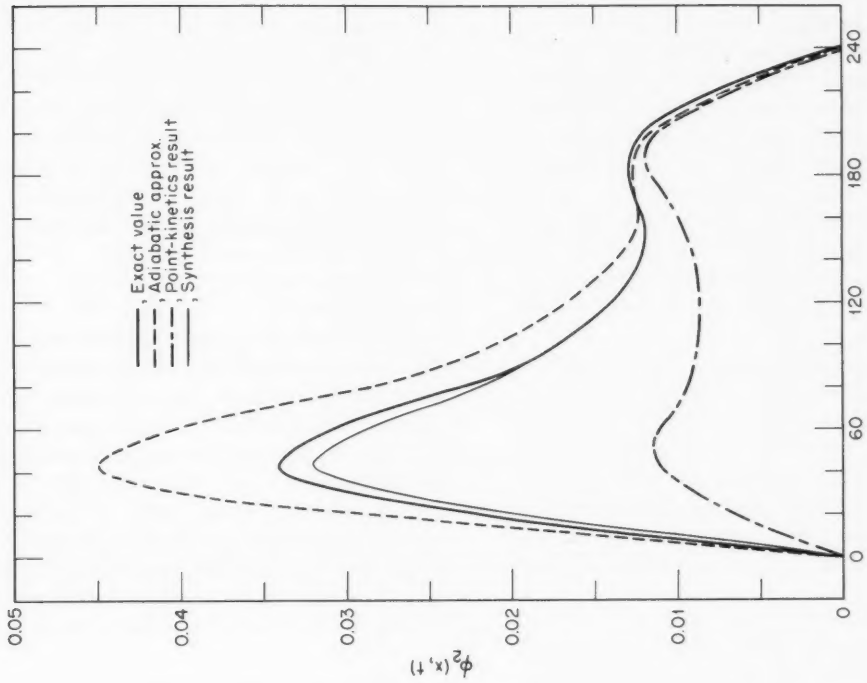

Fig. 2 Thermal-flux distribution at 0.8 sec for a delayed-critical transient in a 240-cm slab thermal core.[3]

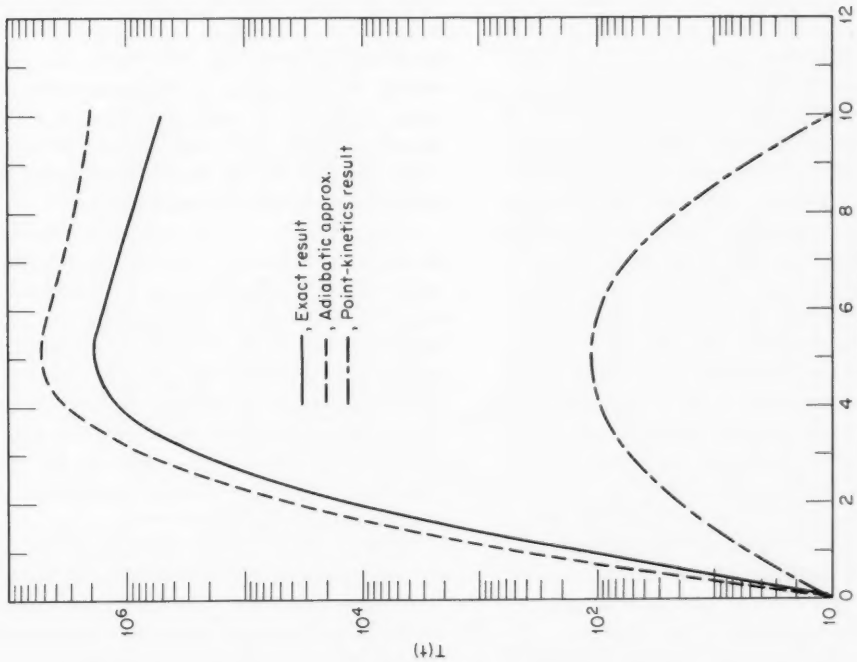

Fig. 1 Flux amplitude for a prompt-critical excursion in a 240-cm slab thermal core.[3]

first harmonic eigenvalues of the unperturbed reactor. Delayed-neutron holdback effects are generally important in transients in the delayed-critical or subcritical regimes, initiated from flux levels comparable to or greater than those obtained during the transients.

Relatively little has been done with respect to studying the reactivity effect of the w/v term via its effect on spatial flux distributions in superprompt-critical transients. It appears, however, that this term can be significant in regions of low absorption,[8,9] such as reflectors, and that it is generally more important for thermal reactors than for fast reactors[9] because $\nu_{th} \ll \nu_{fast}$.

Spatial flux shift effects become more complicated when feedback is considered. Johnson, Gyftopoulos, and Radd[10] considered the effect of spatial flux tilting with feedback for a small (60-cm slab) thermal reactor model. They analyzed the transient resulting from a positive step change in the fission cross section in a quarter of the core, using uniform and distributed feedback models. Even for such a small core, spatial flux-shape changes due to the perturbation and subsequent feedback effects were significant. More recently, Yasinsky[11] has made an extensive analysis of spatial effects in rod-ejection accidents in thermal seed–blanket reactors. Several commonly employed procedures for defining point-kinetics parameters were examined. His results indicate not only that spatial effects are important in the analyses but also that it is difficult to specify a prescription for defining fixed parameters of a point-kinetics model which will ensure a conservative resultant prediction. The influence of feedback on the spatial flux distribution in one of the transients considered by Yasinsky is indicated in Fig. 3.

Kessler[12] and Jackson and Kastenberg[13] have studied the effect of spatial flux tilting on fast reactor transients, with feedback effects included. Kessler[12] demonstrated that point kinetics can be considerably in error for superprompt-critical transients in 300-MW(e) liquid-metal fast breeder reactors (LMFBRs). Jackson and Kastenberg[13] also considered an LMFBR, as represented by a 300-cm slab. The total power resulting from the introduction of a step material change worth \$1.36 into two ends of the slab is shown in Fig. 4. The two space–time (exact) calculations differed only in the spatial distribution of the feedback. For the uniform feedback the two point-kinetics models bracketed the correct solution, but both point-kinetics models overpredicted the correct solution for the distributed-feedback model.

The importance of spectral changes in transient analyses has been examined for LMFBR models. Meneley and Ott[14] considered the transient resulting from a spatially uniform linear increase in plutonium concentration worth \$15.29/sec. Small spectral changes that occurred were due to the increased capture cross section of uranium arising from Doppler broadening. The point-kinetics model was adequate to predict this transient, in which the spectral changes were rather small. Stacey[15] considered transients resulting from extensive sodium loss, with uranium Doppler feedback, and found that the significant spectral shifts associated with sodium loss profoundly affected the results.

Construction of effective delayed-neutron yields, which account for the difference in spectra of delayed and prompt neutrons, is a common stratagem. Yasinsky and Foulke[16] recently reexamined this procedure for a nonuniform mixture containing several fissionable isotopes and found that suitable spatially averaged effective yields could be defined for a few-group model but that large errors resulted when the physical delay fractions were used. Saphier and Yiftah[17] showed that transient calculations are quite sensitive to the choice of the delayed-neutron spectra.

QUASI-STATIC METHODS

As mentioned previously, the point-kinetics equations are exact when appropriate neutron-flux and importance distributions are used in defining the integral parameters that characterize the model. Although the assumption of time-independent distributions is implicit in common usage, this is not an inherent feature, and point-kinetics formulations in which the flux and/or adjoint distributions were time dependent have been presented.[18-20]

The idea of recomputing flux and/or adjoint distributions at various times during a transient, and recalculating the parameters of a point-kinetics model based on these revised distributions, was one of the earliest, as well as one of the most persistent, methods suggested for incorporating spatial and spectral changes in a reactor transient analysis. Methods of this genre are known as quasi-static techniques and differ among themselves primarily with regard to the manner in which the flux and/or adjoint distributions are recalculated during the transient.

Henry and Curlee[21] introduced the adiabatic method, in which the eigenfunction (λ mode) of the static neutron-balance equation corresponding to the instantaneous reactor configuration is computed at selected times and employed to recalculate the parameters of the point-kinetics model. The importance

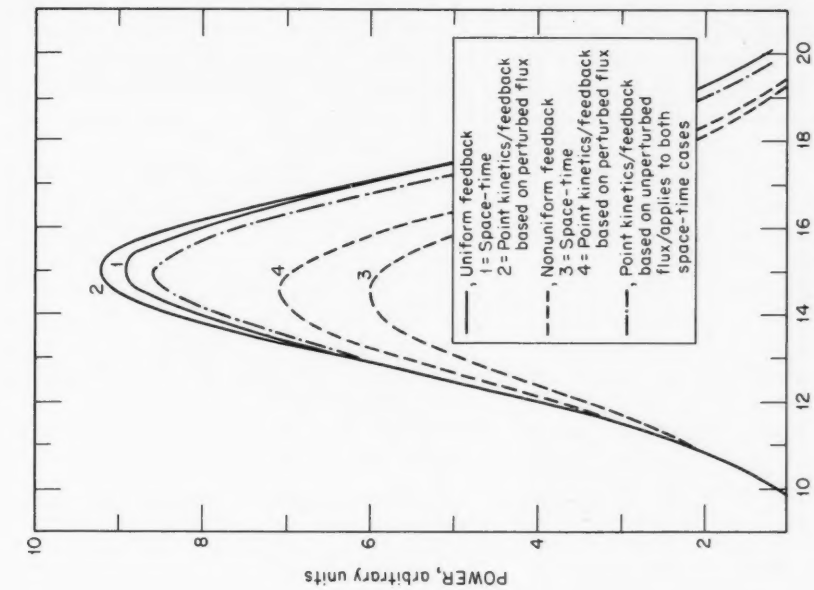

Fig. 4 Spatially dependent and point-kinetics comparisons for the total power in a 300-cm slab LMFBR core following a step insertion of $\Delta k/\beta = 0.68$ in each end (60 cm).[13]

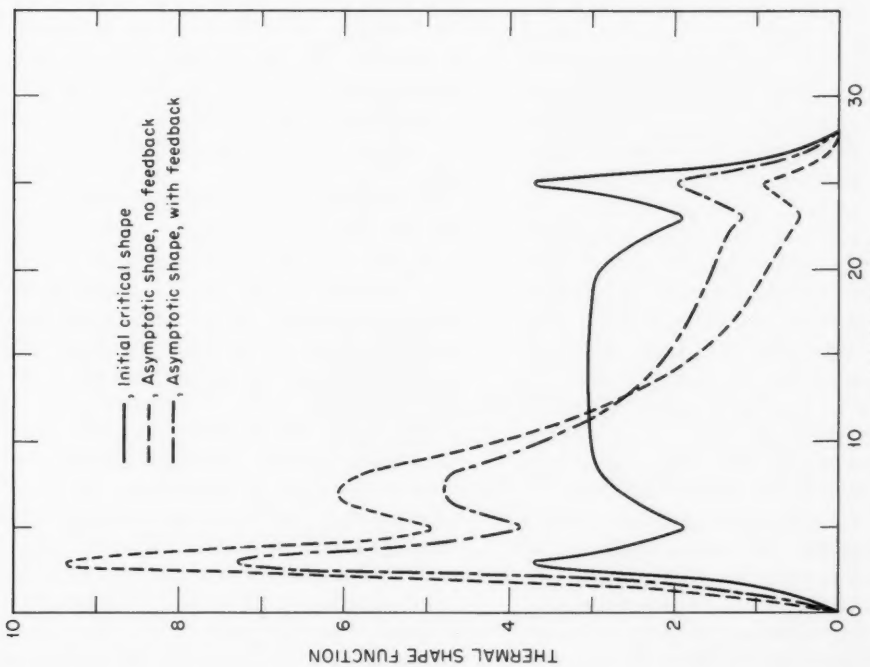

Fig. 3 Thermal-flux distribution for a rod-ejection transient in a 140-cm slab thermal seed–blanket reactor.[11]

distribution corresponding to the initial configuration is used throughout a transient. Aside from the transparent computational difficulty associated with obtaining some measure of consistency between the neutronics and the thermal–hydraulic portions of the calculation, this method does not account for the effect of delayed neutrons in holding back flux tilts or for the effect of the w/v term. The method has been generally satisfactory for transients in which delayed-neutron holdback is unimportant;[9,21,22] e.g., transients originating from low power, transients in the superprompt-critical regime, and transients in small reactors. However, for delayed-critical and subcritical transients originating from appreciable power levels in large reactors, failure to account for delayed-neutron holdback is a serious deficiency of the adiabatic method.[3–5] There is also an important prompt-neutron dynamics effect that the adiabatic model fails to treat properly when the instantaneous period approaches the neutron lifetime in reactors with multiple zones having different prompt-neutron lifetimes. When feedback produces a rapid change in reactivity in the beryllium-reflected SNAP reactor, the delay associated with prompt neutrons in the reflector causes the adiabatic model to be seriously in error.[23]

A typical example of a case in which the adiabatic method fails is illustrated in Figs. 1 and 2.

Ott and Meneley[24] factorize the neutron flux into a time-dependent amplitude function (which is to be obtained as the solution of the point-kinetics equations) and a space- and energy-dependent shape function (which is to be recomputed at intervals throughout the transient). The shape function is formally time dependent. When this factorized expression is substituted into the original kinetics equations, an equation for the shape function results which explicitly accounts for the delayed-neutron distribution and the time derivative which gives rise to the w/v term. The equation for the shape function must be solved iteratively with point-kinetics equations (whose parameters depend on the shape function) and with any feedback equations being considered. For transients in which important changes in the spatial and spectral flux distribution occur more slowly than important changes in the overall neutron-flux level, many time steps in the point-kinetics calculations can be taken before it is necessary to recompute the shape function. An example of the point-kinetics reactivity resulting from a localized ramp perturbation in a thermal-reactor model is shown in Fig. 5. The curves labeled QX1 and WIGLE refer to the quasi-static and exact (finite-difference) calculations, whereas the curve labeled

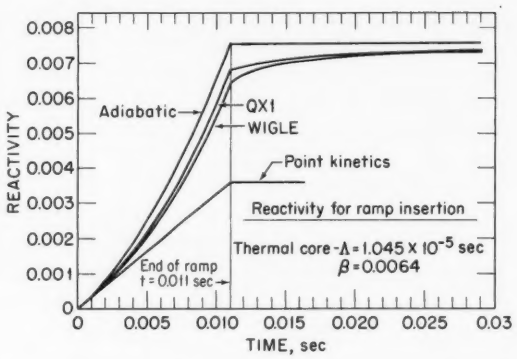

Fig. 5 Equivalent point-kinetics reactivity computed by different methods for a positive ramp insertion in a portion of a 240-cm slab thermal reactor.[24]

point kinetics is based on the point-kinetics model with the initial flux and importance distribution used in computing parameters.

When convergence between the shape function and point-kinetics solutions is required to be sufficiently tight, the quasi-static method of Ott and Meneley yields a solution that approaches the exact solution,[9] which provides a convenient internal check for more approximate calculations. Experience with one-dimensional fast reactor transients, primarily in the superprompt-critical regime, indicates that the method is considerably more economical than a direct solution of the space- and energy-dependent kinetics equations.[9] Interaction strategies that have evolved for use with the quasi-static method were recently reported by Meneley et al.[25]

Galati[26] proposed a model similar to that of Ott and Meneley[24] in which the shape functions are obtained by solving the natural-mode equations iteratively. The natural-mode equations, which are obtained from the neutron and precursor kinetics equations by assuming an exponential time dependence, describe the shape exactly when an asymptotic period occurs. The essence of the method is to approximate changes in physical properties by a histogram and to use the corresponding fundamental natural mode to represent the shape function during each interval. The method is valid if the time intervals between shape function calculations are simultaneously long enough that an asymptotic period obtains and short enough that the histogram-type change in physical properties is a reasonable approximation. The importance function is also recalculated for each time interval. Results ob-

tained with this model indicate that it may be more economical than a direct solution for superprompt-critical transients but that recomputation of the importance functions is necessary for accuracy,[26] which is in substantial agreement with Meneley's experience.[9]

NUMERICAL INTEGRATION

In contrast to the work discussed in the previous section, in which the intent was to retain the point-kinetics formalism, another considerable body of work has been devoted to the direct integration of the space- and energy-dependent neutron kinetics equations. For the most part, this work has dealt with the situation in which the spatial dependence was represented by a finite-difference diffusion-theory approximation and the energy dependence was represented by a multigroup approximation.

Although fully explicit and fully implicit integration algorithms have been employed to some extent, numerical stability problems associated with the former, and truncation errors associated with the latter, have motivated the study of semi-implicit algorithms.

Fully explicit algorithms are those for which the flux at each mesh point and each energy group at time $t + \Delta t$ may be evaluated independent of the flux at other mesh points and/or energy groups, in terms of fluxes at many mesh points and energy groups evaluated at time t (forward difference) or at times t, $t-\Delta t$, $t-2\Delta t$, etc. (e.g., Runga–Kutta). Stability of these simplest of methods requires time steps smaller than the reciprocal of the magnitude of any of the eigenvalues of the matrix associated with the kinetics equations[27] (the natural-mode eigenvalues). Because these eigenvalues can be $\sim -10^4$ for thermal neutrons and $\sim -10^8$ for fast neutrons, time steps of $\sim 10^{-4}$ and $\sim 10^{-8}$ sec would be required for thermal and fast reactors, respectively. Thus a large number of relatively inexpensive (in computation time) time steps are required for practical problems.

Fully implicit algorithms (e.g., backwards difference) are those for which the fluxes at all mesh points and energy groups at time $t + \Delta t$ must be solved for simultaneously. The equation for the flux at a given mesh point and energy group at time $t + \Delta t$ involves the fluxes at other mesh points and energy groups evaluated at time $t + \Delta t$ but involves only the flux at the same mesh point and energy group evaluated at time t. Such methods are generally stable, and the allowable time-step size is limited only by truncation error. Thus a relatively smaller number of expensive time steps characterize fully implicit methods.

Two categories of semi-implicit algorithms have been developed. In the first category the fluxes at all mesh points and energy groups at time $t + \Delta t$ must be solved for simultaneously. The equation for the flux at a given mesh point and energy group involves the fluxes at many mesh points and energy groups evaluated at time t. In the second category of semi-implicit algorithms, the fluxes at some, but not all, of the mesh points and energy groups evaluated at time $t + \Delta t$ must be solved for simultaneously.

The best known of the semi-implicit methods in the first category is the "θ method," which is employed in the widely used WIGL[28] (1D) and TWIGL[29,30] (2D) codes. In this algorithm the entire neutron-balance operator acts upon the flux at $t + \Delta t$ and at t, reduced by multiplicative factors θ and $1-\theta$, respectively, and a similar operation occurs for the delayed-neutron precursors.[31] In the limits $\theta \to 0$ and 1, the algorithm becomes fully explicit and fully implicit, respectively, and $\theta = \frac{1}{2}$ corresponds to the Crank–Nicholson algorithm.

A similar semi-implicit algorithm in the first category is the "time-integrated" method[5] used in the RAUMZEIT code.[32] This algorithm also features the entire neutron-balance operator acting on the flux at $t + \Delta t$ and at t, but with the elements of the operator modified by scalar factors that arise from integrating the time-dependent equations over the interval t to $t + \Delta t$ subject to the assumption of linearly varying reaction rates. Unpublished numerical studies by the author indicate that the time-integrated and θ methods, with $\theta = \frac{1}{2}$, yield essentially identical results for transients ranging from subcritical to superprompt critical and that the accuracy of both methods deteriorated less rapidly with increasing time-step size than for the fully implicit method. However, for sufficiently large time steps, both the time-integrated and $\theta = \frac{1}{2}$ methods exhibited oscillatory solutions not observed with the fully implicit method.

Rhyne and Lapsley[33] recently proposed an algorithm based on a weighted residual technique and denoted the WR method, which is similar to the θ and time-integrated methods in that the entire neutron-balance operator acts on the fluxes at times $t + \Delta t$ and t. However, the discrete approximation to the time-derivative terms involves a three-point difference relation, which introduces the fluxes evaluated at $t-\Delta t$ into the algorithm for the fluxes at $t + \Delta t$. Numerical studies[34] indicate that this method deteriorates in accuracy less rapidly than the θ method, with $\theta = 1$ or

$\frac{1}{2}$, when the time-step size is increased. Moreover, the solutions obtained with the WR algorithm have not been observed to exhibit oscillations for large time steps, as is the case for the $\theta = \frac{1}{2}$ and the time-integrated methods. On the basis of the small amount of evidence available, the WR method seems to be an advance over the θ and time-integrated methods. However, the former has not yet been subjected to the extensive use that the latter two have experienced.

The semi-implicit methods of the first category have in common the fact that the entire neutron-balance operator acts on the flux at time $t + \Delta t$, which means that the flux at all mesh points and energy groups must be solved for simultaneously. This presents no difficulty for few-group one-dimensional problems for which the solution may be obtained by a forward and backward sweep of the spatial mesh, inverting a matrix of rank equal to the number of groups at each mesh point. However, for many-group and/or multidimensional problems, iterative methods must be invoked. This motivated the development of semi-implicit methods of the second category.

Many of these methods have been examined by Hansen and his colleagues,[35] who first perform an exponential transformation. Hence it is appropriate to digress for a moment to discuss an exponential transformation that is performed to reduce truncation error. The flux at each mesh point and energy group and the percursor density at each mesh point are written, within each time-step interval, as the product of an exponential term and a second term that is assigned an undetermined time dependence. If the exponential terms are approximated reasonably accurately, the second term will exhibit a small and presumably smooth variation that can be represented adequately by a low-order difference approximation. The method was used initially with the point-kinetics model, and the exponents were chosen as the reciprocal periods associated with the solution to the inhour equation with material properties pertinent to the time interval. When Pluta, Hübschmann, and Lill[36] extended the method to the coupled-core equations, they suggested that the exponents be estimated from the logarithm of the ratio of the two most recent values of the variable. Subsequent developments have utilized some variant of this latter idea.

After performing an exponential transformation, Andrews and Hansen[37] decomposed the neutron-balance operator so that the terms that coupled the fluxes at different mesh points but in the same group operated on the fluxes at time $t + \Delta t$, whereas the terms that coupled the fluxes in different energy groups but at the same mesh point operated on the fluxes at time t. In this manner it is only necessary to solve simultaneously for the fluxes in a given group, and repeat for each group, which can be done readily for one-dimensional problems. This algorithm can be shown to be unconditionally stable[37] and is the basis of the one-dimensional multigroup code GAKIN.[38]

When the GAKIN method is applied to two-dimensional problems, the terms in the neutron-balance operator that couple the fluxes at different mesh points in a given group are more involved (five-point rather than three-point difference relations) than for the one-dimensional case, and it is necessary to solve for the fluxes at time $t + \Delta t$ iteratively. An alternate procedure has been suggested by McCormick and Hansen,[39] who replace the coupling in one of the two dimensions by a buckling based on the most recent solution. The direction in which the buckling replacement is made alternates each time step. In this manner the solution for the two-dimensional flux at $t + \Delta t$ is obtained by solving a set of one-dimensional problems, one for each mesh point in the other dimension. This method has not been tested extensively.

A somewhat different separation of the neutron-balance operator for two-dimensional problems has been developed by Reed and Hansen[40] and by Denning, Redmond, and Iyer.[41] The basis of this method, known as the alternating-direction explicit (ADE) method, is to separate the neutron-balance operator so that the terms describing the coupling among fluxes at different mesh points at time $t + \Delta t$ are based on only a two-point difference relation for one dimension. Using the known value of the flux on the boundary, the algorithm becomes explicit when the mesh is traversed sequentially. The direction of the spatial coupling is alternated on successive time steps. Reed and Hansen[40] find that the exponential transformation significantly reduces the truncation error associated with the ADE algorithm. The method has been shown to be stable, but has not undergone extensive numerical testing.

The alternating-direction implicit (ADI) method has also been examined for two-dimensional problems by Hageman and Yasinsky[42] and by Wight and Hansen.[43] In this method the neutron-balance operator is separated so that at time $t + \Delta t$ the coupling among fluxes in a given group at different mesh points is one-dimensional, with the most recent values of the fluxes in the other dimension used to evaluate the coupling term in that direction. The direction of the coupling alternates on successive time steps. Hageman and Yasinsky[42] have developed a variant of this

method, known as ADI-B^2, in which the coupling term in the other direction is replaced by a buckling evaluated from fluxes at time t. The ADI method is stable but has large truncation error. Wight and Hansen[43] found that the exponential transformation reduced the truncation error, but the method was no longer unconditionally stable. Experience with the method has been limited.

Semi-implicit methods of the second category require much less effort per time step than semi-implicit methods of the first category, but have a larger truncation error. For comparable accuracy, many relatively economical time steps are required for methods of the second category, whereas fewer more costly time steps are required for methods of the first category. Comparative studies[39-43] are inconclusive regarding which type method requires the least computational time for two-dimensional problems. Hageman and Yasinsky[42] found the ADI method to be comparable to or better than the θ method for simple model problems (uniform cores) but found the θ method to be definitely superior for nonmodel problems. They found the ADI-B^2 method to be superior to the ADI method and comparable to or better than the θ method for nonmodel problems. The ADE method was found to be somewhat better than the ADI or GAKIN methods.[35] Reed and Hansen[40] found the ADE method to be comparable to the θ method. Denning, Redmond, and Iyer[41] found the ADE method to be superior to the θ method for superprompt-critical transients but inferior for delayed-critical transients.

Several studies of numerical integration methods have been made. These studies were based on nodal or modal approximations. Fuller, Meneley, and Hetrick[44] have generalized the earlier work of Kaganove and Brittan on the method of undetermined parameters for the spatially dependent kinetics equations. Umar and Ram[45] have proposed a time-varying parameter method based on the separation of the neutron-balance operator into a constant and time-varying part. Neither of these methods has been compared with other algorithms. Clark and Margolis[46] have studied various integration algorithms for the multimode representation of the spatially dependent kinetics equations. Hurwitz[47] proposed a parametric projection method for solving the coupled-core equations. Belleni-Morante[48] showed that the coupled-core equations could be cast in integral form and that methods similar to those employed previously for the integral form of the point-kinetics equations could be used to obtain a numerical solution.

Two studies dealing with the theoretical foundations of the neutron kinetics equations have been made. Henry[49] has given a general derivation of the space-dependent multigroup kinetics equations from a variational functional. He considered the spectral synthesis (overlapping-group equations) and parallel-group equations, as well as the few-group equations. Stacey[50] derived the multigroup equations with flux- and adjoint-weighted group constants for the case when the weighting functions could vary with time and position. He found that new terms arose because of spatial and temporal variations in the weighting functions. Stacey also examined the positivity properties of the generalized equations and considered the question of the consistency between the discrete approximation to the adjoint equations and the mathematical adjoint to the discrete approximation of the multigroup kinetics equations.

As a point of reference, it should be noted that the quasi-static methods discussed in the previous section can be viewed as indirect methods for numerically integrating the space- and energy-dependent kinetics equations, when the solutions for the shape and amplitude functions are iterated to consistency and the approximations associated with the particular formulation are valid. In particular, the improved quasi-static method proposed by Ott and Meneley[24] involves no approximations other than the numerical ones used in obtaining the difference algorithms from the differential equations.

At present, one-dimensional few-group problems can be solved expeditiously, and multigroup problems can be solved in a reasonable amount of time (tens of minutes). For those cases in which the flux amplitude is changing much more rapidly than the spatial or spectral distribution, the improved quasi-static method is more economical than the semi-implicit methods. However, when the spatial or spectral distribution is changing rapidly relative to the time scale of the transient, the latter methods are to be preferred.[9] Two-dimensional calculations are another matter, however, and computing times for realistic problems are on the order of hours.

For practical applications, solution of the relevant feedback equations must be included in comparisons of accuracy, efficiency, and stability. There has been little attention to this important question, which suggests a potentially fruitful area for future research.

A number of approximate methods have been developed to decrease the computing time required to solve the space- and energy-dependent neutron kinetics equations. Associated with these methods, of course, is

a certain loss of detail and/or accuracy. The next three sections of this article are devoted to a discussion of such methods.

COARSE-MESH FEW-GROUP APPROXIMATIONS

The most obvious stratagem for reducing the computing time associated with the multigroup finite-difference method is to reduce the number of mesh points and/or groups, relative to what would normally be considered adequate to calculate the static neutronics properties of the reactor. This reduction may be done simply without modifying the computational algorithm, or it may be done in conjunction with a redefinition of the algorithm.

A coarse-mesh few-group solution may be obtained with any of the previously mentioned codes or with codes that are inherently limited to a coarse mesh, such as FREAK.[51] Relatively little work has been published indicating the tradeoff of accuracy for computational economy as the number of mesh points and/or groups is reduced. Unpublished work by Wade[52] indicates that mesh spacings larger than a neutron migration length can introduce large errors.

For thermal reactors a two- or three-group transient analysis is generally assumed to be adequate on the basis of the success of this type of group structure in static analyses, although this assumption does not appear to have been checked extensively. For fast reactors, on the other hand, approximately 10 to 30 groups are generally felt to be necessary for static analyses, and thus also for transient analyses. Again, this assumption has not been examined sufficiently to draw general conclusions.

Hitchcock, Hansen, and Henry[53] compared the asymptotic periods calculated for delayed-critical transients with 16 groups with those calculated with 8 and 4 groups, where the constants for the 8- and 4-group calculations were obtained by collapsing the 16-group constants with simple flux weighting. They found that, even though the 8- and 4-group models agreed well with the 16-group model in the static eigenvalue, disagreement in asymptotic periods of 6% (8 groups, fast reactor), 31% (4 groups, fast reactor), −2.7% (8 groups, thermal reactor), and −5.3% (4 groups, thermal reactor) was noted. Several workers have subsequently examined this problem and concluded, as summarized by Henry,[54] that the difficulty in accounting properly for the lower energy of the delayed-neutron spectrum is due to the failure of the group collapsing with flux weighting. Flux–adjoint weighting appears to satisfactorily resolve this discrepancy, as does the simpler prescription of just using flux–adjoint weighting to define effective delay fractions. Mortenson and Putnam[55] also discuss this problem, as does Meneley,[56] who finds that as few as nine carefully chosen groups (with flux-weighted constants) may be adequate to describe fast reactor transients.

Stacey[15,57] investigated the use of spectral synthesis (overlapping-group) methods as an alternative to the conventional few-group methods for fast reactor transient analysis. The basis of these methods is the synthesis of the energy dependence of the neutron spectrum from precomputed trial spectra. He examined sodium-voiding problems with Doppler feedback and found that solutions obtained with only two trial spectra matched 26-group solutions to within a few percent in transients in which sufficient spectral changes took place so that conventional two-group calculations (with flux-weighted and flux- and adjoint-weighted group constants) were in error by an order of magnitude. The spectral synthesis method seems capable of yielding a better representation of spectral changes than does a conventional few-group model of equivalent computational complexity. However, the positivity properties associated with the latter do not occur for the former, which could potentially lead to difficulty. In addition, the greater amount of coupling among equations in the spectral synthesis method implies that new iteration schemes may be needed for multidimensional problems.

A number of methods have been proposed for arriving at an algorithm for coarse-mesh difference equations which is more accurate than the conventional type of difference algorithm. These methods have in common the assumption of some knowledge about the spatial distribution between mesh points.

Riese[58,59] assumed that a reactor could be broken up into many large regions, the flux within each being represented by a low-order polynomial function of position. Using this assumption to obtain trial functions for use in a variational functional, he arrived at a finite-difference algorithm, in which the equations are more highly coupled than in the conventional algorithm. This algorithm is the basis of the VARI-QUIR (2D) code.[58] Koen and Hansen[60] used a similar procedure. Yasinsky and Foulke[61] recently demonstrated that the use of overlapping piecewise continuous polynomials led to one-dimensional finite-difference algorithms that were significantly more accurate than the conventional algorithms for mesh spacings, which are large compared to a neutron migration length.

Bobone[62] proposed a procedure similar to that of Riese but based it on an expansion of the flux within each region in solutions to the Helmholtz equation characteristic of that region. By requiring flux and current continuity in a least-mean-square sense at region interfaces, he obtained what amounted to coarse-mesh finite-difference equations.

Alcouffe and Albrecht[63] have applied the methods of variational synthesis (to be discussed in a subsequent section) to obtain finite-difference algorithms. They expanded the flux shape within a given region in a single precomputed spatial trial function, which may change at discrete times. Using this trial function in a variational functional, they obtained equations for the combining coefficients appropriate to the different regions of a reactor. These equations may be interpreted as finite-difference algorithms.

These improved coarse-mesh algorithms are promising, but, with the exception of VARI-QUIR, they have not been tested extensively. They are closely related to the modal and nodal methods discussed from a somewhat different viewpoint in the next two sections.

Saji and Axford[64] proposed a heterogeneous model in which fuel rods were treated as line sources. Their model was restricted to rods embedded in a uniform medium. This type model is more appropriate for reactors with relatively few large fuel elements than for present power reactors in which large numbers of fuel elements are better treated by homogenization. This does not mean that heterogeneities are unimportant, for certainly they must be treated in computing feedback effects associated with fuel and coolant temperature. However, the neutron-flux calculation can probably be performed quite satisfactorily with a homogenized model.

MODAL/SYNTHESIS METHODS

A variety of methods, having in common the expansion of part or all of the spatial dependence in known functions with undetermined expansion coefficients that depend upon the remaining spatial variables (if any) and time, have been developed in an attempt to obtain an economical, but accurate, spatial approximation. These methods have been variously labeled as modal-expansion or synthesis methods. The appropriate equations are obtained by substituting the assumed expansion for the flux in the space- and energy-dependent neutron and precursor kinetics equations, weighting with a function that depends on the same spatial variables as the expansion functions, and integrating over those spatial variables. This is repeated for as many different weighting functions as there are expansion functions to obtain equations equal in number to the unknown expansion coefficients. An equivalent derivation, and identical equations, results from the application of a semidirect variational technique.

The resulting approximate equations are either ordinary (time) or partial (space and time) differential equations, depending on whether all or part of the spatial dependence, respectively, is expanded. These equations must then be numerically integrated, following a finite-difference approximation to the remaining space dependence. Methods in which all the spatial dependence is expanded, resulting in ordinary differential equations for the time-dependent expansion coefficients, are known as "time-synthesis" methods. "Space–time" synthesis is the term used for those methods in which only part of the spatial dependence is expanded.

Two rather different classes of spatial functions have been investigated for the expansion of the flux. In the earlier analyses the fundamental and higher harmonic eigenfunctions of some neutron-balance operator characteristic of the initial configuration of the reactor were chosen as expansion functions. Recent work has concentrated more on the use of expansion functions, which are the fundamental solutions of the neutron-balance equations evaluated for different configurations of the reactor. These latter functions are referred to as "synthesis" functions to distinguish them from the former, which are referred to as "eigenfunctions."

A number of different eigenfunctions were examined by Kaplan[65] for the property of "finality," which means that the equations for the different expansion coefficients are not coupled. He examined (1) λ eigenfunctions, which are the eigenfunctions of the static neutron-balance operator; (2) w eigenfunctions, which are generated by an operator similar to the static neutron-balance operator but with a w/v term that arises from the flux time derivative, a $(1-\beta)$ multiplying the fission term, and w acting as the eigenvalue; and (3) the natural eigenfunctions, which are generated by the operator representing neutron plus precursor plus feedback equations with time derivatives replaced by w in each equation, and with w acting as the eigenvalue. Only the latter eigenfunctions possess the property of finality, and then only when no external change is made to the properties of the reactor.

Henry[66] found that the eigenvalues of the natural eigenfunctions occurred in clusters containing a number of eigenvalues equal to the sum of the number of

neutron energy groups and the number of delayed-neutron precursor groups, when no feedback equations were considered. By postulating that the eigenfunctions corresponding to all the eigenvalues in a cluster have identical spatial (and angular) shapes, he defined a set of "inhour" eigenfunctions having certain useful orthogonality properties. Henry and Kaplan[67] subsequently presented a formalism for relating the natural eigenvalue to a linear functional which can be evaluated using the easier to compute λ eigenfunctions. (In general, the natural eigenfunctions are complex and have been computed successfully in one-dimensional geometries only, whereas the λ eigenfunctions can be readily generated by conventional static codes if node lines can be identified by symmetry.)

Foulke and Gyftopoulos[68] applied the natural eigenfunctions to interpret oscillator experiments in the NORA reactor[69] and to transient analyses. Numerical experiments indicated that the asymptotic tilt resulting from a given perturbation could be directly correlated with the ratio of the fundamental-to-first harmonic natural eigenvalues. Comparison with direct numerical solution indicated that, to obtain satisfactory accuracy for a transient following a step perturbation in a local region of width Δx, at least $M+1$ harmonics are needed, where M is the lowest spatial harmonic whose wavelength is less than $2\Delta x$.

Garabedian and Lynch[70] considered a Fourier-series expansion for a multiregion slab reactor, with the expansion functions being orthogonal on the interval defined by the slab width. Their results implied that a rather large number of such expansion functions would be required to represent the effect of localized perturbations.

Mathews[71] derived a spatially dependent kinetics model based on a two-λ-mode expansion. He indicated how conventional perturbation theory codes could be utilized to evaluate the model parameters.

Modal models based on eigenfunction expansions do not appear to be practical for calculating transients resulting from localized perturbations in multiregion reactors. This impracticality stems from either the large number of eigenfunctions required or from the difficulty associated with computing the eigenfunctions in complicated geometries, or both, depending upon the type of problem and the types of eigenfunctions.

This has motivated an effort to develop modal models based on expansion functions which are more or less tailored to represent flux shapes anticipated during a transient and which are possible to calculate for realistic geometries. Such models are usually referred to as synthesis models, and the expansion functions are sometimes known as synthesis functions, a designation which will be adopted in this article.

Dougherty and Shen[72] derived one of the earliest synthesis approximations, employing a semidirect variational method. They also introduced the use of "Green's functions" expansion functions, which are computed from the static neutron-balance equation by setting the fission cross section to zero and using a source that is nonzero only in a localized region. The source is taken as the fission source for the critical reactor, which must be obtained by solving the static neutron-balance equation. When the reactor is separated into a number of complementary regions for the purpose of generating Green's functions, the resulting model is expected to be capable of representing changes that occur uniformly throughout any one of these same regions and to represent many combinations of such changes. The success of such a method in analyzing transients in reactor models composed of a few large regions, in one or more of which a uniform perturbation had occurred, was demonstrated by Dougherty and Shen and more recently by Rohr and Becker.[73] Carter and Danofsky,[74] Stevenson and Gage,[75] and Yasinsky[76] chose an application for which the method seems particularly well suited, the analysis of transients in a system composed of an array of physically separated cores. A comparison made by Yasinsky with a direct numerical integration of the finite-difference equations for a one-dimensional two-group model, consisting of three 70-cm-thick fast reactor cores separated by 48 cm of blanket material, is shown in Fig. 6. The perturbation consisted of a 0.5% ramp decrease in the absorption properties of the right core in the time interval $0 < t < 0.5$ sec. Two synthesis solutions are shown. Solution 2 was obtained with a model that used three Green's functions expansion functions, each of which was the solution of a static problem with only one of the cores present. (These expansion functions are similar to, but slightly different from, the Green's functions of Dougherty and Shen.) A model that used three whole-reactor static solutions corresponding to the material configurations at three different times during the transient was used to obtain solution 1. Both synthesis solutions agreed well with the direct solution for this loosely coupled core. For more tightly coupled cores, Yasinsky found the first type of synthesis solution (whole-reactor expansion functions) to be somewhat more accurate.

Kaplan, Marlowe, and Bewick[77] introduced the use of time-dependent flux-synthesis methods with whole-reactor expansion functions chosen to "bracket" the extreme flux shapes anticipated during a transient.

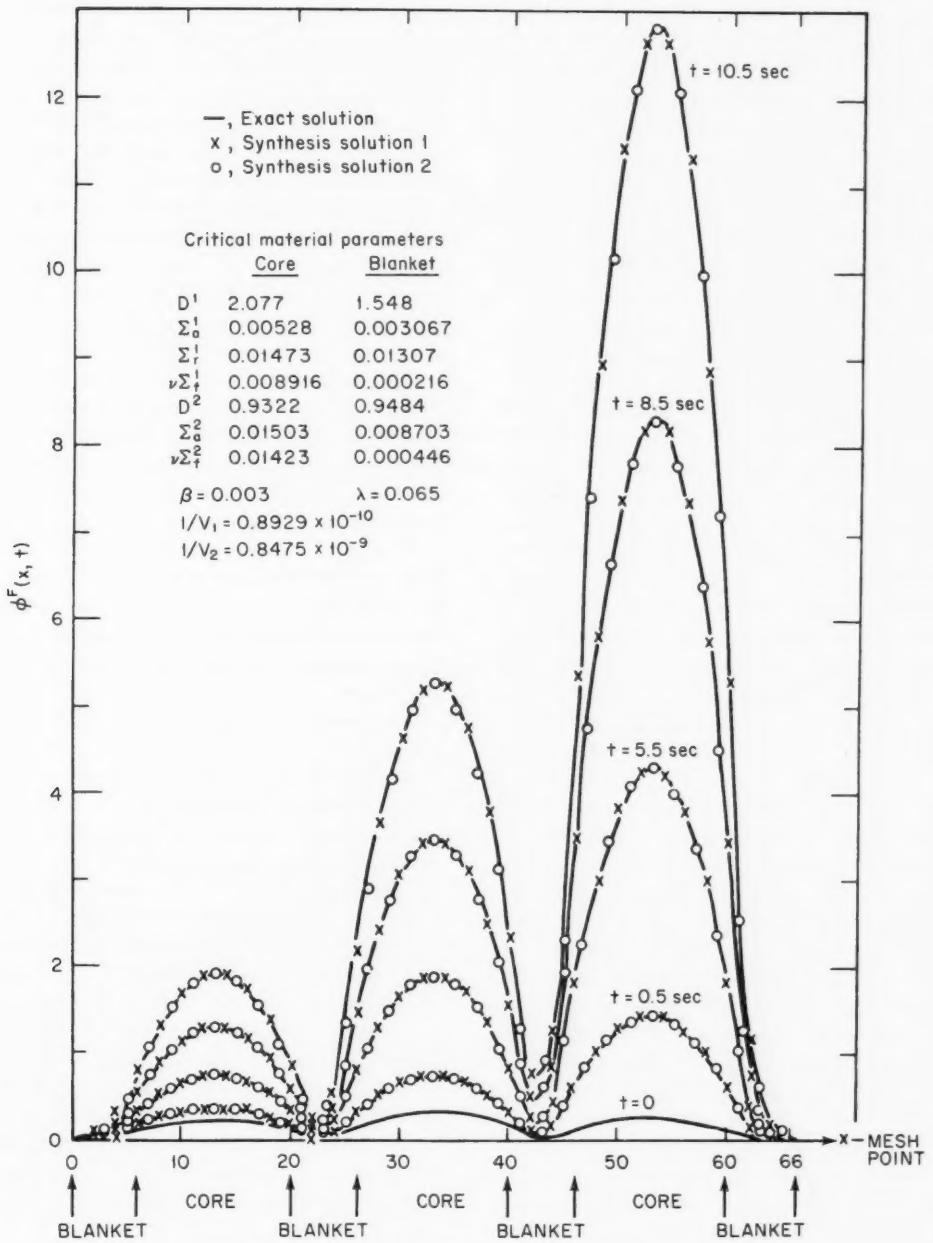

Fig. 6 Fast-flux distributions in a slab representation of a modular fast reactor assembly.[76]

These flux shapes can be computed for realistic geometries with standard codes. Both the time-synthesis and space–time-synthesis approximations, using whole-reactor expansion functions, have been extensively tested.[3,77-83] The general conclusion is that the methods are capable of yielding quite accurate solutions when appropriate expansion functions are used. Unfortunately the synthesis equations do not possess any type of positivity properties, and one anomalous situation has been reported in which a spurious solution was obtained.[80,81]

Space–time synthesis seems preferable to time synthesis for multidimensional problems. It is difficult to synthesize the transient flux shape along the direction of a moving control rod with a relatively small number of expansion functions, but it is relatively easy to synthesize the flux distribution in a plane perpendicular to the control-rod motion and to calculate directly the variation of the expansion coefficients along the direction of the control-rod motion. Moreover, the dimensionality of the calculations that must be performed to obtain expansion functions is less than the dimensionality of the problem for space–time synthesis but not for that of time synthesis.

The selection of appropriate expansion functions can normally be motivated by the circumstances of the transient. However, delayed-neutron holdback[79] (in subcritical and delayed-critical transients initiated from power), the w/v term arising from the flux time-derivative term[8] (prompt-supercritical transients), and temperature feedback can have a profound effect on the flux shape and can make the choice of an appropriate expansion function something of an art.

Yasinsky's work[82] serves to illustrate the methodology involved in, and the accuracy typical of, synthesis calculations. One of the models studied was a portion of a large seed–blanket thermal reactor. The first transient was induced by a mild decrease in absorption cross sections and a slight increase in downscattering cross section in an upper portion of a vertical seed region over a 0- to 0.2-sec interval. The space–time synthesis solution used three expansion functions that were one-dimensional static (fundamental λ mode) solutions; the first two for x slices through the two unperturbed axial regions and the third for an x slice through the axial region with the maximum perturbation present. The thermal-flux distribution computed with the synthesis model is compared with a direct solution (TWIGL) in Fig. 7.

Another transient was calculated for this same model, but with the perturbed region extending further down and with the perturbation occurring in a 0- to 0.02-sec interval. As seen in Fig. 8, the synthesis calculation does not agree with the direct solution as well in this transient as in the delayed-critical transient illustrated in Fig. 7. Adams[8] traced the error to the effect of the w/v term in the metal and water regions that separated the seed and blanket regions on the flux shape and found that using expansion functions that accounted for this effect markedly improved the results of the synthesis calculation.

The recent development of discontinuous flux synthesis has increased the flexibility and capability of the method. Yasinsky[84] used a formalism that permitted different sets of expansion functions to be used during different time intervals. This enabled the expansion functions most appropriate for a given interval to be used, without requiring that an unnecessarily large number of functions be used in any given interval. Kessler[12] used this same technique and proposed an iterative method for improving on the expansion functions to account for the effect of temperature feedback.

Yasinsky[85] and Stacey[86] extended the earlier work on discontinuous static flux synthesis to provide the capability of using different sets of expansion functions in different zones perpendicular to the plane of the expansion function (e.g., if a three-dimensional reactor is to be calculated, one set of x–y functions may be used in the region $z_1 < z < z_2$, another set in the region $z_2 < z < z_3$, etc.). Adams[8] has shown that some of the synthesis calculations reported by Yasinsky[82] can be improved and made more economical (two rather than three expansion functions) by using axially discontinuous synthesis.

Stacey[86] extended the multichannel synthesis formalism to time-dependent problems. This formalism allows different sets of expansion functions to be used in different regions (channels) in the plane in which the expansion functions are defined, or allows a given set of expansion functions to be combined differently in different channels. Similar formalisms have been studied by Alcouffe and Albrecht[63] and by Fuller, Meneley, and Hetrick.[44] Stacey[86] compared the multichannel (MC) and conventional (SC) synthesis methods for a series of one-dimensional models subjected to a sequence of strong local perturbations. Using rather general expansion functions not specifically tailored to the transient, he found that the multichannel feature (i.e., the ability to combine the expansion functions differently in different regions) considerably enhanced the accuracy of the calculation. The flux distributions (normalized) computed by different synthesis models, all using the same expansion functions, are shown in

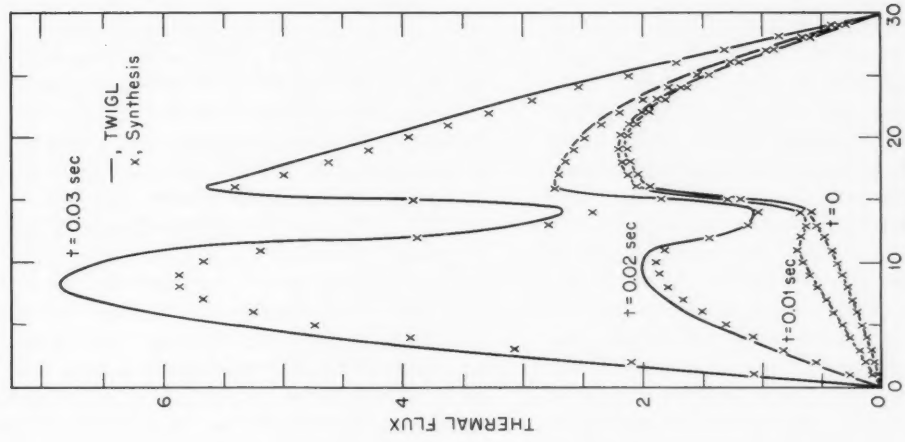

Fig. 8 Thermal flux at x mesh point 8 for prompt-supercritical transient in light-water breeder reactors.[82]

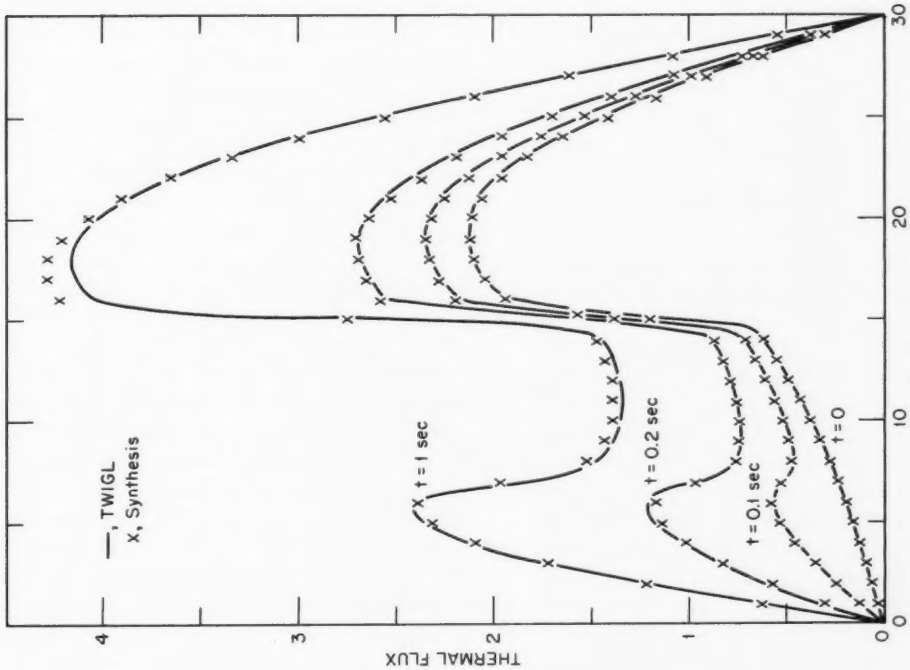

Fig. 7 Thermal flux at x mesh point 8 for delayed-critical transient in light-water breeder reactors.[82]

Fig. 9 for one such transient. Agreement with an exact (finite-difference) solution (RAUMZEIT) improves as the number of channels increases.

Variational methods have played an important role in the development of synthesis approximations. Dougherty and Shen,[72] Kaplan, Marlowe, and Bewick,[77] and Köhler[87] introduced variational functionals having the neutron kinetics equations as Euler equations. Becker[88] suggested the inclusion of a boundary term in the functional of Kaplan, Marlowe, and Bewick[77] which also made it stationary with respect to arbitrary endpoint variations, thus strengthening the theoretical foundation. Yasinsky,[84] Stacey,[86,89] Lewins,[90] Becker,[91] Kessler,[12] and Woodruff[92] considered variational functionals that admit trial solutions that are discontinuous in time, thus enabling synthesis equations that use different expansion functions in different time intervals to be developed. Yasinsky,[85] Stacey,[86,89] Alcouffe and Albrecht,[63] and Woodruff[92] introduced variational functionals that admit trial solutions that are discontinuous in space, thus leading to axially discontinuous and/or multichannel synthesis models. Becker[93] indicated how a least-squares variational method could be applied to time-dependent synthesis problems.

Wachspress[94] and Steele[95] have summarized variational flux-synthesis methods in recent reviews. Wachspress presented a critical review of methods used for spatial, spectral, and space–time synthesis, tracing the historical development and emphasizing the common basis. Steele presented a synopsis of recent work in spatial and space–time synthesis but did not make a critical comparison. Kaplan[96] and Stacey,[97] as well as Wachspress,[94] have reviewed the theoretical basis of the synthesis or modal-expansion method.

In production use are computer codes that analyze transients in few-group three-dimensional reactor models represented by as many as $\sim 10^6$ spatial mesh points, using the space–time synthesis method. Ignoring the time required to compute the two-dimensional expansion functions and from them the parameters of the synthesis model, which is considerable, calculational times for these transients are of the same order as for few-group one-dimensional problems. At present,

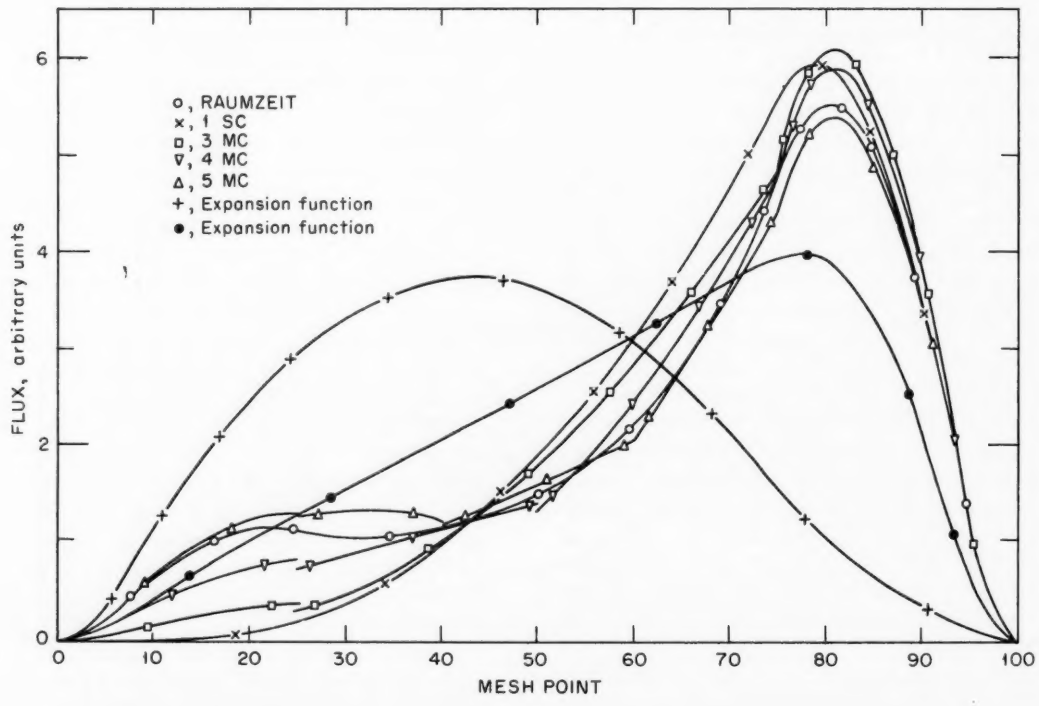

Fig. 9 Flux distribution at 1.0 sec for a 100-in. slab thermal reactor: comparison of multichannel and single-channel syntheses.[86]

no other method provides this magnitude of capability for such a relatively modest expenditure of computation time.

NODAL/COUPLED-CORE METHODS

When a reactor can be readily visualized as consisting of several cores, or regions, with a weak neutronic interaction, it may be possible to adequately represent the kinetic behavior by a system of coupled point-reactor equations, one for each core. The coupling should represent the neutronic interaction among the cores, or regions. Such a model is quite appropriate for an array of cores embedded in a reflector or blanket in which the neutronic interaction is not sufficient to significantly affect the flux distribution within any core, and it was to such reactors that the method was originally applied. Subsequently the method has been applied to reactors consisting of several large contiguous regions. In principle, the theory can be formulated to apply to either type reactor. However, the coupling parameters are generally evaluated with some static-flux and importance distributions within each core, or region, and these coupling parameters are assumed to remain constant during a transient. This procedure is more appropriate for separated cores, within each of which the flux and importance distributions are to a good approximation separable in space and time, than to contiguous regions of a large core, within each of which the flux or importance distribution may change appreciably during a transient.

Avery[98] developed the first coupled-core model within the framework of energy-dependent diffusion theory. His equations are based on the interaction of the partial fission sources in a given core caused by neutrons originating in that and other cores. Avery defined the partial fission source in core j due to neutrons originating in core k as the product of the total fission source in core j (calculated for some static-flux distribution), and the fractional importance in core j due to neutrons originating in core k. For evaluation of the fractional importance, static flux and importance distributions and a partial flux due to neutrons originating in reactor k are needed. The latter is computed as the solution to a source problem obtained by setting the fission cross section to zero everywhere and taking a static fission distribution in reactor k as the source, a procedure identical to that used to generate Green's functions expansion functions[72] in a modal technique. Source coupling parameters were then defined as the ratio of partial-to-total fission sources. Partial lifetimes were also defined in terms of these partial fluxes and an importance distribution. Prompt and delayed neutrons were assumed to have the same coupling parameters and partial lifetimes.

In applying the theory to coupled, thermal–fast reactors, Avery[99] chose to represent the reactor by coupled point-reactor equations for the fast and thermal neutrons. In this case, partial sources and partial fluxes were defined for the fast- and thermal-energy regions. Cockrell and Perez[100] extended Avery's formalism to the framework of neutron transport theory and introduced spatial and spectral coupling simultaneously. Their spatial coupling parameters are defined in terms of surface integrals.

Komata[101] recently demonstrated that Avery's formalism can be derived in a straightforward manner with the assumptions that (1) the delayed and prompt-fission spectra are identical, (2) the adiabatic approximation is valid, and (3) the spatial flux-distribution changes are much slower than the flux amplitude. Gandini and Salvatores[102] have applied perturbation theory to Avery's formalism to obtain expressions for changes in coupling parameters and partial lifetimes consequent to a perturbation in reactor properties.

Baldwin[103] presented a different formalism, which is obtained by directly introducing a source term into the point-kinetics equation for each core to represent the interaction with other cores. Baldwin assumed that the flux in each core was on an asymptotic period in order to derive a generalized inhour equation, but he could have arrived at coupled-core kinetics equations by relaxing this assumption to space–time separability of the flux in each core. Baldwin assumed that the spatial flux distribution in each core was the fundamental-mode diffusion-theory solution for that core, which implies an assumption that neutrons arriving from other cores appear in the fundamental mode. He also introduced a time-delay term for neutrons that originate in one core and arrive in another core. Schwalm[104] generalized Baldwin's model to multigroup transport theory. In contrast to the formalism of Cockrell and Perez,[100] Schwalm's equations couple the neutrons in one energy group in many cores and the neutrons in one core in many energy groups, but not in many energy groups in many cores directly. Harris and Fluharty[105] derived a similar model with the coupling parameters defined in terms of integrals over region surfaces which were evaluated from integral transport theory with a first-flight kernel.

Another class of coupled-core models, in which the coupled kinetics equations are derived directly from

the transport equation by integration over the spatial domain of each core, is generally attributed to Hansen.[106] He wrote coupled equations for the vector flux in a core due to neutrons originating in that core and for the vector flux in a core due to neutrons originating in other cores. Evaluation of the coupling parameters, which are a function of the delay time, can be extremely complicated in this model. For the purpose of evaluating the coupled-core parameters, the flux is assumed to be space–time separable within each core. Belleni-Morante[107] showed that, in transforming the transport equation into integral form, the surface terms lead to time delays. In later work[108] he proved that the existence of a distribution function for delay times is necessary due to the energy distribution of interacting neutrons. Kaplan[109] presented a similar derivation, but it was based on neutron diffusion theory and involved coupling parameters only between contiguous regions, which could be evaluated by performing surface integrals based on assumed flux and importance distributions.

Plaza and Köhler[110] derived coupled-core equations similar to Hansen's by integrating the importance-weighted transport equation for the entire vector flux. By explicitly introducing space–time separability of the flux within each core in a manner similar to that by Henry[18] for the point-kinetics equations, they arrived at coupled-core equations involving surface coupling terms for coupling parameters. Belleni-Morante[111] presented a derivation similar to this, but without explicitly assuming space–time separability or introducing the importance function.

Common to all the coupled-core/nodal formulations is a practical difficulty in computing the parameters of the model, particularly the interaction parameters (coupling parameters and delay times) in an appropriate manner. The use of static-flux and importance distributions characteristic of the initial static configuration to evaluate the model parameters is the standard practice (e.g., Seale and Hansen[112]). The fact that these distributions and hence the model parameters (especially the coupling parameters) may change during a transient has not yet been treated in a satisfactory manner. Hassan and Miley[113] determined coupling parameters by using the inverse kinetics method on a solution obtained with a finite-difference code. This technique appears to be limited to cases in which the coupling is predominantly in one direction (the case they considered) or in which two identical cores are involved. Wade and Rubin[114] have shown that the deleterious effect of a changing intranodal flux distribution on the coupling parameters could be partially nullified by empirically selecting coupling parameters so that extreme flux distributions characteristic of a transient are matched in a least-mean-square sense. (Their work was concerned with contiguous regions rather than with separate cores.) Asahi, An, and Oyama[115] used perturbation theory to obtain time-dependent coupling parameters, which they related to the higher spatial modes of the reactor. Köhler et al.[116] found that time-dependent coupling parameters could significantly influence a transient calculation but that delay times have a negligible effect for most transients of interest in fast reactor safety. Belleni-Morante[117] found that first-flight neutrons could significantly affect the interaction of coupled cores, which casts some doubt on models derived from neutron diffusion theory for very fast transients. He also developed a formalism embodying time-dependent coupling parameters.[118]

The application of coupled-core, or nodal, methods has been primarily to reactors composed of physically separated cores, such as those proposed for rocket propulsion or for one fast breeder reactor. Applications have also been made to reactors composed of several large contiguous regions, especially the coupled fast–thermal reactor concepts. Representative examples are given in Refs. 119–121.

The relation between the nodal and modal models has been examined by Wade,[122] who derived coupling parameters for a nodal model from a modal expansion in discontinuous expansion functions. Stacey[86] also commented on this relation, noting that the multichannel synthesis formalism reduces to a nodal model when a single expansion function is used and constitutes an extended nodal model, which can account for the nonseparability of the intranodal flux distribution when more than one expansion function is used.

Comparative reviews of the basic theory of coupled-core models have been made by Köhler[123] and by Adler, Gage, and Hopkins.[124] The various models are similar in many respects, and a consistent derivation of the different models from a common formalism would serve to emphasize the similarities and differences. Extensive numerical comparisons with more exact methods are needed to quantitatively evaluate the various formalisms.

EXPERIMENTS

A variety of experiments have been performed in which spatial neutronic effects were important. Some of these experiments were intended to provide data for

the verification of spatial-dependent kinetics models or for the determination of certain parameters of such models. Such experiments are discussed in this section. Spatial and spectral neutronic phenomena have also "contaminated" many experiments intended for other purposes, requiring appropriate corrections to be made. Experiments of this latter class are beyond the scope of this review.

Chezem et al.[121,125,126] summarized experiments on two uranium–graphite-fueled, beryllium-reflected Kiwi reactors. Reactivity coupling between the two reactors at equal power was determined experimentally as changes in control-rod position from isolated critical settings and was checked with asymptotic period measurements with the control rods fixed in the isolated critical positions. Reactivity coupling parameters at 6-, 9-, and 16-ft separations were 24.7, 11.9, and 3.3 cents, respectively. Conventional zero-power transfer functions obtained by oscillating reactivity in one of the reactors at frequencies up to 700 rads/sec compared well with the prediction (dotted line) of Baldwin's[103] coupled-core model, as shown in Fig. 10. The driving core is PARKA, and the following core is TNT. Pulsed-neutron experiments that exhibited damped oscillations in the passive core following a pulse in the active core were also performed. Hopkins and Adler[127] demonstrated that reflected coupled-core equations with a time delay could be formulated to yield complex roots, thus suggesting a theoretical confirmation of the observed oscillatory response.

Mihalczo[128] reported the results of Rossi alpha and pulsed-neutron experiments performed on pairs of unreflected, highly enriched uranium cylinders. His analysis was based on a coupled-core model with coupling parameters and delay times determined by Monte Carlo calculations. The calculated asymptotic decay constant agreed with the results of the Rossi alpha measurements to within 3.4%.

Hassan and Miley[129] compared one-dimensional finite-difference calculations (WIGL[28]) with experiment for a pulse propagating through a D_2O-moderated natural-uranium assembly (4- by 5-ft base by 4 ft high) which was coupled to the University of Illinois TRIGA reactor through a graphite thermal column. Three lattices were studied, varying in k_{eff} from 0.0 to 0.92. Using a model that predicted the steady-state flux distribution quite well, they were able to predict the attenuation of pulse amplitude, delay time, and pulse widths quite accurately, except near the end of the assembly. Their results are summarized in Figs. 11 and 12. They note that the results are quite sensitive to the homogenization procedure used in constructing the model parameters.

Ohanian and Diaz[130,131] also compared one-dimensional finite-difference calculations (WIGL[28]) with pulse-propagation experiments using the University of Florida SPERT assembly, which is a tank 8 ft long and 3 ft high and which has a variable width. The SPERT F-1 fuel rods (4 to 8% enriched UO_2) were arrayed in H_2O to form side-reflected cores with metal-to-water ratios (M/W) of 0.5, 1.0, and 1.5. Clean and cadmium-rodded experiments were performed. In general, the calculational model did not predict the static characteristics of the assembly satisfactorily; this may account, at least in part, for the fact that "the WIGL results do not accurately predict the dynamic response of these essentially simple systems which were studied."[130] The authors found a correlation between the agreement obtained in the space–time studies and that obtained in the static studies. Assemblies with higher M/W and with the cadmium rod present were more in error than clean assemblies with M/W = 0.5. Sensitivity of the results to small changes in the transverse buckling, obtained by a 1D transverse buckling iteration or by measurement, was noted by the authors. The rate at which the pulse propagates and the amplitude attenuation were consistently over-predicted, and the dispersion of the pulse was under-predicted. Results for one of the better-modeled assemblies (clean, M/W = 0.5) are illustrated in Fig. 13 (FWHM = full-width at half-maximum).

A series of space–time kinetics experiments has been performed in the Solid Homogeneous Assembly (SHA) at Knolls Atomic Power Laboratory (a thermal-spectrum assembly) for the express purpose of testing calculational models.[132] The side-reflected core, 5-ft long with a square cross-sectional area of 1 ft^2, consisted of a homogeneous mixture of paraffin, enriched UO_2 powder, and ZrO_2. For large longitudinal flux tilts with significant delayed-neutron hold-back, the core was decoupled by a polyethylene slab into two identical halves, resulting in an eigenvalue separation of ~0.6%. Transients were induced by introducing step perturbations near one end. The three-dimensional space–time synthesis model used for the transient calculation was verified by comparison with static foil-activation traverses,[133] asymptotic period measurements, and eigenvalue separation obtained by a static-flux-tilt method[6] and a two-detector noise correlation method.[134] Transient detector responses at several longitudinal positions agreed well with predicted values. An example is illustrated in Fig. 14 (the numbers indicate the experimental result

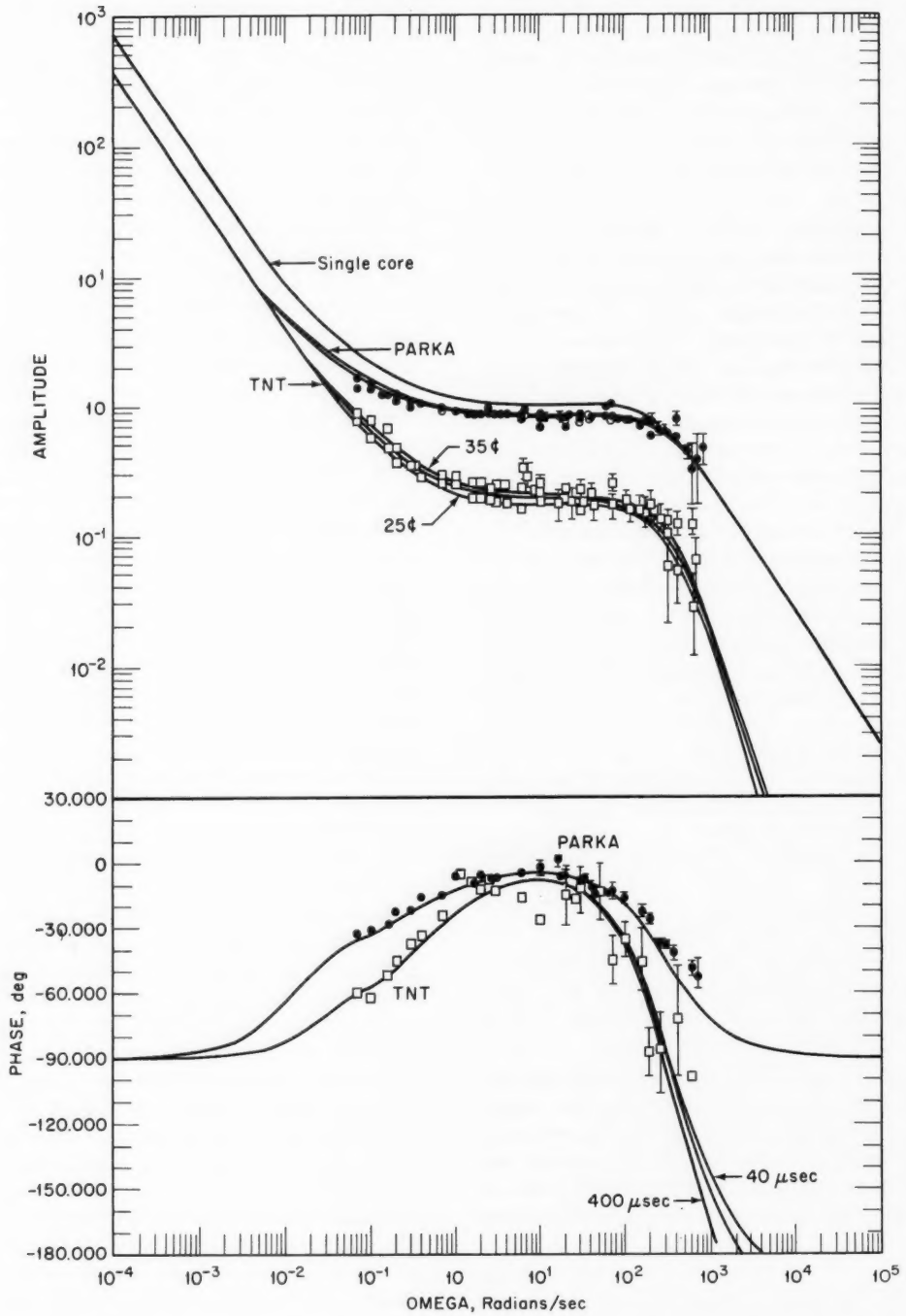

Fig. 10 Transfer function of Kiwi coupled-core reactor system at 6-ft separation.[125] Zero power; lag time 40, 130, and 400 μsec.

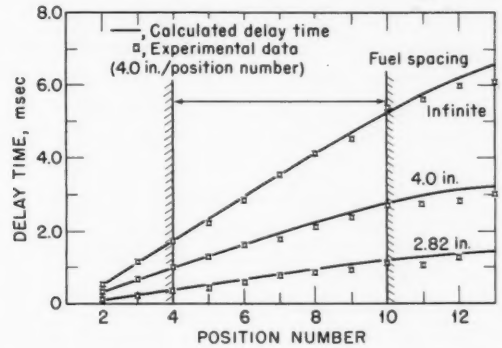

Fig. 11 Delay times for pulse propagation in a D_2O-moderated uranium assembly.[129]

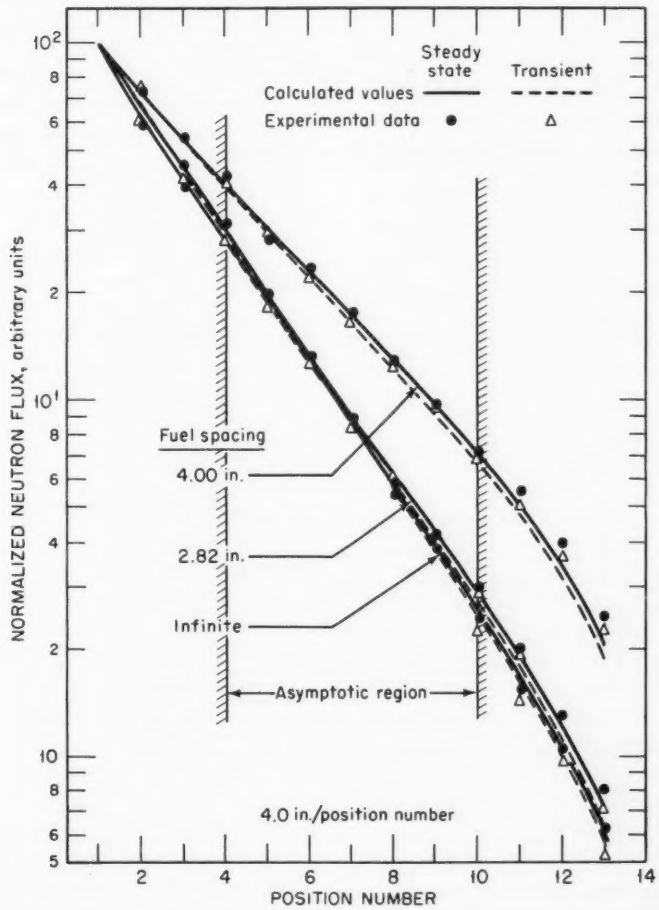

Fig. 12 Attenuation of steady-state flux and of pulse peak amplitude in a D_2O-moderated uranium assembly.[129]

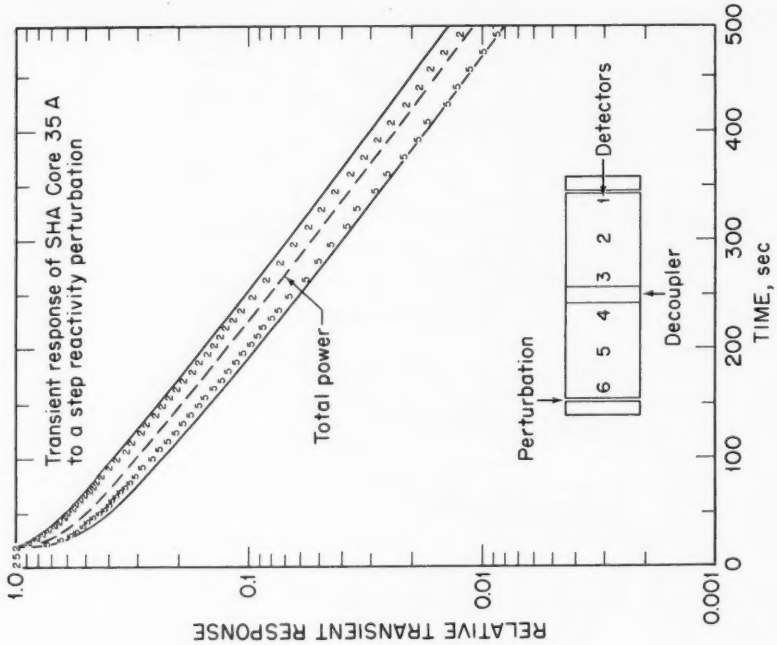

Fig. 14 Transient flux tilts in a homogeneous UO_2, paraffin-moderated assembly: comparison of theory and experiment.[132]

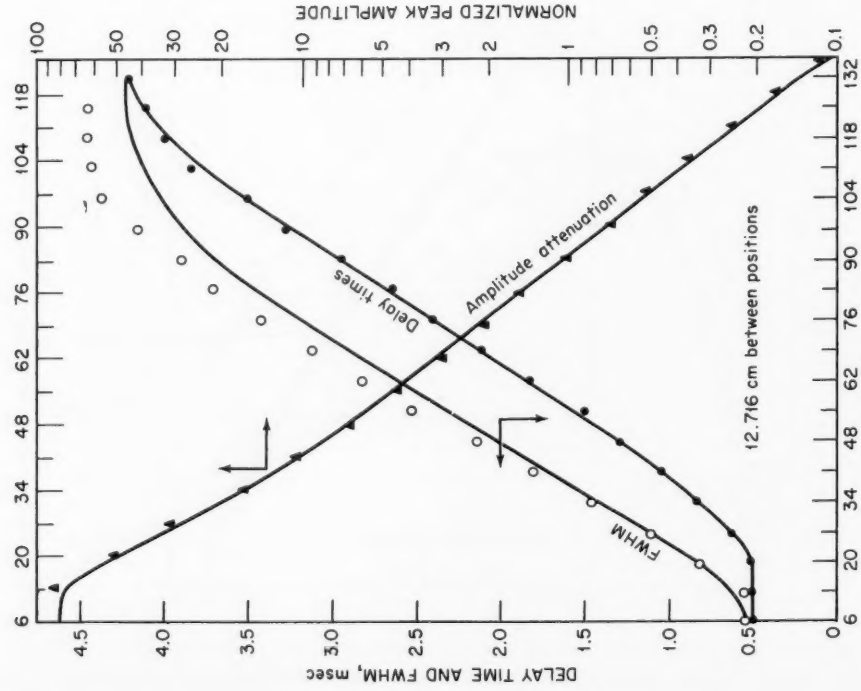

Fig. 13 Delay times, FWHM, and amplitude attenuation for pulse propagation in an H_2O-moderated assembly with SPERT-1 fuel.[131]

for the corresponding detector location, and the line indicates the corresponding prediction). The authors concluded that, if the core is well modeled statically, including the perturbation worth and the eigenvalue separation, the transient response is then predicted accurately by a few-group space–time synthesis model.

A number of authors have used spatially dependent kinetics models to predict the transfer function relating a localized perturbation to a localized detector response. Foulke and Gyftopoulos[68] applied a natural-mode expansion to infer the natural-mode eigenvalue from the NORA experiments.[69] They found good agreement for the amplitude and phase of the fundamental natural eigenfunction corresponding to the prompt thermal-group component as inferred from the data relative to theory, but poor agreement was obtained for higher harmonics. Cohn, Johnson, and MacDonald[135] developed a method for computing the transfer function with conventional static codes and obtained relatively good agreement with the NORA data. Wakabayaski and Hoshino[136] reported relatively good agreement between the transfer function measured in the SHE assembly and calculations based on a two-region analytical solution using the pole expansion method.[137] Saji[138] also compared the NORA data with the results of a *w*-mode analysis and reported favorable agreement.

Two-detector noise cross correlation has been used to infer the coupling parameter in a two-core model from sink frequencies in the cross power-spectral density. Boynton and Uhrig[139] applied this technique to the UFTR-10 at the University of Florida, and Hendrickson and Danofsky[140] and Hendrickson and Murphy[141] used this in analyzing the Iowa State UTR-10. Albrecht and Seifritz[142,143] used a similar procedure in analyzing data from the Karlsruhe Argonaut reactor. Albrecht and Danofsky[144] reported good agreement with these latter experiments below the first sink frequency using a modal-expansion model with Green's functions expansion functions.

Kinetics experiments in the two-slab Karlsruhe Argonaut[145] have been interpreted with coupled-core and modal-expansion models. Borgwaldt et al.[146] inferred coupling parameters from rod-drop experiments which agreed quite well with the result obtained by Albrecht and Seifritz from noise cross-correlation experiments. Edelmann, Murley, and Stegemann[147] analyzed Rossi alpha experiments with a modal-expansion method and obtained relatively good agreement on asymptotic decay constants. Earlier results are summarized in Ref. 148.

The available experimental evidence, which is quite limited, indicates that a calculational model capable of predicting certain static characteristics of an assembly will be successful in predicting the outcome of transients carried out in that assembly if delayed neutrons are treated properly. Important static characteristics, in this regard, are eigenvalue, flux distribution, worth of the perturbation which produces the transient, flux tilt in response to that perturbation, and perhaps others. Additional experiments in relatively clean assemblies, which can be modeled with minimal ambiguity, should be performed to establish this conclusion more firmly. Experiments on more-realistic assemblies should then be conducted to assess empirically the validity of the procedures used to evaluate the parameters of the calculational models used for transient analyses.

SUMMARY

Ample theoretical evidence has accumulated in recent years to establish that the conventional point-kinetics model, with fixed parameters averaged over spatial and spectral neutron-flux and importance distributions which are implicitly assumed to remain unchanged during a transient, may be significantly in error in failing to account for changes in these distributions. In large and/or loosely coupled thermal reactors, spatial changes are quite significant; spectral changes are less important, in general, and may be treated satisfactorily by a few-group representation. Spectral changes appear to be more important than spatial changes in fast reactors, although the spatial dependence of spectral changes is certainly important. Investigation of these effects is much more advanced for thermal reactors than for fast reactors. However, a general criterion for when these effects are important has not been established for either reactor type.

Efforts to account for these effects quasi-statically by reevaluating the parameters of a point-kinetics model at different times during a transient or by direct solution of the multigroup finite-difference equations have evolved to the point that accurate and economical codes exist for the solution of problems in one-space dimension, and attention is presently focused on the development of efficient algorithms for two-dimensional problems. Quasi-static methods appear to be superior to direct methods for transients in which the change in flux amplitude is much more rapid than the change in spatial and/or spectral flux distribution but inferior if this condition is not satisfied, although sufficient numerical testing to verify this remains to be done. Of the direct methods, semi-implicit techniques

appear to be most promising, although it is not clear at this time whether the fully coupled or the alternating, partially coupled algorithms are superior.

Nodal/coupled-core and modal/synthesis approximations have been extensively developed. The methods are more economical than direct or quasi-static methods, in general, and have been applied to realistic, multidimensional reactor models. The nodal methods have been relatively successful for describing transients in systems consisting of an array of separate cores, and relatively less successful when applied to a system composed of contiguous regions. The major problem associated with the nodal method is the computation of coupling parameters. Space–time synthesis methods have been used to compute detailed three-dimensional transient power distributions and represent the most highly developed capability presently employed in reactor transient analysis, as far as detail of representation is concerned. Synthesis methods suffer the drawback that the requisite skill in selecting appropriate expansion functions is usually acquired empirically, and the success of synthesis methods depends strongly on the selection of appropriate expansion functions.

The synergism of methods for calculating the neutron-flux distribution and methods for calculating the relevant feedback phenomena should be given more attention. Comparisons of numerical integration schemes and quasi-static methods should be done with consideration for the feedback equations. The incorporation of feedback effects into synthesis functions and nodal model parameters should likewise be examined.

Although the theoretical basis of space- and energy-dependent reactor kinetics seems to be in good shape, more numerical comparisons are needed between methods. Perhaps the greatest need is for more experimental data against which the theory and modeling procedures can be tested. Analysis of existing experiments seems to indicate that a calculational model that adequately predicts certain static characteristics will also predict transients adequately if delayed-neutron phenomena are properly treated. This may well be so, but additional experimental evidence to this effect would go a long way toward establishing a sound foundation for space- and energy-dependent transient reactor analysis.

Finally, much more work should be done to evaluate the practical importance of accounting for spatial and spectral effects, and the relative adequacy of the various approximate methods for doing so, in realistic transient analyses. The work to date has established the qualitative nature of these effects and has provided some measure of their potential magnitude but has been confined for the most part to somewhat hypothetical transients with idealized treatments of feedback. Initiation mechanisms, control-system response, and feedback mechanisms are often of overriding importance in determining the course of a transient, and the practical importance of an error in predicting the transient flux distribution is measured in terms of damage to reactor components.

REFERENCES

1. S. Kaplan, A. F. Henry, S. G. Margolis, and J. J. Taylor, Space–Time Reactor Dynamics, in *Proceedings of the Third International Conference on the Peaceful Uses of Atomic Energy, Geneva, 1964,* Vol. 4, p. 41, United Nations, New York, 1965.
2. W. M. Stacey, Jr., Xenon-Induced Spatial Power Oscillations, *Reactor Technol.*, **13**(3): 252 (Summer 1970).
3. J. B. Yasinsky and A. F. Henry, Some Numerical Experiments Concerning Space–Time Reactor Kinetics Behavior, *Nucl. Sci. Eng.*, **22:** 171 (1965).
4. K. Ott and J. T. Madell, Quasistatic Treatment of Spatial Phenomena in Reactor Dynamics, *Nucl. Sci. Eng.*, **26:** 563 (1966).
5. W. M. Stacey, Jr., and C. H. Adams, The Time-Integrated Method: A Quasi-Static Neutron Space–Time Approximation, *Trans. Amer. Nucl. Soc.*, **10:** 251 (1967).
6. D. C. Wade and R. A. Rydin, An Experimentally Measurable Relationship Between Asymptotic Flux Tilts and Eigenvalue Separation, in *Symposium on Dynamics of Nuclear Systems,* Tucson, 1970, University of Arizona Press, to be published.
7. S. Kaplan and S. G. Margolis, Delayed Neutron Effects During Flux Tilt Transients, *Nucl. Sci. Eng.*, **7:** 276 (1960).
8. C. H. Adams, Knolls Atomic Power Laboratory, private communication.
9. D. A. Meneley, Argonne National Laboratory, private communication.
10. S. O. Johnson, E. P. Gyftopoulos, and M. E. Radd, Effects of Flux Shape Changes on Power Excursion Behavior, *Trans. Amer. Nucl. Soc.*, **8:** 221 (1965).
11. J. B. Yasinsky, On the Use of Point Kinetics for the Analysis of Rod-Ejection Accidents, *Nucl. Sci. Eng.*, **39:** 241 (1970).
12. G. Kessler, Space-Dependent Dynamic Behavior of Fast Reactors Using the Time-Discontinuous Synthesis Method, *Nucl. Sci. Eng.*, **41:** 115 (1970).
13. J. F. Jackson and W. E. Kastenberg, Space–Time Effects in Fast Reactor Dynamics, *Nucl. Sci. Eng.*, **42:** 278 (1970).
14. D. A. Meneley and K. O. Ott, Spectral Effects in Liquid-Metal Fast Breeder Reactor Transients, *Trans. Amer. Nucl. Soc.*, **12:** 706 (1969).
15. W. M. Stacey, Jr., Spectral Synthesis Applied to Fast Reactor Dynamics, *Nucl. Sci. Eng.*, **41:** 249 (1970).

16. J. B. Yasinsky and L. R. Foulke, On the Use of Effective Delayed-Neutron Fractions for Few-Group Space–Time Analysis of Light Water Breeder Reactors, *Trans. Amer. Nucl. Soc.*, **13:** 280 (1970).
17. D. Saphier and S. Yiftah, The Effect of Errors in the Delayed-Neutron Data on Fast Reactor Static and Dynamic Calculations, *Nucl. Sci. Eng.*, **42:** 272 (1970).
18. A. F. Henry, Neutron Kinetics, Sec. 5.2 in Naval Reactor Physics Handbook, A. Radkowsky (Ed.), USAEC Report 7030, Vol. I, p. 855, Superintendent of Documents, U. S. Government Printing Office, Washington, 1964.
19. E. P. Gyftopoulos, General Reactor Dynamics, in *The Technology of Nuclear Reactor Safety*, T. J. Thompson and J. G. Beckerly (Eds.), Vol. 1, Chap. 3, p. 175, The M.I.T. Press, Cambridge, Mass., 1964.
20. M. Becker, A Generalized Formulation of Point Nuclear Reactor Kinetics Equations, *Nucl. Sci. Eng.*, **31:** 458 (1968).
21. A. F. Henry and N. J. Curlee, Verification of a Method for Treating Neutron Space–Time Problems, *Nucl. Sci. Eng.*, **4:** 727 (1958).
22. D. L. West, M. P. Kalman, J. E. Boyden, R. C. Stirn, and J. J. Barth, Use of the Adiabatic Approximation in Prompt-Critical, Large-Core Reactor Excursion Analyses, *Trans. Amer. Nucl. Soc.*, **8:** 497 (1965).
23. J. F. Jackson, W. F. Rhoades, and L. I. Moss, Analysis of SNAPTRAN-1 and -2 Reactor Kinetics Experiments, USAEC Report NAA-SR-11850, Atomics International, 1967.
24. K. O. Ott and D. A. Meneley, Accuracy of the Quasistatic Treatment of Spatial Reactor Kinetics, *Nucl. Sci. Eng.*, **36:** 402 (1969); also in Conference on Industrial Needs and Academic Research Reactor Kinetics, USAEC Report BNL-50117, p. 192, Brookhaven National Laboratory, 1968.
25. D. A. Meneley, G. K. Leaf, A. J. Lindeman, T. A. Daly, and W. T. Sha, A Kinetics Model for Fast Reactor Analysis in Two Dimensions, in *Symposium on Dynamics of Nuclear Systems*, Tucson, 1970, University of Arizona Press, to be published.
26. A. Galati, The Metastatic Method in Nuclear Reactor Core Kinetics Calculations, *Nucl. Sci. Eng.*, **37:** 30 (1969).
27. K. F. Hansen, Comparative Review of Two-Dimensional Kinetics Methods, USAEC Report GA-8169, Gulf General Atomic Incorporated, 1967.
28. A. F. Henry and A. V. Vota, WIGL-2—A Program for the Solution of the One-Dimensional, Two-Group, Space–Time Diffusion Equations Accounting for Temperature, Xenon, and Control Feedback, USAEC Report WAPD-TM-532, Westinghouse Electric Corp., Bettis Atomic Power Laboratory, 1965; also, A. V. Vota, N. J. Curlee, and A. F. Henry, WIGL-3—A Program for the Steady-State and Transient Solution of the One-Dimensional, Two-group Space–Time Diffusion Equations Accounting for Temperature, Xenon, and Control Feedback, USAEC Report WAPD-TM-788, Westinghouse Electric Corp., Bettis Atomic Power Laboratory, 1969; also, M. E. Radd, WIGLE-40, A Two-Group Time-Dependent Diffusion Theory Program for the IBM-7040 Computer, USAEC Report IDO-17125, Idaho Nuclear Corporation, 1965.
29. J. B. Yasinsky, M. Natelson, and L. A. Hageman, TWIGL—A Program to Solve the Two-Dimensional, Two-Group, Space–Time Neutron Diffusion Equations with Temperature Feedback, USAEC Report WAPD-TM-743, Westinghouse Electric Corp., Bettis Atomic Power Laboratory, 1968.
30. J. B. Yasinsky and L. A. Hageman, On the Solution of the Time-Dependent Group Diffusion Equations by an Implicit Time Differenced Iterative Method, in Proceedings of Conference on the Effective Use of Computers in the Nuclear Industry, USAEC Report CONF-690401, p. 55, April 1969.
31. T. A. Porsching and A. F. Henry, Some Numerical Methods for Problems in Reactor Kinetics, USAEC Report WAPD-T-2130, Westinghouse Electric Corp., Bettis Atomic Power Laboratory, 1968.
32. C. H. Adams and W. M. Stacey, Jr., RAUMZEIT—A Program to Solve Coupled Time-Dependent Neutron Diffusion Equations in One Space Dimension, USAEC Report KAPL-M-6728, Knolls Atomic Power Laboratory, 1967.
33. W. R. Rhyne and A. C. Lapsley, Numerical Solution of the Time- and Space-Dependent Multigroup Neutron Diffusion Equations, *Nucl. Sci. Eng.*, **40:** 91 (1970).
34. W. R. Rhyne, Further Experience with Implicit Time-Differencing Methods for Two-Dimensional Reactor Kinetics, *Trans. Amer. Nucl. Soc.*, **13:** 281 (1970).
35. K. F. Hansen, Finite-Difference Solutions for Space Dependent Kinetics Equations, in *Symposium on Dynamics of Nuclear Systems*, Tucson, 1970, University of Arizona Press, to be published.
36. P. R. Pluta, W. G. Hübschmann, and G. W. Lill, Kinetics of Coupled Thermal-Fast Spectrum Power Reactors, in *Coupled Reactor Kinetics*, p. 360, C. G. Chezem and W. H. Köhler (Eds.), Texas A&M Press, College Station, Tex., 1967.
37. J. B. Andrews and K. F. Hansen, Numerical Solution of the Time-Dependent Multigroup Diffusion Equations, *Nucl. Sci. Eng.*, **31:** 304 (1968).
38. K. F. Hansen and S. R. Johnson, GAKIN—A One-Dimensional Multigroup Kinetics Code, USAEC Report GA-7543, Gulf General Atomic Incorporated, 1967.
39. W. T. McCormick, Jr., and K. F. Hansen, Numerical Solution of the Two-Dimensional Time-Dependent Multigroup Equations, in Proceedings of Conference on the Effective Use of Computers in the Nuclear Industry, USAEC Report CONF-690401, p. 76, April 1969.
40. W. H. Reed and K. F. Hansen, Alternating Direction Methods for the Reactor Kinetics Equations, *Nucl. Sci. Eng.*, **41:** 431 (1970).
41. R. S. Denning, R. F. Redmond, and S. S. Iyer, A Stable Explicit Finite-Difference Technique for Spatial Kinetics, *Trans. Amer. Nucl. Soc.*, **12:** 148 (1969); also, S. S. Iyer, The Numerical Solution of the Space–Time Reactor Kinetics Equations Using an Alternating Direction Explicit Procedure, Ph.D. Thesis, Ohio State University, 1969.
42. L. A. Hageman and J. B. Yasinsky, Comparison of Alternating Direction Time-Differencing Methods with Other Implicit Methods for the Solution of the Neutron Group-Diffusion Equations, *Nucl. Sci. Eng.*, **38:** 8 (1969).

43. A. L. Wight and K. F. Hansen, Solving Reactor Kinetics Equations by Alternating-Direction Implicit Method, *Trans. Amer. Nucl. Soc.*, **12:** 620 (1969).
44. E. L. Fuller, D. A. Meneley, and D. L. Hetrick, Weighted-Residual Methods in Space-Dependent Reactor Dynamics, *Nucl. Sci. Eng.*, **40:** 206 (1970).
45. A. Umar and K. S. Ram, Coupled-Core Kinetics by Time-Varying-Parameter Method, *Trans. Amer. Nucl. Soc.*, **12:** 706 (1969).
46. W. G. Clarke and S. G. Margolis, The Multimode Synthesis Approximation for Space–Time Reactor Dynamics, USAEC Report WAPD-TM-635, Westinghouse Electric Corp., Bettis Atomic Power Laboratory, 1967.
47. H. Hurwitz, A Simplified Nonlinear Model for Qualitative Study of Reactor Distribution Transients, *Nucl. Sci. Eng.*, **23:** 183 (1965).
48. A. Belleni-Morante, The Kinetic Behavior of a Reactor Composed of G Loosely Coupled Cores, *J. Nucl. Energy*, **10:** 547 (1964).
49. A. F. Henry, Few-Group Approximations Based on a Variational Principle, *Nucl. Sci. Eng.*, **27:** 493 (1967).
50. W. M. Stacey, Jr., General Multigroup and Spectral Synthesis Equations, *Nucl. Sci. Eng.*, **40:** 73 (1970).
51. M. A. Perks, FREAK, A Fast Reactor Multigroup Kinetics Program in Conference on Applying Computing Methods to Reactor Problems, USAEC Report ANL-7050, p. 395, Argonne National Laboratory, 1965.
52. D. C. Wade, Knolls Atomic Power Laboratory, private communication.
53. J. T. Hitchcock, K. F. Hansen, and A. F. Henry, Spectral Effects in Multigroup Kinetics, *Trans. Amer. Nucl. Soc.*, **12:** 291 (1969).
54. A. F. Henry, Review of Computational Methods for Space-Dependent Kinetics, in *Symposium on Dynamics of Nuclear Systems*, Tucson, 1970, University of Arizona Press, to be published.
55. G. P. Mortenson and G. E. Putnam, Pitfalls in Reactor Kinetics Calculations, in *Symposium on Dynamics of Nuclear Systems*, Tucson, 1970, University of Arizona Press, to be published.
56. D. A. Meneley, in Reactor Development Program Progress Report, December 1969, USAEC Report ANL-7655, Argonne National Laboratory, Jan. 29, 1970.
57. W. M. Stacey, Jr., Spectral Synthesis Methods in Fast-Reactor Dynamics, in *Symposium on Dynamics of Nuclear Systems*, Tucson, 1970, University of Arizona Press, to be published.
58. J. W. Riese and G. Collier, VARI-QUIR: A Two-Dimensional Time-Dependent Multigroup Diffusion Code, USAEC Report WANL-TNR-133, Westinghouse Electric Corp., Astronuclear Laboratory, 1963.
59. J. W. Riese, A Variational Technique for Space–Time Neutron Diffusion, *Trans. Amer. Nucl. Soc.*, **7:** 22 (1964).
60. B. V. Koen and K. F. Hansen, Numerical Solution of the Coupled Core Kinetics Equations, *Trans. Amer. Nucl. Soc.*, **11:** 167 (1968).
61. J. B. Yasinsky and L. R. Foulke, Space–Time Methods for Movable Fuel Problems, in *Symposium on Dynamics of Nuclear Systems*, Tucson, 1970, University of Arizona Press, to be published.
62. R. Bobone, Analytic Solution of the Time Linearized Kinetics Equations in Multiregion Reactors in the Diffusion Approximation, *Trans. Amer. Nucl. Soc.*, **10:** 568 (1967).
63. R. E. Alcouffe and R. W. Albrecht, A Generalization of the Finite-Difference Approximation Method with an Application to Space–Time Nuclear Reactor Kinetics, *Nucl. Sci. Eng.*, **39:** 1 (1970).
64. G. Saji and R. A. Axford, Space–Time Kinetics for Heterogeneous Reactor Models, *Nucl. Sci. Eng.*, **35:** 319 (1969).
65. S. Kaplan, The Property of Finality and the Analysis of Problems in Reactor Space–Time Kinetics by Various Modal Expansions, *Nucl. Sci. Eng.*, **9:** 357 (1961).
66. A. F. Henry, The Application of Inhour Modes to the Description of Nonseparable Reactor Transients, *Nucl. Sci. Eng.*, **20:** 338 (1964).
67. A. F. Henry and S. Kaplan, Some Applications of a Multimode Generalization of the Inhour Formula, *Nucl. Sci. Eng.*, **22:** 479 (1965).
68. L. R. Foulke and E. P. Gyftopoulos, Application of the Natural Mode Approximation to Space–Time Reactor Problems, *Nucl. Sci. Eng.*, **30:** 419 (1967).
69. P. T. Hansson and L. R. Foulke, Investigations in Spatial Reactor Kinetics, *Nucl. Sci. Eng.*, **17:** 528 (1963).
70. H. L. Garabedian and R. E. Lynch, Nonlinear Reactor Kinetics Analysis, *Nucl. Sci. Eng.*, **21:** 550 (1965).
71. R. L. Mathews, Two Mode Kinetics Equations, USAEC Report KAPL-M-6576, Knolls Atomic Power Laboratory, 1966.
72. D. E. Dougherty and C. N. Shen, The Space–Time Neutron Kinetic Equations Obtained by a Semidirect Variational Method, *Nucl. Sci. Eng.*, **13:** 141 (1962).
73. P. C. Rohr and M. Becker, Time-Synthesis Using Discontinuous Green's Functions Modes, *Trans. Amer. Nucl. Soc.*, **12:** 619 (1969).
74. N. Carter and R. Danofsky, The Application of the Calculus of Variations and the Solution of Coupled Core Kinetics Equations, in *Coupled Reactor Kinetics*, p. 249, C. G. Chezem and W. H. Köhler (Eds.), Texas A&M Press, College Station, Tex., 1967.
75. M. G. Stevenson and S. J. Gage, Application of a Coupled Fission Mode Approach to Modular Reactor Kinetics, *J. Nucl. Energy*, **24:** 1 (1970).
76. J. B. Yasinsky, On the Application of Time-Synthesis Techniques to Coupled-Core Reactors, *Nucl. Sci. Eng.*, **32:** 425 (1968).
77. S. Kaplan, O. J. Marlowe, and J. Bewick, Application of Synthesis Techniques to Problems Involving Time Dependence, *Nucl. Sci. Eng.*, **18:** 163 (1964).
78. J. A. Bewick and S. Kaplan, Test of the Time Synthesis Approach for the Solution of Reactor Kinetics Problems, USAEC Report WAPD-TM-641, Westinghouse Electric Corp., Bettis Atomic Power Laboratory, 1966.
79. R. A. Rydin, Time Synthesis—A Study of Synthesis Modes and Weighting Functions, *Trans. Amer. Nucl. Soc.*, **10:** 569 (1967).
80. W. M. Stacey, Jr., Space–Time Nuclear Reactor Kinetics Development at KAPL, in Conference on Industrial Needs and Academic Research in Reactor Kinetics, USAEC Report BNL-50117, Brookhaven National Laboratory, p. 380, 1968.

81. C. H. Adams, R. A. Rydin, and W. M. Stacey, Jr., A Numerical Study of Single-Channel Flux Synthesis, *Trans. Amer. Nucl. Soc.*, **11**: 169 (1968).
82. J. B. Yasinsky, Numerical Studies of Combined Space–Time Synthesis, *Nucl. Sci. Eng.*, **34**: 158 (1968).
83. N. Suda, Approximate Solution to Space Dependent Kinetics Problems, *J. Nucl. Sci. Technol. (Tokyo)*, **5**: 377 (1968).
84. J. B. Yasinsky, The Solution of the Space–Time Neutron Group Diffusion Equations by a Time-Discontinuous Synthesis Method, *Nucl. Sci. Eng.*, **29**: 381 (1967).
85. J. B. Yasinsky, Combined Space–Time Synthesis with Axially Discontinuous Trial Functions, USAEC Report WAPD-TM-736, Westinghouse Electric Corp., Bettis Atomic Power Laboratory, 1967.
86. W. M. Stacey, Jr., A Variational Multichannel Space–Time Synthesis Method for Nonseparable Reactor Transients, *Nucl. Sci. Eng.*, **34**: 45 (1968).
87. W. H. Köhler, Variational Method for Prompt Neutron Kinetics, *Nukleonik*, **8**: 203 (1966).
88. M. Becker, On the Inclusion of Boundary Terms in Time-Dependent Synthesis Techniques, *Nucl. Sci. Eng.*, **22**: 385 (1965).
89. W. M. Stacey, Jr., Variational Functionals for Space–Time Neutronics, *Nucl. Sci. Eng.*, **30**: 448 (1967).
90. J. Lewins, Time-Dependent Variational Theory, *Nucl. Sci. Eng.*, **31**: 160 (1968).
91. M. Becker, Asymmetric Discontinuities in Synthesis Techniques for Initial-Value Problems, *Nucl. Sci. Eng.*, **34**: 343 (1968).
92. W. L. Woodruff, Some Improvements in Variational Flux Synthesis Methods, USAEC Report ANL-7696, Argonne National Laboratory, 1970.
93. M. Becker, Semidirect Least-Squares Variational Methods and Initial-Value Problems, *Trans. Amer. Nucl. Soc.*, **10**: 550 (1967).
94. E. L. Wachspress, Variational Methods and Neutron Flux Synthesis, in Proceedings of Conference on the Effective Use of Computers in the Nuclear Industry, USAEC Report CONF-690401, p. 271, April 1969.
95. M. L. Steele, Variational Techniques as a Method for Multidimensional Reactor Calculations, *Reactor Technol.*, **13**(1): 73 (Winter 1969–1970).
96. S. Kaplan, Synthesis Methods in Reactor Analysis, *Advan. Nucl. Sci. Technol.*, **3**: 233 (1965); also, Variational Methods in Nuclear Engineering, *Advan. Nucl. Sci. Technol.*, **5**: 185 (1969).
97. W. M. Stacey, Jr., *Modal Approximations: Theory and an Application to Reactor Physics*, The M.I.T. Press, Cambridge, Mass., 1967; also, A General Modal Expansion Method for Obtaining Approximate Equations for Linear Systems, *Nucl. Sci. Eng.*, **28**: 438 (1967).
98. R. Avery, Theory of Coupled Reactors, in *Proceedings of the Second United Nations International Conference on the Peaceful Uses of Atomic Energy, Geneva, 1958*, Vol. 12, p. 182, United Nations, New York, 1958.
99. R. Avery et al., Coupled Fast-Thermal Power Breeder Critical Experiment, in *Proceedings of the Second United Nations International Conference on the Peaceful Uses of Atomic Energy, Geneva, 1958*, Vol. 12, p. 151, United Nations, New York, 1958.
100. R. G. Cockrell and R. B. Perez, Kinetic Theory of Spatial and Spectral Coupling of the Reactor Neutron Field, in *Neutron Dynamics and Control*, Tucson, Ariz., April 1965, D. L. Hetrick and L. E. Weaver (Coordinators), AEC Symposium Series, No. 7, (CONF-650413, p. 323), 1966.
101. M. Komata, On the Derivation of Avery's Coupled Reactor Kinetics Equations, *Nucl. Sci. Eng.*, **38**: 193 (1969).
102. A. Gandini and M. Salvatores, New Perturbation Method for Coupled Reactors, *Nukleonik*, **12**: 80 (1969).
103. G. C. Baldwin, Kinetics of a Reactor Composed of Two Loosely Coupled Cores, *Nucl. Sci. Eng.*, **6**: 320 (1959).
104. D. Schwalm, On a Derivation of the Multigroup Kinetics Equations of Coupled Reactors, Euratom Report EUR-2416.e, 1965.
105. D. R. Harris and R. G. Fluharty, Coupled Region Kinetics Formulations, in *Symposium on Dynamics of Nuclear Systems*, Tucson, 1970, University of Arizona Press, to be published.
106. C. G. Chezem, G. E. Hansen, H. H. Helmick, and R. L. Seale, The Los Alamos Coupled Reactor Experience, USAEC Report LA-3494, Los Alamos Scientific Laboratory, 1967.
107. A. Belleni-Morante, The Reactor Kinetics Equations as a Direct Consequence of the Boltzman Equation, *Nukleonik*, **8**: 33 (1965).
108. A. Belleni-Morante, Delay-Time Distribution Function in Coupled Reactor Kinetics, *Nukleonik*, **10**: 217 (1967).
109. S. Kaplan, Nodal Analysis, in Naval Reactors Physics Handbook, A. Radkowsky (Ed.), USAEC Report 7030, Vol. I, p. 961, Superintendent of Documents, U. S. Government Printing Office, Washington, 1964.
110. H. Plaza and W. H. Köhler, Coupled-Reactors Kinetics Equations, *Nucl. Sci. Eng.*, **26**: 419 (1966).
111. A. Belleni-Morante, Neutron Transport in a Reactor Composed of Two Loosely Coupled Cores, in *Coupled Reactors Kinetics*, C. G. Chezem and W. H. Köhler (Eds.), p. 176, Texas A&M Press, College Station, Tex., 1967.
112. R. L. Seale and G. E. Hansen, Calculation of Interaction Parameters for Loosely Coupled Reactor Systems, in *Coupled Reactor Kinetics*, C. G. Chezem and W. H. Köhler (Eds.), p. 218, Texas A&M Press, College Station, Tex., 1967.
113. H. H. Hassan and G. H. Miley, A Determination of the Dynamic Coupling Coefficient, *Trans. Amer. Nucl. Soc.*, **11**: 575 (1968).
114. D. C. Wade and H. H. Rubin, A Nodal Calculation of a Space–Time Transient Using Coupling Coefficients Which Account for Changing Internodal Leakages, *Trans. Amer. Nucl. Soc.*, **10**: 250 (1967).
115. Y. Asahi, S. An, and A. Oyama, On the Two-Point Approximation Equation of Reactor Kinetics, *J. Nucl. Sci. Technol. (Tokyo)*, **4**: 315 (1967).
116. W. H. Köhler, C. Y. Ho, H. Plaza, and N. B. Poulsen, Influence of Time-Dependent Coupling Coefficients and Delay Times of the Kinetics of a Modular Fast Reactor Core, in *Fast Reactor Physics*, Symposium Proceedings, Karlsruhe, 1967, Vol. I, p. 529, International Atomic Energy Agency, Vienna, 1968 (STI/PUB/165).

117. A. Belleni-Morante, Effect of First-Flight Neutrons on Coupled Reactor Kinetics Behavior, *J. Nucl. Energy,* **21:** 867 (1967).
118. A. Belleni-Morante, The Kinetic Behavior of a Reactor Composed of Two Loosely Coupled Cores with Time-Dependent Coupling Coefficients, *Nukleonik,* **8:** 291 (1966).
119. P. R. Pluta, Coupled-Core Kinetic Behavior, in *Neutron Dynamics and Control,* Tucson, Ariz., April 1965, D. L. Hetrick and L. E. Weaver (Coordinators), AEC Symposium Series, No. 7, (CONF-650413, p. 544), 1966.
120. M. V. Dyos and F. M. Heck, The Current Status of Analytical Methods for Calculating the Kinetic Behavior of Loosely Coupled Fast Reactor Cores, in *Proceedings of the International Conference on the Safety of Fast Reactors,* pp. III-6.1–6.7, Aix-en-Provence, 1967, Commissariat à l'Energie Atomique, Paris, 1967.
121. C. G. Chezem and W. H. Köhler (Eds.), *Coupled Reactor Kinetics,* Texas A&M Press, College Station, Tex., 1967.
122. D. C. Wade, Nodal Space–Time Kinetics Models Interpreted in Terms of Modal Expansions, *Trans. Amer. Nucl. Soc.,* **11:** 168 (1968).
123. W. H. Köhler, Summary of Derivations of Coupled Point Reactor Kinetics Equations, in *Coupled Reactor Kinetics,* p. 192, C. G. Chezem and W. H. Köhler (Eds.), Texas A&M Press, College Station, Tex., 1967.
124. F. T. Adler, S. J. Gage, and G. C. Hopkins, Spatial and Spectral Coupling Effects in Multicore Reactor Systems, in *Coupled Reactor Kinetics,* p. 521, C. G. Chezem and W. H. Köhler (Eds.), Texas A&M Press, College Station, Tex., 1967.
125. H. H. Helmick, C. G. Chezem, and R. L. Seale, Los Alamos Coupled Reactor Experiments, *Trans. Amer. Nucl. Soc.,* **8:** 222 (1965); also Report LADC-8516.
126. H. H. Helmick and C. G. Chezem, Summary of Coupled KIWI Experience, in *Coupled Reactor Kinetics,* p. 29, C. G. Chezem and W. H. Köhler (Eds.), Texas A&M Press, College Station, Tex., 1967.
127. G. C. Hopkins and F. T. Adler, Transfer Functions and Response for Coupled Core Reflected Systems, in *Coupled Reactor Kinetics,* p. 42, C. G. Chezem and W. H. Köhler (Eds.), Texas A&M Press, College Station, Tex., 1967.
128. J. T. Mihalczo, Rossi-α and Pulsed Neutron Measurements in Subcritical Coupled Uranium-Metal Cylinders, in *Coupled Reactor Kinetics,* p. 484, C. G. Chezem and W. H. Köhler (Eds.), Texas A&M Press, College Station, Tex., 1967.
129. H. H. Hassan and G. H. Miley, Verification of Space–Time Reactor-Kinetics Analysis by Experiments, *Nucl. Sci. Eng.,* **40:** 449 (1970).
130. M. J. Ohanian and N. J. Diaz, Research on Neutron Pulse Propagation in Multiplying Media, Report IN-1366, Idaho Nuclear Corporation, 1969.
131. N. J. Diaz and M. J. Ohanian, Space–Time Kinetics Studies in a Large Close-to-Critical H_2O–UO_2 Assembly, *Trans. Amer. Nucl. Soc.,* **12:** 236 (1969).
132. R. A. Rydin, J. A. Burke, W. E. Moore, and K. W. Seemann, Space–Time Kinetics Experiments and Calculations for Loosely Coupled Cores, *Trans. Amer. Nucl. Soc.,* **13:** 698 (1970); also to be published in *Nuclear Science and Engineering.*
133. R. A. Rydin, J. Burke, F. Feiner, K. W. Seemann, and W. M. Stacey, Jr., Static Measurements Preparatory to Space–Time Kinetics Experiments in the SHA, *Trans. Amer. Nucl. Soc.,* **12:** 653 (1969).
134. J. A. Burke, W. E. Moore, R. A. Rydin, and K. W. Seemann, Time Domain Noise Measurements in Loosely Coupled Cores, in *Symposium on Dynamics of Nuclear Systems,* Tucson, 1970, University of Arizona Press, to be published.
135. C. E. Cohn, R. J. Johnson, and R. N. MacDonald, Calculating Space-Dependent Reactor Transfer Functions Using Statics Techniques, *Nucl. Sci. Eng.,* **26:** 198 (1966).
136. J. Wakabayaski and T. Hoshino, Study of the Transfer Function of SHE Critical Assembly, in *Coupled Reactor Kinetics,* p. 421, C. G. Chezem and W. H. Köhler (Eds.), Texas A&M Press, College Station, Tex., 1967.
137. T. Hoshino, J. Wakabayaski, and S. Hayaski, New Approximate Solution of Space- and Energy-Dependent Reactor Kinetics, *Nucl. Sci. Eng.,* **23:** 170 (1965).
138. G. Saji, Excitation of Higher Space Modes in Reactor Transfer Function Measurement (Part I), *Nucl. Sci. Eng.,* **32:** 93 (1968).
139. A. R. Boynton and R. E. Uhrig, Evaluation of Two-Region Reactor Parameters by Random Noise Measurements, *Nucl. Sci. Eng.,* **18:** 220 (1964).
140. R. A. Hendrickson and R. A. Danofsky, Measurement of the Reactivity Coupling Coefficient in the Iowa State UTR-10, in *Coupled Reactor Kinetics,* p. 506, C. G. Chezem and W. H. Köhler (Eds.), Texas A&M Press, College Station, Tex., 1967.
141. R. A. Hendrickson and G. Murphy, Cross Spectral Density Measurements in a Coupled-Core Reactor, *Nucl. Sci. Eng.,* **31:** 215 (1968).
142. R. W. Albrecht, and W. Seifritz, Fundamental Properties of the Coherence Function in Symmetrical Two-Node Systems, *Nukleonik,* **11:** 143 (1968).
143. W. Seifritz and R. W. Albrecht, Measurement and Analysis of the Coupled Core Coherence Function in a Two-Node Symmetrical Reactor, *Nukleonik,* **11:** 149 (1968).
144. R. W. Albrecht and R. A. Danofsky, Analytical Experimental Correlations in Space-Dependent Coherences, *Trans. Amer. Nucl. Soc.,* **12:** 708 (1969).
145. H. Meister, K. H. Beckhurts, W. Häfele, W. H. Köhler, and K. Ott, The Karlsruhe Fast-Thermal Argonaut Reactor Concept, German Report KFK-217, 1964.
146. H. Borgwaldt et al., Reactor Dynamics Topics Recently Investigated at Karlsruhe, in Conference on Industrial Needs and Academic Research in Reactor Kinetics, USAEC Report BNL-50117, Brookhaven National Laboratory, p. 322, 1968.
147. M. Edelmann, T. E. Murley, and D. Stegemann, Investigation of Prompt Neutron Kinetics in the Fast-Thermal Argonaut-Reactor STARK by Noise Analysis, in *Coupled Reactor Kinetics,* p. 390, C. G. Chezem and W. H. Köhler (Eds.), Texas A&M Press, College Station, Tex., 1967.
148. M. Edelmann, G. Kussmaul, H. Meister, D. Stegemann, and W. Väth, Pulsed Source and Noise Measurements on the STARK Reactor at Karlsruhe, in *Pulsed Neutron Research,* Symposium Proceedings, Karlsruhe, 1965, Vol. II, p. 799, International Atomic Energy Agency, Vienna, 1965 (STI/PUB/104).

General References

D. K. Butler and D. A. Meneley, Recent Developments in Fast Reactor Kinetics, *Nucl. Safety*, **11**: 289 (1970).

N. E. Carter, Review of Physics Methods Used for Computing the Kinetic Behavior of Large Power Reactors, USAEC Report BNWL-738, Battelle–Northwest, 1968.

A. F. Henry, Review of Computational Methods for Space–Time Kinetics, in Proceedings of Conference on the Effective Use of Computers in the Nuclear Industry, USAEC Report CONF-690401, April 1969; also in *Symposium on Dynamics of Nuclear Systems*, Tucson, 1970, University of Arizona Press, to be published.

C. Hsu and T. P. Mulcahey, Methods for Studying Space-Dependent Reactor Dynamics, *Reactor Fuel-Process. Technol.*, **11**(4): 172 (Fall 1968).

S. Kaplan, A. F. Henry, S. G. Margolis, and J. J. Taylor, Space–Time Reactor Dynamics, in *Proceedings of the Third International Conference on the Peaceful Uses of Atomic Energy, Geneva, 1964*, Vol. 4, p. 41, United Nations, New York, 1965.

W. M. Stacey, Jr., *Space–Time Nuclear Reactor Kinetics*, Academic Press Inc., New York, 1969.

J. B. Yasinsky, Notes on Nuclear Reactor Kinetics, USAEC Report WAPD-TM-960, Bettis Atomic Power Laboratory, 1970.

Testing of Nuclear Power Reactors

By Joseph A. Thie*

A most important time in the life of a nuclear power plant is the transition period—known as reactor commissioning—between the end of construction and the start of routine operation since many testing activities take place. Extensive testing is required to satisfy legitimate concerns for safe operation; however, much of the testing is undertaken because nuclear plants are complex installations, the technology is new in comparison to others, and there is some deserving fetishism regarding safety.

The current status of testing and the intricacies of this commissioning for the large reactor power plants in the United States are described and discussed critically in this article. Startups of early experimental and prototype plants have been reviewed before.[1-3] However, the testing needs of present-day commercial reactors differ from these. The much simpler startups of research reactors have been discussed in the literature,[4,5] as has been the Calder Hall type.[5]

REASONS FOR TESTING

Many reasons, of various origins, justify a test program. Some principal ones will be mentioned here. It is not possible to assign a relative importance to these reasons. Organizations involved do not have identical interests and, hence, have somewhat different motives for specific tests. Moreover, even within an organization, different groups (for example, the legal and physics departments) might rank their reasons differently.

Proving design safety by means of a test is a widely admitted motive, with such related factors as protecting the public and plant personnel and also protecting equipment needed for safe operation. Because of the complex interrelations among systems and their components in a power plant, safety implications are far reaching.

Testing is also done for economic reasons. Prevention of damage to equipment is an obvious motive. Furthermore, if a test uncovers a weakness or malfunction that could ultimately cause some reactor incident—with or without equipment damage—the accompanying loss of operating time has economic consequences.

Proving conformity with licensing regulations or codes is a feature that permeates the entire program. Safety motives mentioned above are perhaps sufficiently general to encompass this. However, the numerical and other safety criteria listed in codes and in the Technical Specifications represent concrete goals. Test reports document the meeting of these criteria.

It may be true that some limited testing is done merely to live up to "expectations," or because of tradition or perhaps suggestions from outside organizations. (An example of the latter might be where regulatory bodies suggest, rather than impose, firm testing requirements.) A reactor contractor and a utility may believe a test to be of little value but "expected"; however, they perform the test because it takes less time and effort than arranging not to. But, the possibility of getting an unexpected result can be cited in defense of performing tests of debated value.

Training opportunities available in the startup of a new reactor are a most important by-product of testing. Procedures are not written to give training per se, but the personnel participating gain valuable experience in carrying them out. Although an operator may have control-room technique from a simulator or elsewhere, preoperational and startup testing gives him a wealth of experience in the reactor plant. This is most

*Consultant, P. O. Box 517, Barrington, Ill. 60010.

advantageous to a utility and is why its personnel typically do the testing under guidance from the reactor contractor. (Because of union working rules at most installations, contractor personnel generally are prohibited from performing many manual aspects of testing and operating.)

Basic operating information generated from test results is required by the control-room operators and their technical and maintenance support staffs and is used throughout the life of the plant. So far it has not been possible for detailed operating data to be supplied in advance, as would be done for "carbon copies" from an assembly line.

With the era of special experimental water reactors essentially past, further development now occurs in the new plants as they are built and operated. Laboratory-proven concepts require demonstration by integrated plant operation. Here, special testing may be added for a first-of-a-kind addition to a reactor. For example, jet pumps first used in Dresden 2 were performance tested in considerable detail.

Finally, contractual requirements (beyond just listing tests by name) manifest themselves in the test program. Well known in this category is the warranty run—the plant demonstrating full-power capability for an extended period of time. However, the contract can impose other testing requirements: for example, if there is a bonus or penalty associated with the maximum power capability, then an accurate and fair determination requires a very detailed test procedure (as on the two Tarapur BWRs).

PROGRAM PHASES

Reactor commissioning is understood as the activity period between the completion of construction and turnover for routine operation. The testing work may be divided into five sequential phases: preoperational or "preop," cold, hot, power, and final. These categories, with slight variations, are adopted by startup teams in organizing their work sequentially in time.

As construction is completed in various systems, their preoperational testing can start, usually concurrent with construction in other systems. Preoperational, as the word implies, means a check-out before normal operation. This check-out is distinct from any prior checking or testing within the construction phase of a system. The plant systems and their components are treated as isolated entities here. Their performance in relation to and concurrent with other system operations is deferred to a later program phase (such as the power phase). In this way, preoperational testing may be overlapped with construction and achieve an overall saving of time.

Cold and hot phases refer to test conditions at room temperature or above, respectively. Fuel loading occurs within these cold and hot phases. (PWRs use pump heat to achieve conditions for hot functional tests of various systems prior to fuel loading; BWRs first load and then use nuclear heat to reach conditions for hot functionals.) Reactor power is of the order of 1 to 5% or less of rated power. Also included in the cold and hot phases are integrated system tests with the reactor shut down. It is usual and advantageous to check out as much of the plant as possible before significant power operation while radiation levels and system contamination are essentially nonexistent.

Power escalation and accompanying tests—the power phase of the program—are the heart of reactor commissioning. Even though there have been prior check-outs, proper plant behavior under normal and slightly abnormal conditions must be demonstrated. As seen below, this part of the program takes place in a series of steps—each step corresponding to a new power level—until full power is attained.

Reaching full power and performing certain tests does not quite finish the commissioning effort. A final phase of the five sequential phases can consist of some retesting if changes to the plant are made or further construction work occurs. In any event, a warranty run at full power will be a part of this final phase before plant acceptance by the utility.

An ideal reactor startup has construction merging into preoperational testing and then into the ensuing phases. The important reactor tests and minor repairs from the time of initial criticality to the time of reaching design power typically take 4 or 5 months. A plant is fortunate if no rescheduling occurs because of unpredictable events. When such schedule slippage occurs, the combined ingenuity of the project manager, his staff, and the utility's staff is brought to bear on the rescheduling. Inherent flexibilities in construction work, as well as in the overlapping phases of commissioning, can minimize or even eliminate substantial economic losses associated with delays in achieving power production.

STARTUP ORGANIZATION

The organization shown in Fig. 1 is "typical" in the sense of specifying the key positions, groups, and committees usually present, although titles vary from plant to plant, as do the specific details of line responsibility and reporting. Where personnel assigned

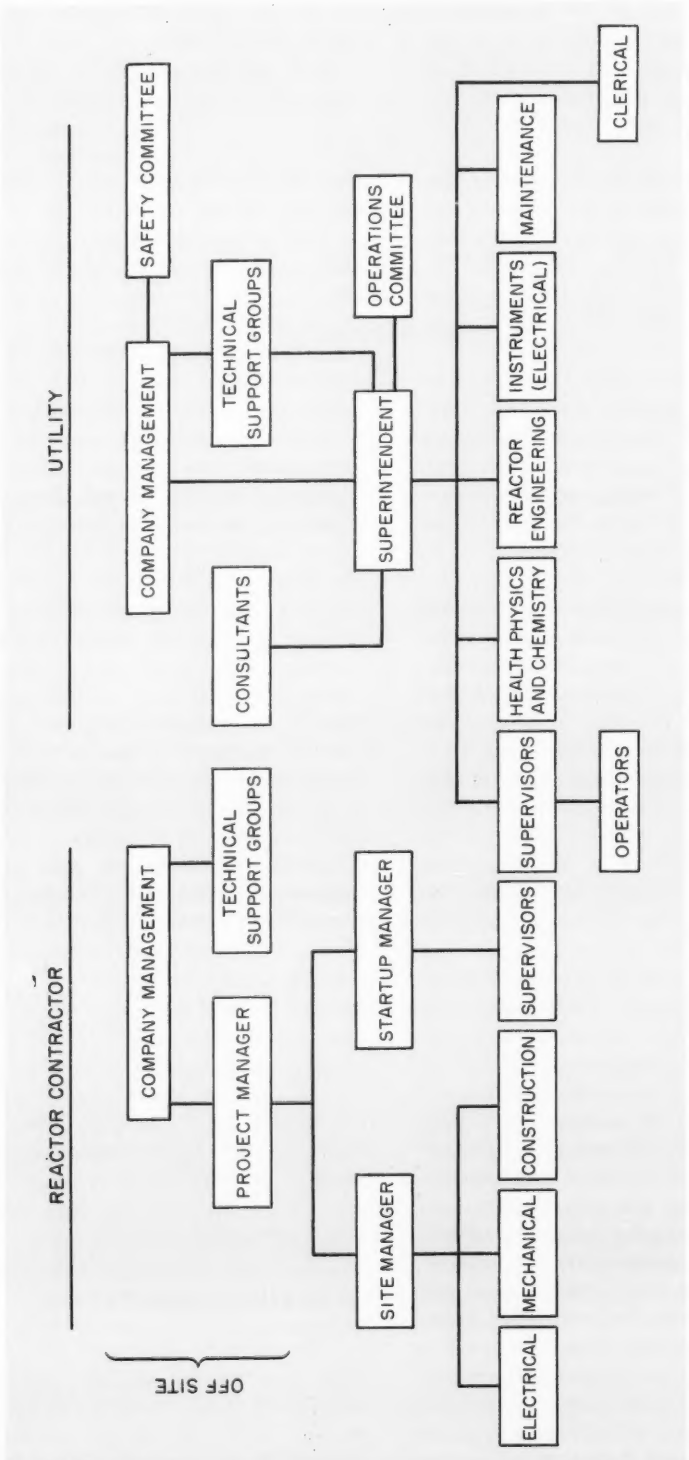

Fig. 1 Typical organization during the time of reactor commissioning.

are limited, one individual may fulfill more than one function. With construction virtually finished, aspects of the organization associated with construction are not shown. Duplication shown in some positions in Fig. 1 (such as shift supervisors of both the supplier and the utility) may or may not, in fact, take place. Of overall significance in responsibilities is the position of utility management as license holder.

plant operational problems, performing special tests, e.g., metallurgical and vibration, and making independent assessment of safety questions.

Good liaison between the design engineering staff and the operating staff is important and of mutual benefit. On one hand, information and experience from startup can be fed back into the general design of the reactor type, leading to subsequent improvements.

Table 1 Organizational Characteristics of Plant Safety Committees*

Characteristic	No.	Qualitative assessment		
		Always	Usually	Occasionally
Range of number of members	5 to 7			
Fraction of members that are off site	0.5 to 0.7			
Specializations of members				
Power-reactor engineering		x		
Operations		x		
Health physics				x
Management		x		
Physics or nuclear analysis		x		
Nonnuclear operation				x
Average time between meetings, 2 months				
Naming of consultants for committee use			x	

*Data for this table have been determined by the author from features written into the charters of committees at five separate power plants. The columns indicate characteristics of all 5, 3 to 4, or 1 to 2 committees.

Apart from contract requirements, factors affecting the extent to which personnel of the reactor supplier are present at the site include:

1. Experience of the utility's staff in startup.
2. Availability of the reactor contractor's personnel.
3. Relative complexity or importance of the work in progress at any given time; for instance, the supplier's site personnel are gradually reduced as commissioning progresses toward its end point.

During startup the amount of technical support needed in specialized areas of reactor technology far exceeds that encountered in normal plant operation. Figure 1 indicates four off-site sources of this support: technical support groups of the utility, technical support groups of the reactor contractor, outside consultants, and a safety committee. The specialties of these individuals are used to assist as needed, on site or off site, when it is not practical to use a permanent staff member. Such specialized needs arise when facing legal and licensing problems, in physics calculations, when analyzing certain test data, and in correcting

On the other hand, certain operating difficulties (or merely inconveniences) can be corrected during startup by an immediate redesign.

Two committees—safety and operations—shown in Fig. 1, usually are functioning at the time of fuel loading. The former advises company management, and the latter advises site management. However, in practice, having the safety committee report to company management is often only an organizational formality, since site personnel at the committee meetings usually obtain recommendations from the committee at first hand. Advising company management by formal committee minutes is an important function in any event.

The safety committee is more active during commissioning than during routine plant operation. Some of its initial activities are to organize itself in accordance with the Technical Specifications as well as utility and member desires (see Table 1); to review procedures (startup, operating, and emergency), plant operations, and design changes; and to conduct special plant audits. Since the majority of the committee's members are generally located off site (since they work either for other companies or elsewhere for the utility),

the judgments are made by primarily disinterested parties. Recently, an American Nuclear Society (ANS) meeting session was devoted to the discussion of safety committees.[6-9] There was general agreement on the need for a safety committee, with advantages from its independent outlook being a prime reason. This was considered to overshadow disadvantages stemming from lack of a committee's knowledge of the power plant in great detail. Many specific points brought out in this ANS session can be of value to existing safety committees.

The operations committee typically is made up of the senior individuals of the various departments in the site organization. Since it reviews all technical problems and policies of the plant, a broad spectrum of opinions is brought to bear on the topics discussed.

At the end of commissioning, the startup organization merges into the permanent operating organization, with the temporary personnel, notably those of the reactor supplier, leaving the site. Their work and responsibilities (except for special long-term advisory and other service or supply arrangements) are mostly assumed by the utility through both its site staff and engineering and management staff elsewhere. For example, the technical expertise involved in the leak rate test of containment would be totally that of the utility when tests subsequent to the first are performed; but, in the case of core physics calculations required for fuel warranty purposes, the reactor supplier might continue them for a small utility (although larger utilities have the preferable arrangement of performing their own calculations here).

PREOPERATIONAL TESTING

At various times during construction and commissioning, the various equipment and system checks made to eliminate difficulties and verify satisfactory performance include:

1. Quality-assurance verification.
2. Reviews of drawings and procedures for construction and operation.
3. Checks and tests during construction, including supervision, inspection, etc.
4. Preoperational testing of components.
5. Limited testing of separate systems, including hot functional tests.
6. Initial integrated plant operation.
7. Routine testing and preventive maintenance.

Primarily items 4 and 5 are discussed in this section, and categories of tests in item 6 are described later. For the most part, preoperational testing and limited system testing occur before fuel loading. But some testing of individual systems is performed after fuel loading, as is, of course, integrated plant operation.

For purposes of a preoperational program, the entire reactor plant is divided into from 20 to 40 systems. Names of tests that are common to the BWR, PWR, and HTGR during preoperational testing are: rad-waste, control rods, nuclear instrumentation, radiation monitors, service water, fire protection, compressed air, primary coolant purification, reactor protection, ventilation, feedwater, emergency power, fuel handling, turbine, and hot functional. Special systems tested in BWRs are: off-gas monitoring, traveling in-core detector, rod-worth minimizer, and main-steam-line monitoring. Special PWR systems include: chemical and volume control, level control (of the pressurizer and of the steam generator), and in-core thermocouples. HTGR preoperational tests include: helium circulators' auxiliaries; helium storage, transfer, and makeup; acoustic detection of steam-pipe ruptures.

Hot functional tests are included here, i.e., the systems are operated with the plant near operating temperature as another check on their performance. The hot functional program, involving many systems, is thus a collection of tests.

Test Procedures

Figure 2 shows a long chain between conception and accepted completion of a test. (Some of this is considered "red tape" by some testing groups, but not necessarily so named by review bodies involved.) This figure shows only a single-procedure (or scope) review process applicable to preoperational and startup tests at each of three points. However, in practice, these can be a series of multiple reviews from different individuals or groups. Such a review might include: the procedure originator's own group, the startup team members who will conduct the test, the utility's engineering staff and their consultants, the reactor plant staff, the AEC's regulatory staff, the operations committee, and the safety committee. So the points in Fig. 2 where review occurs can involve significant amounts of elapsed time. Reviews lead to comments more often than to the simple acceptance or rejection paths shown in Fig. 2. These comments, if adopted, can be written into the procedure.

With many similar reactors of a given type (BWR or PWR) from a few major suppliers, it is not surprising that written procedures are largely inherited—in many

instances virtually word for word. This has advantages of using proven methods and also requiring less manpower for test preparation. But a disadvantage is that a tendency toward procedure rigidity can develop and possibly discourage improvements.

A written procedure is prepared prior to conducting all preoperational tests. Although the specific format varies with plants, the general content of preoperational test procedures is likely to have many of the features of Table 2, some explicitly and others implicitly.

Similarly, there are written procedures for the 15 to 30 startup tests for reactor operation. These tests,

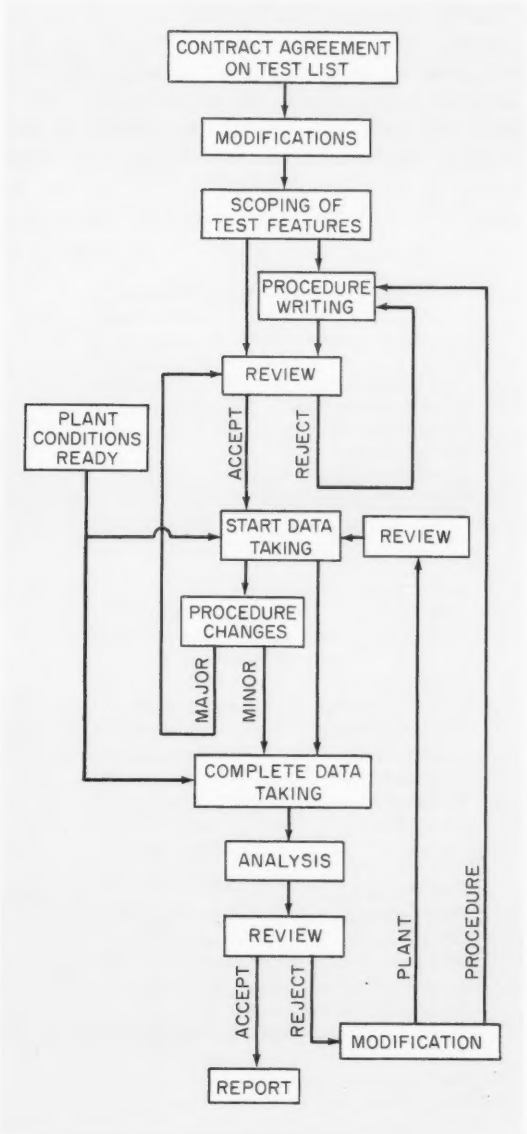

Fig. 2 Flow chart of the steps involved in performing a test.

Table 2 Typical Features of a Preoperational Test for a Simplified Hypothetical Instrument Calibration

Test features	Illustration (hypothetical test)
Purpose of test	Calibration and verification of functions.
Descriptive summary	A standardized input is measured, and settings are adjusted to achieve calibration.
References	Equipment manuals and the plant's operating manual.
Prerequisites and initial conditions to prevail	Installation complete; certain power sources energized.
Special test equipment needed and associated instructions	Standard input source; electrical test instruments.
Detailed procedures	A description of wiring connections; a list of switch and adjustment positions; etc.
Limitations and cautions	Maximum input that might damage the equipment.
Data sheets, with guides for acceptable or expected data	All variables, instrument dial settings, and remarks listed in multicolumn data sheets.
Checklists corresponding to steps in the procedure	Observer's initials appearing at each significant step (such as an alarm occurring at the proper value of a variable).
Actions required if there are deviations from expected performance	Special settings to be changed to achieve calibration.
State in which equipment is to be left after the test	Removal of jumper wires and other temporary measures.
Manpower requirements	One man in the control room, one man elsewhere.
Sign-off sheets for test personnel and their management	Provisions for signatures and dates as well as statements of exceptions, such as an indicating light to be ordered and replaced.

many of which are repeated at various conditions, are usually more complex than preoperational tests because the reactor is operating and many systems are concurrently involved. However, the total testing time is likely to be less than for the preoperational program, which should have eliminated the "bugs" system by system.

Besides having the features of preoperational tests, startup tests are more elaborate in such areas as acceptance criteria, data analyses, and supporting documents. Explicit limits referred to in some plants as "level 1" criteria are given for major design criteria and Technical Specifications. Lesser "level 2" criteria are merely design predictions or expectations which, if not met, should not interrupt the testing program while an analysis for the explanation is being made.

With startup tests involving reactor operation more complex than preoperational tests, it is not surprising that more extensive analysis of the test data is frequently needed to complete the test. The procedure outlines this analysis with a goal of making it straightforward and easy to perform immediately at the site. Also, sufficient supplementary information is in the procedure, its appendixes, or supporting documents, to permit this on-the-spot data analysis. Among the supporting documents of value to startup personnel in test performance and analysis are: technical specifications, operating and equipment manuals, calculations and examples of detailed analysis, topical reports of the reactor contractor relevant to the test program, test program reports from similar reactors, and appendixes to the procedures covering special needs of some tests.

Beyond the formal content, a good procedure should:

- Be independent of calculations and of results from other reactors. The sequential procedure steps must detect an unsafe or potentially damaging situation before it happens. One must not blindly assume the validity of the design or other experience.
- Be clear and easy to follow. This implies being concise and perhaps using appendixes for extensive supplementary material. It also implies having enough information to be self-sufficient, if in the hands of experienced personnel.
- Contain some operating flexibility. The testing and operating staff should have whatever leeway is compatible with safety and other criteria of review and regulating bodies rather than being required to perform time-consuming operations that are more arbitrary than necessary.
- Use data sheets based on prior experience with the same test elsewhere, but provide ample room for additional data and remarks.

TYPES OF STARTUP TESTS

Tables 3 to 6 divide the specific tests named in several recent and representative license applications to the AEC[10-13] into four categories: physics tests at startup (Table 3), plant-system tests at power (Table 4), dynamics tests (Table 5), and instrumentation tests (Table 6). These tests occur in the cold, hot, and power phases of the commissioning program. A particular reactor supplier will vary his test list only a little from reactor to reactor. For PWRs, no two suppliers use identical series of tests; a particular reactor program would specifically list most of the tests in the composite shown here and, within these

Table 3 Physics Tests at Startup*

BWR[10]
Fuel loading
Control-rod sequence
Shutdown margin
Rod calibrations
Core-performance evaluation
Axial power distribution
Rod-pattern exchange
Composite of PWRs[11,12]
Core loading
Initial critical
Nuclear design check of hot critical-rod groups
Minimum shutdown verification
Rod calibrations
Effects of temperature and boron
Power coefficients
Rod worth at power
Unit startup
Core power distribution
Xenon worth
HTGR[13]
Fuel loading
Pulsed-neutron measurements (precritical)
Critical
Pulsed-source reactivity measurements (shutdown)
Loading adjustment
Differential rod worth (cold)
Reactivity effects of helium and temperature
Power coefficients
Rod worth at power

*In this and subsequent tables, a comparison can be made of the somewhat similar tests for the three different reactor types.

Table 4 Plant-System Tests at Power

BWR[10]
Chemical and radiochemical
Radiation measurements
Control-rod drives
System expansion
Core-isolation cooling
High-pressure coolant injection
Relief valves
Process computer
Electrical output and heat rate
Vessel temperature
Composite of PWRs[11,12]
Shield survey
Station control-rod drop
Nuclear-steam-supply-system heat balance
Turbine-generator startup
Unit-load steady-state test
Load cycle
HTGR[13]
Helium purification
Shield survey
Performance of turbine and steam plant
Circulating-water system
Primary coolant helium and auxiliaries
Vessel performance

Table 5 Dynamics Tests

BWR[10]
Vibration of vessel internals
Main-steam-line isolation valve
Recirculation-pump trips
Flow control
Turbine trip
Generator trip
Pressure regulator
Bypass valve
Feedwater-temperature and -flow changes
Loss of power
Flux response to rods
Composite of PWRs[11,12]
Load swing
Step load reduction
Station trip
Plant automatic control
Control valves
Partial-length-rods maneuvering
Dynamic control-rod drop
Induced xenon power oscillations
HTGR[13]
Plant automatic control
Xenon buildup and decay

Table 6 Instrumentation Tests

BWR[10]
Startup-range performance
Intermediate-range calibration
Local-power-instrument calibration
Averaging-power-instrument calibration
Composite of PWRs[11,12]
Power-range-instrument calibration
Thermocouple/RDT intercalibration
Power distribution from out-of-vessel detectors
HTGR[13]
Plant instrumentation and protective-system performance

tests, generally accomplish the purposes of other tests not specifically named in the program.

Physics Tests

Listings with approximately the same titles usually have the same general test method. But there are notable exceptions, such as PWRs approaching criticality initially by boron dilution in the water rather than by control-rod withdrawal. In general, however, physics-testing methods are equally applicable to all reactor types, and only the mechanics of performing the test may differ.

From year to year there is some variation in the list of tests performed, with the physics tests being cut back perhaps more than the other categories. As examples, the earlier BWRs would have criticality tests on a minimum critical mass core prior to any on a fully loaded core. Formerly, considerable effort was aimed at special reactivity effects—such as for BWR poison curtains or individual fuel elements. Also, at one time more interest was shown in flux distribution details—such as gamma scanning of irradiated fuel elements. The same overall abbreviation of cold physics testing over the years is also manifested in the PWRs. In both reactor types this is basically because:

- Comparisons of calculations and experiments have proved to be generally good.
- Calculations give better accuracy than before.
- Physics of sister plants in a given generation differ little.

A recognition that considerable reactor testing time can be saved by elimination of some physics tests also played a role in their curtailment. However, physics data at operating conditions are important and are still taken. A safety-oriented objection to testing reduc-

tions; whether in physics or other categories, is a lesser probability of detecting construction errors or defects manifested by unexpected behavior. The opinion is expressed here that a very thorough study extending over the experience of many commissionings is required to develop and justify abbreviations in current testing practices. If better quality assurance during construction sufficiently reduces the probability of certain defects, it can be reasonable to take advantage of this in planning tests. However, the ability to test for the unexpected must be retained. Such things should be weighed carefully before changes in testing programs are made. It could be most financially rewarding for utilities to optimize the balance between, on the one hand, economic losses associated with a completed plant not producing full power during most of the testing and, on the other hand, risks of economic losses from a shutdown due to a defect not revealed because of inadequate testing.

Plant-Systems Power Tests

Table 4 lists steady-state tests in which the performance of systems is proved under power-operating conditions. Most of these (as are many of the tests in Tables 3, 5, and 6) are repeated at various power levels during a stepwise approach to full power. Some sets of testing powers (expressed as percentage of full power) in use as stopping points after the hot functionals are:

Water reactors: 15–20%, 25–30%, 50%, 70–75%, 90%, and 100%.

HTGR: 25%, 40%, 60%, 80%, and 100%.

Whether a particular test is performed at one, a few, or all of these stopping points depends on the extent to which its data are significantly power dependent, confidence with which results can be predicted, safety or economic consequences of unexpected results, and time required or relative ease in performing the test. For example, relief valves might be tested only at 25% power, but radiation measurements would be made at most of the stopping points during escalation.

Not indicated in Table 4 are final system check-outs at the operating temperature if reactor operation is not intimately associated with the check-out, or if the operating manual—rather than a special procedure—suffices for operator instructions, e.g., locating and correcting steam leaks. Such check-outs are documented, nevertheless, even though not as part of a startup procedure.

Health-physics and chemistry departments perform shield survey and coolant chemistry tests, support the test engineers, and perform routine monitoring of the facility and its personnel as well.

Not listed is the warranty test after 100% power is achieved, usually consisting of 100 hr of operation, because the various plants use different formalities in integrating this into the program. The contract can require either that a few test procedures (especially power measurements) be repeated during the warranty run, or that a special 100-hr-acceptance test procedure be followed to take the required data. This test, along with plant changes and retests resulting from initial testing and operating, occurs in the final phase of reactor commissioning.

Dynamic Tests

When a reactor transient or time-dependent behavior is a principal feature in a startup test, this test is categorized in the lists of Table 5. These tests primarily involve the effects of transients in coolant flow and system pressure—effects on the core as well as effects on the remainder of the plant. Objectives of dynamic tests are:

1. Establishing the reactivity effect on the core (and ensuing consequences such as power and heat-flux transients) to be in accordance with designed safety.

2. Determining the response of equipment to be according to design requirements.

3. Giving the operators training in coping with transient events that can occur later in the life of the plant.

Most dynamic tests take place on a time scale of seconds, as may be judged by those listed in Table 5, and the essential data can be taken rather quickly. However, there are two exceptions: testing of the effects of spatial xenon transients in the large PWRs has taken hours; when a reactor scram is a natural consequence of the test, it becomes a time-consuming factor in the overall program to restart.

Results of present dynamics testing differ quantitatively from the results of physics testing. A frequent goal of physics tests is numerical determination of a specific reactor parameter by deductive calculations from data, e.g., a reactivity effect. The custom in dynamics testing of water reactors is to report largest observed deviations from steady state, with few additional deductions. On the other hand, in fast reactors (not represented in Table 5), dynamic parameters (time constants, for example) have been determined from their transient tests.[14] Such information also could be obtained in other reactor types.

Instrumentation Tests

In the preoperational phase there are extensive instrument calibrations based on simulated test signals if the parameter being measured is not available—for example, currents from in-core detectors not being measurable until reactor operation. However, during startup testing all instruments eventually measure the required physical parameters. Earlier calibration work can be checked, or initial calibrations can be made. Thus Table 6 shows the instrument tests to be primarily calibrations.

Although there are fewer tests in this test list than in the other three categories, the devotion of efforts to instrumentation is not correspondingly small. Rather, the instrumentation department, in collaboration with test engineers: installs special instruments, transducers and their readouts, required for certain tests; corrects instrument malfunctions and possibly even design defects as they develop; gives control systems final adjustments; and performs routine checks and recalibrations. Some of this work is formalized in the test procedures of Tables 3 to 5 in which instrument installations, calibrations, and adjustments are a part.

PERFORMING TESTS

Figure 2 shows that data taking can commence when a sequence has been planned to accommodate each test at its proper time, when it has been accepted, and when the plant is at proper test conditions. Some features of a carefully selected sequence are:

1. Proving safe operation before reaching each stage or step, tests providing assurance of safe operation at that stage having been performed, and having allowed the progression between steps to take place safely.
2. Scheduling tests leading to shutdowns at convenient times, perhaps when additional construction is to start or when system load requirements permit.
3. Enough flexibility to permit rescheduling when unforeseen events require.
4. Efficient utilization of the extra testing personnel who are not part of the normal plant staff.

In the actual performing of a test, the required data are taken by technicians, operators, and supervising engineers. In some preoperational tests this may consist of checking off a list of proper performance characteristics. On the other hand, extensive tabulations of data may be required in startup tests during reactor plant operation. Current testing customs are designed around the data being recorded and analyzed by the test personnel, often in a laborious fashion, giving the staff a valuable insight into the operations—a very good training technique. Immediate data reduction and evaluation on the site (with or without computer assistance) are features of most tests.

However, computerized data logging is now possible and accelerates testing if it is utilized for that purpose. This method of assisting testing probably will receive the same favorable reception from the operating and testing staff as did the simple reactivity computer; a number of plants have saved time in rod calibrations by an on-line conversion of the neutron-flux transient to excess reactivity.

The path in Fig. 2 from data taking to the final report normally is straightforward—analysis and review being the only steps interposed. With a well-written procedure, the immediate review by test personnel is a simple verification that acceptance criteria have been met. As a check, other groups, such as the operations committee, safety committee, and technical supporting engineers, also review the data.

However, where the test program is not progressing smoothly, some of the complications of Fig. 2 occur. In the order of more common to less common (also decreasing total delay time resulting), these are:

1. The plant is not ready for the test because of construction (due to labor difficulties, procurement delays, etc.), licensing, repairs, spurious scrams, redesigning, or other delays.
2. A test is unsuccessful and, rather than demonstrating its acceptance criterion, requires repeating—possibly after plant or procedure modifications. Otherwise, it is customary to accept tests as successfully completed to avoid delays, even though their less significant parts may have shown problems or may not be quite finished. However, there is an understanding that the minor items will eventually be resolved, and these are identified in the test report as such.
3. A halt in performing a test comes about before it is completed and requires procedure or plant changes beyond the jurisdiction of supervisory personnel.

Written reports, such as the following, demonstrate accomplishment of the test goals and are valuable references for the design and operating staffs:

- Data sheets of the procedure, associated computer data logs, and instrument charts.
- Preliminary report giving immediate analysis.
- Final topical report giving any additional analysis.
- Special reports as a result of malfunction or unexpected results.

• Supplementary plant operations records: logs, department records, committee minutes, memoranda, etc.

UTILIZATION OF RESULTS

When a test has been completed, there is both immediate and long-term utilization of results. It is evident that shortcomings pointed out by the test are of immediate interest. Also, results allow immediate progression to another test: for example, calibration of nuclear instruments at a low power is needed to escalate to a higher power.

Many specific parameters and calibrations are a useful result of testing and are of long-term value to the operating staff, e.g., reactivity effects of temperature, power, and fission products; characteristics of control rods such as their worths and scram times; and calibration curves for instruments.

Design groups compare experimental data with their expectations, possibly improving their design methods. A notable example is the spatial distribution of power in the core; if design methods of calculating this distribution agree with experiments, there is a possibility of increasing the rated core power, due to a lesser need for large safety margins. Also, where new equipment is being used, one can expect more than the usual interest by the designers.

Some original test data eventually are used for comparison with future tests, either at the same reactor or at some other. Thus control-rod scram times become norms for future comparison. Critical control-rod patterns or boron concentrations are base points from which changes in core reactivity are measured. The maintenance staff might use preoperational test measurements of equipment characteristics as norms when making future checks of the same or replacement equipment.

RELATIONS WITH GOVERNMENT

The importance attached to an adequate testing program has recently been brought out by the AEC's Regulatory Staff issuing guidelines for assistance to applicants: "Guide for the Planning of Preoperational Testing Programs," and "Guide for the Planning of Startup Programs." Although not firm safety standards (in the sense as a vessel code for example), these nevertheless do set forth regulatory positions on safety issues pertaining to testing.

Test results are used, among other reasons, to document compliance with governmental regulations. Periodic inspections at the reactor site by the AEC's Division of Compliance occur subsequent to and throughout the testing period. Preoperational test data results are reviewed for regulatory determination of readiness for fuel loading. Data of both preoperational and startup testing are compared with requirements in the Technical Specifications and with other safety standards as well.

It is not unusual for test results to be submitted to the Division of Reactor Licensing, to support a change in the plant's Technical Specifications. For example, a license may permit operation at limited power. If test data show a higher power to be possible and safe, then they become an important part of the application for a license change.

Although not a formalized part of initial operation, there is often some "debugging" of the plant's Technical Specifications. This is true especially for newer types of plants or innovations in regulations. Part of this debugging involves the licensee's arriving at workable interpretations where he is not clear on the intent. Another part is securing changes to unworkable requirements in the license, should these develop.

Some tests are conducted as a result of recommendations made by the Advisory Committee on Reactor Safeguards in their review of the reactor in the licensing process. They may suggest that the AEC's regulatory staff pursue a matter with the utility, the result often being the incorporation of additional tests into the program for reasons of safety.. A current example is vibration testing of vessel internals.

Relations of the plant to other regulatory bodies—such as fire inspectors or state radiation and environmental control agencies—have not significantly influenced startup tests. However, an influence of the same nature as the AEC's could result if test documentation of compliance with special regulations is required.

DISCUSSION

The preceding represents what has evolved as customary and typical in reactor commissioning in the United States, rather than what may be optimum—if indeed there is an optimum. From the standpoint of the utility, a minimum loss of power due to testing time is optimum—with the constraint that testing must be adequate to ensure the detection of defects and the obtaining of necessary information. It is this constraint that defies arriving at a mathematical optimum. Difficult judgments from experience of many startups are required to define any minimal acceptable

program. Some general observations may be made on what is felt to be the strong and weak points of current practice. Regarding the former, some key features that have contributed to the success of many startups to date are:

- Experienced personnel at the site to supervise and conduct the tests.
- Adequate technical assistance throughout the testing—starting with the contractual commitment and continuing through completion of testing.
- Assurances of trouble-free operation from a quality-assurance program and other items discussed above in preoperational testing.
- A set of carefully planned and, if possible, previously proved procedures.
- Skill in scheduling and having the flexibility of rescheduling to accommodate the unexpected.
- Good relations with regulatory bodies, labor, and equipment suppliers.

On the other hand, it is not difficult to find weak points and inefficiencies in specific startup or preoperational test programs of some reactors:

- The red tape associated with Fig. 2, although providing advantages of checks and balances, can be responsible for inefficiencies and time delays.
- "Deadwood" tests, inherited from previous reactors, may no longer be needed, and a better balanced program might result with their replacement by those having promise of more useful information.
- A false economy exists if expensive reactor operating time is used to achieve convenience in data taking or save some data analysis time—especially if computers can be used to log data and to assist with corrections in their analyses.
- Inflexibility of procedures or personnel in regard to changes can result in some wasted effort.
- Lack of smooth working inter- and intraorganizational relations can be a general impediment during testing.

Finally, a few speculations can be listed with respect to improvements that might come about in reactor commissioning and inure to the benefit of all concerned:

1. To the extent computer data logging and other automated aids are operable and factored into the startup tests, one can expect more information from less testing time.

2. A study of specific startup programs from an efficiency standpoint may lead to better use of startup time. A concept of multipurpose tests might develop where several tests can be combined and performed concurrently.

3. Better and earlier liaison between the reactor plant organization and outside groups (governmental and environmental agencies, for example) should be capable of resolving problem areas well before, rather than at the time of, fuel loading.

4. Industry standardization in test methods and quantitative acceptance criteria on results would streamline much of the complexity depicted in Fig. 2.

5. A considerably more open publication, dissemination, and criticism of test results than now exists should also be most beneficial.

REFERENCES

1. Nucleonics staff, A Perspective on Startup Experience, *Nucleonics*, 23(3): 46 (1965).
2. S. D. MacKay, Testing Nonnuclear Components and Systems, *Nucleonics*, 23(3): 48 (1965).
3. J. A. Thie, Reactor Loading and Physics Tests, *Nucleonics*, 23(3): 52 (1965).
4. E. L. Cox, Startup and Operating Experience at the University of Missouri (Columbia) Research Reactor, *Nucl. Safety*, 10(4): 337 (1969).
5. J. Shaw, *Reactor Operation*, Permagon Press, Inc., New York, 1969.
6. W. F. Witzig and N. J. Palladino, Role of Operations and Safety Committees for Nuclear Power Plants, *Trans. Amer. Nucl. Soc.*, 12(2): 790 (1969).
7. L. E. Minnick, Safety Committee Experience in Nuclear Power Plant Operation, *Trans. Amer. Nucl. Soc.*, 12(2): 790 (1969).
8. R. J. Nertney, Safety Committee Experience and Effectiveness, *Trans. Amer. Nucl. Soc.*, 12(2): 791 (1969).
9. D. D. Lanning, Who Needs a Nuclear Power Reactor Safety Committee? *Trans. Amer. Nucl. Soc.*, 12(2): 792 (1969).
10. Northern States Power Company, Final Safety Analysis Report (Monticello), Appendix D, USAEC Report Docket 50-263, 1969.
11. Virginia Electric & Power Company, Final Safety Analysis Report, Part B, Vol. 4 (Surry Power Station), USAEC Report Docket 50-280, 1970.
12. Duke Power Company, Final Safety Analysis Report (Oconee), USAEC Report Docket 50-269, 1970.
13. Public Service Company of Colorado, Final Safety Analysis Report, Vol. 3 (Fort St. Vrain), USAEC Report Docket 50-267, 1969.
14. M. L. Batch and A. E. Klickman, Evaluation of Noise Analysis for the Enrico Fermi Reactor, Report APDA-NTS-13, Atomic Power Development Associates, Inc., January 1968.

AEC Critical Review Series

Aerodynamic Characteristics of Atmospheric Boundary Layers

ERICH J. PLATE, Argonne National Laboratory and Karlsruhe University

May 1971

In the last few decades many meteorologists, physicists, and engineers have contributed to such an extent to our understanding of atmospheric boundary layers that a reasonably complete physical picture of the flow processes is available. In this book Professor Plate has summarized what is known about mean flow conditions and has developed his subject in four chapters covering four aspects of boundary layers. For each of these areas, recent research is surveyed and integrated into a coherent account of mean properties of wind and temperature fields. A series of suggestions is given for future research to extend the limits of our knowledge, with particular emphasis on laboratory experiments.

198 pages, 7 by 9¾ inches
Library of Congress Catalog Card Number: 70-611329

Available for $3.00 as TID-25465 from
National Technical Information Service
U. S. Department of Commerce
Springfield, Virginia 22151

NUCLEAR SCIENCE ABSTRACTS

The U. S. Atomic Energy Commission, Division of Technical Information, publishes *Nuclear Science Abstracts (NSA)*, a semimonthly journal containing abstracts of the literature of nuclear science and engineering.

NSA covers (1) research reports of the U. S. Atomic Energy Commission and its contractors; (2) research reports of government agencies, universities, and industrial research organizations on a worldwide basis; and (3) translations, patents, books, and articles appearing in technical and scientific journals.

Complete indexes covering subject, author, source, and report number are included in each issue. These indexes are cumulated and sold separately.

Availability

SALE *NSA* is available on subscription from the Superintendent of Documents, U. S. Government Printing Office, Washington, D. C. 20402, at $42.00 per year for the semimonthly abstract issues and $38.00 per year for the cumulated-index issues. Subscriptions are postpaid within the United States, Canada, Mexico, and all Central and South American countries, except Argentina, Brazil, Guyana, French Guiana, Surinam, and British Honduras. Subscribers in these Central and South American countries, and in all other countries throughout the world, should remit $52.50 per year for subscriptions to semimonthly abstract issues and $47.50 per year for the cumulated-index issues. The single-copy price for the abstract issues is $1.75 postpaid, with this exception: Add one-fourth of $1.75 for mailing to the countries to which the $52.50 subscription rate applies.

EXCHANGE *NSA* is also available on an exchange basis to universities, research institutions, industrial firms, and publishers of scientific information. Inquiries should be directed to the Division of Technical Information Extension, U. S. Atomic Energy Commission, P. O. Box 62, Oak Ridge, Tennessee 37830.

Subscription Information

Technical Progress Reviews may be purchased from Superintendent of Documents, U. S. Government Printing Office, Washington, D. C. 20402. *Nuclear Safety* at $3.50 per year (six issues) for each subscription or $0.60 per issue; *Reactor Technology* at $3.00 per year (four issues) for each subscription or $0.75 per issue; *Isotopes and Radiation Technology* at $2.50 per year (four issues) or $0.70 per issue.

Postage and Remittance

Postpaid within the United States, Canada, Mexico, and all Central and South American countries except Argentina, Brazil, Guyana, French Guiana, Surinam, and British Honduras. For these Central and South American countries and all other countries: add, for each annual subscription, $1.00 for *Nuclear Safety* and $0.75 for each of the other journals; for single issues, add one-fourth of the single-issue price. Payment should be by check, money order, or document coupons, and MUST accompany order. Remittances from foreign countries should be made by international money order or draft on an American bank payable to the Superintendent of Documents or by UNESCO book coupons.